An Injectable Degradable Porous Polymer Scaffold for Tissue Engineering and Drug Delivery

Aliasger K. Salem

BSc (Hons.), MRSC

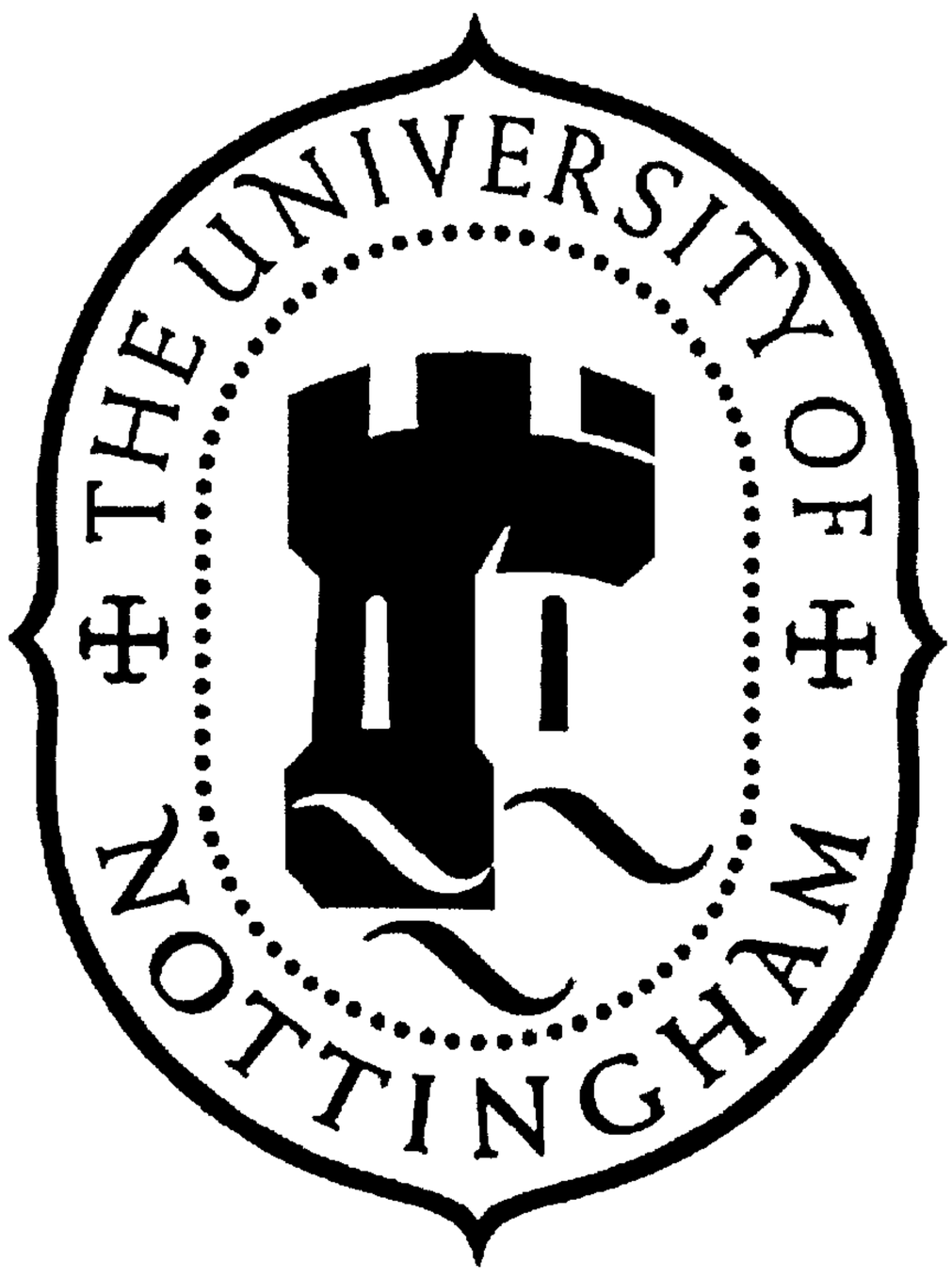

A thesis submitted to the University of Nottingham for the degree of Doctor of Philosophy

November 2001

Results presented in thesis are featured in the following publications:

Salem, A. K.; Cannizzaro, S.M.; Davies, M.C.; Tendler, S.J.B.; Robert, C.J.; Williams, P.M.; Shakesheff, K.M. (2001). Synthesis and Characterisation of a Degradable Poly (lactic acid)-Poly (ethylene glycol) Copolymer with Biotinylated End Groups. *Biomacromolecules*, 2, 2, 575-580

Salem A. K.; Stevens R.; Pearson R.G.; Davies, M.C.; Tendler, S.J.B.; Robert, C.J.; Williams, P.M.; Shakesheff, K.M. (2001). Interactions of fibroblasts and endothelial with defined pore features. *Journal of Biomedical Materials Research*, in press.

Salem, A. K.; Rose, F.R.A.J.; Davies, M.C.; Mitchell J.R.; Robert, C.J.; Stolnik S.; Tendler, S.J.B.; Williams, P.M.; Shakesheff, K.M. (2001). Porous polymer and cell composites that self-assemble *in situ*. *Nature*, submitted.

INDEX

ABSTRACT

Cell transplantation on biodegradable scaffolds is an established approach in tissue engineering to the problem of the regeneration of diseased or damaged tissues. As cells grow and organise themselves, they secrete their own extracellular matrix, while the polymer degrades into natural metabolites resulting in eventual natural tissue replacement. Polymeric materials used for these scaffolds must satisfy a number of requirements. These include defined cell-interactive properties, porosity, biodegradability, mechanical and controlled release properties.

To date, scaffolds have been designed to conform to these requirements. However, the need to preform defined three-dimensional structures requires prior knowledge of the dimensions of the defect or cavity to be filled. Furthermore the general use of toxic solvents in the processing of these scaffolds prevents the incorporation of biological agents and cells during fabrication. Therefore, poor transportation of cells through the scaffolds can result in low cell seeding efficiencies. Finally such scaffolds require an invasive operation for transplantation of the material.

In contrast a number of injectable materials have been proposed and investigated. The transformation from liquid pre-cursor to gel in such systems

can, however, require cell harmful trigger signals such as UV exposure or pH changes. Furthermore, these injectable gels lack a porous structure preventing effective cell migration and restricting tissue formation and vascularisation to the barrier of diffusion for signalling and nutrient molecules.

The work in this thesis presents a scaffold that is both injectable and conforms to the requirements of water-insoluble porous scaffolds. This starts with the synthesis of a biotinylated poly (lactic acid)-poly (ethylene glycol) (PLA-PEG) copolymer. The polymer is degradable, protein resistant and cell interactive when used in conjunction with biotinylated cell adhesive peptides. The biotin unit tethered to the PEG-PLA also provides the polymer with self-assembling properties when used in conjunction with avidin.

In contrast to alternative injectable materials, the scaffold presented in this thesis is porous. This porosity is necessary for tissue ingrowth and vascularization. Therefore, before progressing on to the manufacture of the scaffold, a systematic study of two cell types involved in vascularisation was carried out over defined pore features. These studies revealed that cell behaviour over pore features was related to cell type, cell density and pore size. This had significant implications for the injectable scaffold in development because proposed advantages were delivery of a variety of cell types, controlled porous structure, and efficient cell seeding.

Microparticles were then manufactured from the PLA-PEG-biotin using a single emulsion manufacturing process. Surface Plasmon Resonance (SPR)

confirmed that these microparticles would bind efficiently to avidin. The condition for optimum self-assembling of particles was then determined using aggregation studies. These studies showed that a critical quantity of avidin was required for microparticles to aggregate together. The ability to aggregate particles of different sizes leads to the potential for controlling scaffold porosity. Rheological testing showed that the scaffold's mechanical properties could be tailored to that of the tissue in which regeneration is required.

The self-assembly of microparticles was also demonstrated to form complex three-dimensional scaffolds without the use of toxic solvents. Scaffolds prepared in simulated tissues maintained shape upon injection. Scaffolds were then self-assembled with cells entrapped within them. Cell viability within the self-assembling scaffolds was confirmed by Alamar Blue assays. *In vivo* studies have demonstrated that cell-scaffold composites permit tissue ingrowth and thus readily undergo vascularisation.

The novel molecular-interaction mechanism of self-assembly of these scaffolds differentiates this material from other injectable systems. The formation of porous scaffolds within a cavity or a soft-tissue could be a pre-requisite for tissue remodelling using new cell sources that are dependent on vascularization and tissue ingrowth. The basic component of the scaffold is a biodegradable microparticle that presents a protein resistant surface with biotinylated moieties. Therefore, standard controlled release technologies and biotin-avidin mediated surface engineering can be combined with the self-assembly to form biomimetic scaffolds that stimulate integrin-mediated cell adhesion and then release growth factors.

ACKNOWLEDGEMENTS

Firstly thanks to my family for support of my ongoing education. Special thanks goes to my direct supervisor Professor Kevin Shakesheff for exceptional support during my studies. Additionally I express my gratitude to my co-supervisors, Professors Martyn Davies and Saul Tendler and Drs Clive Roberts and Phil Williams for their advice during my time here. Thanks go to the EPSRC for funding.

For their assistance with advice and help during my studies, I thank members of the Tissue Engineering Group, LBSA, the advanced drug delivery group, the National Centre for Macromolecular Hydrodynamics (NCMH), Orthopaedics at the University of Southampton and the central microstructure facility at the Rutherford-Appleton Laboratories. Specifically, I thank Dr Scott Cannizzaro for advice on polymer synthesis, Dr Robert Stevens for help with photolithographic techniques, Dr Richard Oreffo for assistance with *in vivo* studies, Professor John Mitchell for rheological guidance and Dr Snow Stolnik for advice on microparticle manufacturing processes.

Finally my gratitude goes to all the people (too numerous to mention) that have made my PhD a pleasure to carry out.

LIST OF FIGURES

LIST OF TABLES

ABBREVIATIONS

^{13}C NMR	^{13}C nuclear magnetic resonance
^{1}H NMR	Proton nuclear magnetic resonance
ABAM	Antibiotic/antimycotic
ANOVA	One-way analysis of variance
Av-Rh	Rhodamine-conjugated avidin
BAEC	Bovine aortic endothelial cells
bFGF	Basic fibroblast growth factior
Biotin-HPDP	N-([6-biotinamido-]hexyl-)3'[2'pyridylthio] propionamide
BMPs	Bone morphogenetic proteins
BuLi	Butyl Lithium
CAD	Computer assisted design
CAM	Chorioallantoic membranes of chick embryos
CMFDA	5- chloromethylflourescien diacetate
CNS	Central nervous system
DCM	Dichloromethane
DMEM	Dulbeccos modified Eagles medium
DMSO	Dimethyl sulfoxide
DSC	Differential scanning calorimetry
Ebeam	Electron beam pattern generator
ECM	Extra-cellular matrix
FCS	Foetal calf serum
FDA	Food and Drug administration
G'	Storage modulus
G''	Loss modulus
GPC	Gel permeation chromatography
HABA	2-4'-Hydroxyazobenzene benzoic acid
HBSS	Hanks Balanced Salts Solution
HMDS	Hexamethyldisilizane
HOS cells	Human osteoblast Sarcoma cells
IPC	Interpolymeric complexes
KOH	Potassium hydroxide
LPCVD	Low-pressure chemical vapour deposition
mps	Microparticles

NGF	Nerve growth factor
NHS	N-hydroxy succinimide
-OH	Hydroxyl end-group
Pa	Pascals
PBS	Phosphate buffered saline
PCL	Poly (ε-caprolactone)
PCS	Photon correlation spectroscopy
PDGF	Platelet derived growth factor
PDLLA	Poly (D,L-lactic acid)
PDLLG	Poly (D,L-lactic acid-co-glycolic acid)
PDMS	Polydimethylsiloxane
PDO	Poly (dioxane)
PEG	Poly (ethylene glycol)
PEO	Poly (ethylene oxide)
PET	Poly (ethylene terepthalate)
PG	Proteoglycan
PGA	Poly (glycolic acid)
PLA	Poly (lactic acid)
PLA-PEG	Poly (lactic acid)-Poly (ethylene glycol)
PLGA	Poly (lactic acid-co-glycolic acid)
PLL	Poly (l-lysine)
PLLA	Poly (L-lactic acid)
PMA	Poly (methacrylic acid)
PMMA	Poly (methyl methacrylate)
PNIPAAm	Poly (N-isopropylacrylamide)
PPO	Poly (propylene oxide)
PS	Poly (styrene)
PTFE	Poly (tetraflouroethylene)
PVA	Poly (vinyl alcohol)
R_D	Rate of decrease in absorbance
RGD	Arginyl-glycyl-aspartate
SCCM	Standard cubic centimetres
SEM	Scanning electron microscopy
$Sn(Oct)_2$	Stannous 2 ethyl hexanoate
SPR	Surface plasmon resonance
TCP	Tissue culture plastic
TEM	Transmission electron microscopy
TFE	Tetrafluoroethanol

CHAPTER 1

INTRODUCTION

1.1 Tissue Engineering

Tissue engineering is an interdisciplinary field that applies the principles of engineering and the biological sciences to offer the possibility to create completely natural tissue and replace failing or malfunctioning organs (Langer and Vacanti 1993).

There are inherent difficulties in current organ and tissue transplantations strategies because donor shortages have resulted in a significant number of patients on the waiting list for operations. This list has increased from 19,095 patients in 1989, to 74,800 by February 2001 in the USA alone (Stock and Vacanti 2001; Vacanti 2001). Furthermore, those patients fortunate enough to receive transplantations are subjected to immunosuppresion therapies for the rest of their lives because of the associated risks of infection and tumor development. The lack of donor tissue availability and donor site morbidity

further hampers transplantation of tissues. Replacement with mechanical devices is limited by an increased risk of inflammation and infection. Mechanical devices also lack the mechanism for self-repair and such devices will not grow concurrently with the patient (Vacanti and Langer 1999; Vacanti and Vacanti 2000; Vacanti 2001).

The potential impact of tissue engineering from both a therapeutic and an economic standpoint is enormous. Organ failures and diseases are increasing with human life expectation. The total health care costs for patients suffering from tissue loss or organ failure exceed $400 billion annually in the USA alone. It has been estimated that the total market for tissue-engineered products in the USA will be $80 billion annually (Peppas and Langer 1994; Davis and Vacanti 1996). The success of alternative donor sources from other species like the pig still remain in doubt, because of potential transferable diseases such as the pig endogenous retrovirus (Stock and Vacanti 2001).

The object of tissue engineering is to regenerate natural tissues from living cells to replace defective or lost tissues and organs. It involves the creation of natural tissue by transplanting cells removed from the patient or a close relative and seeded into an implant which serves as both an adhesive substrate and a physical support for the isolated cells. Using cells from the same genotype avoids many of the problems associated with immune rejection of foreign tissue. As these cells are capable of proliferation, a small number of harvested cells can be expanded until a cell mass sufficient to replace the organ function

is achieved. Therefore, it is not required to sacrifice the entire organ of the donor (Cima *et al.* 1991) (Vacanti *et al.* 1994).

Tissue engineering can be classified into two main areas: *in vivo* and *in vitro* tissue engineering. Once a tissue can be generated on a large scale *in vitro*, it can then become a viable supply of new tissue for patients. *In vitro* tissue engineering thus requires a specifically designed environment for regeneration. This is in contrast to the *in vivo* approach, where most of the materials necessary for tissue regeneration are automatically provided by the host living body. To date, it has only been possible to proliferate singular cell types *in vitro* and thus the formation of only simple avascular structures is possible. Therefore, *in vitro* tissue engineering, whilst theoretically desirable, is currently limited to tissues such as dermis, epidermis and articular cartilage (Eaglstein and Falanga 1998; Christenson 1999; Edelman 1999; Atala and Nyberg 2000).

Tissue regeneration *in vivo* attempts to achieve natural regeneration of tissues and organs by harnessing the natural healing process of the body. For large defects, it is necessary to use a scaffold as support for the tissue to grow. The scaffold may be used either with or without cell seeding prior to implantation. Scaffolds without cells just serve to imitate the natural extra-cellular matrix (ECM) of the body. Tissue regeneration is, in this case, dependent on the ingrowth from the surrounding tissue in a process, which is known as tissue induction. Vascularisation of a scaffold is a typical example of tissue induction (Mikos *et al.* 1993).

Tissues engineering using scaffolds with cells have been studied to restore the function of several tissues such as liver (Moghe 1996), blood vessels (Niklason and Langer 1997), nerve (Bellamkonda and Aebischer 1994), skin (Pachence 1996), cartilage (LeBaron and Athanasiou 2000) and bone (Hutmacher 2000). Significant challenges to this approach include the design and fabrication of a suitable scaffold able to promote cell adhesion and to support cell growth, proliferation and differentiation and induced formation of natural tissue. In many cases, biocompatible, biodegradable polymers are utilised to either induce surrounding tissue and cell ingrowth or to serve as a temporary scaffold for transplanted cells to attach, grow, and maintain differentiated functions (Christenson *et al.* 1997).

The original hypothesis that cells on polymer scaffolds could give rise to organised tissue extended from the following biological observations:

1. Most tissues undergo constant remodelling (Healy *et al.* 1996).
2. Dissociated mature cells can reorganise themselves into their native histological structures when placed in ideal cell culture conditions (Marler *et al.* 1998).
3. While isolated cell populations are capable of histological reorganisation, this is limited when they are delivered as a cell suspension because they lack a template to guide restructuring (Kim and Mooney 1998).

4. The quantity of tissue for implantation is restricted by diffusion requirements for gas and nutrient exchange (Marler *et al.* 1998).

The strategy of tissue engineering generally involves the following steps (Figure 1.1): Depending on the target organ, a suitable cell source is identified, isolated, and produced in sufficient numbers (Bonassar and Vacanti 1998; Stock and Vacanti 2001). Then a biocompatible material that can be used as a cell substrate or cell-encapsulation material is isolated or synthesised and processed into the required shape (Cima *et al.* 1991). The material is seeded uniformly with cells, which can then be grown in a bioreactor (Burg *et al.* 2000) and finally the material-cell construct is placed into the target *in vivo* site, where depending on the site and the structure, vascularization may be necessary (Kim and Mooney 1998).

1.2 Polymer Scaffolds

A key element in a number of tissue engineering approaches is the use of a polymer scaffold (Vacanti *et al.* 1994). Isolated cells injected into the body at random cannot form new tissue on their own (Cima *et al.* 1991; Marler *et al.* 1998). They require a specific environment in which a supporting material acts as a template for the *in vitro* cell seeding and the subsequent re-implantation into the host with the aim of tissue formation. Using a degradable scaffold on which cells grow and organize themselves can potentially achieve this.

Isolated cells

Biodegradable
Polymer scaffold

Cells seeded onto scaffold. As cells produce extracellular matrix and proliferate, synthetic polymer scaffold degrades

In Vitro Tissue
Engineering

In Vivo Tissue
Engineering

Grow tissue
in bioreactor

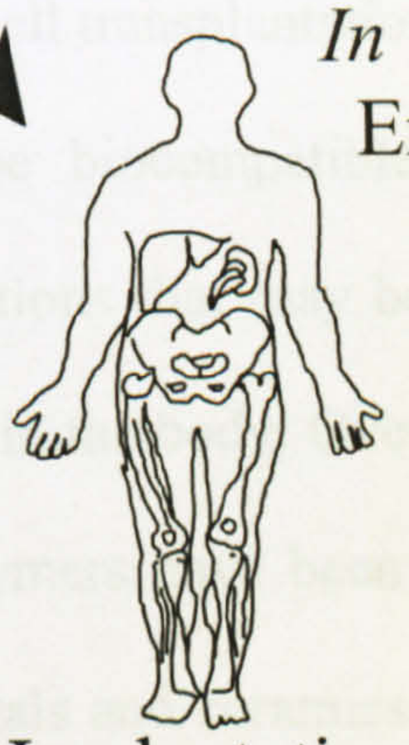

Implantation

Figure 1.1 Schematic representation of a typical tissue engineering approach. Specific cell populations are harvested from the appropriate tissue and seeded onto a biodegradable polymer scaffold.

As the cells begin to secrete their own extracellular matrix, the polymer degrades and is eventually eliminated from the body, resulting in completely natural tissue replacement (Peter *et al.* 1998).

The work in this thesis presents the development of a novel *in situ* solidifying porous scaffold for tissue engineering. The review in this chapter will thus attempt to introduce the materials commonly used for scaffolds in tissue engineering, the design criteria of scaffolds in tissue engineering and the methods that are currently established for manufacturing porous scaffolds.

1.2.1 Materials for scaffolds in tissue engineering

The first step in the design of a scaffold for cell transplantation is the choice of a suitable material. The material must be biocompatible and preferably biodegradable to avoid the risk of complications that may be associated with the long-term presence of a foreign material in the body. Over the last century, materials such as metals, ceramics and polymers have been extensively used for surgical implantations (Kohn 1996). Metals and ceramics have contributed to major advances in the medical field, particularly in orthopaedic tissue replacement (Agrawal 1998). These materials, in comparison to polymers, however are difficult to process and lack biodegradability. The use of polymers can be sub-divided into two categories: natural polymers and synthetic polymers.

1.2.1.1 Natural derived polymers

Proteins and sugars derived from natural extracellular matrices, such as collagen and glycosaminoglycan, have been used to repair nerve (Labrador *et al.* 1998), skin (Pachence 1996), cartilage (LeBaron and Athanasiou 2000) and bone (Winn *et al.* 1999). Chemical crosslinking by glutaraldehyde has been proposed to control the stability and degradation rate of these matrices, whereas porosity has been controlled using both chemical and physical techniques (Cavallaro and Kemp 1994). However, collagenous scaffolds that have been crosslinked with glutaraldehyde can exhibit immunogenicity, calcification and fibrous scarring during long term implantation (Cima *et al.* 1991).

Transplantation scaffolds fabricated from natural polymers can suffer from some major disadvantages such as poor mechanical performances. Collagen, hyaluronate, fibrin and gelatin, for an example lack mechanical strength. They can also provoke adverse tissue reactions and immune responses and they may promote undesired cell behaviour (Cima *et al.* 1991; Moghe 1996). However, numerous natural materials have found wide use in tissue engineering applications. Chitosan is a natural polysaccharide, whose structural characteristics are similar to glycosaminoglycans. Chitosan is highly soluble in an acidic environment and insoluble under neutral conditions. It has been used in a variety of biomedical applications, such as haemodialysis membranes, drug delivery systems, artificial skin, orthopaedic and dental coating materials

(Chuang *et al.* 1999; Chenite *et al.* 2000; Park *et al.* 2000). Alginates are also water-soluble polysaccharides which have the ability to form crosslinked gels in the presence of multivalent ions thus providing potential for a number of applications in drug delivery and tissue engineering (Rowley, 1999). Alginate is widely available (isolated from seaweed), has low diffusional barriers for nutrients and reasonable biocompatibility. However, the calcium ions on which gelation is dependent can be lost in the body (Kim and Mooney 1998).

1.2.1.2 Synthetic polymers.

There is a wide variety of synthetic polymers that have been investigated for biomaterial and tissue engineering applications. Poly (vinyl alcohol) (PVA), poly (N-isopropyacrylamide) (PNIPAAm) and its derivatives have for example, been shown to have great potential as delivery vehicles for cartilage and the pancreas. The non-degradable crosslinks and toxic crosslinking molecules used with polymers such as PNIPAAm are however drawbacks in the use of these materials (Li *et al.* 1998; Lee and Mooney 2001; Peng and Cheng 2001).

The use of biodegradable materials has proven to be immensely important in medical applications over the last three decades. Polymers prepared from glycolic acid and lactic acid have found a multitude of uses in the medical industry, beginning with the biodegradable sutures first approved in the 1960s (Cima *et al.* 1991).

Since that time, diverse products based on lactic and glycolic acid and on other materials such as poly (ε-caprolactone) homopolymers and copolymers have been accepted for use as medical devices (Yin and Baker 1999; Ural *et al.* 2000). Table 1.1 describes the properties of some of these common biodegradable polymers. In addition to these approved materials, a great deal of research continues on polyanhydrides (Burkoth and Anseth 2000), polyorthoesters (Heller 1994), polyphosphazenes (Schacht *et al.* 1996) and other biodegradable polymers (Peppas and Langer 1994).

The degradation mechanism varies with each of these polymer types. For example, polyorthoesters are surface eroding, whilst polyphosphazenes degradation rate can be controlled by changes in the structure of the side-chain rather than the backbone as with the polyesters.

The molecular properties of an increasing number of synthetic polymers such as molecular weight, molecular weight distribution, composition and molecular architecture can be manipulated to modify their physico-mechanical properties (Gopferich 1996). Given the high processing ability for synthetic polymers, it is thus possible to have porous materials with well-controlled microstructure and good mechanical properties (Lu and Mikos 1996).

Polymer	Melting point (°C)	Glass-Transition Temp (°C)	Modulus (Gpa)	Degradation Time (months)
PGA	225-230	35-40	7.0	6 to 12
PLLA	173-178	60-65	2.7	>24
PDLLA	Amorphous	55-60	1.9	12 to 16
PCL	58-63	(-65)-(-60)	0.4	>24
PDO	N/A	(-10)-0	1.5	6 to 12
PGA-TMC	N/A	N/A	2.4	6 to 12
85/15 PDLLG	Amorphous	50-55	2.0	5 to 6
75/25 PDLLG	Amorphous	50-55	2.0	4 to 5
60/35 PDLLG	Amorphous	45-50	2.0	3 to 4
50/50 PDLLG	Amorphous	45-50	2.0	1 to 2

Table 1.1 Properties of common biodegradable polymers.

1.2.1.3 Poly α-hydroxy acids

An important class of synthetic biodegradable polymers includes polyesters and copolyesters of lactic and glycolic acid (Figure 1.2) (Peter *et al.* 1998). They are among the few synthetic polymeric materials approved for human clinical use by the Food and Drug Administration (F.D.A.).

Due to their high versatility, the aliphatic polyesters derived from lactic acid and glycolic acid are the synthetic biodegradable polymers most commonly employed in medical and pharmaceutical applications including surgical sutures (Matsusue *et al.* 1992), drug delivery systems (Hubbell 1998), orthopaedic and reconstructive implants. These polymers are furthermore widely tested as biodegradable matrices to be used in transplantation of a variety of cells, such as osteoblasts (Ishaug-Riley *et al.* 1998), chondrocytes and hepatocytes (Kaufmann *et al.* 1997).

Extensive research has been carried out to assess the regenerative potentials of different organs using porous biodegradable polyester materials as scaffolds for cell transplantation (Freed *et al.* 1994).

Poly (lactic acids) can be prepared by two different routes: firstly, by polycondensation of lactic acid and secondly by ring-opening polymerisation of the cyclic dimer. Depending on the initiator, the polymerisation of lactide may follow three different reaction mechanisms:

PLA PGA

Figure 1.2 Poly (lactic acid) (PLA) and poly (glycolic acid) (PGA) structures

1. A cationic mechanism
2. An anionic mechanism
3. An insertion mechanism (Kricheldorf and KreiserSaunders 1996)

Cationic polymerisation has very few initiators and the products are of low molecular weight. C^{13} nuclear magnetic resonance spectroscopy (^{13}C NMR) also showed that the polymers of lactide and glycolide produced were not truly random copolymers (Kricheldorf and Kreiser 1987).

With anionic polymerisation of L-lactide there is a 10-20% racemization observed suggesting that chain-transfer reactions with the monomer via deprotonation takes place (Kricheldorf and Boettcher 1993). High molecular weights can only be obtained by a combination of butyl lithium (BuLi) and crown ethers, however lithium is a toxic material (Kricheldorf and KreiserSaunders 1996).

One of the best methods for polymerisation of lactides is the insertion mechanism using stannous 2-ethylhexanoate ($Sn(Oct)_2$) (Kricheldorf and KreiserSaunders 1996; Li *et al.* 1996). $Sn(Oct)_2$ is a permitted food additive in numerous countries, which means that its toxicity is extremely low compared to other heavy metal salts. $Sn(Oct)_2$ is also highly efficient and allows almost complete conversion even at monomer/catalyst ratios as high as 10^4:1 (Kricheldorf *et al.* 1995). Random copolymers are possible and the risk of racemization is low. This has been confirmed by work done to gain information on monomer sequences by ^{13}C NMR on PLGA polymers prepared

using $Sn(Oct)_2$ (Kricheldorf *et al.* 1985). Furthermore, when the polymerisation of L-lactide was catalysed with $Sn(Oct)_2$ in the presence or absence of alcohol, the molecular weights parallel the lactide/alcohol ratio, but never the lactide/Sn ratio. Polymerisations conducted at low lactide/catalyst ratios in the absence of an alcohol yield poly (lactic acids) with a low content of 2-ethylhexanoate end-groups. Proton nuclear magnetic resonance spectroscopy (^1H NMR) of chloroform ($CHCl_3$) solutions also demonstrated that $Sn(Oct)_2$ forms stronger complexes with alcohol and weaker complexes with lactide. The reaction between lactide and hydroxyl (OH) end-groups is bound by an Sn atom via two sp^3d^2 orbitals (Figure 1.3) (Kricheldorf *et al.* 1995).

The racemic poly (DL-lactic acid) (PDLLA) is amorphous and has a lower glass transition point than the two stereoregular polymers, poly (D-lactic acid) (PDLA) and poly (L-lactic acid) (PLLA).

The copolymers of lactide and glycolide are less crystalline than the two homopolymers of the two monomers. Poly (lactic acid), because of the methyl group is more hydrophobic than the poly (glycolic acid) and water uptake increases as the glycolide ratio in the copolymer increases.

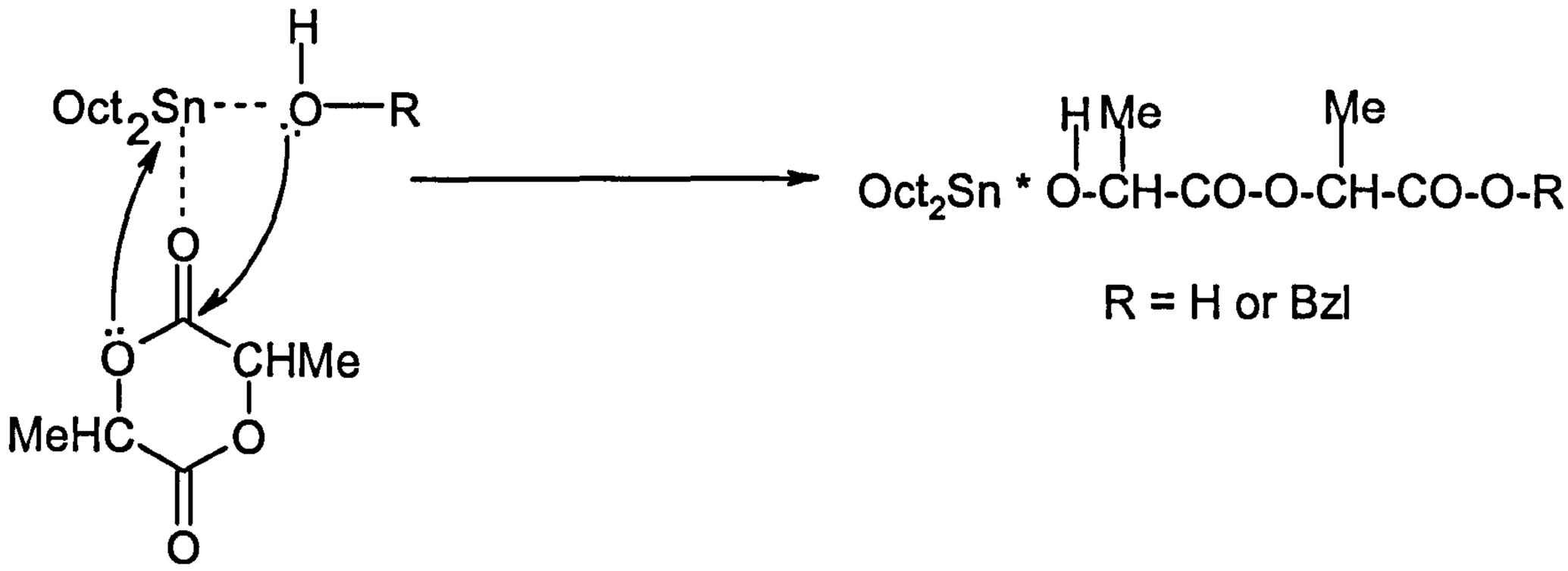

Figure 1.3 Stannous octoate and its complexation with the hydroxyl group to ring-open lactide(Kricheldorf *et al.* 1995)

The general crystallisation behaviour of poly (L-lactic acid) has been characterised and the equilibrium melting point and the glass transition temperature were found to be 215°C and 55°C respectively (Kalb and Pennings 1980). The *in vivo* and *in vitro* degradation of PLLA occurs through hydrolytic degradation (Figure 1.4) (Lu *et al.* 2000). This is controlled not only by the water diffusion within the polymer matrix, but also by the release of the water-soluble acid oligomeric by-products. Consequently, the degradation profile is found to be dependent on a number of parameters, such as porosity, size and shape of the device. (Holy *et al.* 1999)

In addition to the degradation rate, copolymerisation of lactides also has decisive effects on mechanical strength, hydrophilicity and biocompatibility of the final biomaterial. For example, biodegradable poly (ethylene glycol)/poly (lactic acid) block copolymers, covering a wide range of compositions and molecular weight have been synthesised. This copolymerisation is an easy way to modulate the hydrophilic/hydrophobic balance (Penco *et al.* 1996).

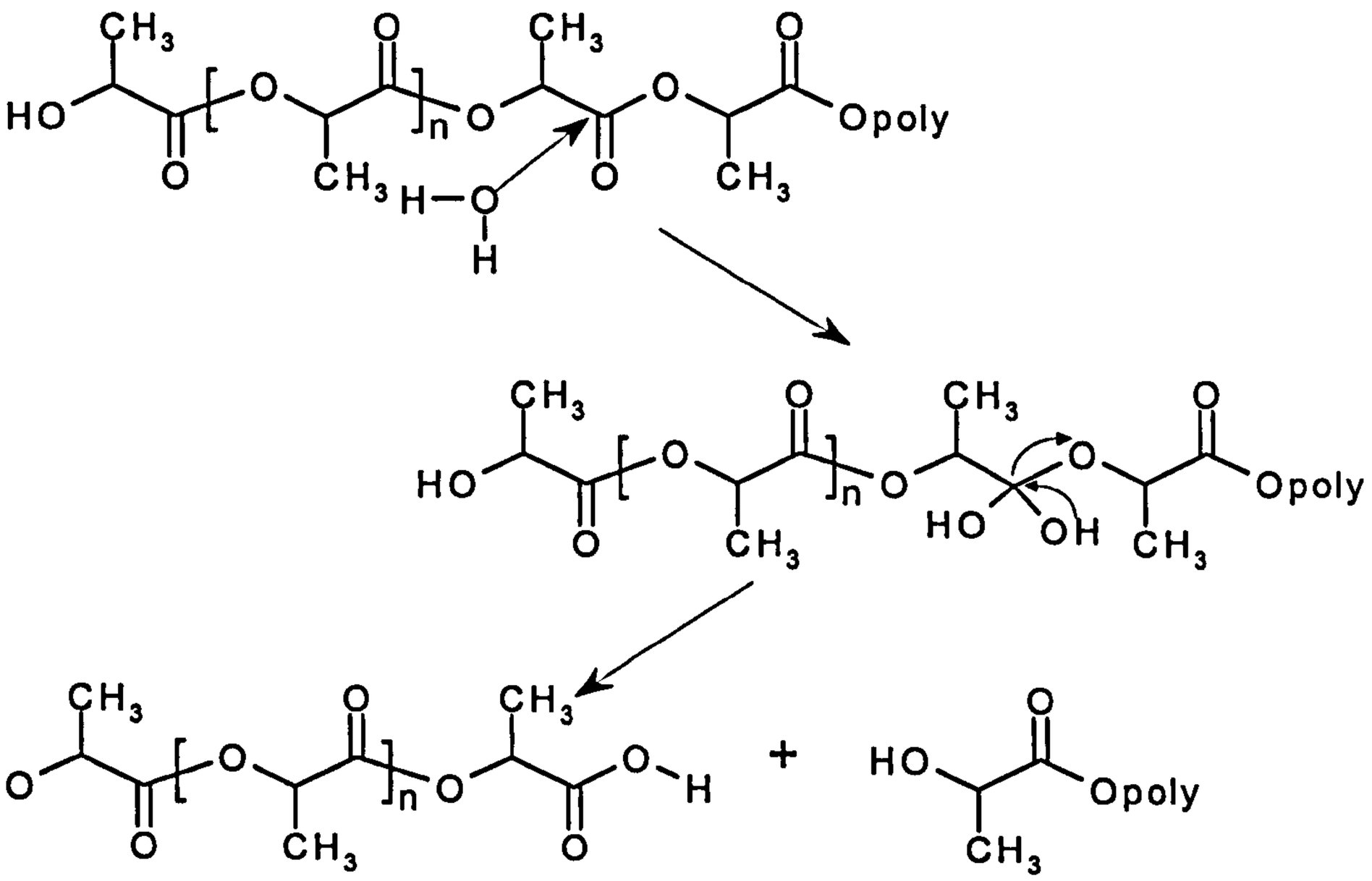

Figure 1.4 The degradation of poly (lactic acid) (Lunt 1998)

1.2.1.4 Poly (ethylene glycol) based copolymers.

The inclusion of PEG in copolymer systems imparts beneficial surface properties within the body when scaffolds are manufactured from the polymer, because of the ability of PEG to repel proteins within aqueous environments (Holmberg *et al.* 1997). This property is a result of the hydrophilic nature of the PEG, which binds water through hydrogen bonding, which then prevents protein binding. This repulsion inhibits the adsorption of proteins to the polymer/scaffold surface and, therefore, prevents many undesirable polymer-cell interactions (Holmberg *et al.* 1997; Deible *et al.* 1998). For an example, in comparison to PLA, nanoparticles made from the PLA-PEG copolymer have increased blood circulation times and been demonstrated to be inert toward proteins of the coagulation system (Uhrich *et al.* 1999).

Various methods have been used to achieve materials with a PEG surface. These include covalent grafting of PEG, which present reactive chain-ends at the surface (Otsuka *et al.* 1998), entrapment of PEG onto the surface (Quirk *et al.* 2000), graft copolymerisation of PEG macro-monomer onto the surface (Rashkov *et al.* 1996), and direct adsorption of PEG onto surfaces in the form of a surfactant or a block copolymer in which one of the blocks is a PEG. Adsorption of amphiphilic PEG-containing block copolymers on the surface allows temporary passivation of the surfaces towards cell and protein adsorption, but such coatings are not stable and the density of PEG achievable on the surface is typically lower than that required for complete passivation.

Furthermore, most of the PEG coated surfaces possess no reactive group on the PEG chain end (Tziampazis *et al.* 2000; Veronese 2001).

Heterobifunctional PEG has different functional groups at both chain ends. When one of the functional end-groups in the heterobifunctional PEG selectivity initiates the polymerization of a hydrophobic monomer, a new heterobifunctional AB block copolymer can be prepared, keeping the other functional group at the PEG chain end available (Otsuka *et al.* 1998). Poly α-hydroxy acids such as PLA are ideal as the hydrophobic segment of PEG based copolymers because the Food and Drug Administration (FDA) approve both PEG and PLA for medical/clinical use. PLA-PEG copolymer systems possess surfactant properties because the PEG block is very hydrophilic and the PLA block is hydrophobic (Zhu *et al.* 1990). Therefore, when PLA-PEG is employed in a fabrication process that uses an aqueous external phase, e.g., particle fabrication by the single emulsion technique, PEG enriches the surface (Hrkach *et al.* 1997). This process is described in more detail in Chapter 5.

There are a variety of techniques by which PLGA-PEG and PLA-PEG copolymers can be synthesised. These vary from the most common method of reacting lactide/glycolide monomers with the hydroxy-terminated groups of PEG using stannous chloride (Deng *et al.* 1990), aluminium tri-isopropoxide (Li and Kissel 1993), isobutylaluminoxane (Chen *et al.* 1997), and stannous octoate ($Sn(Oct)_2$) (Kricheldorf and Meierhaack 1993; Kricheldorf *et al.* 1995; Li *et al.* 1996) to chain extension reactions on PLGA thermal oligomers by a

polycondensation reaction using α,ω-bis-hydroxylated oligomers, such as polyethyleneglycols.(Penco *et al.* 1998)

A difficulty encountered with surfaces designed for specific biological recognition such as the antigen-antibody interactions is the non-specific adsorption of other proteins (Veronese 2001). In this regard, the protein-resistant properties of a PEG surface are advantageous. Ligands including proteins, peptides and sugars can be attached to the distal end of these PEG chains creating substrates that recognize a specific molecule with minimised nonspecific adsorption of other components (Veronese 2001). This approach has been shown to be useful in regionally selective microarchitectured scaffolds fabricated from biodegradable polymers for spatial organization of co-cultured cells with different functions. A similar surface engineering was performed by Patel *et al.*, who developed a method of generating micron-scale patterns of any biotinylated ligand on the surface of a biodegradable block copolymer of PLA and PEG (Patel *et al.* 1998). The polymer is biodegradable and resistant to non-specific protein adsorption, and the biotin moiety at the distal end of the PEG segment allows surfaces to be biospecific by binding avidin-conjugated ligands. The synthesis and characterisation of PLA-PEG-biotin, which forms the foundation of our self-assembling scaffold, is discussed in Chapter 3.

1.2.2 Design criteria for polymer scaffolds in tissue engineering.

There are a number of biological, physical and chemical conditions required for the implementation of scaffolds for cell transplantation and tissue ingrowth. These are broadly split into five main categories:

1. Biocompatibility and/or cell-interactive properties
2. Porosity
3. Biodegradability
4. Mechanical properties
5. The use of the scaffold in controlled release.

1.2.2.1 Biocompatibility and cell-polymer interactions

Cells recognize synthetic materials through a complex protein layer, which forms immediately on the material upon contact with body fluids (Drumheller.P 1998). This relation between material properties and cellular responses, mediated by the intervening protein layer, has complicated the development of biomaterials. Before the advent of biodegradable materials in the use of surgical procedures, polymer implants were intended to remain inert, thus unaffected by reactions with the surrounding tissues. As a result, cell-polymer interactions were first studied for the purpose of preventing or at least minimising the interactions (Agrawal 1998). Recent progress has been made by incorporating biologically active structures into the material, to permit direct

cellular interaction with the material (Drumheller and Hubbell 1995). These advances are based on the molecular biology of cell adhesion; specifically, the identification of small domains in the adhesion proteins of the extracellular matrix that bind to adhesion receptors on the surface of cells has been critical (Figure 1.5)(Drumheller.P 1998). Oligopeptide copies of these adhesion-promoting peptides can be synthesized and incorporated into materials, either in the bulk or as surface modifications. These approaches toward biofunctionalization provide a method to control biological interactions directly through material design.

Hubbell and co-workers have characterized the conditions under which the minimal cell binding oligopeptide sequences such as arginyl-glycyl-aspartate (RGD), which are found in many cell adhesion proteins, is capable of supporting adhesion in cells such as the fibroblast (Massia and Hubbell 1990). It was observed that a surface density of 10 fmol/cm^2 of surface coupled RGD ligand was enough to promote normal cell spreading, clustering of the cell-surface receptors, and organization of a normal cytoskeleton, corresponding to about 140nm distance between peptide ligands (Massia and Hubbell 1991).

Numerous schemes have been developed for the incorporation of such adhesion ligands into both biostable and biodegradable polymer surfaces. These methods are generally based on adsorption, physical immobilisation or covalent binding. Quirk *et al* have developed a physical entrapment method whereby PLA is exposed to a partial solvent system containing poly L-lysine (PLL).

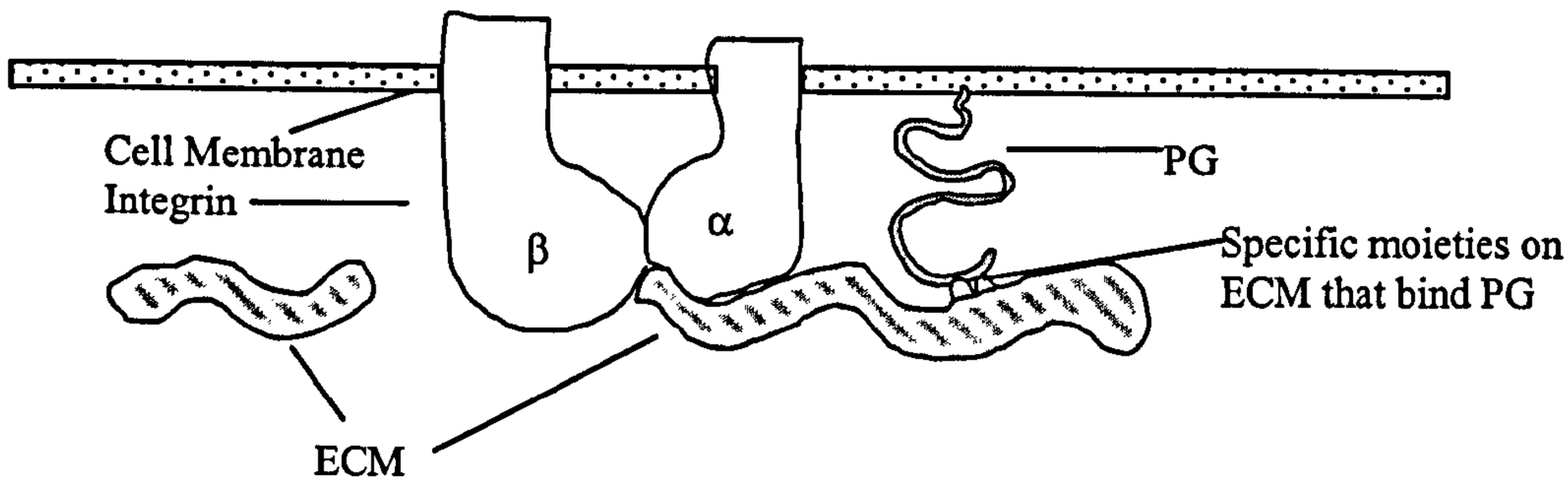

Figure 1.5 Integrin/proteoglycan (PG) interactions in cell-extracellular matrix (ECM) adhesion adapted from (Drumheller and Hubbell 1995)

This causes the formation of a gel layer in the PLA in which PLL diffuses into. Addition of a non-solvent excess results in immobilisation of the PLL. The attachment of RGD to PLL prior to this surface modification has been demonstrated to greatly enhance cell interactions (Quirk *et al.* 2001). Langer and co-workers at the Massachusetts Institute of Technology (MIT) have developed copolymers of the poly (lactic acid) with lysine providing sites for facile grafting of such peptide-based adhesion ligands (Barrera *et al.* 1993; Hrkach *et al.* 1995; Cook *et al.* 1997). A further method for presenting peptide sequences is the PLA-PEG-biotin copolymer developed by Shakesheff and co-workers. The universal coupling system via a biotin:avidin:biotin sequenced approach avoids possible disadvantages of covalent chemical attachments such as harsh reaction conditions and inefficient coupling or purification methods and allows for the facile surface presentation of peptides such as RGD (Cannizzaro *et al.* 1998). Clearly, the modification and functionalisation of polymer surfaces is a very active area of research. Microlithography techniques, which allow fine control of the surface texture is another illustration of surface modification in view of controlling, cell adhesion (Curtis and Clark 1990). Such techniques are reviewed further in Chapter 4 where lithography was employed to assess cell interactions with defined pore features, which are an important aspect of three-dimensional porous scaffolds.

1.2.2.2 Pore size and morphology

Three-dimensional porous polymer matrices possess several advantages for tissue reconstruction, including an increased area for cell anchorage and an

increased volume for cell growth, migration and effective fluid-phase transport of nutrients (Vacanti *et al.* 1994). The morphology of scaffold pores can critically determine the performance of an implanted scaffold, including the rate of tissue ingrowth. A high surface area favours cell attachment and growth, whereas a large pore volume is required to accommodate and subsequently deliver a cell mass sufficient for tissue repair (Freed *et al.* 1994). This has been demonstrated by transplantation of hepatocytes for the engineering of new liver tissue. (Cima *et al.* 1991; Kaufmann *et al.* 1997). When scaffolds are implanted *in vivo*, porous polymeric implants are often invaded by vascularized fibrous tissue. Predicting such behaviour is important because ingrowth in this manner can improve the survival of cells such as the hepatocytes, but has also shown to dramatically decrease the porosity of the implant (Mikos *et al.* 1993) (Mooney *et al.* 1997). Table 1.2 shows that pore size, not chemical composition, has the predominant influence on the vascularization of an implant. Implants show optimal vascular induction, where pores are large enough for cell and tissue infiltration but not large enough to allow fibrous deposit (Sharkawy *et al.* 1998). Larger pores have also been shown to round macrophages, resulting in favourable angiogenic factor secretion, whilst smaller pore sizes, lead to macrophage spreading, which promotes fibroblast proliferation (Padera and Colton 1996).

Highly porous biomaterials are also desirable for the easy diffusion of waste products from the implant (Mikos *et al.* 1993; Kim and Mooney 1998), which is a major requirement for regeneration of highly metabolic organs such as the liver and pancreas.

Pore size (μm)	Site	Material	Vascular penetration	Observations	Ref.
5-700 (pore size)	Subcutaneous	PVA	Yes	Vascularisation at 60 μm near to normal tissue.	(Sharkawy *et al.* 1997; Sharkawy *et al.* 1998; Sharkawy *et al.* 1998)
30, 60 and 100 μm (internodal distance)	Subcutaneous	PTFE	Yes	Largest degree of vascularisation at internodal distances of 60 μm	(Salzmann *et al.* 1997; Williams *et al.* 1997)
30-60 (internodal distance)	Hamster dorsal skin flaps for 10 d	PTFE	Yes	Microvessels grow most effectively at larger internodal distance of 60 μm	(Clowes *et al.* 1986; Clowes *et al.* 1987)
1, 22 and 30 μm (fibril length)	Artery	PTFE	No	Higher vascular density with larger fibril lengths of 30 μm	(Menger *et al.* 1990)
0.02-15 (pore size)	Subcutaneous	PTFE Cellulose acetate, mixed-esters cellulose, acrylic copolymer	No	Vascular capsules containg blood vessels with larger pore sizes from 5-15 μm Avascular capsules with smaller pore sizes	(Brauker *et al.* 1995; Padera and Colton 1996)

Table 1.2 Effect of pore size in biomaterials on vascularization.

Table 1.3 shows the influence of porosity on diffusion and permeability properties. The surface area/volume ratio of a porous material depends on the density and average diameter of the pores. The optimum porosity varies with tissue types such as cartilage with minimal porosity constraints, to liver which requires pores with a minimum diameter of 60μm (Athanasiou *et al.* 1998) (Cima *et al.* 1991; Kaufmann *et al.* 1997). A scaffold suitable for organ and tissue regeneration must also contribute towards the organisation and direction of cell growth and ECM production. It has been shown that porous matrices with well-defined networks of interconnected pores take a significant role in this organization (Freed *et al.* 1994; Lu *et al.* 2000). The degree of porosity also has a significant impact on the rate of degradation with higher porosities reducing pH levels by easy removal of acidic oligomers thereby preventing autocatalytic degradation (Lu *et al.* 2000).

1.2.2.3 Biodegradability

When the ECM production is large enough to provide cells with a natural environment, the polymer scaffold degrades away at a controlled rate. Ideally, it should be completely resorbed, and natural physiological and metabolic pathways should eliminate the biodegradation products in order to avoid risks of unfavourable tissue reactions.

The ideal lifetime of a biodegradable polymer scaffold depends on the application and particularly on the time required for the tissue or organ regeneration.

Pore size (μm)	Material	Vascular density (no. Per mm^2)	Permeability ($x10^{-5}$ cm/s)
700	PVA	55	0.71
60	PVA	116.3	3.89
5	PVA	73.7	1.37
5	PTFE	67.5	0.65
0.5	PTFE	35.2	1.47
0	PVA	30.5	1.62

Table1.3 Effect of porosity in biomaterial implants on transport properties (Sharkawy *et al.* 1997; Sharkawy *et al.* 1998; Sharkawy *et al.* 1998).

Thus, the success of a biomaterial in tissue engineering depends largely on how its biodegradation rate can be controlled. Certain scaffolds are thought to exhibit accelerated degradation at times owing to autocatalysis, which may be as a function of porosity. Poly α-hydroxy acids break down through a hydrolytic degradation pathway that leads to lactic acid/glycolic acid, which enter the tricarboxylic acid cycle and are eventually excreted. Thus, as these materials undergo hydrolytic breakdown, they release acidic by-products. An acidic environment can accelerate hydrolysis of these polymers (Lunt 1998; Holy *et al.* 1999). If the implants are structurally able to allow sufficient fluid flow through the interior, the by-products can be evacuated quickly. If however, diffusion is restricted by a non-porous environment, acidic by-products can accumulate within the implant resulting in adverse reactions from the surrounding tissue (Agrawal *et al.* 2000) (Mooney *et al.* 1995). One of the major advantages of degradation is that the scaffold can act as a controlled release device delivering growth factors over a sustained period of time (Sheridan *et al.* 2000).

1.2.2.4 Scaffolds as controlled release devices

A last criterion, which can influence the choice of polymer as biomaterial, is the possibility of incorporating bioactive molecules, such as drugs or growth and differentiation factors (Lee *et al.* 2000). Indeed, the controlled release of tissue-specific growth factors from the polymer scaffold may in some cases, considerably enhance the process of organ and tissue regeneration. Examples of growth factors include nerve growth factor (NGF) for nervous tissue regeneration (Bellamkonda and Aebischer 1994; Smith and Browne 1998), basic fibroblast growth factor (bFGF) for wound healing (Bonassar and Vacanti 1998), bone morphogenetic proteins (BMPs)

for cartilage (Saltzman *et al.* 1999) (Fujisato *et al.* 1996) and bone remodelling (Hollinger and Leong 1996), and angiogenic growth factors for the control of vascularization (Sondell *et al.* 1999). In tissue-engineered devices, there are two different potentially different delivery systems. Growth factors can be incorporated directly into the scaffold during or after fabrication (Babensee *et al.* 2000). In a biodegradable system, the growth factor would be released as the scaffold degrades to induce tissue regeneration. Growth factor, directly incorporated into a biodegradable polymer scaffold, is released by a diffusion-controlled mechanism that is regulated by the median pore size (Whang *et al.* 1998). The protein can also be released by an erosion mechanism or a combination with diffusion. Alternatively, the growth factor delivery device, in the form of microparticles, nanoparticles, fibres or injectable complexes, can be incorporated into the scaffold (Mooney *et al.* 1996). This method of delivery is also desirable because growth factors have short biological half-lives. For an example, platelet derived growth factor (PDGF) has a half-life of less than two minutes when injected intravenously (Babensee *et al.* 2000).

Specific growth factors, released from the delivery device would aid in the induction of cell migration, proliferation and differentiation or improve engraftment of seeded cells, supported by the polymer scaffold, for more efficient tissue regeneration (Babensee *et al.* 2000). There should be no interference of the growth factor delivery device and the tissue engineered device. The two components should function synergistically. Growth factors released from a device may interact with matrix proteins in the scaffold or in the surrounding tissue to enhance their local bioavailability or provide increased stability (Babensee *et al.* 1998; Lee *et al.* 2000). A novel approach to the use of growth factors is to immobilise them onto the surface

of scaffolds, which in conjunction with adhesive peptides, could mimic membrane-anchored growth factors such as heparin-binding epidermal growth factor (Ito 1998).

In summary, cell scaffolds for tissue engineering should meet several design criteria:

1. The surface should permit cell adhesion and growth (Hench 1998).
2. Neither the polymer nor its degradation products should provoke inflammation or toxicity when implanted *in vivo* (Peter *et al.* 1998).
3. The material should be reproducibly processable into three-dimensional structures.
4. There should be controlled porosity in order to provide a high surface area for cell-polymer interactions, sufficient space for extracellular matrix regeneration, and minimal diffusional constraints during *in vitro* culture (Tjia and Moghe 1998).
5. The scaffold should resorb once it has served its purpose of providing a template for the regenerating tissue, since foreign materials carry a permanent risk of inflammation (Ronneberger *et al.* 1997).
6. The scaffold degradation rate should be adjustable to match the rate of tissue regeneration by the cell type of interest (Ratner *et al.* 1990; Freed *et al.* 1994).

Such scaffolds should allow attachment of isolated cells to a polymeric support structure that has suitable surface properties for guiding the reorganisation and growth of cells. These should be designed so that the cells could survive by diffusion once the cell-polymer construct was implanted. Ideally, the cell-polymer construct would become vascularized in conjunction with expansion of the cell mass following

implantation, and both these processes could be influenced if desired by release of appropriate growth factors at the site (Fausto *et al.* 1995). The ability of scaffolds to conform to all these conditions is also highly dependent on the manufacturing process.

1.2.3 Manufacturing methods

The conventional processing techniques and porogen methods used in the polymer industry are unsuitable for producing medical implants. Indeed, additives are commonly used, such as surfactants, plasticizers, stabilizers and lubricants, which can be toxic to cells. The properties of the polymer, the components involved and the shape of the scaffold required dictate the choice of processing technique for the manufacture of polymer scaffolds (Thomson *et al.* 1995).

The traditional methods for scaffold fabrication include fiber bonding, solvent casting, membrane lamination and melt molding (Thomson *et al.* 1995; Lu and Mikos 1996). Mooney *et al* demonstrated that an effective method of stabilizing PGA scaffolds was to spray solutions of PLLA/PLGA in chloroform (1-15% w/v) over a PGA mesh using a nitrogen stream to atomize the polymer solution. Since PGA is very weakly soluble in chloroform, the PGA fibres are effectively unchanged by the process (Mooney *et al.* 1996). Porosity in scaffolds is commonly formed by particulate leaching. This is achieved by evaporating chloroform from solutions of PLLA containing sodium chloride particles. These polymer films with entrapped salt particles are then leached in water to remove the particles resulting in highly porous films (Kaufmann *et al.* 1997). These same films can then also be formed into hollow

tubes (Mooney *et al.* 1995). A similar system has been used by Shoichet and co-workers where glucose crystals were dispersed within a PLGA solution in dimethyl sulfoxide (DMSO) (Holy *et al.* 1999). These methods appear to be however, most effective for only thin films or structures with thin walls.

Novel methods of manufacturing scaffolds include a prototyping technology that has been developed at MIT where a binder is expelled through a print head nozzle onto a powder bed. The scaffold is built by layers of powder and binder in a method that can create complex three-dimensional shapes. The highly toxic solvents however prevent incorporation of biological agents such as cells or growth factors during fabrication (Hutmacher 2000). Wintermantel *et al* have developed a novel method for scaffold formation using minimally invasive approaches. They introduced a thread like material and delivered it through an injection canal (e.g. cannula). A fluid stream acted as a carrier for the "lycra monfil^{TM}" based material, which was unreeled from a spool creating a porous scaffold in the form of a tangle (Wintermantel *et al.* 1996). Langer and co-workers have produced macroporous polymer foams by a hydrocarbon templating method in which a viscous polymer solution of PLA in chloroform and a particulate hydrocarbon porogen such as paraffin was compacted in a Teflon mold. The polymer/ solvent/ porogen phase was then extracted in a hydrocarbon solvent, such as hexane which is a non-solvent for the polymer but miscible with the polymer solvent. This resulted in the porogen becoming extracted and rapid precipitation of a porous polymer phase (Shastri *et al.* 2000).

Defined three-dimensional biodegradable foams have also been shaped by lamination of highly porous PLLA and PLGA membranes previously prepared by solvent casting

and salt leaching. The membranes with the appropriate shape are solvent impregnated, then stacked up in a three-dimensional assembly with continuous pore structure. Computer-assisted modelling can then help to design templates with the desired implant shape. The *in vivo* prevascularization of these laminated foams has been demonstrated by the injection of a sufficient mass of e.g. hepatocytes for liver regeneration (Mikos *et al.* 1993). Finally Mooney *et al* have demonstrated that the use of supercritical carbon dioxide (CO_2) is a promising approach in creating polymer scaffolds (Mooney *et al.* 1996). This was achieved by exposing poly α-hydroxy acids to CO_2 gas (5.5 MPa, 72 hr). The CO_2 gas pressure was decreased resulting in thermodynamic instability and the dissolved CO_2 nucleated and formed pores within the polymer matrix. As the method avoids the use of organic solvents, it is possible to then incorporate growth factors into the scaffold without loss of biological activity (Howdle *et al.* 2001).

1.3 *In situ* solidifying biomaterials

There are a number of applications in tissue engineering and drug delivery that require the development of novel biomaterials that can be transformed from liquid precursors to solids in the final form. Applications for the use of *in situ* transforming materials include cell delivery; barriers for tissue regeneration guidance; injectable temporary scaffolds for tissue regeneration; tissue adhesives for healing and injectable controlled release devices for local drug delivery (Hubbell 1996; Hubbell 1996; Hubbell 1998).

However, the most significant advantages of *in situ* transformation from liquid precursors to solids are, that large objects can be delivered via minimally invasive

surgical devices, and that implants can be made that conform to complex tissue shapes.

The ideal injectable polymer would need to satisfy the following design criteria:

1. It would polymerise *in situ* in a timely fashion without detrimental effects to the surrounding tissue such as a temperature rise.
2. It should fill defects of various shapes and sizes and have the correct mechanical and physical properties for a particular application.
3. It would maintain these mechanical properties as it degrades.
4. It must degrade into biocompatible degradation products according to a predetermined degradation profile, have a long shelf life, be sterilizable without loss of its properties, and be available to the surgeon in the sterile operating field on short notice (Hubbell 1996; Hubbell 1998; Peter *et al.* 1998).

In recent years, materials have been developed that can operate near body temperature, use non-toxic solvents, are based on macromolecular and hydrophilic precursors and do not liberate cytotoxic leaving groups as the transformation proceeds. These include materials that are converted from biologically acceptable liquid precursors into solids by photochemically initiated free radical reactions. For example, Hubbell and co-workers have copolymerised oligomers such as lactic or glycolic acid at the hydroxyl end groups of polyethylene glycol (PEG) blocks. Acrylating the resulting terminal hydroxyls resulted in the formation of a telechelic diacrylate of the ABA block copolymer of polyethylene glycol (B) and poly (lactic

acid) (A) (Han and Hubbell 1996). The water-soluble diacrylate yields a crosslinked hydrogel when polymerised. These materials have potential as mechanical barriers in controlled healing. This was demonstrated when the photopolymerisation process was used to block the deposition of blood clots on the arterial surface of an injury in animal studies, resulting in favourable wound healing (Hubbell 1996). Similarly, a method has been developed at MIT which can encapsulate chondrocytes through a photopolymerising system consisting of poly (ethylene oxide)–dimethacrylate and a polyethylene glycol semi-interpenetrating network (Elisseeff *et al.* 1997).

Photoinitiated polymerisation is also possible with more hydrophobic macromolecular precursors that yield on transformation, rigid materials that are capable of bearing mechanical loads. For example, unsaturated macromers based on polyesters formed from fumaric acid, polyethylene glycol and polypropylene fumarate which can be polymerised *in situ* to form materials that may also be useful in the repair of bone (Peter *et al.* 1997; He *et al.* 2000).

In addition to transformations based on free radical polymerisation, other groups have recently contributed new technologies for *in situ* transformation, based on alternative mechanisms of solidification. Such transformations may occur because of a change in pH or temperature, ionic crosslinking, solvent exchange or crystallisation. Block copolymers of polyethylene glycol and propylene glycol, for example, display a lower critical solution temperature and can form liquids at cold temperatures and gels at body temperatures. Kim and co-workers have developed block copolymers of poly (lactic acid) with polyethylene glycol, and these copolymers display an upper critical solution temperature, forming liquids at temperatures around 45°C and gels at body

temperature (Jeong *et al.* 1997). Another thermally triggered system that combines ionic crosslinking has been proposed by Westhaus and Messersmith. In their system, liposomes with entrapped calcium chloride were suspended in an aqueous alginate solution. When heated to 37°C, the liposomes released calcium ions into the alginate solution crosslinking it into a gel (Westhaus and Messersmith 2001). These injectable materials clearly have great potential in the development of non-invasive therapies in tissue-engineering and drug delivery.

1.4 Aims of project:

This introductory chapter has established the concept of tissue engineering. Materials used as scaffolds for tissue growth are required to have defined properties; favourable cell-polymer interactions, porosity, degradability, mechanical strength and controlled release properties. Recent advances in the field have also demonstrated novel materials that can transform *in situ* thereby providing a minimally invasive technique for delivery of polymer/polymer-cell constructs. A major obstacle with these *in situ* transforming materials, in comparison to traditional water-insoluble scaffolds is that such hydrogels lack large interconnected porous networks and, hence, the barrier of diffusion to signalling and nutrient molecules limits tissue formation. In addition, the mechanism of gelation may damage cells, hence, prohibiting co-administration of the cells.

The work presented in this thesis shows the development of an injectable material that is not only minimally invasive but also fulfils the requirements of scaffolds used in tissue engineering applications. The polymer designed for this application is degradable and capable of facile engineering to present a cell-adhesive surface. The scaffold is porous with tailorable mechanical properties and is also capable of controlled release (e.g. growth factors). The novel crosslinking process provides a highly effective method of seeding the scaffold with viable cells that are distributed throughout. Chapter 3 describes the synthesis and characterisation of the polymer that forms the foundation of the scaffold. The pore-cell interaction is then probed in Chapter 4 to gain a deeper understanding of the relationship between them. Finally in Chapter 5 and 6, the development of the injectable porous scaffold is described: from

the physico-chemical properties through to the self-assembly of three-dimensional scaffolds and the entrapment and delivery of viable cells.

CHAPTER 2

THEORY OF INSTRUMENTAL METHODS

The studies presented in this thesis have utilized a range of analytical techniques. These range from methods used to characterise the bulk and surface properties of the polymer to methods that characterise the formation of our polymer scaffold, both quantitatively and qualitatively. This chapter provides a brief theoretical background to some of the analytical techniques used. Specific experimental details are then additionally described within the materials and methods section of each of the results chapters.

2.1 Polymer characterisation:

2.1.1 Differential Scanning Calorimetry (DSC)

Differential scanning calorimetry (DSC) is a technique for studying thermal transitions in materials such as polymers (Mi and Zheng 1998). The DSC equipment has an adiabatic chamber which houses two pans, one to hold the polymer sample and the other acts as a reference pan, which is left empty. Each pan is located above a heater that applies heat to each of the pans at a specific controlled heating rate. Both heaters are electronically controlled so as to achieve the same temperature in both pans. The pan containing the sample thus has a larger heat output. The difference in the heat output of the sample heater and the reference heater at a given temperature provides the heat flow, which when divided by the heating rate results in the heat capacity of the sample. DSC can thus yield valuable thermal information on materials like biodegradable polymer. A plot of the heat flow against temperature will show shifts, for an example, at the glass transition temperature, T_g, above which polymers have a higher heat capacity. Outputted data is recorded and analysed by established software that extracts the measured data. DSC analysis requires a sample of only a few tens of milligrams in mass, and between five and six millimetres in diameter.

2.2 Quantitative measurement of scaffold formation

2.2.1 Surface Plasmon Resonance (SPR)

SPR is a technique that enables the real-time monitoring of dynamic processes, such as the interaction of biomolecules with a surface, without the need for labelling molecules. SPR can provide information regarding both the extent of biomolecular attachment to a surface and the kinetics involved with such processes. In this thesis, SPR has been employed in studies detailed in Chapters 3 and 5; to investigate the biotin-avidin mediated interaction of our self-assembling scaffold.

When light travels through a transparent medium, for example glass, the proportion of light which is reflected off the glass interface increases as the angle of incidence increases until a critical angle, θ_c, is reached after which all the light is reflected back (total internal reflection).

In SPR, a glass slide is coated on one side with a thin film of noble metal (typically silver or gold). At a specific angle greater than θ_c, the light is no longer totally internally reflected. At this angle, termed the SPR angle (θ_{spr}) the incoming light is able to couple with free oscillating electrons (plasmons) in the metal film. Coupling occurs when the wave vector of the non-propagating evanescent wave emanating from the surface equals the oscillating frequency of the surface electrons causing them to resonate i.e. a surface plasmon is resonantly excited. The transfer of energy from the incident light to the metal

film causes a reduction in the intensity of the reflected light, which can be detected.

Surface plasmons can only occur at the interface between two materials with different dielectric constants, for example a metal-water interface. The wave vector of a surface plasmon is influenced by the refractive index of the dielectric medium above the metal surface. The distance over which this technique is sensitive to refractive index changes is of the order of the wavelength of light employed. If the index immediately above the metal surface changes, for example because of biomolecules attaching to it, then a change in the angle of incidence is needed to generate resonance. Therefore, SPR can be utilized to profile the attachment of biomolecules from a bulk solution to a surface by monitoring the θ_{spr} with respect to time.

2.2.1.1 SPR Instrumentation

The SPR system (Ortho Clinical Diagnostics, Chalfont St. Giles, U.K) employed for traces obtained in Chapters 3 and 5 is shown schematically in Figure 2.1. A laser light source operating at a wavelength of 780 nm was focussed through a glass prism and onto the underside of a thin silver film (approximately 50 nm thick) supported on a glass slide (Ortho Clinical Diagnostics, Chalfont St. Giles, U.K). The glass slide was optically coupled to the prism using immersion oil (Stephens Scientific, Riverdale, New Jersey, U.S.A.). In Chapters 3 and 5, the silver films were modified, to present biotin surfaces.

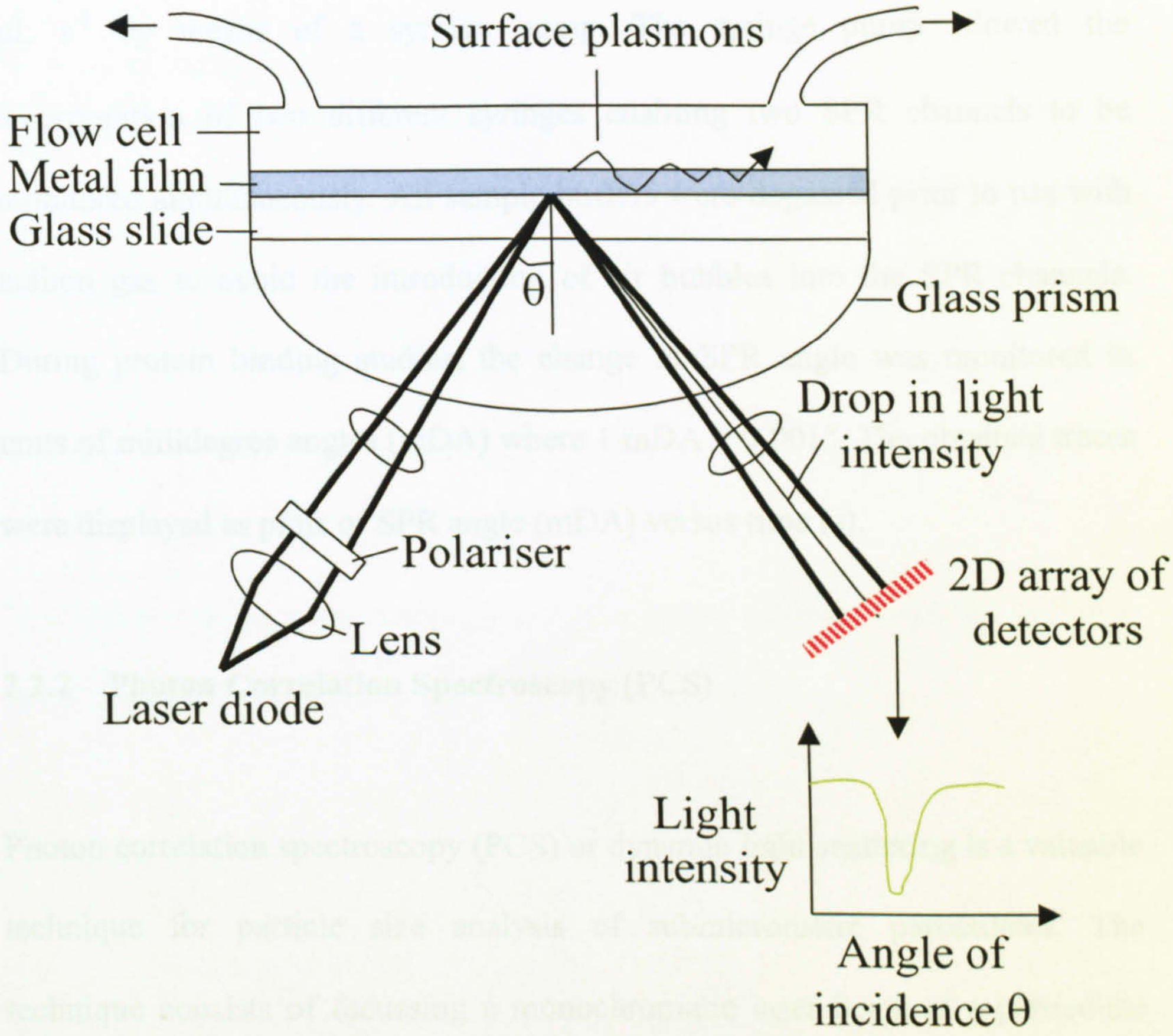

Figure 2.1 Schematic of SPR adapted from (Green *et al.* 1997; Green *et al.* 1999)

The reflected light was focussed onto an array of charge-coupled detectors and their data output processed within the SPR software. The flow of liquid across the silver surface was confined to three isolated flow channels within a thermoregulated copper block (equilibrated at 34°C). Sample solutions of 1 ml were introduced through a loop valve system to the flow channels at a rate of 4 $\mu L\ s^{-1}$ by means of a syringe pump. The syringe pump allowed the incorporation of two different syringes enabling two SPR channels to be monitored simultaneously. All sample buffers were degassed prior to use with helium gas to avoid the introduction of air bubbles into the SPR channels. During protein binding studies, the change in SPR angle was monitored in units of millidegree angles (mDA) where 1 mDA = 0.001°. The obtained traces were displayed as plots of SPR angle (mDA) versus time (s).

2.2.2 Photon Correlation Spectroscopy (PCS)

Photon correlation spectroscopy (PCS) or dynamic light scattering is a valuable technique for particle size analysis of submicrometre particulates. The technique consists of focussing a monochromatic laser beam at a particulate dispersion and analysing the statistical intensity fluctuations of the scattered light. These fluctuations are due to the random Brownian motion of the particles, the rate of which is inversely proportional to the particle size at constant temperature.

Experimentally, a photo multiplier is used to detect the scattered light at 90°C to the incident beam and the average scattered intensity is correlated as a

function of the correlation time τ_c. the derived intensity decay or autocorrelation function $G(\tau_c)$ is directly related to the diffusion coefficient of the particles, C_D:

$$G(\tau_c) = 1 + \exp(-2C_D Q^2 \tau_c)$$

Q is the scattering vector given by:

$$Q = (4\pi/\lambda)\sin(\theta/2)$$

Where λ is the wavelength of the incident light and θ is the scattering angle.

The hydrodynamic diameter, D_{hyd}, is then obtained directly from the diffusion coefficient by means of the Stokes-Einstein equation:

$$C_D = kT/3\pi\eta D_{hyd}$$

Where k is the Boltzmann constant, T is the absolute temperature and η the solvent viscosity.

For polydisperse systems, the autocorrelation function consists of a sum of exponentials. The simplest treatment of such systems to provide the average particle size and the polydispersity index of the distribution is cumulant analysis. This method assumes that the distribution of exponentials is unimodal, and so the mean size is described by the "best fit average"

exponential. The log of the normalised correlation function is fitted to a polynomial of the following form:

$$\mathrm{Log_e}(G(\tau_c)) = K_0 - K_1\tau_c + \tfrac{1}{2} K2\tau_c^2 \ldots\ldots\ldots$$

Where K_0, K_1, K_2..... are the coefficients of the cumulants fit determined by a simple least squares fitting procedure. K_1 describes the average diffusion coefficient, C_D:

$$K_1 = 2Q^2C_D$$

This yields the average *hydrodynamic particle diameter*, D_{hyd}

2.2.2.1 PCS instrumentation

The PCS equipment used was a Malvern 4700 series instrument (Malvern Instruments, Malvern, U.K.) with vertically polarised light supplied by an argon-ion laser (Cyonics, San Jose, U.S.A.) operated at 20 mW. The nanoparticle dispersions were diluted using filtered, deionised water to achieve a suitable scattering intensity. Six 30 second measurements of each sample were made at a temperature of 25.0 ± 0.1°C and at a measuring angle of 90°C to the incident beam. The correlation decay functions were analysed by the cumulants method to determine the average particle diameter and polydispersity index. The values presented are the mean of two replicate samples together with the standard deviation.

2.2.3 Coulter LS230

Aggregate structure has been known to be of great importance in solid-liquid separation processes such as sedimentation and influences the strength of the aggregates. Particle characterization by light-scattering techniques has the advantage of allowing estimation of a wide range of particle size in a rapid and non-destructive manner. (Selomulya *et al.* 2001)

The evolution of size of the aggregates was monitored using a particle size analyser (Coulter LS230). The instrument applies the principle of forward light scattering by particles to measure the particle size distributions. The size distributions were estimated by fitting the intensity of the scattered light (λ = 750 nm) as a function of the scattering angle (θ = 0.017-34°C). They were then compared by the instrument to the scattering patterns of spherical particles of the same size calculated by the Mie model of light scattering by particles with significant differences only if particles are very non-spherical.

2.2.4 Sedimentation

Sedimentation ranks as one of the oldest methods of particle size measurement and is capable of providing accurate results with good size resolution. Although a very large number of measurement methods have been based on sedimentation, most vary only in the method used to study the gradual separation of the particles, and the fundamental physics of the system – the settling of particles in a gravitational field is identical to all.

A remote system of estimating the amount of material in suspension at a particular point would be an effective method of monitoring sedimentation. An ideal technique would be to use a light beam passing through the suspension, and estimate the particle concentration from the attenuation of the light beam. This can be achieved by UV-Vis spectroscopy, which measures the attenuation of a beam of light after it passes through a sample. Absorption measurements can be at a single wavelength or over a range of spectrum. The particle concentration can be obtained from the absorption by assuming that the particles cause a loss of light from the beam which is proportional to their cross-sectional area. Particles of diameter d will obscure an area, which is proportional to the square of their diameter; the obscured area a_d is written as:

$$a_d = k_d d^2$$

where k_d is a constant dependent on the shape of the particles (e.g. it is $\pi/4$ for spherical particles).

2.2.5 Rheological determination of mechanical properties

2.2.5.1 Principles of dynamic (oscillatory) rheological measurements

In oscillatory rheological measurements, a small amplitude sinusoidal strain with frequency ω (rad s^{-1}) is applied to the system, and the sinusoidal stress that is generated is measured simultaneously.

This is illustrated schematically for a viscoelastic system in Figure 2.2, which shows the stress response to a sinusoidal strain of amplitude γ_0. The amplitude of the stress is τ_0 and it oscillates with the same frequency, but out of phase. The phase angle shift between the two is given by:

$$\theta_p = \Delta t.\omega$$

where Δt is the time shift between the two waves. If a sinusoidal strain wave were applied to a perfectly elastic solid (Hookean solid), the resultant stress wave would be completely in phase with the strain ($\theta=0^0$). In contrast, for a purely viscous liquid (Newtonian liquid) the stress would be exactly 90° out of phase with the strain (maximum stress corresponding to maximum strain rate). The behaviour of a viscoelastic material lies somewhere in between these two extremes and the phase shift ($0^0 < \theta < 90°$) depends on the relative amounts of elastic and viscous behaviour at the frequency of oscillation.

In oscillatory shear, the complex shear modulus G^*, describes the relationship between the stress and strain. G^* is vectorially resolved into two components; the elastic or storage modulus, G' (the real part of the complex modulus) and the viscous or loss modulus, G'' (the imaginary part of the complex modulus):

$$G^* = G' + iG''$$

From the stress and strain amplitudes (τ_0 and γ_0 respectively) and the phase angle shift, θ, it is possible to determine all three moduli as follows:

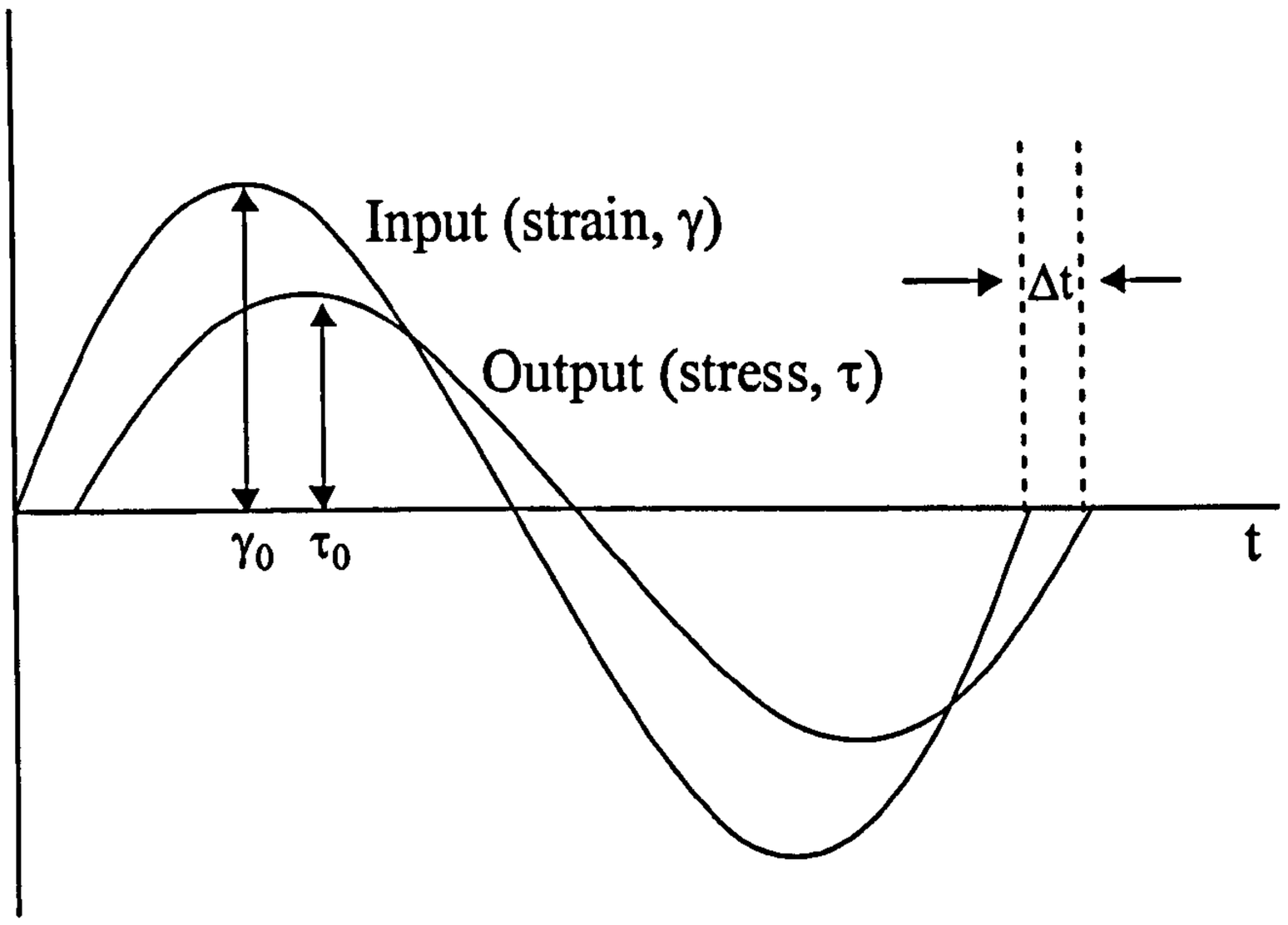

Figure 2.2 The relationship between harmonic shear strain (γ) and harmonic shear stress (τ) for a viscoelastic material adapted from Bohlin software.

$$|G^*| = \tau_0 / \gamma_0$$

$$G' = |G^*| \cos \theta$$

$$G'' = |G^*| \sin \theta$$

G' is a measure of the energy stored elastically by the system, whereas G'' is a measure of the energy dissipated as viscous flow.

2.2.5.2 Rheological measurements

Dynamic (oscillatory) measurements were performed using a Bohlin rheometer interfaced with an IBM computer. This instrument operates in the frequency range 10^{-3}-20 Hz and it has interchangeable torsion bars covering a wide range of sensitivities. In this work, measurements were made using a frequency range of 0.01 - 5 Hz at 37 ± 0.1°C. A cone and plate method using a 40mm diameter cone with a 4° cone was employed in these studies. A solvent trap was fitted to prevent sample skinning or drying. Each sample was allowed to rest for 10 minutes before making the rheological measurements. Initially the frequency was kept constant at 1 Hz and the strain amplitude increased stepwise (*strain sweep*), whilst measuring the rheological parameters G^*, G' and G''. This enables the linear viscoelastic region to be defined, where G^*, G' and G'' are independent of the strain amplitude at the given frequency. Measurements were

then made in the linear viscoelastic region as a function of frequency, at a fixed strain amplitude (*frequency sweep*).

The measuring system in the instrument used a series of form factors to calculate shear stress and shear strain. Shear stress was equal to C1 multiplied by the torque, whilst shear rate was equal to C2 multiplied by the angular velocity. In the cone and plate method employed, C1 was 1/(2/3 x r3) and C2 was 1/θ where r was the radius of the cone and θ was the cone angle in radians. The viscosity was then calculated by dividing shear stress by shear rate.

2.3 Qualitative assessment of scaffold formation

2.3.1 Confocal Microscopy

Confocal microscopy is a technique used to gain high resolution views of thick specimens by rejection of out of focus scattering (Tjia and Moghe 1998)(Figure 2.3). This is achieved by an arrangement of diaphragms, which, at optically conjugated points of the path of the rays, act as a point source and as a point detector respectively. Rays that are out of focus are suppressed by the detection pinhole. The depth of the focal plane is, besides the wavelength of light, determined in particular by the numerical aperture of the objective used and the diameter of the diaphragm. At a wider detection pinhole, the confocal effect can be reduced. To obtain a full image, the image point is moved across the specimen by mirror scanners.

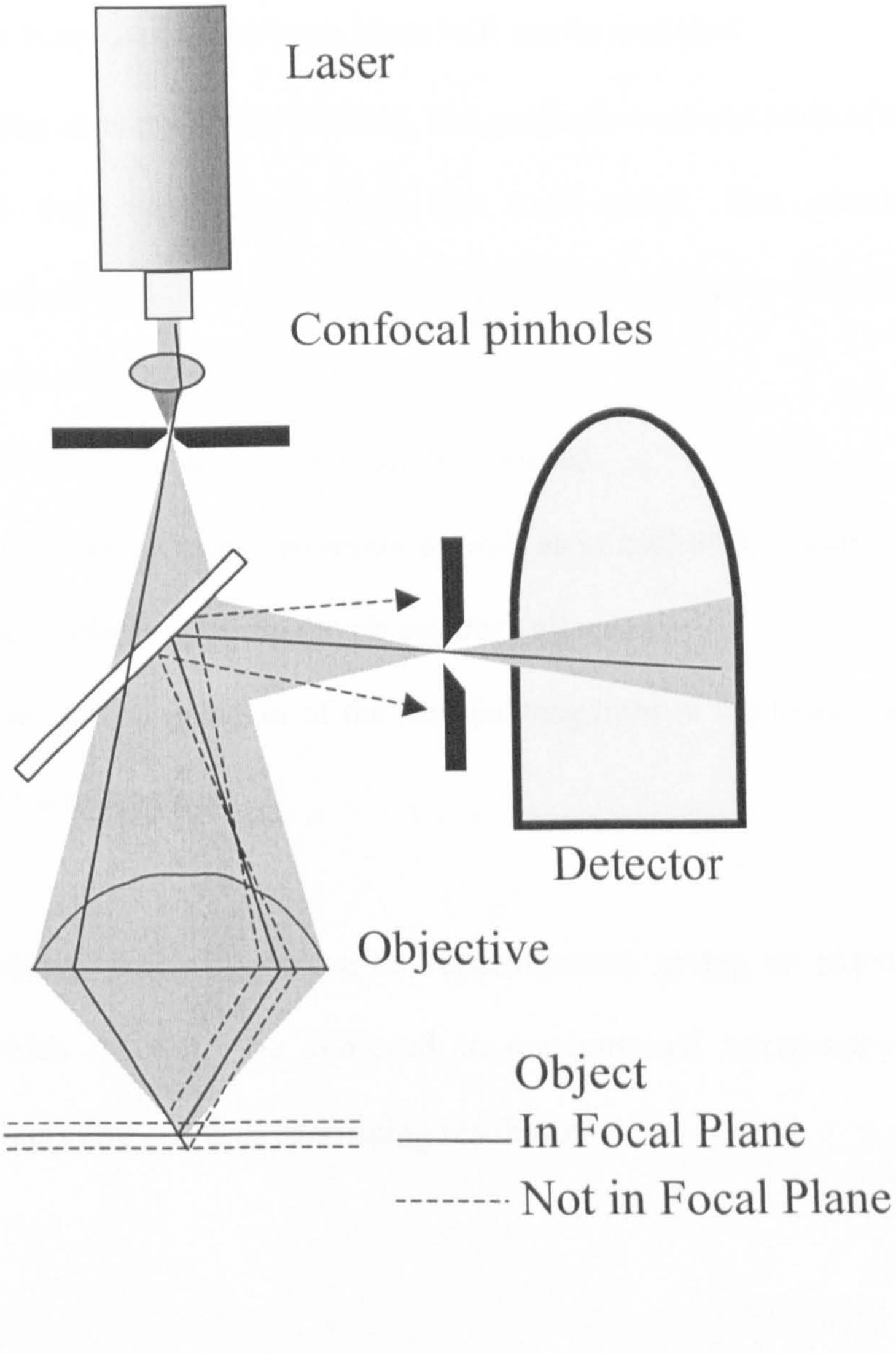

Figure 2.3 Schematic of Confocal microscope adapted from Leica website.

The emitted/reflected light passing through the detector pinhole is transformed into electrical signals by a photomultiplier and displayed on a computer monitor screen. Major improvements offered by a confocal microscope over the performance of a conventional microscope are:

1. Light rays from outside the focal plane will not be recorded.
2. Defocussing does not create blurring, but gradually cuts out parts of the object as they move away from the focal plane. The practical consequence is that these parts become darker and eventually disappear. This feature is called optical sectioning.
3. True three-dimensional data sets can be recorded.
4. Scanning the object in x/y-direction as well as in z-direction (along the optical axis) allows viewing the object from all sides.
5. Due to the small dimension of the illuminating light in the focal plane, stray light is minimized.

By image processing, many slices can be superimposed, giving an extended focus image which can only be achieved in conventional microscopy by reduction of the aperture and thus sacrificing resolution.

CHAPTER 3

SYNTHESIS AND CHARACTERISATION OF A DEGRADABLE POLY (LACTIC ACID) – POLY (ETHYLENE GLYCOL) COPOLYMER WITH BIOTINYLATED END GROUPS.

3.1 Introduction

The criteria for the use of synthetic polymeric biomaterials as scaffolds in tissue engineering have been established in Chapter 1. The ability to develop materials that are capable of being processed into porous degradable scaffolds that mimic cellular recognition is a desirable strategy in tissue engineering. Similarly, materials that are capable of *in situ* transformations have great potential in facilitating minimally invasive therapies. In Chapter 3, we describe the synthesis of a polymer that can be processed into a scaffold that can comply with the requirements of both traditional water-insoluble porous scaffolds and injectable biomaterials. This material thus forms the foundation of our injectable self-assembling scaffold.

3.1.1 The biotin-avidin interaction in biomedical applications

The binding of biotin and avidin is an established interaction in biomedical applications. Although many other ligand-binder interactions are described in the literature, the biotin-avidin or, biotin-streptavidin interaction has some unique characteristics that make it ideal as a general bridge system in a diverse range of uses (González *et al.* 1997). For an example, changes in pH and repeated washings do not break the non-covalent interaction of the biotin and avidin bridge because its binding constant is 10^{-15} M^{-1}, which is one of the strongest known biological interactions. The binding process is specific, ensuring it is the target molecule that is bound. Because biotin is a small molecule of 244.31 Daltons in size, conjugation of biotin with macromolecules can be achieved without significantly affecting their targeting ability (Diamandis and Christopoulos 1991; Lindqvist and Schneider 1996; González *et al.* 1997).

Table 3.1 lists the potential biomedical applications that use the biotin-avidin interaction. These include drug targeting, immunological assays, nucleic acid hybridisation assays, flow cytometry, electron microscopy, affinity chromatography, surface modification and attachment of biotin to membranes of cells. Avidin is also often used as a model for predicting protein interaction behaviour (Kaasgaard *et al.* 2001).

Applications	Biotinylated moieties	Avidin conjugate
Immunological assays, flow cytometry, cell sorting, immunohistochemistry, western blots, nucleic acid hybridisation	Enzymes (ALP, β-galactosidase, glucose oxidase, HRP), anti-immunoglobulins	Enzymes (ALP, β-galactosidase, glucose oxidase, HRP) flourophores (flourescien, coumarins, rhodamines, phycoerythrin, Texas Red), Eu^{3+}-chelates, polystyrene, chemiluminescent labels
Glyconjugate studies, mitogenic stimulations studies	Lectins	
Localization of lectin receptors	Anti-Lectins	
Electron Microscopy	Ferritin, hemocyanin	Ferritin, gold
Affinity Chromatography	Agarose, cellulose, hormones, liposomes, latex particles	Agarose
Amplification assays, receptor-ligand interaction studies	Anti-avidin, anti-streptavidin	
Nucelic acid hybridisation, molecular mass marker, DNA sequencing	Nucleotides, DNA	Magnetic particles
Hybridoma production	Cells	

Table 3.1 Applications of the biotin-avidin interactions: (Green 1965; Leary *et al.* 1983; Diamandis and Christopoulos 1991; Chern *et al.* 1996; Lindqvist and Schneider 1996; Lynch *et al.* 1996; González *et al.* 1997; Kaiser *et al.* 1997; Mahal *et al.* 1997)

Immobilized avidin/streptavidin can be used to purify and characterize various moieties of interest. For example, magnetic particles conjugated with avidin have been used to retrieve biotinylated DNA. Solid substrates used in this manner also purify DNA binding substances or separate cells tagged with biotinylated antibodies. Biotin modified submicron latex particles have been used to separate mixtures of avidin and lysozyme effectively (Chern *et al.* 1996). The avidin was subsequently recovered from the particles by using 8M pH 1.5 guanidine-HCL solutions or autoclaving. Lynch *et al* have carried out comprehensive studies on the aggregation kinetics of biotinylated liposomes for affinity purification (Lynch *et al.* 1996; Lynch *et al.* 1996).

Drug delivery applications for the biotin-avidin interaction include HIV and cancer treatment. For example, the potential of combining the avidin-biotin system with nanoparticle technology has recently been demonstrated in carrier systems with biotinylated drug derivatives for antisense therapy for HIV infections (Coester *et al.* 2000). Furthermore, whilst effective radioimmunotherapy in cancer therapy is limited by slow antibody clearance from the circulation, which results in low tumour to blood ratios and restricts the dose of radiolabelled anti-tumour antibody that can be safely administered. Avidin and streptavidin clearing agents have been shown to effectively complex and clear radioactive biotinylated antibodies from the circulation via the reticuloendothelial system (Marshall and Pedley 1996). Whilst immunogenicity of avidin limits its use in such applications, PEG modification of avidin has been shown to reduce the immune response.

Conjugation of biotin to polymers, proteins and sugars can be carried out in a number of ways. Table 3.2 lists a selection of the available biotin labelling strategies for polymers, proteins and carbohydrates. Other methods of avidin binding include direct conjugation of the polymer to avidin. For an example, Stayton and co-workers have developed a series of polymer-streptavidin complexes. This was achieved by reacting an S-H group from cysteine on the streptavidin with derivatized vinyl sulfone groups on the copolymer. One example is a poly (N-isopropylacrylamide)-streptavidin conjugate that displays temperature dependent binding of biotin. The polymer binds biotin at room temperature and releases it at 37°C. They have also produced a pH-sensitive copolymer of NIPAAm and acrylic acid and conjugated this copolymer to streptavidin. Lowering the pH caused the polymer to collapse blocking biotin binding. Raising the pH caused the polymer to fully hydrate allowing biotin to bind. Furthermore, poly (2-propylacrylic acid)-streptavidin complexes have been shown to have pH dependent haemolytic properties capable of disrupting membranes of red blood cells (Stayton *et al.* 1995; Ding *et al.* 1999; Lackey *et al.* 1999).

3.1.2 Poly (lactic acid)-polyethylene glycol-biotin (PLA-PEG-biotin)

Poly (lactic acid)-polyethylene glycol-biotin (PLA-PEG-biotin) is a degradable polymer with protein resistant properties and a universal linkage system that allows both self-assembly of the polymer and that can undergo rapid surface engineering in aqueous media to create biomimetic surfaces (Figure 3.1) (Cannizzaro *et al.* 1998).

Moiety for biotinylation	Reactive group on moiety	Biotinylation reagent	Conditions	Ref
Poly (ethylene glycol)	Functionalised NH_2 group	NHS-biotin	DMF/ET_3N for 24hr at room temp.	(Kaiser *et al.* 1997)
Proteins	Amine	N-hydroxy-succinimide ester of biotin (NHS-biotin)	Alkaline (pH 9.1) bicarbonate solution.	(Diamandis and Christopoulos 1991)
	sulfhydryl	Iodoacetyl-LC-biotin		
	Tyrosyl, hystidyl	*p*-diazobenzoylbiocytin		
	Carboxyl groups	Biotin hydrazide	A water soluble carbodiimide reaction	
Poly vinylpyrrolidone	Radical inititated polymerisation of N-vinyl pyrrolidone	Derivatized azonitrile initiator with biotin	Solution polymerisation in dimethylformamide	(Ganachaud *et al.* 1995)
Glycoproteins	Sugar moities	Biotin-LC-hydrazide	Oxidising vicinal hydroxyl groups into aldehydes using $NaIO_4$. Reaction found to be inferior to biotin-NHS	(Diamandis and Christopoulos 1991)
Poly (pyrrole-biotin)	Pyrrole ammonium derivative	Pyrrole modified biotin	Electro-copolymerisation of Pyrrole ammonium derivative with pyrrole modified biotin by controlled potential electrolysis	(Cosnier and Lepellec 1999)

Table 3.2 Biotin labelling strategies for polymers, proteins and carbohydrates

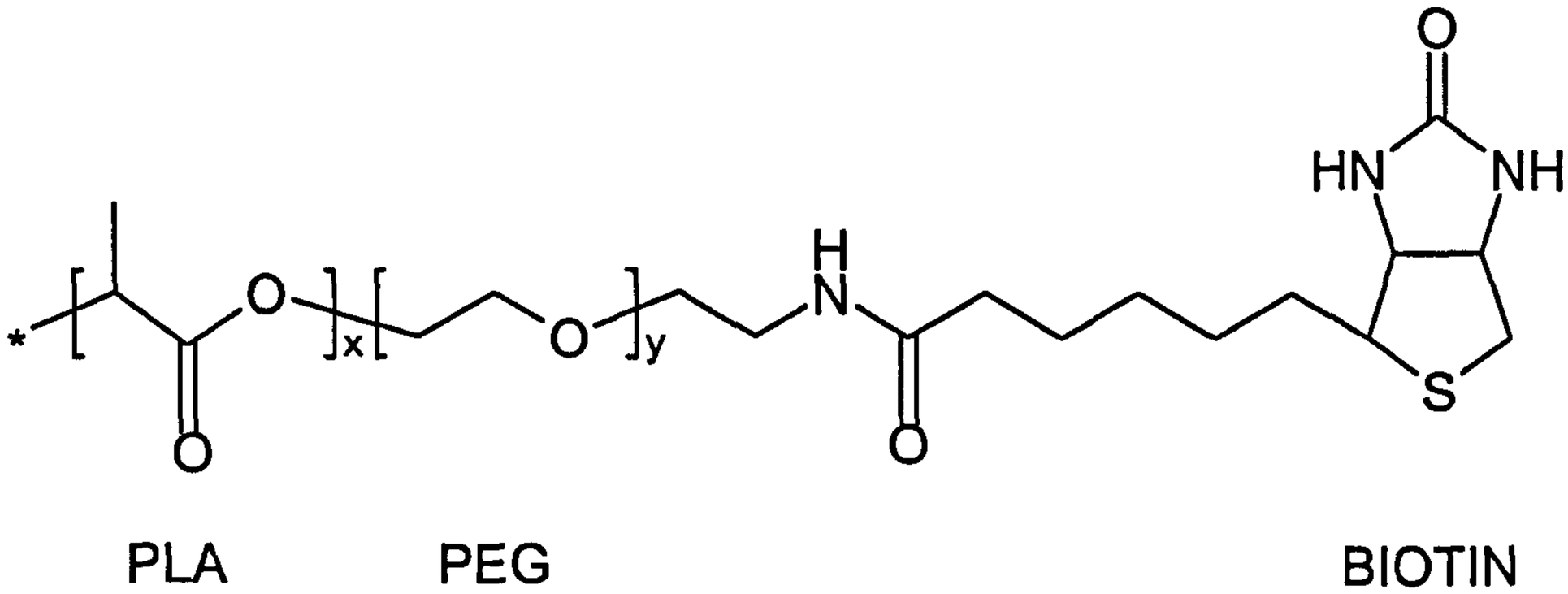

Figure 3.1 Structure of PLA-PEG-biotin

Surface engineering and self-assembly of this polymer is dependent on biomolecular interactions between the biotin end group and the protein avidin. PLA-PEG copolymers and their use as an effective biomaterial in drug delivery and tissue engineering has been discussed in Chapter 1. PLA is the backbone of the polymer and provides structural integrity to any scaffold (Agrawal *et al.* 1997; Hench *et al.* 1998; Lu *et al.* 1996; Han *et al.* 1996). Polyethylene glycol (PEG) has long been considered an attractive biomaterial because of its ability to resist protein adsorption (Holmberg *et al.* 1997; Deible *et al.* 1998; Holmberg *et al.* 1997 ; Park *et al.* 1998; Park *et al.* 1999). In PLA-PEG-biotin, PEG acts as a spacer group for the biotin thus improving biotin-binding capabilities by reducing steric hindrance. To utilise biotin in this manner, it is covalently linked to the PEG. Although traditionally covalently linked biotin derivatives showed greatly reduced affinities for avidin due to steric hindrance. High affinity and metastability of avidin-biotin interaction could be restored when 7-27 atom spacers were introduced between the biotin and the peptides. These spacers, however, were not effective against other steric hindrances created because the four-biotin binding sites on avidin are organised in two pairs on opposite sides of the receptor protein. Steric repulsion between adjacent biotinylated derivatives, thus allows the exploitation of only one site per pair in practice (Green 1965). The use of PEG spacers, however, optimises the biotin–avidin interaction when compared to that of avidin and *d*-biotin because the flexibility of the PEG chains further reduces the interaction of the individual components and decreases non-specific binding (Kaiser *et al.* 1997). Each biotin moiety on the PLA-PEG-biotin attaches to one of the four biotin binding sites on the tetrameric protein avidin leaving available binding pockets

for any biotinylated peptide sequences or ligands (Green *et al.* 1965; Lindqvist *et al.* 1996; González *et al,* 1997; Weisenhorn *et al.* 1992; Hendrickson *et al.* 1989; Diamandis *et al.* 1991).

Finally, when compared to the conditions used in covalent coupling strategies, avidin-based surface engineering of PLA-PEG-biotin has the advantage of being rapidly completed in a mild aqueous environment, with simple washing and purification steps (Figure 3.2). It therefore may eliminate the potential of damage to ligands. In addition, any motif that can be biotinylated can be presented at the surface of PLA-PEG-biotin based biomaterials, and precise control over the density of surfaces composed of mixtures of motifs can be achieved. PLA-PEG-biotin has been shown to have favourable responses from endothelial cells when presenting RGD sequences to the surface using this technique (Cannizzaro *et al.* 1998). This therefore has the potential to be a valuable system for the manufacture of tissue engineering scaffolds or matrices. The four biotin binding sites in avidin also combines a potentially effective method of self-assembling with the advantageous properties of the PLA-PEG based systems.

An important factor in the design of new biomaterials is reproducibility in terms of chemical, physical and biological properties. PLA-PEG-biotin can be synthesised in two steps: Biotin attachment to bi-functional PEG followed by PLA attachment to PEG-Biotin by ring-opening polymerisation of the lactide. The polymerisation is possible using two methods; solution polymerisation or melt polymerisation.

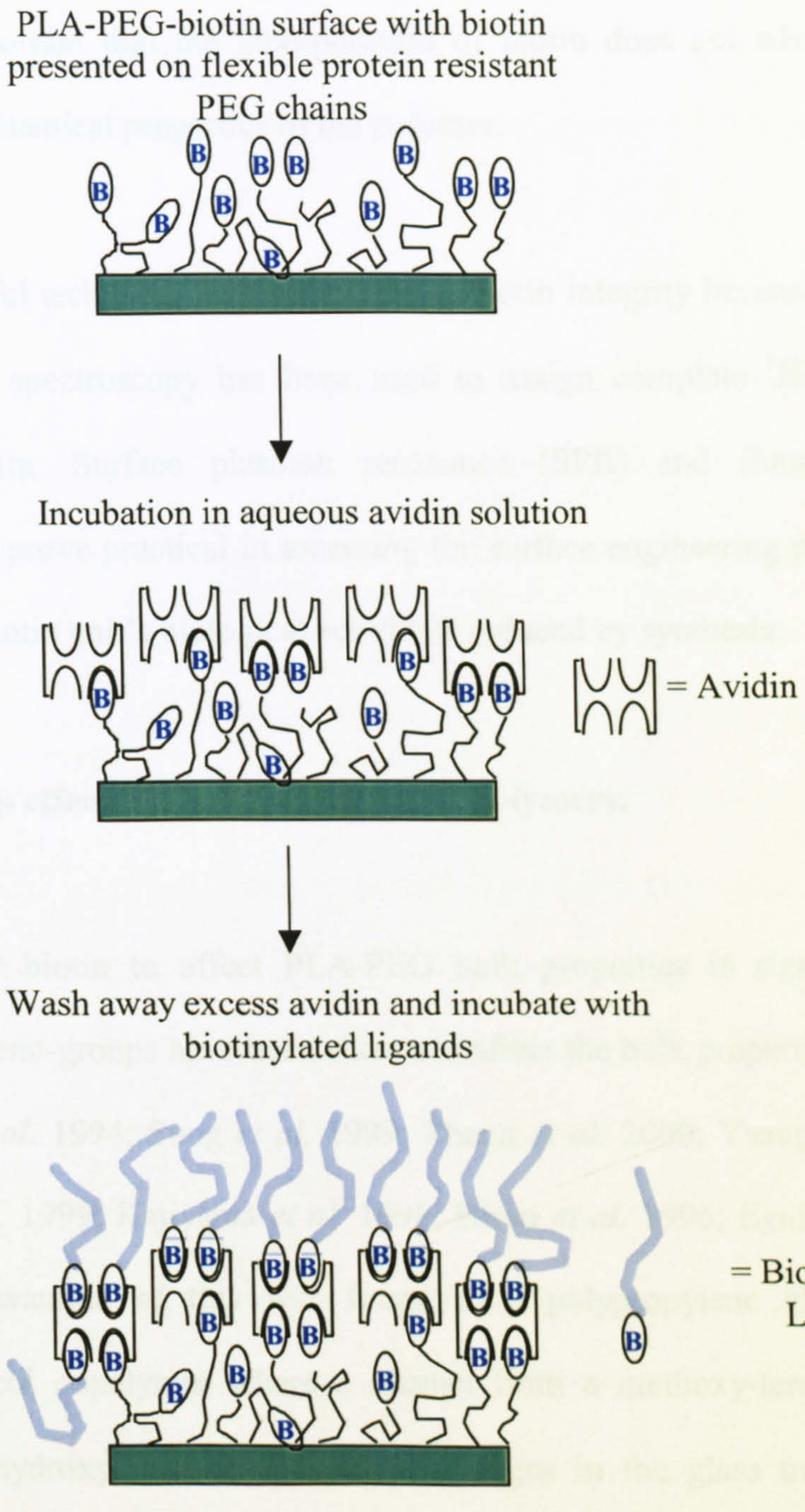

Figure 3.2 Schematic of surface engineering approach of PLA-PEG-biotin adapted from (Patel *et al.* 1998)

Given the vigorous conditions of synthesis, it is essential that the manufacture of the polymer does not alter the biotin structure or its molecular recognition. Equally, it is important that the incorporation of biotin does not adversely affect the physicochemical properties of the polymer.

^{1}H-NMR is a useful technique for characterising biotin integrity because two-dimensional (2D) spectroscopy has been used to assign complete ^{1}H-NMR spectra of *d*-biotin. Surface plasmon resonance (SPR) and fluorescent spectroscopy then prove practical in assessing the surface engineering process and whether the biotin unit's biological activity is reduced by synthesis.

3.1.3 End-group effects on bulk properties of polymers.

The potential for biotin to affect PLA-PEG bulk properties is significant because polymer end-groups have been shown to affect the bulk properties of a polymer (Kim *et al.* 1994; Sung *et al.* 1999; Zhang *et al.* 2000; Yasugi *et al.* 1999; Tracy *et al.* 1999; Kajiyama *et al.* 1998; Hirao *et al.* 1996; Eguiburu *et al.* 1995). An example of this was found in a polypropylene glycol – polyethylene glycol copolymer where a change from a methoxy-terminated end-group to a hydroxyl end-group lead to changes in the glass transition temperature ranging from 12°C to 20°C. This was attributed to interactions with the hydroxyl end-group and the ether oxygens on the backbone of the polymer and end-to-end hydrogen-bonding interactions (Yoon *et al.* 1997). Further examples of changes in thermal properties because of end-group hydrogen bonding have been seen with poly (ethyl ethylene-*b*-ethylene

oxide)(PEE-PEO) diblock copolymers with pyridine-benzoic acid end groups, which displayed heterodimeric hydrogen bonding. Whilst short blocks of PEO did not crystallise out, the binding of the end groups produced PEO blocks long enough to be detected by differential scanning calorimetry (DSC) (Zhang and Moore 2000).

The potential for an end-group to change the glass transition temperature is important because too low a Tg can produce a material that is too sticky to handle and too high a Tg can produce a material that is not easily processed. It is therefore important to reproducibly synthesize a material with a suitable Tg. For an example, it has been shown that the Tg has a significant effect on relaxation behaviour of PDLLA tablets (Steendam *et al.* 2001). The Tg is also important because it is directly related to the degradation properties of the polymer. This was illustrated by Li *et al* who have shown that as PLA degrades, the Tg changed from 46.4°C initially, decreasing to 29.2°C after 21 days (Li and McCarthy 1999)

Varying the end group of the polymer itself can also alter polymer degradation rates. For example autocatalytic degradation due to carboxylic acid groups, may be slowed by blocking the end groups. (RothenWeinhold *et al.* 1997) Microparticles made of PLGA with free carboxyl groups at the polymer terminus were compared with microparticles with capped PLGA, which had ester linkages at the polymer terminus resulting in a more hydrophobic alkyl end. Comparing the capped polymer to the uncapped PLG (similar molecular weight but different end-group) showed that the uncapped end-group polymer

degraded 2-3 fold faster *in vitro* and 3-4 times faster *in vivo* than the capped polymer. The uncapped PLGA degraded faster than the capped in part because it took up water at a faster rate than the capped polymer (Tracy *et al.* 1999).

Given that the biotin interaction with avidin involves establishing 36 hydrogen bonds (excluding water molecules) and the presence of both ether and ester oxygens along the backbone of the polymer, it is feasible that biotin as an end-group could influence the bulk properties of PLA-PEG in a similar manner (Rosano *et al.* 1999). Therefore we also undertook a systematic study to assess the impact of the biotin end-group on the PLA-PEG.

3.2 Experimental Section

3.2.1 Materials

α-hydroxy-ω-amine PEG (Mw 3,400) and methoxy-terminated PEG (Mw 3,000) were purchased from Shearwater Polymers. DL-lactide was purchased from Purac and stored at 0°C under nitrogen. N-hydroxy succinimide (NHS) biotin was purchased from Pierce & Warriner. Stannous II octanoate [$Sn(Oct)_2$] and all solvents were purchased from Sigma/Aldrich (Poole, UK). Stannous II octanoate was stored under vacuum and used as received following a nitrogen purge and ^1H NMR checks for impurities.

3.2.2 Synthesis of PLA-PEG-biotin

Synthesis of Biotin-PEG-OH

α-hydroxy-ω-amine PEG (1g) was dissolved into acetonitrile (2ml). Methylene chloride (1ml) & Et_3N (80μl) were added and the mixture then stirred for 1 minute. After addition of NHS-Biotin (0.250g), the reactants were stirred overnight under argon. The reaction was worked-up by the slow addition of diethyl ether (40ml) to precipitate the polymer, which were then filtered on a Buchner funnel and washed with diethyl ether. The isolated material was then dissolved in hot isopropanol (70°C) to give an opaque-cloudy solution. The polymer was reprecipitated on cooling; this product was then analysed for biotin attachment by ^1H-NMR spectroscopy.

Removing water impurities and aqueous impurities from Biotin-PEG-OH

The polymer (350 mg) was dissolved into toluene (70ml) and refluxed with a Dean-Stark trap and a condenser. 70% of the toluene was removed by distillation. The polymer was isolated on a rotary evaporator. To remove residual solvent, the polymer was dried under vacuum (Edwards RV8) for 2 days.

Preparation of PLA-PEG-biotin

The graft polymerisation of lactide on Biotin-PEG-OH by solution polymerisation.

Glassware was silanized by rinsing with a 5% methyltrichlorosilane solution in toluene; rinsed with acetone and left overnight to dry at 130°C. A 50ml round-bottom flask was charged with Biotin-PEG-OH (0.35g). Lactide (2g) was transferred into the round-bottom flask, diluted with 10ml toluene, and the round-bottom flask capped and placed in the dessicator. The round-bottom flask was then taken out of the dessicator and heated to 60°C until the contents went into solution. $Sn(Oct)_2$/toluene (0.1g in 1ml) was then added and the reaction was then brought to reflux at 110°C for 4 hours under argon. Following this, the reaction vessel was equipped with a Dean-Stark trap and any remaining solvent was removed by vacuum rotary evaporator. The remaining viscous material was heated to 140°C; a melt, which was left for one

hour under argon. The reaction mixture was allowed to cool after which it was dissolved in approximately 10ml dichloromethane. This polymer solution was then added drop-wise to a cold stirring solution of 100ml diethyl ether. The final product was isolated by vacuum filtration and lyophilised overnight. Approximately 2.0g of white powder was isolated.

The graft polymerisation of lactide on Biotin-PEG-OH by melt polymerisation

This method was as described for the solution polymerisation with the exception that the contents were not diluted with toluene. The round-bottom flask with lactide (2g) and Biotin-PEG-OH (0.35g) was sealed under argon and heated at 140°C for 16 hours before being reprecipitated as previously described.

3.2.3 Preparation of PLA-PEG by melt and solution polymerisation

Synthesis as described for PLA-PEG-biotin substituting Biotin-PEG-OH with Me-PEG-OH. Synthesis of low-content lactide PLA-PEG-biotin by melt and solution polymerisation were completed as described for PLA-PEG-biotin using 0.2g lactide.

3.3 Instrumentation Methods

3.3.1 Nuclear magnetic resonance spectroscopy (NMR)

Proton ^1H NMR spectra were recorded on a Bruker ARX-250 spectrometer at 250MHz. ^1H-NMR chemical shifts were measured in parts per million (ppm) relative to $CHCl_3$ in $CDCl_3$ and DMSO in DMSO-d_6.

3.3.2 Gel permeation chromatography (GPC)

GPC studies were conducted using degassed chloroform as the eluent with a sample concentration of 0.2% w/v, an injection volume of 100µl, columns consisting of 2xPlgel 5 µm (300x7.5mm), a flow rate: 1.0 ml/min. Studies were carried out at ambient temperature and a pressure of 70 bar. The detector used DRI and polystyrene (Easical PS-2) was used to calibrate the system.

3.3.3 Differential scanning calorimetry (DSC)

DSC thermograms were recorded with a Perkin Elmer CCA7 analyser and a Perkin Elmer TAC 7/DX. The heating rate was 10°C a minute with a quenching rate of 200°C a minute. Values of glass transition temperatures (Tg) were taken from the midpoint of the transition region.

3.3.4 Surface plasmon resonance (SPR)

The SPR equipment (Ortho Clinical Diagnostics, Chalfont, St-Giles, UK) employs a Kretschmann configuration with a monochromatic laser source of 780nm wavelength. The glass slides used had a 50nm silver layer on one side. These were coated with samples from a 3mg/mL chloroform solution spun-cast with 100μL at 2000 rpm. This resulted in films that gave time-dependent SPR angle (θ_{SPR})(in millidegrees mDA) which is the angle at which the minimum in light intensity occurs. Avidin (Sigma, Poole, UK) was made up to 5×10^{-7} M in dibasic phosphate buffer (10 mM, pH 7.4), which also acted as the medium for washing. The flow rate was 0.24 mL/min and binding of avidin was determined over 1000 second time periods. Injection of the avidin solution took place approximately 100 seconds after the start of each run. Results were taken from at least 8 repeats

3.3.5 Fluorescent spectroscopy studies using the [2-4'-hydroxyazobenzene benzoic acid] (HABA)/avidin reagent.

Spectroscopy studies were completed on a Beckman DU-600 spectrometer at a fixed wavelength of 500 nm at 37°C. The average read time was 0.5 seconds and the read mode [Abs]. Three blanks were read followed by three readings of the HABA/avidin in 1ml cuvettes. Each polymer sample was recorded 3 times over a subset of 4 repeats. The assay was completed by measuring the absorbance of the avidin-HABA complex at A_{500} before and after it has been placed over a film of PLA-PEG-biotin of known surface area. The absorption

decreases proportionately to the biotin present on the surface because biotin displaces HABA due to its higher affinity for avidin. The change in absorbance can then be used to calculate the amount of biotin present (Green *et al.* 1965).

3.4 Results and Discussion

The attachment of biotin to H_2N-PEG-OH was achieved through N-hydroxy-succinimide chemistry (Figure 3.3). The graft polymerisation of lactide to the HO-PEG-biotin proceeds through a ring-opening polymerisation mediated by the $Sn(Oct)_2$ complex suggested by Kricheldorf (Kricheldorf *et al.* 1995). $Sn(Oct)_2$ has energetically favourable free d orbitals and can thus act as trans-esterification catalysts for alcohols and esters including lactones.(Kricheldorf *et al.* 1995) The octoate groups act mainly as mono-dentate ligands in $Sn(Oct)_2$. In consequence, there are three sp^3d^2 orbitals free. The high lewis acidity leads to the need for another ligand so that $Sn(Oct)_2$ can form a more stable tetrahedral or quadratic configuration of four occupied orbitals. This ligand is the OH group of PEG-Biotin.

The first step involves a co-ordination between the catalyst and the OH- end group of the PEG-Biotin. Binding of the lactone then catalyses the reaction because complexation of the lactone polarises its carbonyl group (Figure 3.3). $Sn(Oct)_2$ also forms strong complexes with water which means that any water impurities present would lead to homo-polymerisation of lactide as illustrated in Chapter 1. For this reason it was very important to silanise all glassware and dry all the reagents especially hydrophilic PEG which has such a great affinity for water.

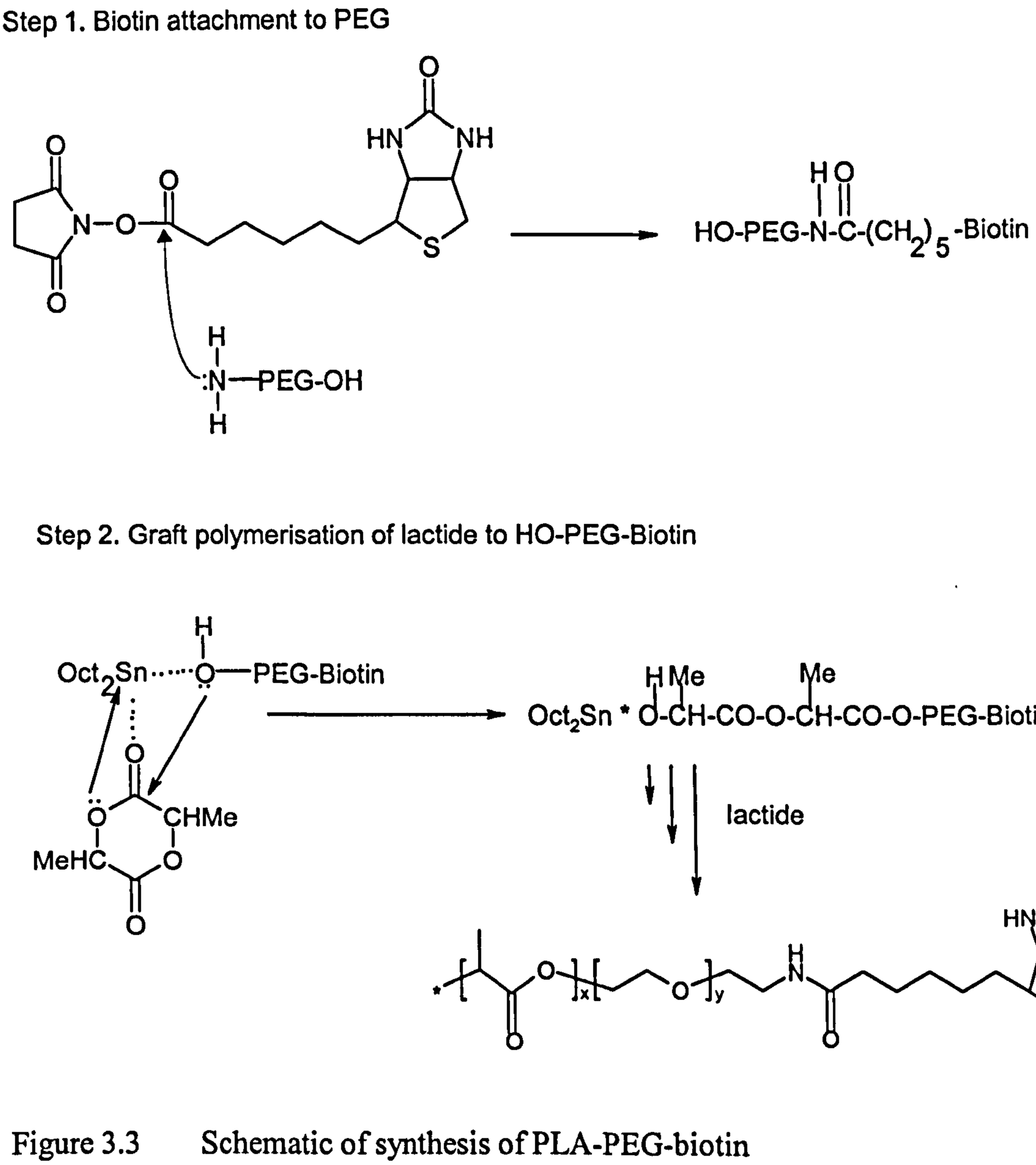

Figure 3.3 Schematic of synthesis of PLA-PEG-biotin

The calculated DP_{PLA} values were found to be in good agreement with theoretical values deduced from the LA/EG ratio in the feed indicating a high yield from the polymerisation (Table 3.3). Further confirmation of this is that no monomer impurity can be detected by ^{1}H NMR, where the NMR shift of the monomer lactide to the poly (lactic acid) has the quartet shift from 5-5.1ppm to 5.1-5.3ppm and the doublet shift from 1.7-1.75ppm to 1.5-1.6ppm (Figure 3.4). Identification of pure PLA-PEG without any PLA homopolymer is seen through GPC spectra. For an example when water impurities were present in a PLA-PEG-biotin synthesis, this resulted in a bimodal peak, one of which was the PLA homopolymer and the other belonging to the PLA-PEG-biotin copolymer. A single peak therefore indicated that a pure polymer had been achieved. NMR analysis on the final product showed no incorporation of octoate end-groups and GPC measurements display a relatively broad molecular weight distribution (Table 3.3).

3.4.1 Evidence of attachment of biotin.

Analysis of HO-PEG-Biotin by ^{1}H-NMR spectroscopy showed the appearance of a triplet at 2.05ppm that can be assigned to the methylene from the biotin chain alpha to the amide and the appearance of a broad singlet belonging to the free amido proton at 7.85 ppm. These signals were not present on the NMR spectra of NHS-Biotin. The biotin group was identified through the two methine protons (H-3, H-4) from the cyclic biotin structure at 4.3 and 4.2ppm and two urea protons (H-1', H-3') from the cyclic biotin structure at 6.45, 6.35ppm (Bates and Rosenblum 1985; Tonan *et al.* 1998).

Polymer	LA/EG In feed	LA/EG[a] In product	DP_{PEG}[b]	DP_{PLA}[b]	Mw	Mn[c]	Tg (°C)	1H NMR shifts (ppm) $CDCl_3$ as ref. CH (PLA)	CH_2 (PEG)	CH_3 (PLA)
PLA-PEG-biotin by melt polymerisation	6.1	5.5	76	418	22680	33440	16	1.56	3.53	5.24
PLA-PEG-biotin by solution polymerisation	6.2	5.3	76	403	22210	32290	17	1.53	3.51	5.22
PLA-PEG by melt polymerisation	6.2	6.8	68	462	27440	36260	14	1.55	3.51	5.20
PLA-PEG by solution polymerisation	6.1	5.8	68	394	23690	31360	16	1.54	3.52	5.23

[a] Determined by using the integration ratio of resonances due to PEG blocks at 3.5ppm (-O-CH_2-CH_2) and to PLA blocks at 1.55ppm (CH_3) in the ^{1}H NMR spectra. [b]$DP_{PEG\text{-}B}$= 3350/44 = 76 and DP_{PEG} = 3000/44 = 68, $DP_{PLA} = DP_{PEG}$ x (LA/EG). [c]Mn = 44 x DP_{PEG} + 72 x DP_{PLA}

Table 3.3 Bulk properties of PLA-PEG and PLA-PEG-biotin by ^{1}H-NMR, GPC and DSC analysis.

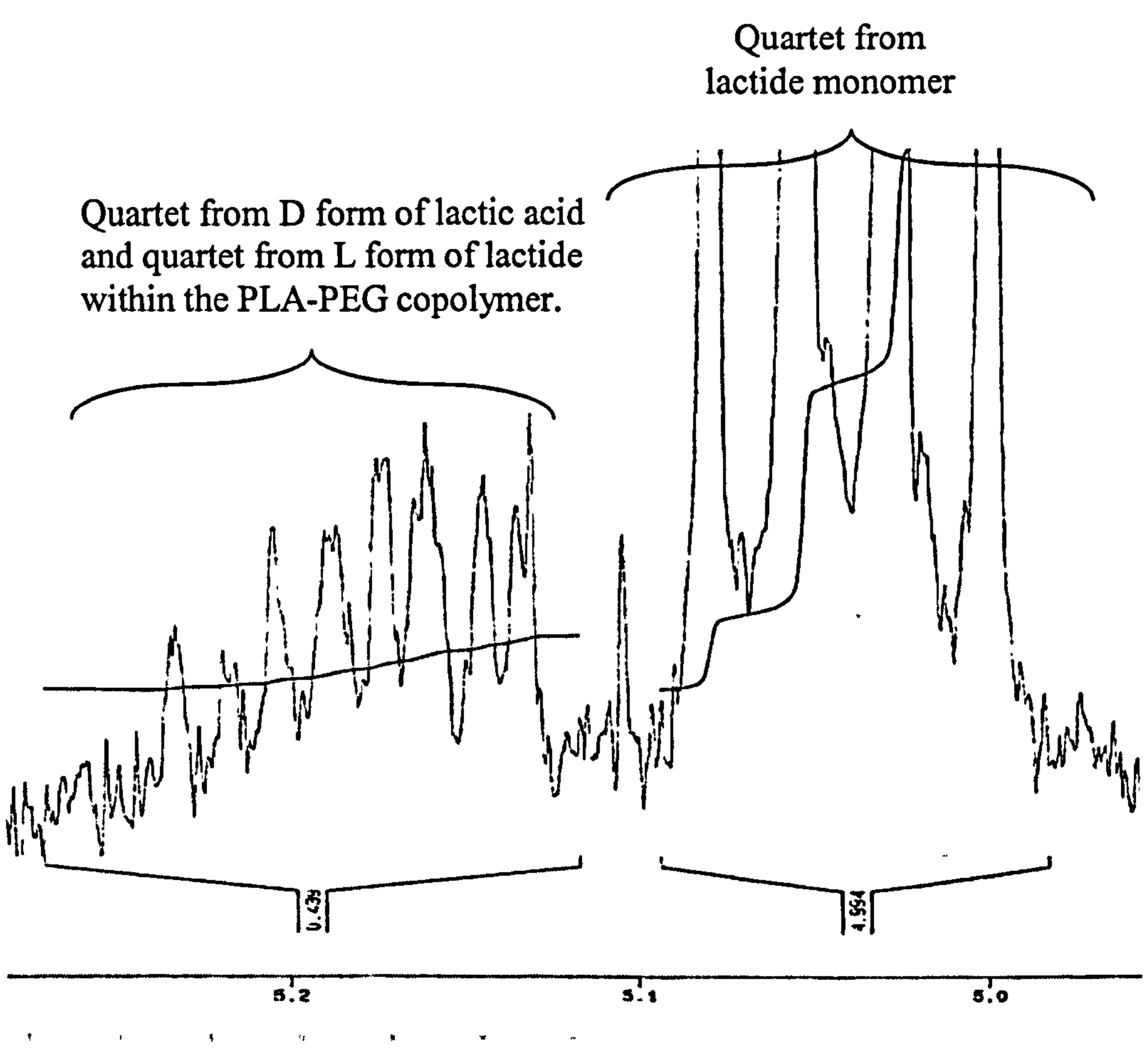

Figure 3.4 Lactide monomer impurity detection in PLA-PEG using ^{1}H NMR.

In NMR spectras of PLA-PEG-biotin (Mw 22210), biotin signals could not be seen as the signal from the PLA overwhelmed the biotin signal. (CH; 1.53 ppm, CH_3; 5.22 ppm). For this reason a low-content lactide, PLA-PEG-biotin was synthesised (0.2g lactide, 0.35g PEG-Biotin). ^{1}H-NMR studies on the low-content lactide PLA-PEG-biotin by solution and melt polymerisation showed that biotin integrity and attachment was maintained after graft polymerisation of lactide to the PEG-biotin, with the biotin protons (H-3, H-4, H-1', H-3') at 4.2, 4.3, 6.35 and 6.45ppm and the amide bond at 7.85ppm still clearly detectable (Figure 3.5). However due to degeneracy in the 1.53ppm and the 5.22ppm region from the PLA signals, SPR and fluorescent spectroscopy using the HABA/avidin complex were necessary to confirm complete biotin binding integrity (Table 3.4). Assessment was also undertaken to resolve whether the route of synthesis showed any effect on the biotin attachment or its binding capabilities, given that melt polymerisation of this polymer had been synthesised at a temperature 30°C higher than solution polymerisation.

SPR analysis measured avidin binding with the PLA-PEG-biotin and PLA-PEG by both synthetic routes. The increase in ϕ_{SPR} from the injection of avidin for the melt polymerised PLA-PEG was 40.90 ± 5.07 mDA and for the solution polymerised PLA-PEG was 42.75 ± 6.48 mDA. The PLA-PEG-biotin by melt and solution polymerisation after injection of avidin gave ϕ_{SPR} shifts of 170.46 ± 4.89 mDA and 181.58 ± 12.19 mDA respectively. There is a clear difference between the PLA-PEG and the PLA-PEG-biotin (Figure 3.6) that is consistent with previous work (Black *et al.* 1999).

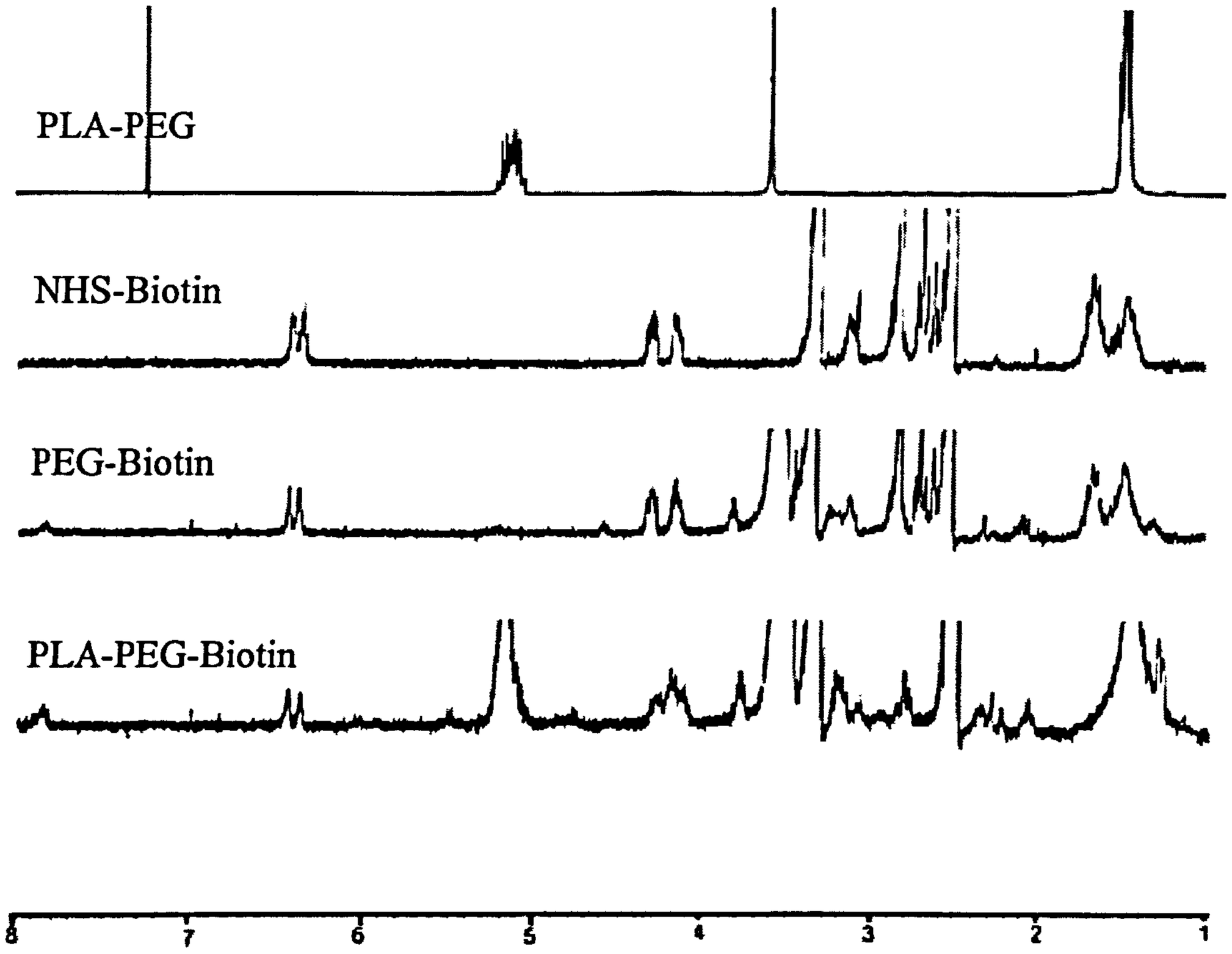

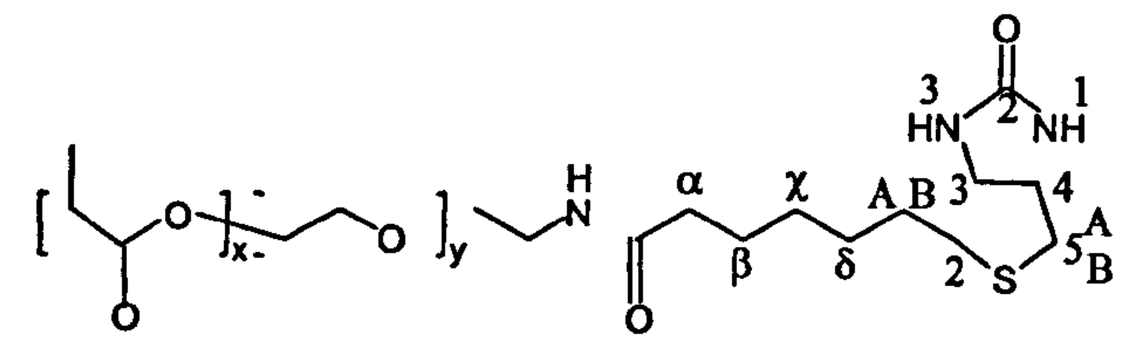

H-2 = 3.36 H-α = 2.05 NH-1' = 6.35
H-3 = 4.2 H-χ = 1.62 NH-3' = 6.45
H-4 = 4.3 H-β = 1.73 NHCO = 7.85
H-5A = 3.01 H-δ = 1.43 PEG = 3.51
H-5B = 2.78 PLA (CH) = 1.53
PLA (CH_3) = 5.22

Figure 3.5 ^{1}H NMR spectras of PLA-PEG, NHS-Biotin, Biotin-PEG-OH, and low molecular weight PLA-PEG-biotin

Polymer	SPR shifts (mDA)	Absorbance value after addition to polymer film in buffer	Absorbance value after addition to polymer film in DME tissue culture media
PLA-PEG-biotin by melt polymerisation	170.46 ± 19.57	1.056 ± 0.002	1.3911 ± 0.006
PLA-PEG-biotin by solution polymerisation	181.58 ± 12.19	1.052 ± 0.003	1.3749 ± 0.006
PLA-PEG by melt polymerisation.	40.90 ± 5.07	1.111 ± 0.010	1.4219 ± 0.005
PLA-PEG by solution polymerisation	42.75 ± 6.48	1.105 ± 0.003	1.4197 ± 0.008

Table 3.4 Surface analysis of biotin integrity and binding capabilities by SPR and fluorescent spectroscopy with the HABA/avidin complex.

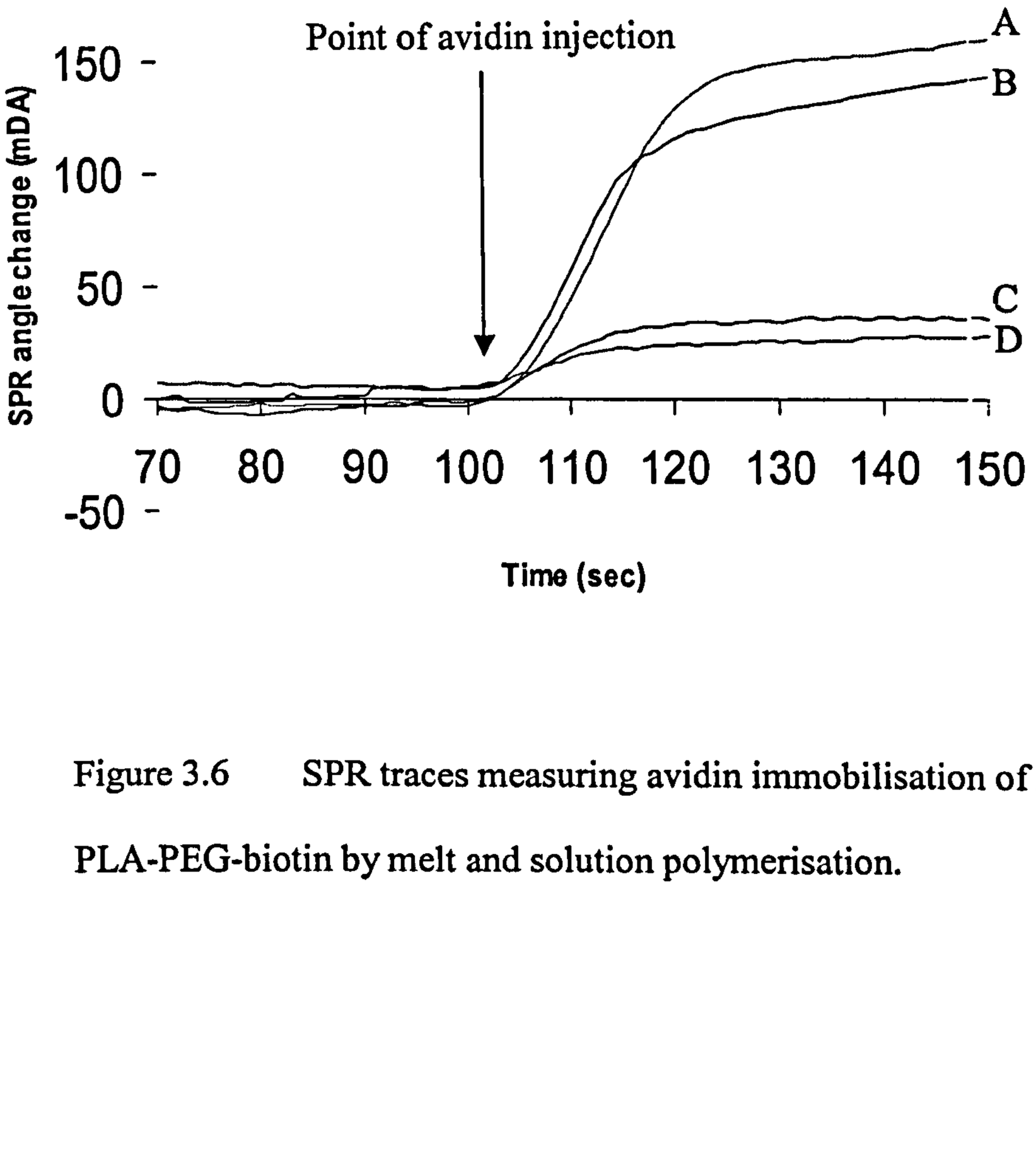

A=PLA-PEG-biotin by solution polymerisation
B=PLA-PEG-biotin by melt polymerisation
C=PLA-PEG by solution polymerisation
D=PLA-PEG by melt polymerisation

Figure 3.6 SPR traces measuring avidin immobilisation of PLA-PEG and PLA-PEG-biotin by melt and solution polymerisation.

The shifts noted with the PLA-PEG surface can be attributed to non-specific interactions, which have been well characterised by Green *et al* (Green *et al.* 1997; Green *et al.* 1999). There was no significant statistical difference in comparisons of polymers synthesised by either melt or solution polymerisation.

Fluorescent spectroscopy studies using the HABA/avidin complex supported SPR data with no decrease in absorbance for the PLA-PEG and a decrease from 1.100 ± 0.004 to 1.052 (equivalent to 625,260 molecules of biotin/μm^2) ± 0.003 and 1.056 (539,010 molecules of biotin/μm^2) ± 0.002 for PLA-PEG-biotin by solution polymerisation and PLA-PEG-biotin by melt polymerisation respectively.

A modification of the HABA/Avidin protocol to assess PLA-PEG-biotin binding under cell culture conditions was to prepare the HABA/Avidin reagent in Dulbecco's modified eagle medium (DMEM) with high glucose, l-glutamine, HEPES buffer and pyrodoxine hydrochloride. The effect of the media was to increase the absorbance from 1.100 ± 0.004 to 1.4254 ± 0.013. This value did not decrease when HABA/Avidin reagent in DMEM was added to a film of PLA-PEG. A decrease was, however, detected from 1.447 ± 0.0026 to 1.3911 ± 0.0059 (625,190 molecules of biotin/μm^2) for a film of PLA-PEG-biotin by solution polymerisation and a decrease from 1.4190 ± 0.0055 to 1.3749 ± 0.0069 (514,670 molecules of biotin/μm^2) for a film of PLA-PEG-biotin by melt polymerisation.

The results show clear evidence of HABA displacement with avidin by the biotin moieties with the PLA-PEG-biotin but no displacement with the PLA-PEG, which is consistent with expectations. This in conjunction with SPR data, which also showed clear differences in θ_{SPR} shifts between the PLA-PEG-biotin and the PLA-PEG, suggests that biotin structural integrity had been maintained together with binding capabilities during synthesis.

3.4.2 Effect of biotin on bulk properties of PLA-PEG

Having shown that the biotin unit was intact, bulk/thermal property analysis through comparisons of PLA-PEG and PLA-PEG-biotin by melt and solution polymerisation was undertaken to see the effect biotin attachment had on the PLA-PEG bulk properties. NMR spectroscopy and GPC studies were completed to ensure that the structural characteristics and molecular weight of the polymer were consistent so that any change in thermal properties were not due to variations other than the end-group. Analysis showed very little difference when characterisation was completed by NMR spectroscopy and GPC (Table 3.3). NMR spectroscopy analysis gave similar integral ratios of PLA to PEG for all four polymers with characteristic peaks for PLA being a doublet (CH) at 1.53 ppm and a quartet (CH_3) at 5.22 ppm and a singlet for PEG (CH_2) at 3.51 ppm. GPC studies gave a mean molecular weight of 24000 ± 2370 confirming that molecular weight differences should not be responsible for any large differences in bulk properties.

DSC data showed that the addition of PEG/PEG-biotin to the PDLLA results in a drop in the glass transition temperature from between 44-50°C for pure PDLLA to 14-17°C for the PLA-PEG/PLA-PEG-biotin copolymer. The monophasic profile displayed by the polymers was constitent with reports that block copolymers derived from D, L-lactide are usually monophasic and do not show first-order phase transitions, because more or less random sequences of D and L lactyl units do not crystallize (Kricheldorf and Meierhaack 1993). There was little difference in thermal properties between the biotinylated and non-biotinylated PLA-PEG and the melt and solution polymerised products suggesting that the biotin end-group does not change the bulk properties of the polymer (Figure 3.7). This was consistent with the work carried out by Kricheldorf *et al.* on the variation of end-groups and synthesis of block copolymers with PEG by anionic polymerisation of lactide where DSC studies showed that thermal properties are predominantly dependent on the PLA: PEG ratio and not the end-group [Kricheldorf *et al.* 1993; Kricheldorf *et al.* 1999; Caibao *et al.* 1996).

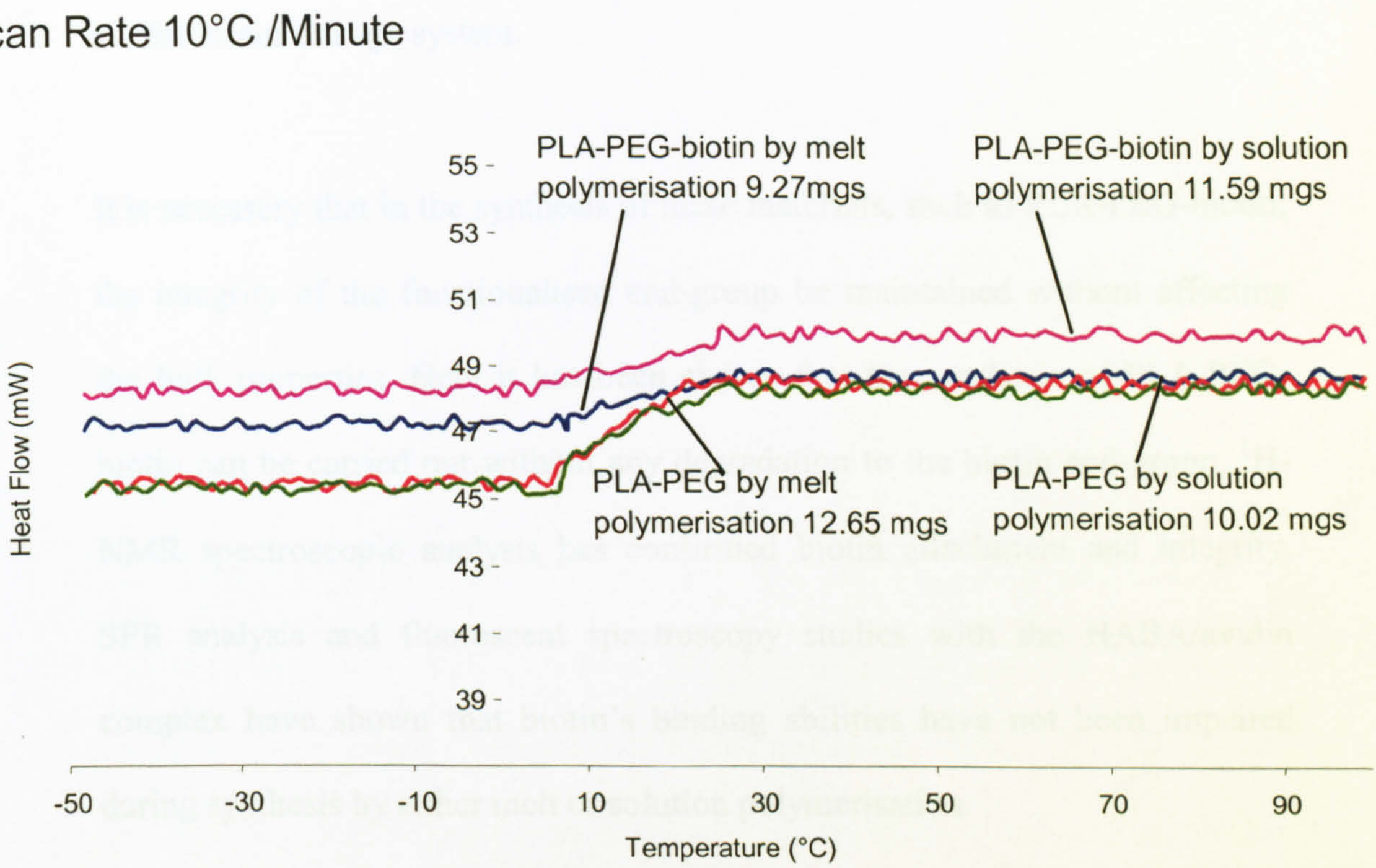

Figure 3.7 DSC thermograms for PLA-PEG-biotin and PLA-PEG by melt and solution polymerisation

3.5 Conclusion

The synthesis of a novel biomaterial that can integrate biological activity into its surface chemistries is described. PLA-PEG-biotin combines the benefits of PLA-PEG based copolymer systems with the advantages of the universal avidin-biotin linkage system.

It is necessary that in the synthesis of these materials, such as PLA-PEG-biotin, the integrity of the functionalised end-group be maintained without affecting the bulk properties. Here it has been shown that the synthesis of PLA-PEG-biotin can be carried out without any degradation to the biotin end-group. ^{1}H-NMR spectroscopic analysis has confirmed biotin attachment and integrity. SPR analysis and fluorescent spectroscopy studies with the HABA/avidin complex have shown that biotin's binding abilities have not been impaired during synthesis by either melt or solution polymerisation.

^{1}H-NMR, GPC and DSC characterisation shows there is no significant effect on bulk properties induced by the biotin end-group. This indicates that PLA-PEG-biotin can be repeatably synthesised with predictable and controllable bulk properties. PLA-PEG-biotin therefore has significant potential for widespread use in drug delivery and diagnostic applications. Furthermore, evidence that the biotin unit and its binding properties are intact and have not compromised the bulk properties of the polymer, provides a material that can form the foundation of our proposed self-assembling porous scaffold.

CHAPTER 4

INTERACTIONS OF FIBROBLASTS AND ENDOTHELIAL CELLS WITH DEFINED PORE FEATURES

The potential for controllable porosity by the proposed self-assembling scaffold is a considerable advantage over other injectable *in situ* transforming biomaterials because non-porous materials limit tissue formation and vascularisation to the barrier of diffusion to signaling and nutrient molecules. Before progressing onto the manufacture, characterisation and assessment of our scaffold in Chapter 5 and 6, it is important to have a fundamental understanding of the pore-cell interaction if scaffold characteristics are to be optimised. Chapter 4 introduces the concepts of cell behaviour over defined features, the methods that are currently used to produce these features and concludes with a systematic study of two model cell types over a series of defined pore features fabricated using photolithographic techniques.

4.1 Introduction

The use of biodegradable polymer scaffolds as templates for tissue engineering has been described for a number of tissue types, including cartilage, liver and nervous tissue (Den Dunnen *et al.* 1993; Bellamkonda and Aebischer 1994; Baldwin and Saltzman 1996; Hutmacher 2000). Within these scaffolds, the seeded cells encounter a high surface area formed by the polymer. This surface is convoluted to form a three-dimensional structure containing many pores (Wake *et al.* 1994; Kaufmann *et al.* 1997; Athanasiou *et al.* 1998; Evans *et al.* 1999). The success of the tissue engineering is dependent on the migration of cells through this porous environment and the maintenance of nutrient diffusion throughout the scaffold after cell colonisation. Ideally, after seeding the cell population should be able to migrate through the scaffold and some pores should remain open to nutrient diffusion as the tissue forms. Further information on the influence of porosity in tissue engineering scaffolds can be found in Chapter 1.

To study the effect of pore diameter on cell migration and morphology we have used microfabrication to form surfaces with defined porosities enabling the study of cell behaviour over these defined topographical features. Two cell types have been chosen for these studies, 3T3 fibroblasts and bovine aortic endothelial cells (BAECs). Cell type choice was made due to the different behaviour of these cells during tissue formation *in vivo*. Fibroblasts tend to fill spaces within tissues and form extracellular matrix, whilst in endothelial, cells

form into tubular architectures in which the integrity of a central lumen is essential to blood vessel function.

4.1.1 The formation of topographical features using photolithography

The advances in microfabrication technologies in the microelectronics industry have led to the potential to study cell behaviour over defined topographical features. The most recent approaches have involved the process of photolithography (Clark *et al.* 1991). Using current silicon chip technologies, a chrome mask can be designed by computer-aided design and transferred and written by electron beam lithography (typically a high voltage 0.1 micron diameter beam containing 1 nA of 20kV over area to be written) (Lawes 1994). The mask produced can then be used to pattern specific designs onto silicon wafers.

A photoresist is used to protect the silicon substrate and exposure to UV light under the designed mask deprotects specified regions for etching. Currently the most effective method for microfabrication is plasma etching (reactive ion etching) because of its ability to etch anisotropically and thus produce deeper microstructure with higher aspect ratios (Lawes 1994; Lawes 1996). Various biocompatible surfaces such as silicon nitride can be etched by selecting the ions specific to the substrate (Clark *et al.* 1991; Kue *et al.* 1999). The etching is achieved by the bombardment of ions in a vacuum. While ions of non-reactive species such as argon will erode most materials, the resultant profiles of the ridges in the etched material are rarely vertical (Lawes 1994). The use of

ions that react chemically with the material is preferred e.g. fluorine ions attack silica glass or oxygen ions etch polymeric plastic materials, essentially by burning. It is not necessary to use the pure gas in forming the ions; it is significantly safer to use for an example, chlorine formed by a discharge in gaseous silicon tetrachloride. The desired ions are usually formed by a discharge in a low-pressure gas and are accelerated by an electric field towards the specimen to be etched. In the reactive ion etching schematic shown in Figure 4.1, the ions are formed in a rf discharge, and as the ions travel much more slowly than the electrons, a d.c. electric field is built up which accelerates the ions towards the substrate. This electric field is of the order of 400 to 4000 V which is not enough to cause implantation of the ions into the substrate (Clark *et al.* 1991; Curtis 1994; Lawes 1994; Lawes 1996). It is rare that the pattern in resist can be used directly; normally it must be transferred into the desired material. This can be done either using additive or subtractive processing. In additive processing the relief pattern in the resist is used as a stencil; material is superimposed on the substrate in areas that are not protected by the resist pattern. This can be done by overcoating with vacuum evaporation, for example, the whole surface with the desired material and immersing the specimen in a flowing stream of solvent that washes away the resist leaving the overcoated material only on the substrate. Thus, the resist is used to protect the regions of the underlying substrate that are not to be etched. Both positive and negative acting resists may be used and thus, by careful design of the mask pattern, a wide variety of microholes, microchannels, micropillars etc may be fabricated with submicron dimensions.

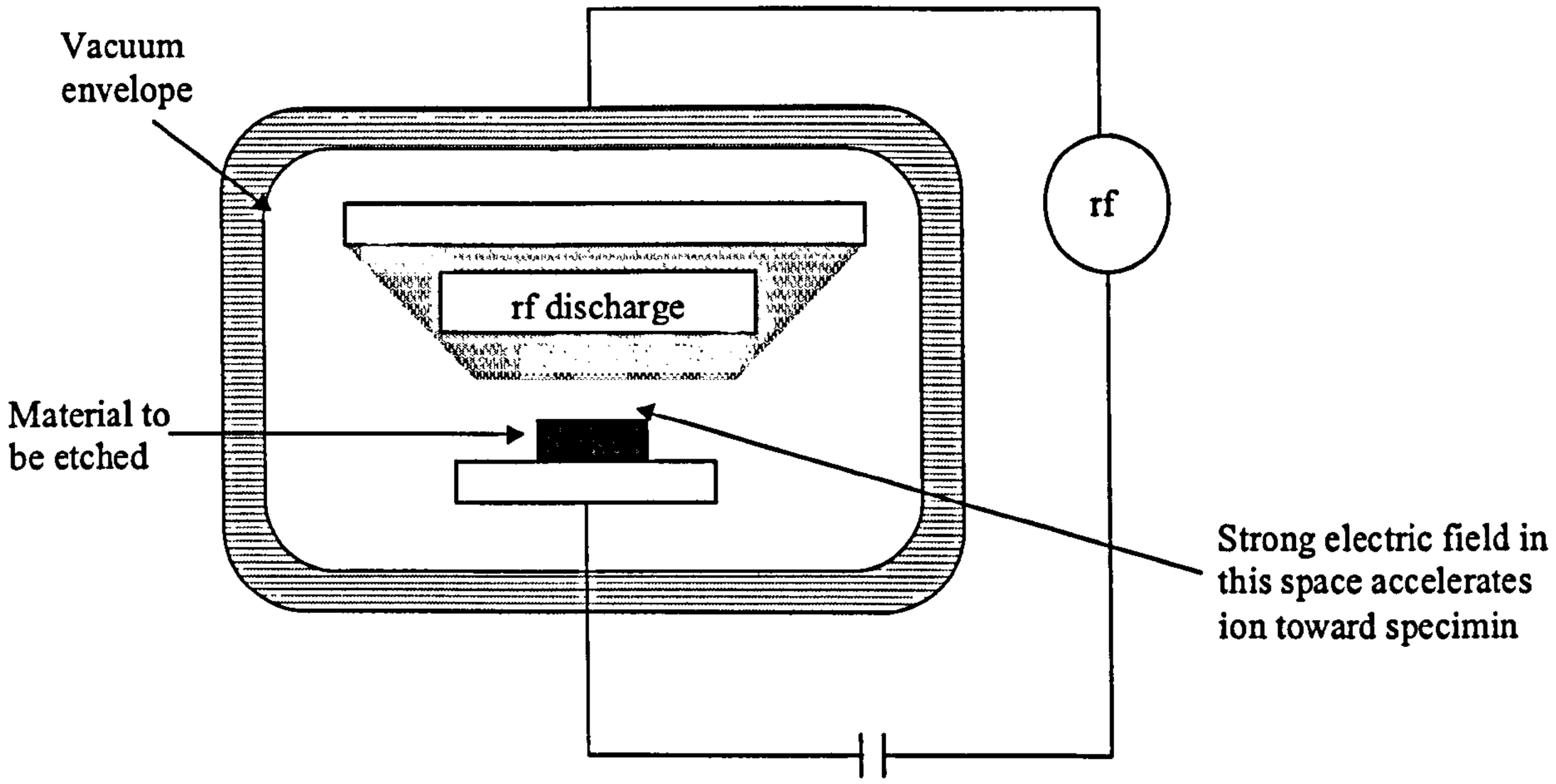

Figure 4.1 Schematic of reactive ion etching machine

Wet chemical etches are not always suitable in nanofabrication as they are normally isotropic in their action making it difficult to make high aspect ratio structures and it is difficult to obtain uniform etching at below 100 nm line widths (Curtis and Clark 1990; Clark *et al.* 1991; Lawes 1996; Curtis and Wilkinson 1997; Curtis and Wilkinson 2001).

4.1.2 Effect of cell behaviour over topographical features

It has been widely reported that a change in surface topography can influence cell behaviour substantially. Table 4.1 provides some examples of the wide variety of features that have been produced and the behaviour of cells over them. Micron-scale roughness has been shown to modify cellular responses in cell culture and to modify biocompatibility and tissue attachment significantly (Vonrecum and Vankooten 1995). This was demonstrated in a comparative study concerning textured and smooth polytetrafluroethylene (PTFE), where exudates obtained from fibroblasts cultured on textured PTFE contained significantly more growth and attachment-promoting activity than those obtained from fibroblasts cultured on smooth PTFE.

Cell spreading and cell shape and their effects on cell growth and cell function have also been shown to be dependent on surface morphology (Singhvi *et al.* 1994; Singhvi *et al.* 1994). For an example, Cook *et al* cultured MDCK cells *in vitro* on microporous membranes and showed that the differentiated state of MDCK cells could be regulated by the microporosity of the surface (Cook *et al.* 1989).

Table 4.1 Cell behaviour over topographical features

Topographical feature	Material	Dimensions of feature	Spatial orientation of features	Fabrication method	Cell type	Cell behaviour observed	Reference
Pores	Filters - uncoated and silicon coated.	Diameter: 0.2-10 μm. Depth not available	N/A	Microporous filter: Nylon dip-coated with PVC/PAN copolymer	*In vivo* studies using canine model	Pores smaller than 0.5 μm: non-adhering, contracting capsules around implants; 1.4-1.9μm pores: adherent capsules but no inflammatory cells on implants. Pores bigger than 3.3 μm: Inflammatory tissue infiltrated 1-2 μm pores: Fibroblasts attached	(Campbell and Von Recum 1989)
Pillars and pores	Poly(methyl methacrylate) (PMMA), Poly (ethylene terepthalate) (PET), polystyrene (PS)	Circular pillars and pores. Diameter: 1, 5, 10 and 50 μm	Uniform array	Laser ablation using masks made by electron-beam lithography, reactive ion etching	Amniotic epithelial cells and Human osteoblasts	1 and 5 μm pillars: Cells stretched between adjacent pillars or engulfed them 10 μm pores: cells attached to edges. 5% increase in resistance to shear force 50 μm PET pillars: greatest adhesion	(Fewster *et al.* 1994)
Grooves	Cast of silicon original using Poly dimethylsiloxane (PDMS)	Square grooves Width 2,5, 10μm Depth 0.5μm	Groove and ridge width equal.	Photolithography and reactive ion etching, UV and glow discharge treatment	Rat dermal fibroblasts	2, 5 μm grooves: stronger orientation than 10 μm grooves. Cell growth on glow discharge treated surface greater than on UV treated surface.	(Denbraber *et al.* 1995)
Grooves	Photoresist, Titanium coated silicon, epoxy replicas	Square and V-shaped grooves Depth: 0.5-60μm	Repeat spacing 30-220 μm, but groove and ridge width not available	Photolithography and anisotropic etching	Porcine periodontal ligament epithelial cells	Migration of cells directed by grooves. Orientations were highest on the smallest repeat spacing. Some cells crossed ridges or descended into grooves. 0.5 μm deep grooves less effective than deeper grooves at directing cells. Lamellae and filipodia of cells seen around edges.	(Brunette 1986)

Table 4.1 Cell behaviour over topographical features *continued.*

Topographical feature	Material	Dimensions of feature	Frequency of features	Fabrication method	Cell type studied	Cellular behaviour	Reference
Grooves	Quartz	Width: 5, 10, 25 μm Depth: 0.5, 1, 2, 5 μm	N/A	Photolithography and reactive ion etching	BHK (fibroblastic) cells	Periodicity of 0.6 μm: Actin condensations observed at topographical discontinuities often at right angles to the groove edge. Vinculin organization similar to that of actin with microtubules observed after 30 min. Taxol reduced elongation. Colcemid increased spreading and reduced orientation and elongation. Cytochalasin D reduced spreading, elongation, and orientation.	(Wojciakstothard *et al.* 1995)
Grooves	Titanium coated silicon, epoxy replicas, photoresist	Square and V-shaped major grooves depth: 5-120 μm Width not available. Minor grooves depth: 2 μm on floor at 54° to major grooves	Repeat spacing: 5-80 μm	Photolithography and anisotropic etching	Human gingival fibroblasts	Major grooves: cells oriented Minor grooves: cell orientation of cells observed in absence of major grooves	(Brunette 1986)
Grooves	Poly(methylmethacrylate) (PMMA)	Width: 2, 3, 6, 12 μm Depth: 0.2, 0.56, 1.10, 1.9 μm	Groove and ridge width equal.	Photolithography and reactive ion etching	Chick embryo cerebral neuron, BHK, MDCK cells.	Increasing depth: Alignment of BHK cells increased Alignment of MDCK cells increased Increasing width: Alignment of BHK cells decreased. No effect on MDCK cells Chick embryo cerebral neurons MDCK cells in groups and not affected by grooves	(Clark *et al.* 1990)

Table 4.1 Cell behaviour over topographical features *continued*

Topographical feature	Material	Dimensions of feature	Frequency of features	Fabrication method	Cell type studied	Cellular behaviour	Reference
Grooves	Quartz and quartz with a poly-l-lysine coating	Width: 130 nm Depth: 100, 210, 400 nm	Groove and ridge width equal.	X-ray lithography and reactive ion etching. Defined masks made by a laser holographic technique.	Chick embryo cerebral neuron, BHK, MDCK cells.	Increasing depth: Alignment of BHK cells increased Elongation of MDCK cells increased, while alignment remained the same. Chick embryo cerebral neurons MDCK cells in groups and not affected by grooves	(Clark *et al.* 1991)
Steps	Poly(methylmethacrylate) (PMMA)	Steps: 1- 18 μm	N/A	Photolithography and reactive ion etching	Rabbit neutrophils, BHK cells, Chick embryonic neural, chick heart fibroblast	1 and 3 μm step heights: Decrease in frequency of ascent 5 μm steps: rabbit neutrophils showed twice the crossing frequency of other cells Increasing step height: less crossing and greater alignment	(Clark *et al.* 1987)
General Roughness	Ti, Ti/Ta alloy, Ti/Al/V alloy	Peak to valley heights: 0.04, 0.36 and 1.36 μm	Random	Alumina emulsion polishing, grinding with SiC paper	Human Gingival fibroblasts	Cells aligned to marks made by grinding. 0.04 μm roughness: 10% of cells oriented. 0.36 μm roughness: 60% of cells oriented. 1.36 μm roughness: 72% of cells oriented.	(Eisenbarth *et al.* 1996)

One proposal has been that topography affects cell behaviour by altering the ability of the extra-cellular matrix (ECM) to absorb to the surface (Meyle *et al.* 1994; Vonrecum and Vankooten 1995). Topographical features have been shown to orient cells in a phenomenon known as "contact guidance" (Brunette 1986; Brunette 1986; Clark *et al.* 1991; Clark 1994; Curtis 1994; Meyle *et al.* 1994; Denbraber *et al.* 1995; Flemming *et al.* 1999). Brunette *et al* for an example showed that major grooves interfered with the cells ability to form long linear cytoskeletal elements, such as microtubules or microfilaments, in the direction of the minor grooves and that the cells tended therefore to be polarized so that they were aligned with the major grooves. It has been suggested that features that involve a change in the direction from one surface configuration into another as produced by hills, pits, valleys, grooves, or edges extending out into the main plane or an edge where two planes meet may be seen as discontinuities (Vonrecum and Vankooten 1995). Cells attach to a surface by a number of contacts including podosomes, dot contacts, point contacts and focal contacts (Meyle *et al.* 1994). These focal adhesions consist of a cluster of ECM-bound integrins that act as a membrane attachment for the actin fibrils inside a cell (Ruoslahti and Obrink 1996; Ruoslahti 1997). There is a great deal of evidence to suggest that there is a concentration of these focal adhesion points at discontinuities (Brunette 1986; Curtis and Clark 1990; Curtis and Wilkinson 1997; Flemming *et al.* 1999). Intracellular proteins involved in the focal adhesions crosslink the actin micro-filaments, whose structure determines cell shape maintenance (Vonrecum and Vankooten 1995). Integrins link the external ECM to the intracellular actin cytoskeleton and it is the presence of the concentrated actin at the discontinuities as detected by

phalloidin staining that confirms the theory of focal adhesion points being formed at discontinuities (Brunette 1986; Curtis and Clark 1990; Vonrecum and Vankooten 1995; Ruoslahti and Obrink 1996; Curtis and Wilkinson 1997; Ruoslahti 1997; Flemming *et al.* 1999).

There are a number of factors involved in the behaviour of cells over topographical features (Clark 1994). Cell density has been shown to have a significant role in the behaviour of cells over a defined surface. When BHK (fibroblastic) cells were compared directly to MDCK (epithelial) cells, MDCK cells in co-culture were often unaffected by topographical features that would strongly orientate single MDCK and BHK cells (Curtis and Clark 1990). Where topographical features are on the nanometre scale, cell-cell interactions have in fact been found to be the more dominant factor in determining cell guidance (Clark *et al.* 1991). There are also clear differences in behaviour between different cell types (Clark 1994; Flemming *et al.* 1999). This may be attributed to different amounts of actin monomer available in different cell types. A cell with less actin monomer will use the majority of this in forming a polymer once in contact with a discontinuity, thus reducing further movement or spreading of the cell and limiting its movement to around the discontinuity (Curtis and Clark 1990). Some cell types may display co-operative behaviour with topographical features. This has been demonstrated when cells migrating along fibres attached to other cells to form "sail sheets" to get from one topographical feature to another where the depth was too great (Curtis and Clark 1990).

4.2 Materials and Method

4.2.1 Silicon Nitride Template Manufacture

Porous silicon nitride membranes were manufactured using a multistage process (Figure 4.2). Double side polished silicon wafers of 300 microns thick were cleaned and coated with low stress silicon nitride using low-pressure chemical vapour deposition (LPCVD). The surface topography design (Figure 4.3) was written to an electron beam pattern generator (Ebeam) and then transferred to two chrome masks, to define the back etch mask and the pore size and layout. Silicon wafers coated on both sides with silicon nitride were dehydrated at 150°C for 30 minutes. On cooling these were coated with hexamethyldisilizane (HMDS) as an adhesion promoter. The back-etching of the wafer was achieved as follows. One side of the wafer was spin coated with 250 microlitres photoresist (AZ5214E) for 60 seconds at 3000 rpm. After a solvent bake at 100°C for 90 seconds, the wafer was exposed to UV light from a mercury vapour lamp. The exposure energy was 100mJcm^{-2}. The exposed resist was developed in a 4:1 mixture of de-ionised water: AZ-400K developer, rinsed with de-ionised water and then spin dried with a nitrogen purge. The substrate was then hard-baked for 30 minutes at 120°C. An oxygen plasma descum was used to remove organic residues from the exposed nitride surface.

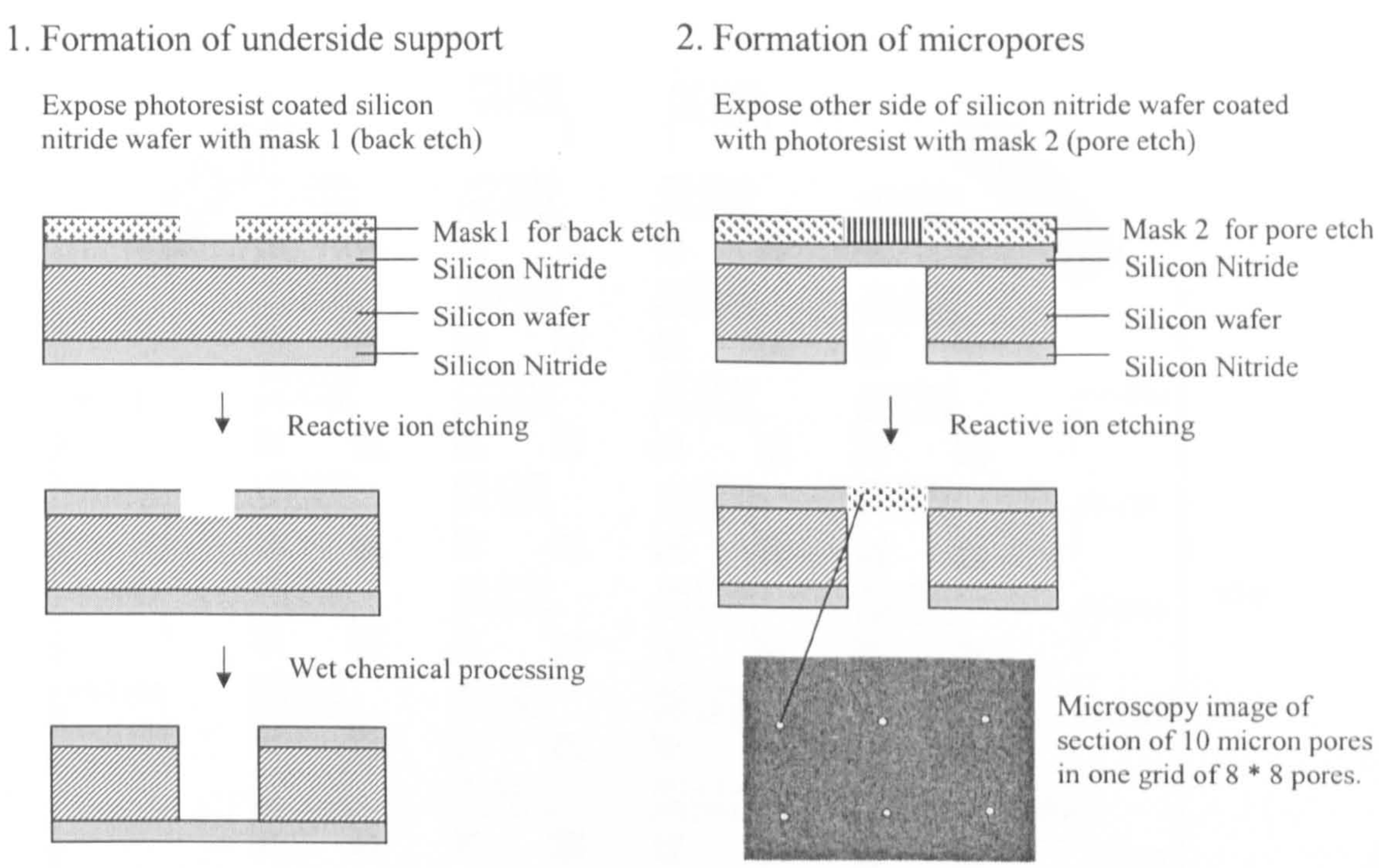

Figure 4.2. Schematic of pore template manufacture.

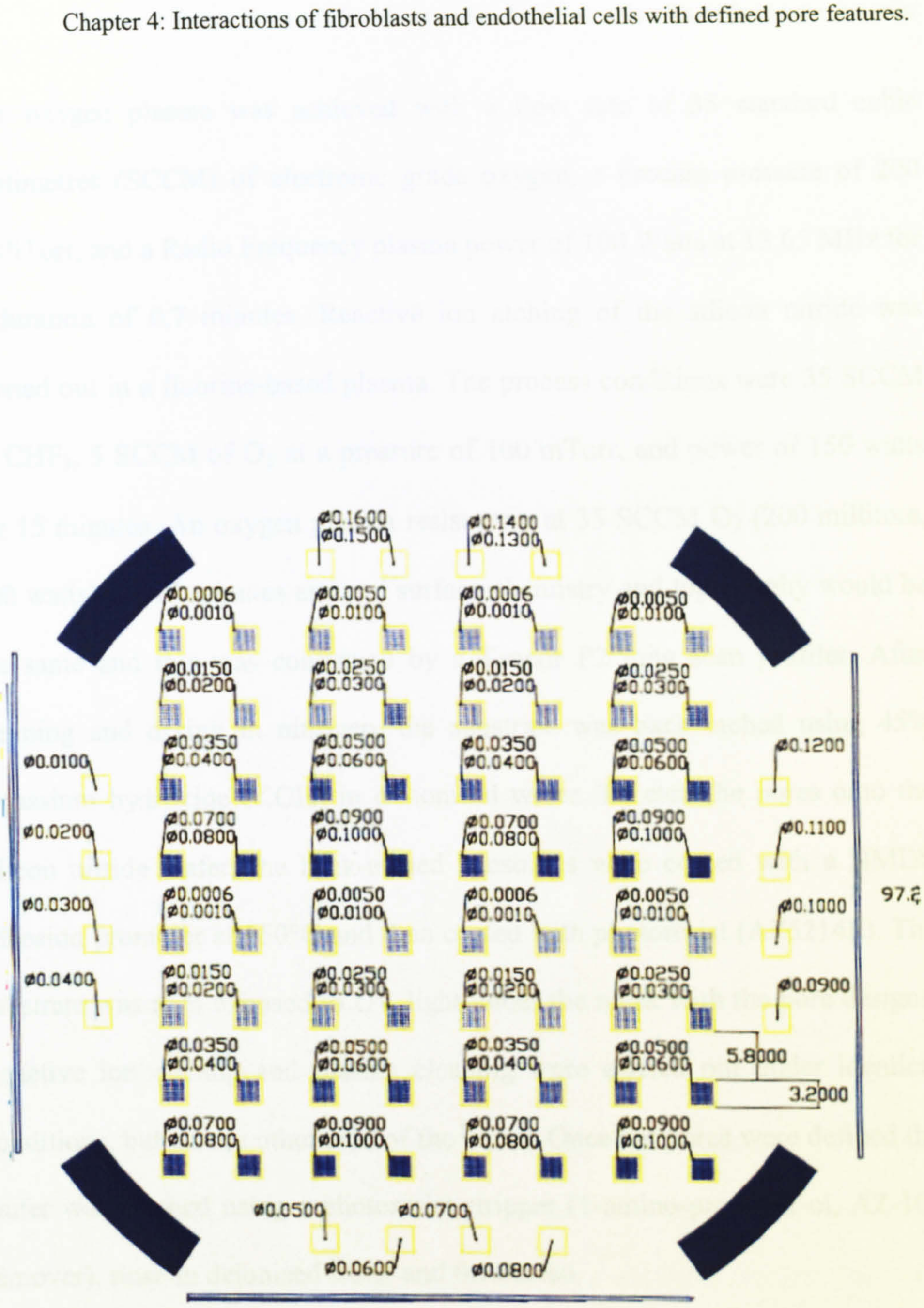

Figure 4.3 Computer aided design (CAD) for pore templates (values in millimetres)

The oxygen plasma was achieved with a flow rate of 35 standard cubic centimetres (SCCM) of electronic grade oxygen, a process pressure of 200 milliTorr, and a Radio Frequency plasma power of 100 Watts at 13.65 MHz for a duration of 0.7 minutes. Reactive ion etching of the silicon nitride was carried out in a fluorine-based plasma. The process conditions were 35 SCCM of CHF_3, 5 SCCM of O_2 at a pressure of 100 mTorr, and power of 150 watts for 15 minutes. An oxygen plasma resist strip at 35 SCCM O_2 (200 millitore, 100 watts) for 15 minutes ensured surface chemistry and topography would be the same and this was confirmed by a Tencor P2 long scan profiler. After cleaning and drying in nitrogen, the substrate was back etched using 45% potassium hydroxide (KOH) in de-ionised water. To etch the pores onto the silicon nitride wafer, the back-etched substrates were coated with a HMDS adhesion promoter at 150°C and then coated with photoresist (AZ5214E). The substrate was then exposed to UV light under the mask with the pore designs. Reactive ion etching and plasma cleaning were carried out under identical conditions, but on the other side of the wafer. Once the pores were defined the wafer was cleaned using a photoresist stripper (1-amino-propan-2-ol, AZ-100 remover), rinse in deionised water and then dried.

4.2.2 Cell Culture

3T3 fibroblasts (ATCC) and bovine aortic endothelial cells (ECACC) were cultured in DMEM supplemented with 10% foetal calf serum, 2 mM L-glutamine, 100 U/ml penicillin, 100 µg/ml streptomycin and 0.25 µg/ml amphotericin B. Cell cultures were incubated at 37°C in a 5% CO_2 enriched

atmosphere. Silicon nitride substrates were coated for 24 hours with 10mg/ml fibronectin dissolved in de-ionised water. Substrates were washed three times with de-ionised water prior to seeding with cells. A cell seeding density of 7000 cells/cm^2 was used in all studies.

3T3 fibroblasts (ATCC) and bovine aortic endothelial cells (ECACC) were co-cultured in DMEM supplemented with 10% foetal calf serum, 2 mM L-glutamine, 100 U/ml penicillin, 100 µg/ml streptomycin and 0.25 µg/ml amphotericin B. Cell cultures were incubated at 37°C in a 5% CO_2 enriched atmosphere. Co-culture studies were carried out by seeding substrates with 3500 cells/cm2 of each cell type in a mixed suspension.

The fibroblasts were treated with using a green chloromethyl derivative of a fluorescein diacetate derivative (CellTracker™, Molecular Probes) to identify the individual cell types in cell coverage calculations. CellTracker™ passes freely through cell membranes, but once inside the cell undergoes a glutathione S-transferase-mediated reaction, producing a cell-impermeant florescent dye-thioether adduct reaction product. Excess unconjugated reagent passively diffuses to the extracellular medium.

Studies with CellTracker™ were completed by adding 11 µl of DMSO (Aldrich) and 1 ml of media to 50 µg of CellTracker™. After mixing and syringe filtering, this was added to a further 11ml of media and placed over the cell culture for 30 minutes after which fresh media was added.

For phalloidin staining of cytoplasmic actin filaments. Cells were fixed in 2% glutaraldehyde for 24 hours, washed with phosphate buffered saline. 0.1% Triton-X was added for 10 minutes; removed and washed. Phalloidin (250 μg/ml) in PBS was then incubated with cells for 30 minutes. The samples were washed several times in phosphate buffered saline.

4.2.3 Microscopy and Time-lapse studies:

Phase contrast images were taken on an optical microscope (Leica DMIRB) attached to a Leica Q500 IW using a colour video camera (JVC TK-C1380). Time-lapse studies were captured on the optical microscope in an environmental chamber (Leica) at 37.1°C (Solent Scientific Incubator Temperature) in a 5% CO_2 enriched environment (Linkam CO 102). Images were taken every 10 minutes over 24 to 48 hour periods. Cell coverage calculations were made using Leica Qwin Software. Florescent images were taken using an absorbance/emission setting of 492-nm/516 nm.

4.2.4 Quantification:

Each set of pores, of a defined size, are set in an 8 by 8 array in a window of 3.2mm by 3.2 mm. Each pore is separated by 320 μm in both the x and y-axis. Differing windows contains set of pores of differing sizes ranging from 5 microns to 100 microns with single pores up to 160 microns in individual windows. Assessments of cell behaviour for quantitative studies were completed by defining cell interaction with the pores into two classifications:

(1) uncovered and (2) covered. Measurements were taken on every pore within a window at set intervals of 4 hours, 24 hours, 48 hours and 72 hours. Further measurements were made every 24 hours as necessary. Repeat studies were then carried out to ensure reproducibility in the results. Statistical analysis of the cell behaviour was calculated using one-way analysis of variance (ANOVA) with a Tukey post-test for the purposes of comparing pairs of group means, from data at each time point.

4.3 Results and Discussion:

4.3.1 Microfabrication of defined pore features

The study of cells over defined pores is important because porosity has been shown to have significant impact on the success of polymer scaffolds in tissue engineering. Two cell types are commonly involved in the vascularization of scaffolds. These are endothelial type cells for blood vessel supply to the scaffold and fibroblastic type cells, which invade the pores within the scaffold. Predicting the behaviour of these cell types is critical because scaffolds invaded with vascularized fibrous tissue has been shown to both increase viability of cells such as hepatocytes and decrease porosity of the scaffold (Mikos *et al.* 1993) (Mooney *et al.* 1997). On this basis, we chose bovine aortic endothelial cells (BAECs) and 3T3 fibroblasts as our model cell types and assessed these under single and co-culture conditions.

The first stage in our experimental design was the manufacture and preparation of our pore features. As described in Chapter 1, pore size and structure is the predominant factor in determining cell infiltration rates and vascularization ability of scaffolds for tissue engineering. These pores vary in size but tend to be between 5 and 100 μm with an optimum porosity having been described at approximately 60 μm (Clowes *et al.* 1986; Clowes *et al.* 1987; Salzmann *et al.* 1997; Sharkawy *et al.* 1997). For this reason, a range of pores from 5 to 100 μm was manufactured.

Pore templates were manufactured using a multistage photolithographic process as described in the methods section. The choice of silicon nitride as a substrate was made because it was able to undergo the photolithographic processes and had been shown to be non-toxic to cell cultures (Kue *et al.* 1999). Plasma ion etching was used to etch the pores into substrate as this provided pores with the highest aspect ratio. Given that changes in surface energy had been shown to have some effect on cell behaviour, all templates were plasma oxygen etched in order to keep surface chemistry and topography the same (Denbraber *et al.* 1995). A Tencor P2 long scan profiler confirmed that the surface topography around the pores was flat. It has also been hypothesized that the behaviour of cells over various topographies is due to the ability of a surface to absorb extra-cellular matrix and this ability is altered over various topographical features. (Vonrecum and Vankooten 1995) For this reason, all samples were coated with a fibronectin solution over a 24-hour period, which in conjunction with the otherwise flat surface should have reduced ECM uncertainties around the pore features.

Each individual pore was assessed before use. As shown in Figure 4.4, a number of pores were found over/underexposed, resulting in damaged pores or pores that had not fully formed. Such pores often left a trace of lithographic material from the washing procedure. These damaged pore features were then omitted from cell culture studies.

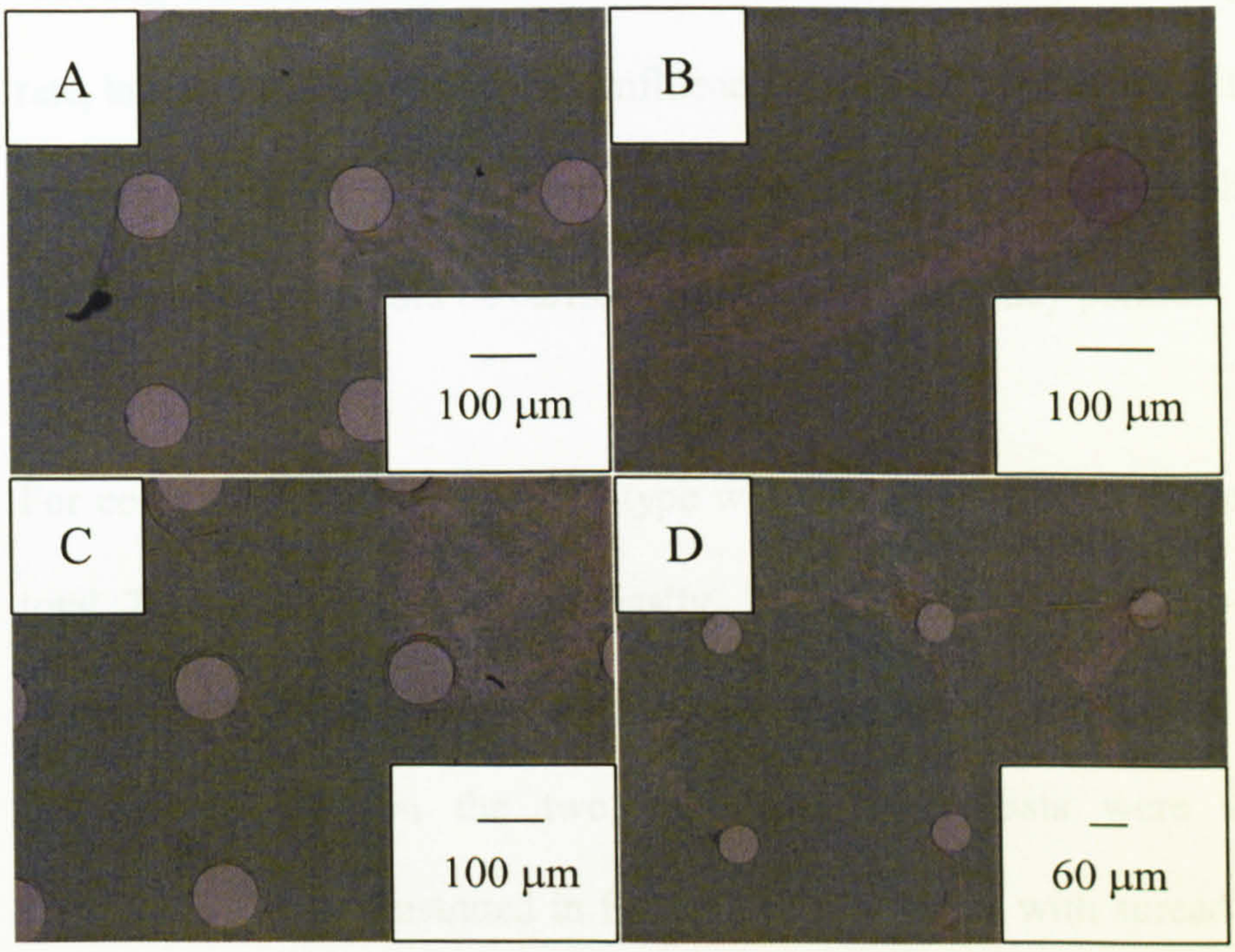

Figure 4.4 Phase contrast microscopy images showing: A/C) overexposed damaged 100 μm pores, B) Underexposed 100 μm pore in which pore has not fully formed and D) overexposed 60 μm pores.

The next stage was to determine an optimal cell seeding density for a short 3-day study that could assess cell behaviour over pore features from low cell populations to high populations. A range of seeding densities from 2000 to 7000 cells/cm^2 was tested on silicon nitride samples. As seen in Figure 4.5, 7000 cells/cm^2 was found to be optimal seeding density for fibroblasts, reaching confluence by 72 hours. Whilst, BAECs had a slower proliferation rate, taking 120 hours to reach confluence. It was decided for consistency that a seeding density of 7000 cells/cm^2 would also be used for endothelial cells and that these studies would be carried out over a longer 5-day period.

For co-culture studies, each cell type was seeded at 3500 cells/cm^2 to make a total 7000 cells/cm^2 seeding density. In the early stages of co-culture, the morphology of fibroblasts and BAECs were found to be quite similar. To differentiate between the two cell types, fibroblasts were stained with Celltracker^{TM}. As illustrated in Figure 4.6, fibroblasts with spread morphology could be observed and the outlines of pores could be seen, thus allowing pore-cell measurements to be made. Measurements were made using light microscopy where both cell types could be observed and then again using fluorescent microscopy where fibroblasts alone could be seen. The difference in the measurements was then assumed to be due to BAEC-pore interactions.

Finally, to prove that cells were covering the pores and not touching the tissue culture plastic below the pore features; pores covered with cells were observed by light microscopy and then the tissue culture plastic below them was focussed on.

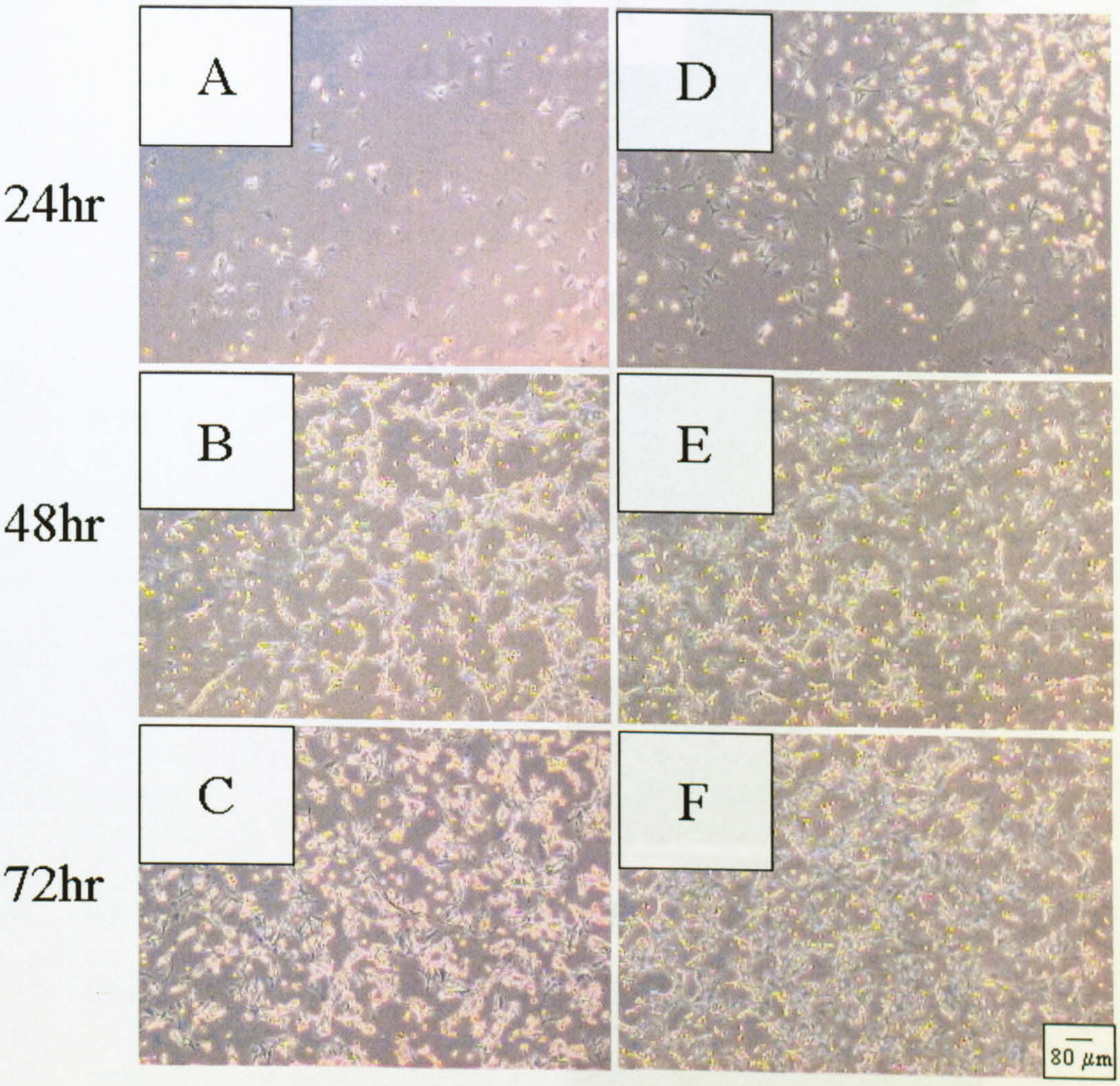

Figure 4.5 Phase contrast microscopy images for determination of optimum cell seeding density.

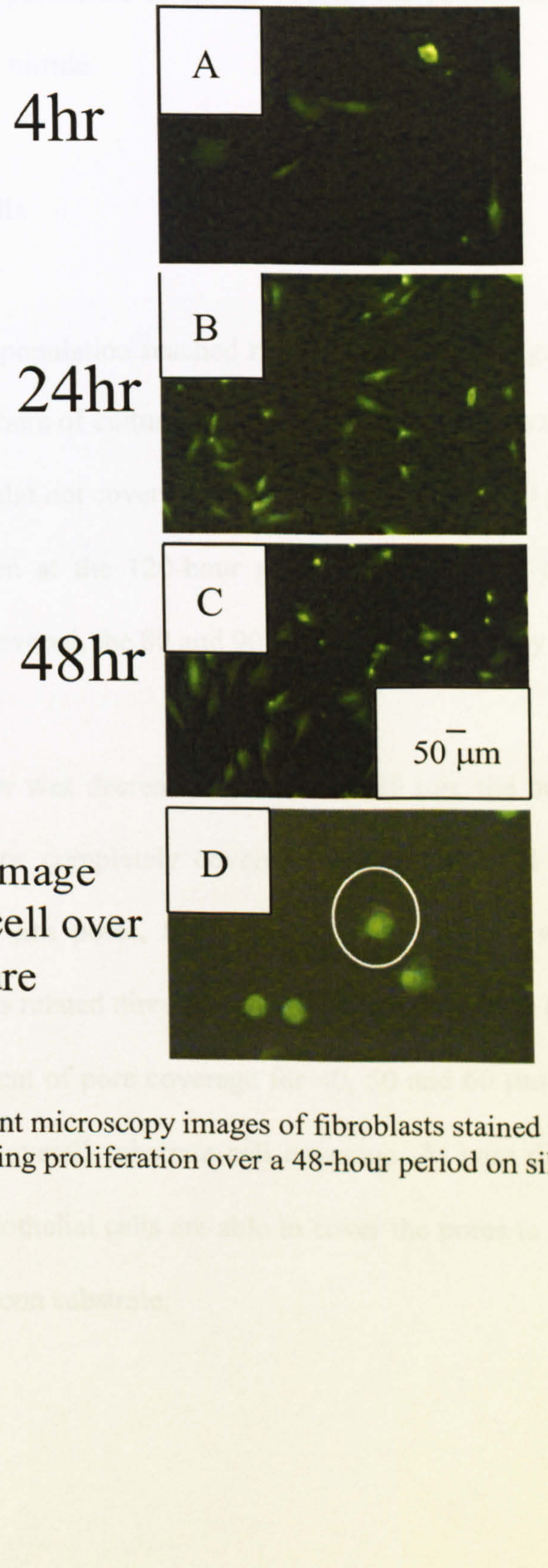

Figure 4.6 Fluorescent microscopy images of fibroblasts stained with CellTracker™ showing proliferation over a 48-hour period on silicon nitride samples

For an example, in Figure 4.7, it can be seen that no cells are present on the TCP below a 160 μm pore covered with fibroblasts. Furthermore, in silicon nitride samples that were damaged during experiments, it was observed that fibroblasts could not proliferate or spread beyond the boundaries of the edges of the cracked silicon nitride.

4.3.2 Endothelial cells

The endothelial cell population reached maximum cell coverage of the silicon substrate after 120 hours of culturing on the samples. As shown in Figure 4.8, the endothelial cells did not cover any part of a pore of 80 or 90 μm diameter at any time point. Even at the 120-hour point, when the rest of surface was essentially entirely covered, the 80 and 90 μm pores were totally uncovered.

As the pore diameter was decreased from 60 to 30 μm, the number of pores that were partially or completely covered by an endothelial cell increased. Considering the 30 μm pores, the probability that a pore was covered or partially covered was related directly to the total pore coverage (Figure 4.8). In comparison, the extent of pore coverage for 40, 50 and 60 μm pore diameters was lower than the overall substrate cell coverage. At pore diameters of less than 30 μm, the endothelial cells are able to cover the pores to the same extent as the rest of the silicon substrate.

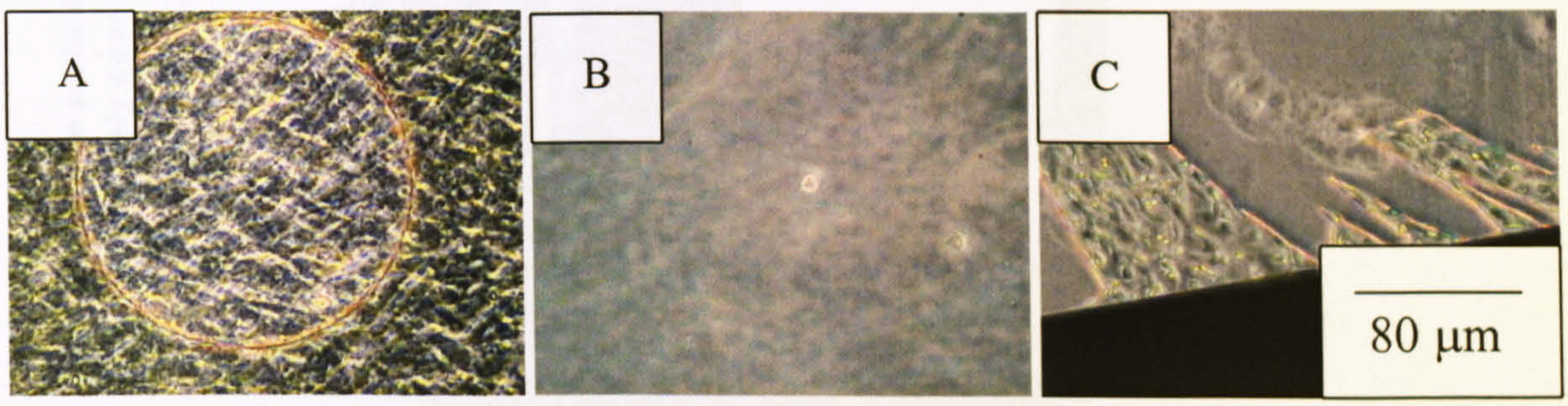

Figure 4.7 Phase contrast microscopy images of A) 160 µm pore covered with fibroblasts, B) Focus on tissue culture plastic below 160 µm pore covered by fibroblasts and C) fibroblasts proliferating within restricted regions of cracked silicon nitride sample.

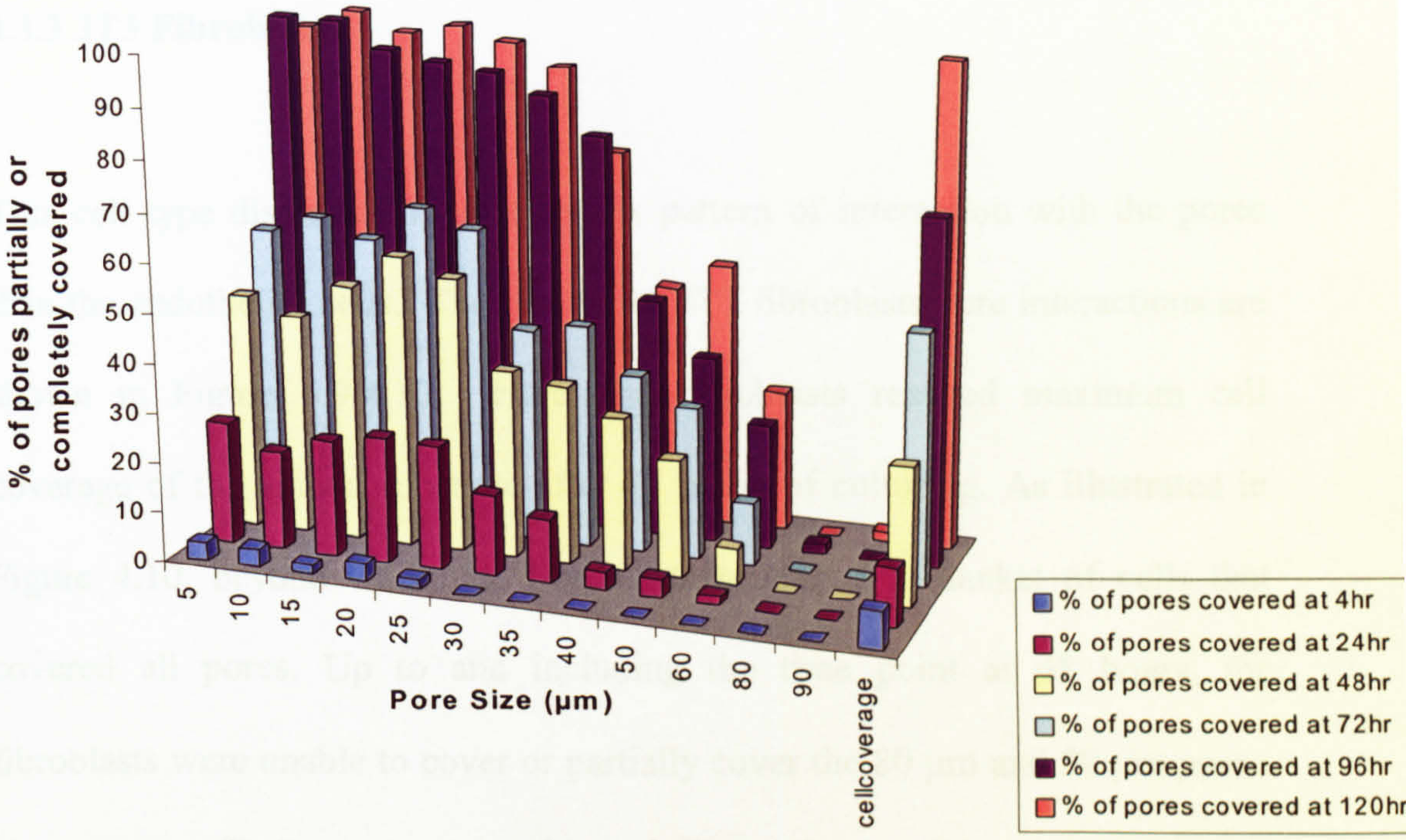

Figure 4.8 Bar chart showing percentage pore coverage with endothelial cells over a 120-hour period.

Overall, it can be concluded that for endothelial cells on this substrate, the cells cannot cover pores of 80 μm or more diameter, are unaffected by pores of 30 μm or less, and a linear relationship exists between cell coverage and pore size between 30 μm and 80 μm.

4.3.3 3T3 Fibroblasts

This cell type displays a more complex pattern of interaction with the pores than the endothelial cells. The results for 3T3 fibroblasts/pore interactions are shown in Figure 4.9/4.10. Here, the fibroblasts reached maximum cell coverage of the silicon substrate after 72 hours of culturing. As illustrated in Figure 4.10, beyond 72 hours, fibroblasts produced a blanket of cells that covered all pores. Up to and including the time point at 48 hours, the fibroblasts were unable to cover or partially cover the 80 μm and 90 μm pores. However, at 72 hours between 20 and 30% of these larger pores became covered.

For the other pore sizes, the trend in fibroblast coverage is less apparent, in comparison with the endothelial cells, with fibroblast coverage found to be more variable. However, in general, fibroblasts were able to cover pores of 50 μm and less.

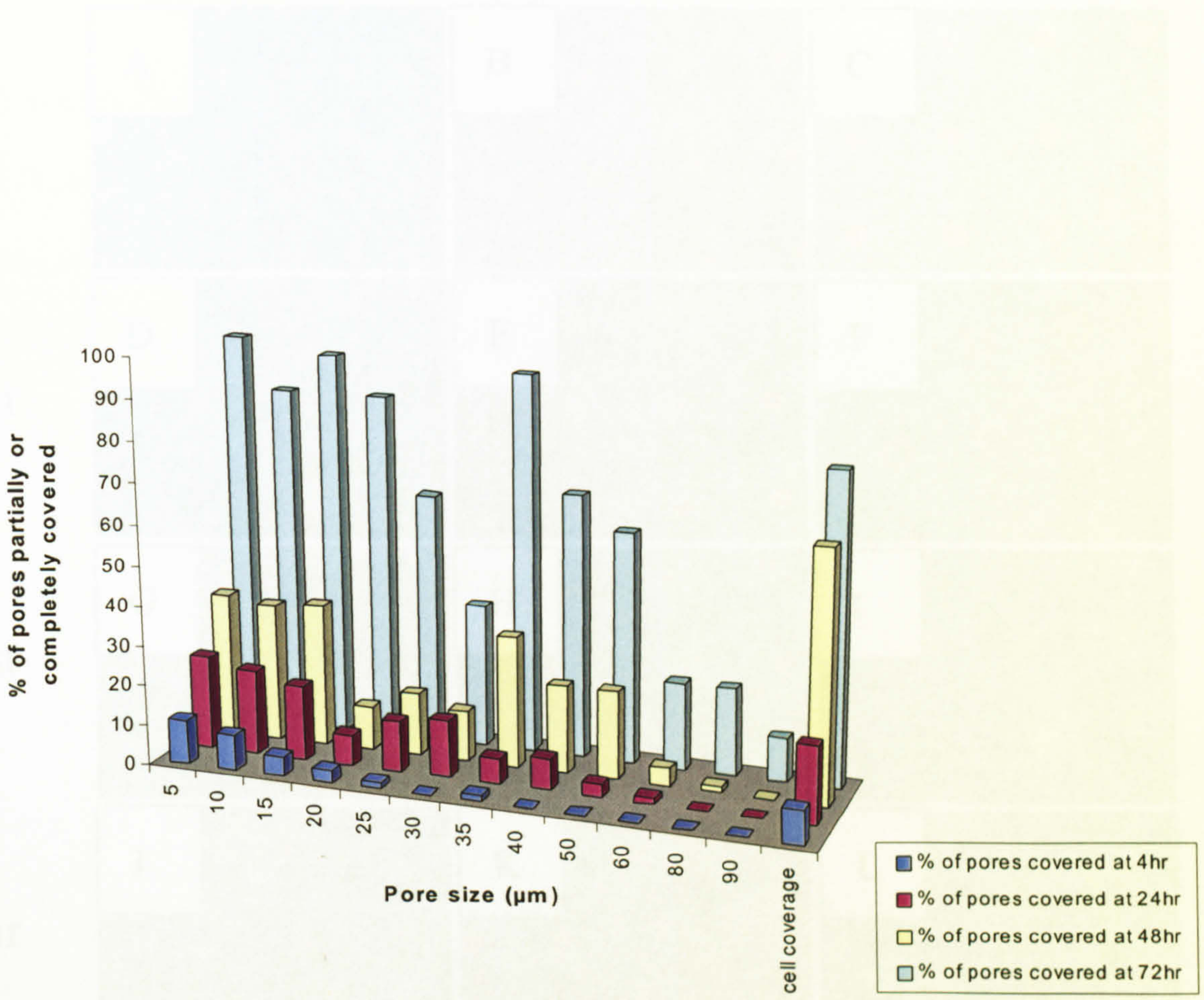

Figure 4.9 Bar chart showing percentage pore coverage with 3T3 fibroblasts over a 72hour period.

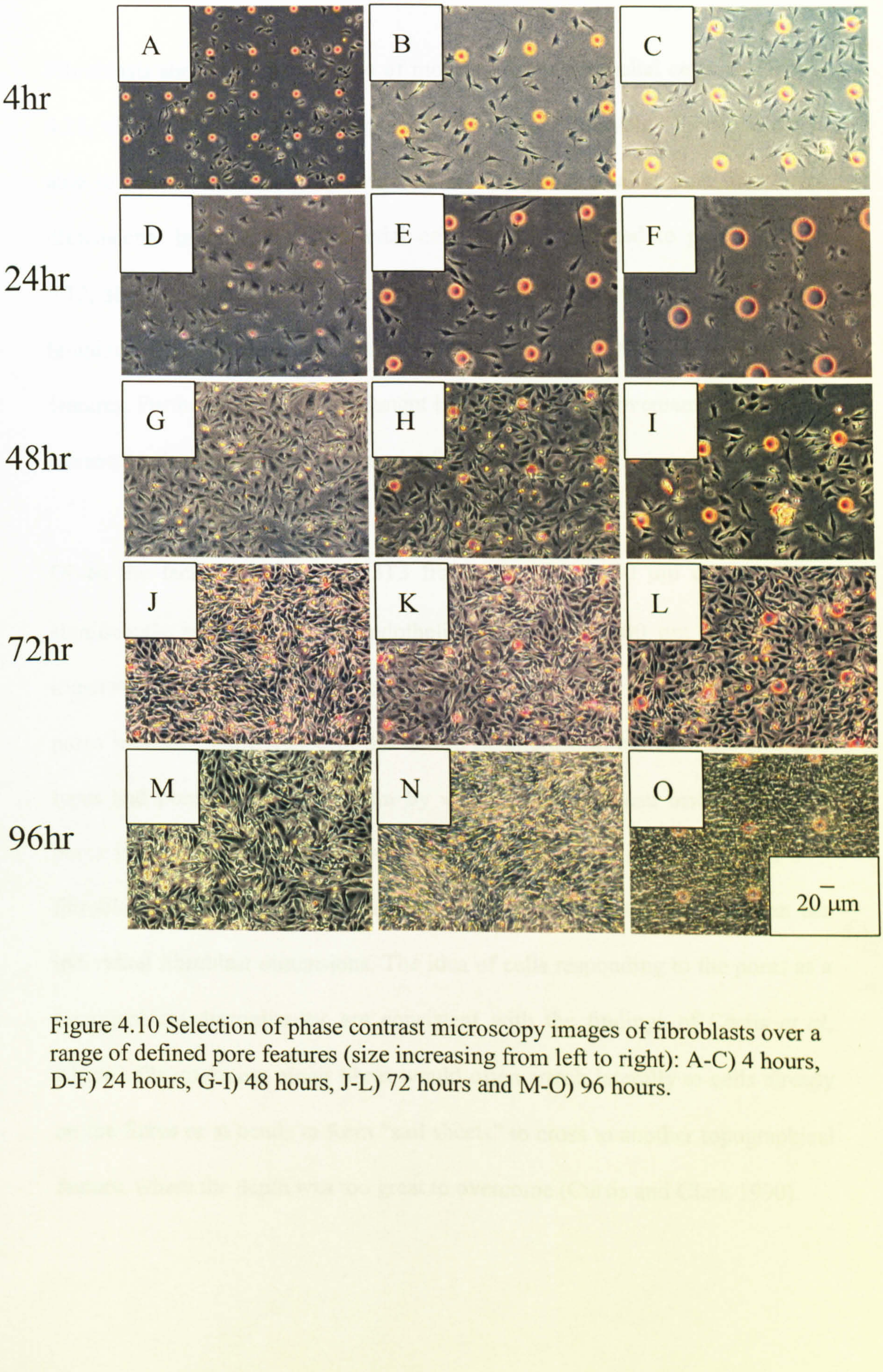

Figure 4.10 Selection of phase contrast microscopy images of fibroblasts over a range of defined pore features (size increasing from left to right): A-C) 4 hours, D-F) 24 hours, G-I) 48 hours, J-L) 72 hours and M-O) 96 hours.

4.3.4 Comparison of endothelial cells and fibroblasts.

Fibroblasts show a greater degree of mobility than endothelial cells. In Figure 4.11, we can see time-lapse images with 10-minute intervals. Fibroblasts are able to move with flexibility over and around pores smaller than their own dimensions. In contrast, endothelial cells become attached to pores. Figure 4.12, shows low cell density images of endothelial cells on a variety of pore templates. The endothelial cells appear to attach preferentially to the pore features. Furthermore, once attachment has taken place, movement is limited to advance and retraction around the pore features.

Given the fact that the spread 3T3 fibroblasts (20 to 50 μm diameter) are significantly smaller then the endothelial cells (60 to 200 μm diameter) as illustrated in Figure 4.13, the ability of the smaller cell type to cover larger pores indicates a difference in the nature of interaction between the two cell types and pores. The mechanism by which fibroblasts can bridge the large pores is shown in Figure 4.14 where time-lapse images show confluent 3T3 fibroblasts use neighbours as supports to cross pore features larger than the individual fibroblast dimensions. The idea of cells responding to the pores as a topographical discontinuity, are consistent with the findings of Curtis *et al*, where cells migrating along fibres would often attach laterally to cells already on the fibres or at bends to form "sail sheets" to cross to another topographical feature, where the depth was too great to overcome (Curtis and Clark 1990).

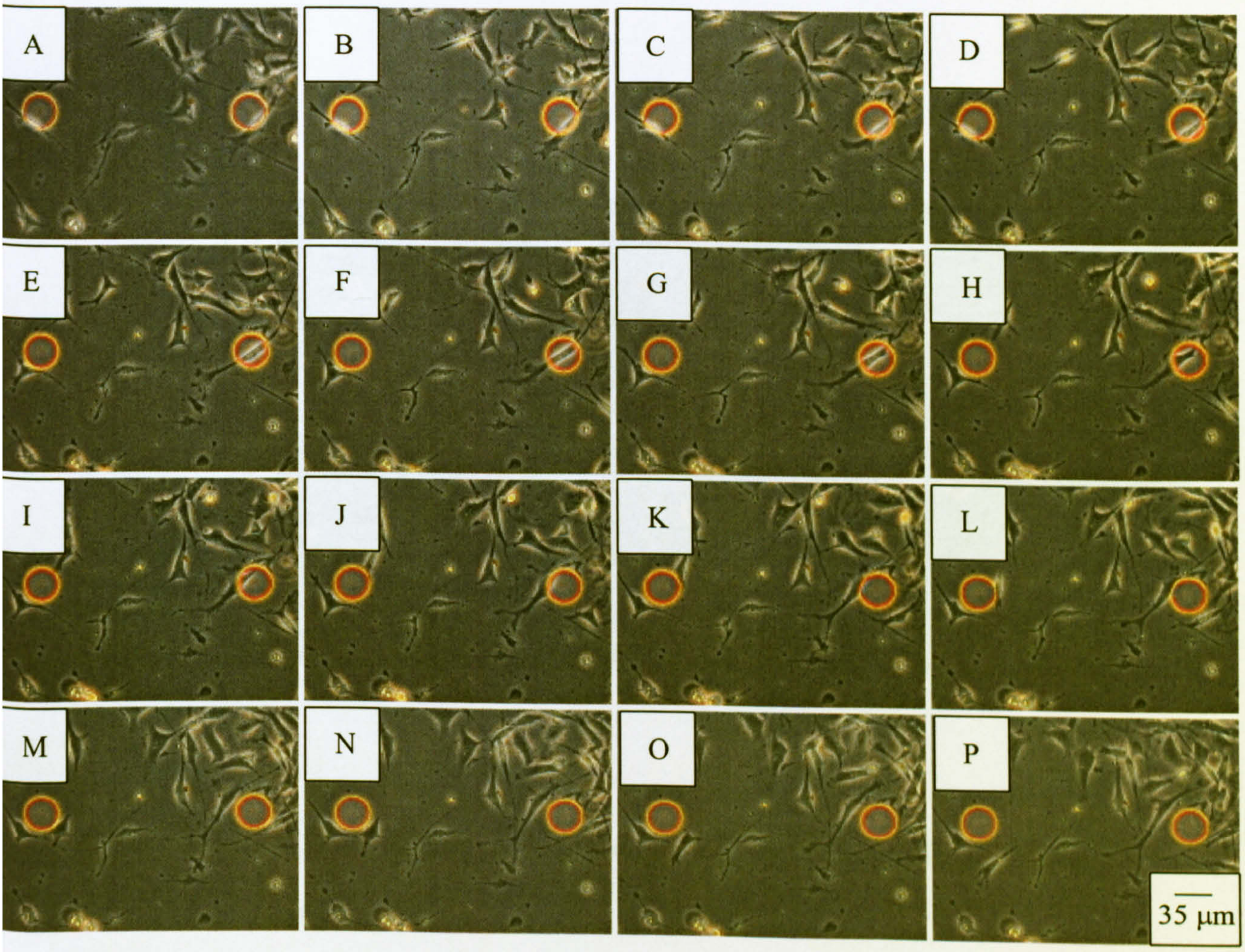

Figure 4.11 Time-lapse images of 3T3 fibroblasts over 35 µm pores: A-P) 10 minute intervals.

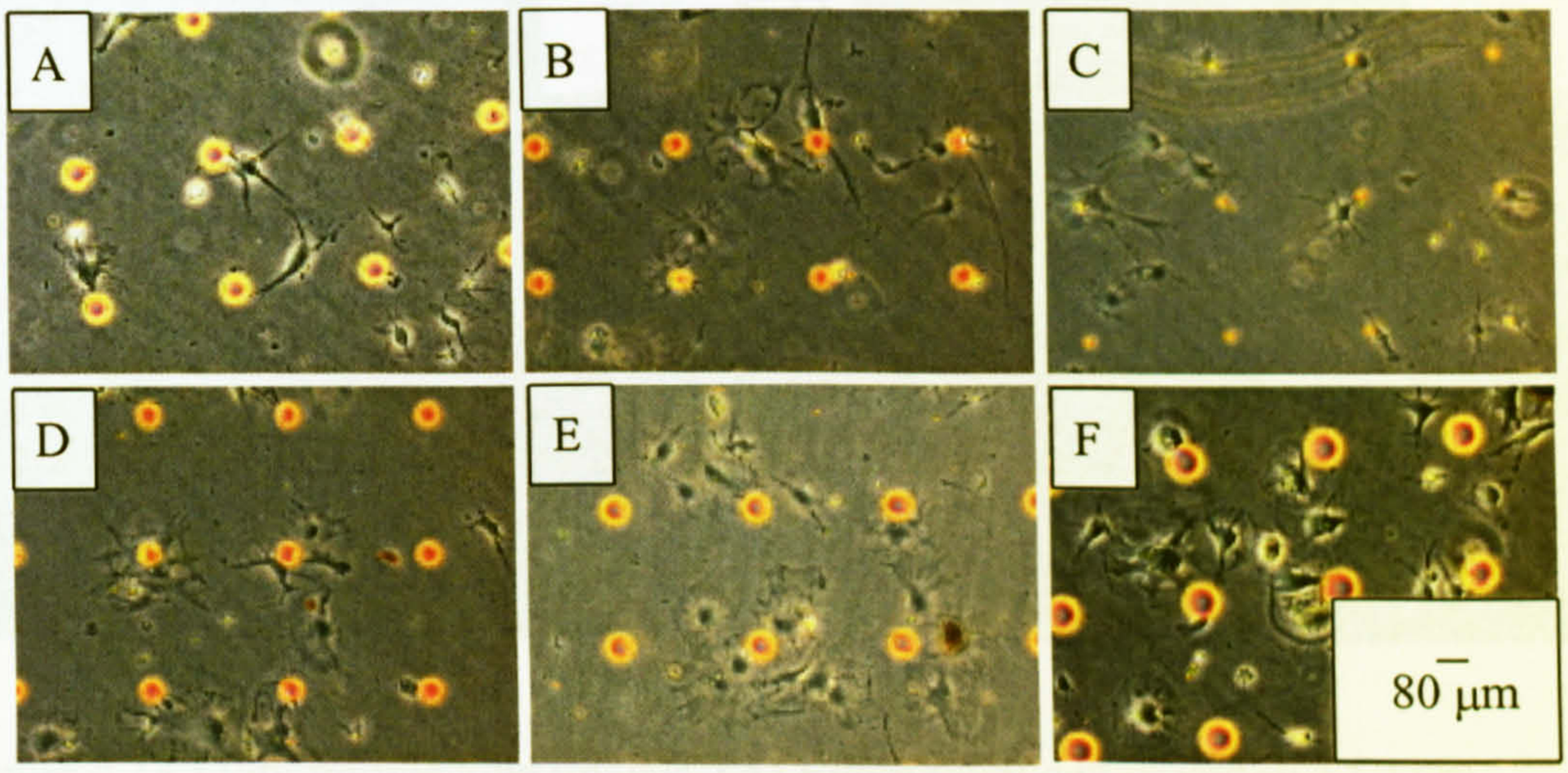

Figure 4.12 Phase contrast microscopy images of endothelial cells attaching to a range of pore features.

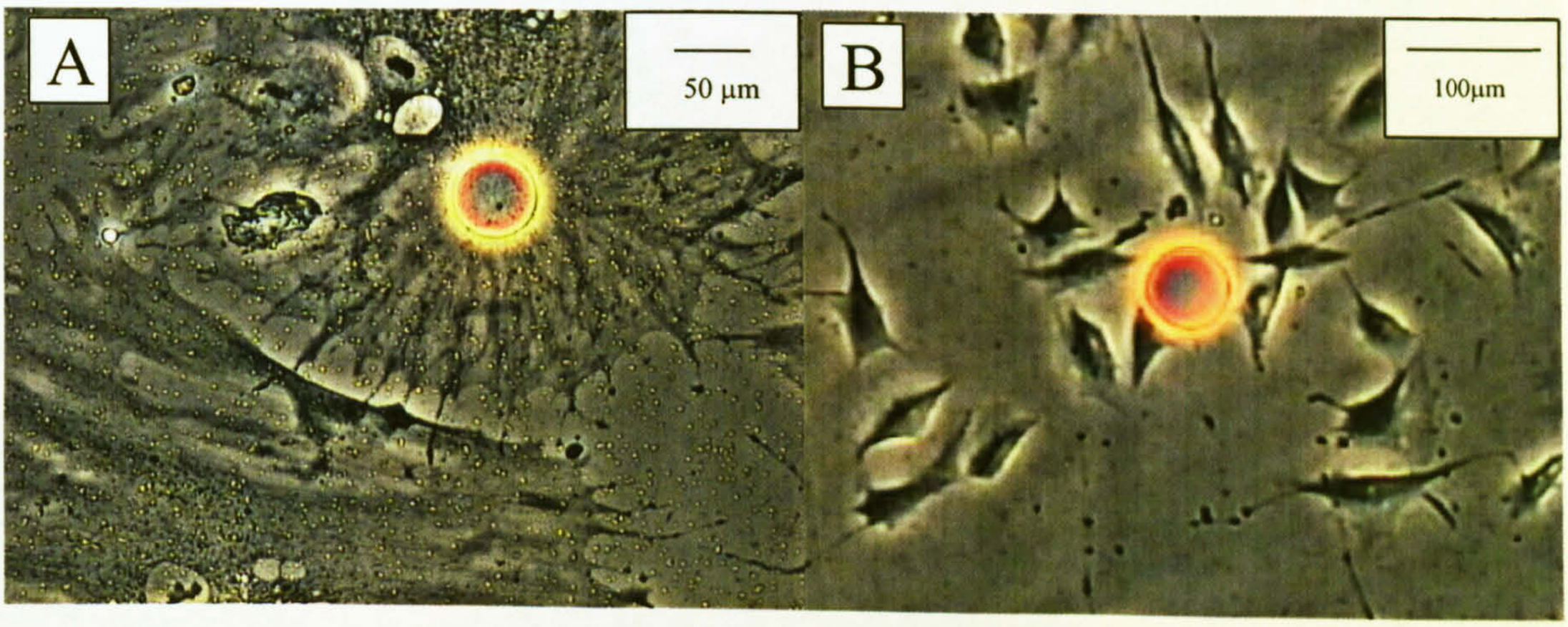

Figure 4.13 Light microscope images (A) Endothelial cell covering a 50 µm pore. (B) 3T3 fibroblasts spreading around 60 µm pore.

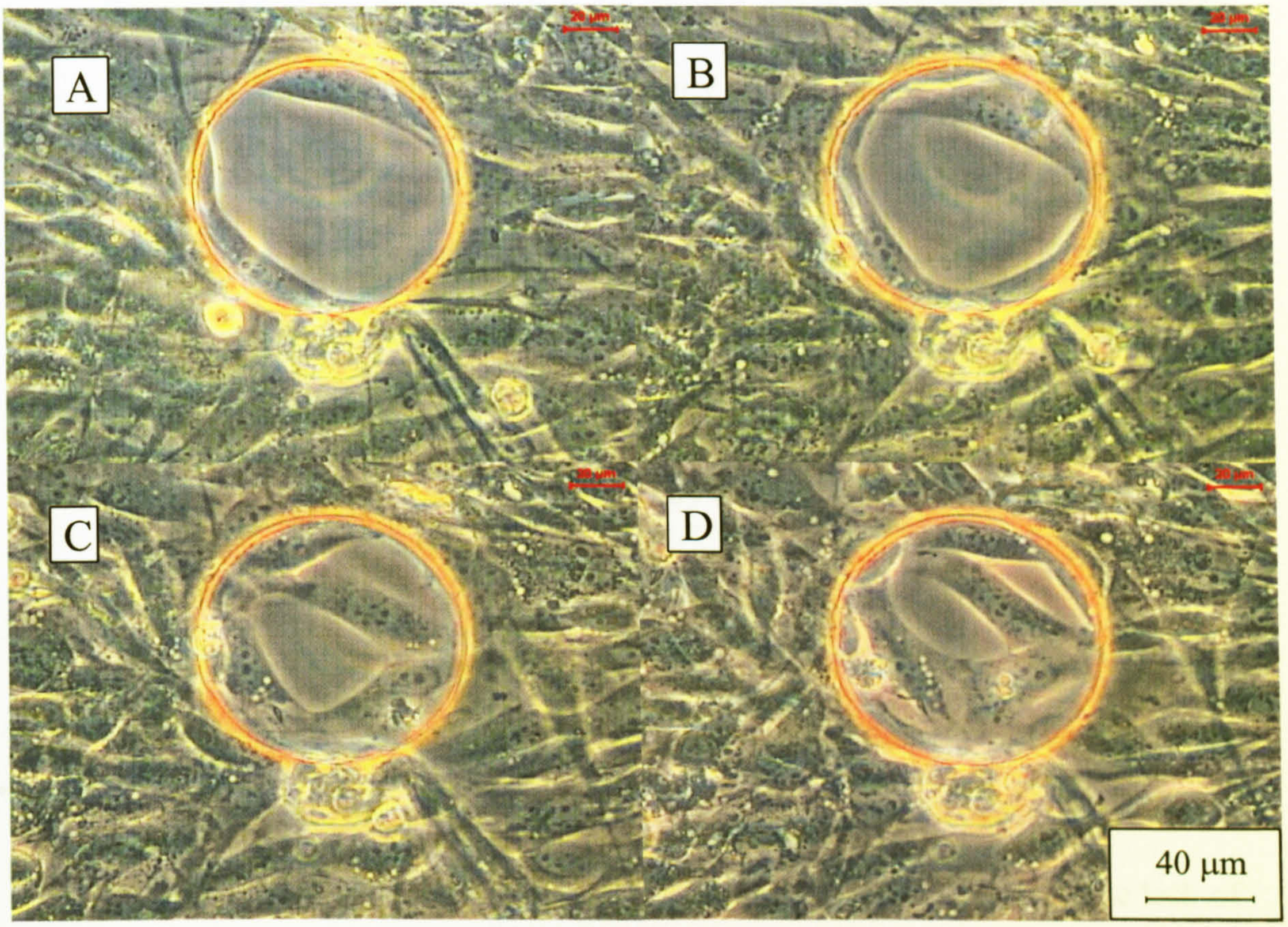

Figure 4.14 Fibroblasts displaying co-operative behaviour at confluence to cross a 100µm pore over a 6-hour period. (A) 0 hours (B) 2.5 Hours (C) 5.0 Hours (D) 6.0 hours.

The difference in the behaviour of the two cell types can be highlighted further through phalloidin staining, which confirms that the cells are responding to the pores as topographical discontinuities. Fluorescence microscopy images in Figure 4.15 show the two cell types around pores fixed with glutaraldehyde and stained with phalloidin. Light intensity cross-sections of the images reveal the lateral variations in the cytoskeletal distribution of each cell type. The cytoskeleton in the endothelial cells (Figure 4.15a) is limited by the boundary of the pore with concentrated regions of cross-linked actin around the edge of the topographical feature. In contrasts, the distribution of cytoskeleton in fibroblasts (Figure 4.15b) is unchanged by the pore boundary.

Thus, the cell's mobility may be reflected by the amount and organisation of actin monomer present in the cell. With the endothelial cells, the actin monomer is polymerised at the pore edge. This results in concentrated regions of cross-linked actin around the edge of the topographical feature. The lack of further actin reflects its reduced ability to form new focal adhesion contacts, thus restricting movement of the cell to near or around the pore. Fibroblasts reorganize and redistribute the actin, which also form focal adhesion points at the edges of the pore. However, the fibroblasts form further focal contacts allowing them to orientate around the pore features and display greater mobility. As a result, the fibroblasts are able to cross the boundary of the pore and then use their neighbouring cells as support structures.

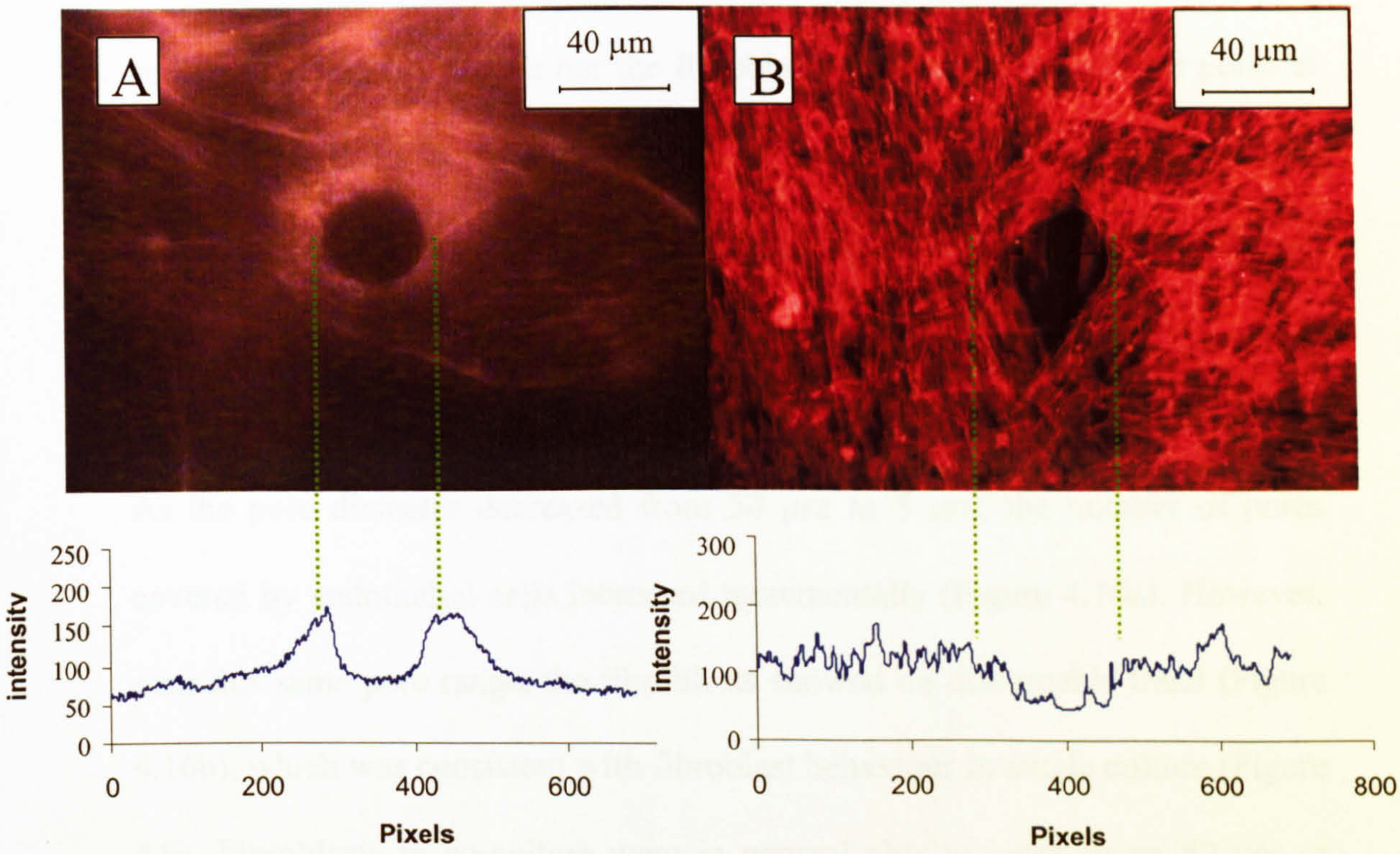

Figure 4.15 Phalloidin stained images with analysis of cross-section to show cytoskeletal distribution of actin at the topographical features with (A) Endothelial cells over a 40-μm pore (B) 3T3 fibroblasts around a 50 μm pore.

4.3.5 Endothelial cells and 3T3 fibroblasts in co-culture

3T3 fibroblasts in co-culture proliferated faster than the endothelial cells, reaching 70% of the cell population at confluence (Figure 4.16). In co-culture, neither the endothelial cells nor the fibroblasts covered 90 or 100 μm pores at any time point. Even at the 96 hours time point, when the rest of the surface was almost entirely covered, the 90 and 100 μm pores remained uncovered (Figure 4.17).

As the pore diameter decreased from 50 μm to 5 μm, the number of pores covered by endothelial cells increased incrementally (Figure 4.16a). However, over this same pore range, the fibroblasts showed no discernable trend (Figure 4.16b), which was consistent with fibroblast behaviour in single culture (Figure 4.9). Fibroblasts in co-culture were in general able to cross pores 50 μm or smaller, once a critical cell density had been achieved. The single culture of fibroblasts showed that a 77% cell density was required before 80 to 90 μm pores would be covered (Figure 4.9). Therefore, with the fibroblasts only reaching a maximum of 70% of the total cell population in co-culture, there was not a sufficient cell density of fibroblasts to cross the 90 or 100 μm pores. This indicates that endothelial cells and fibroblasts will not co-operate in crossing the pore features. The addition of endothelial cells thus has an inhibitory effect by preventing fibroblast-to-fibroblast co-operation over pore features in the co-culture.

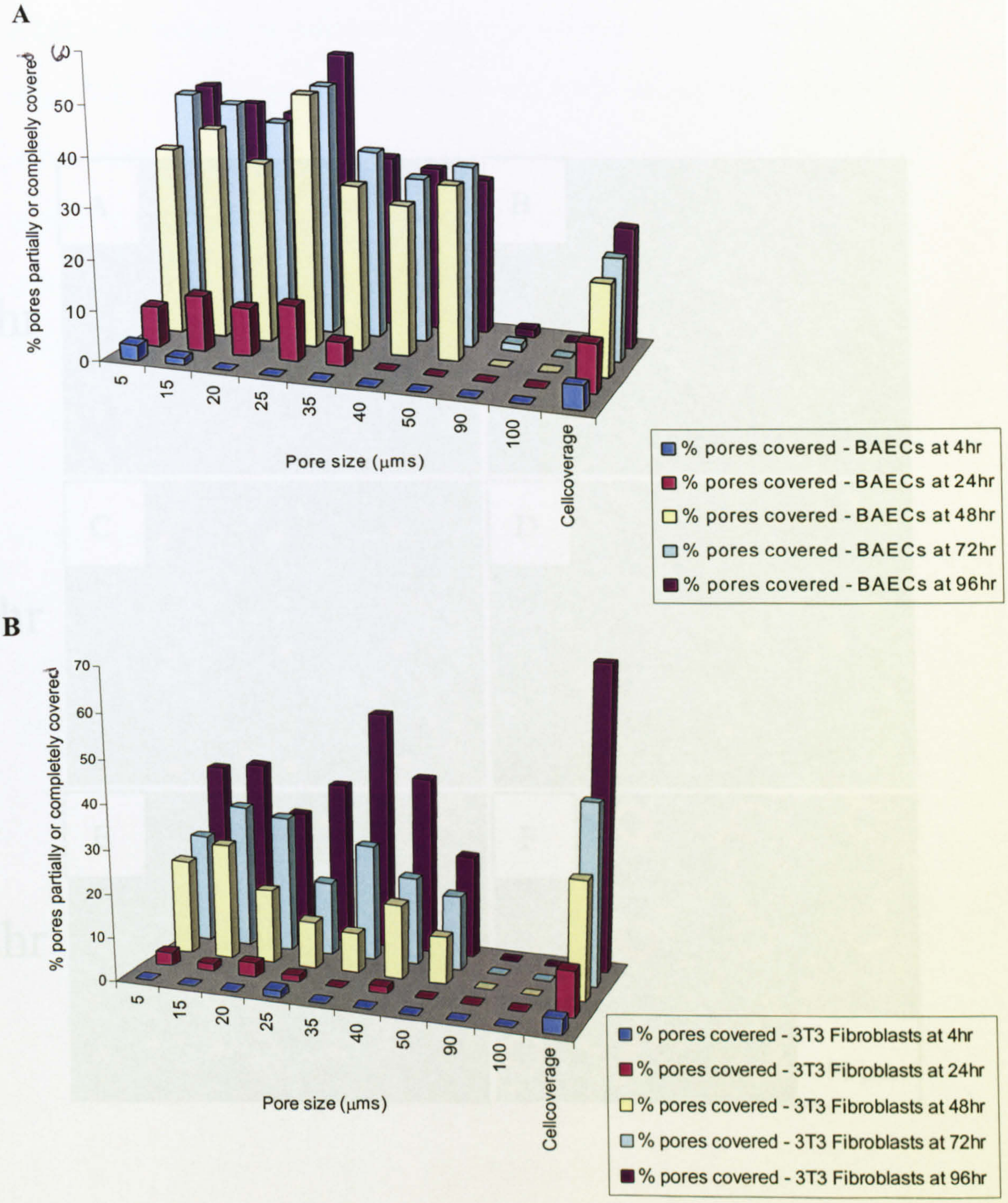

Figure 4.16 Bar charts showing percentage pore coverage by a) endothelial cells in a endothelial-fibroblast co-culture and b) fibroblasts in a endothelial-fibroblast co-culture over a 96hr period.

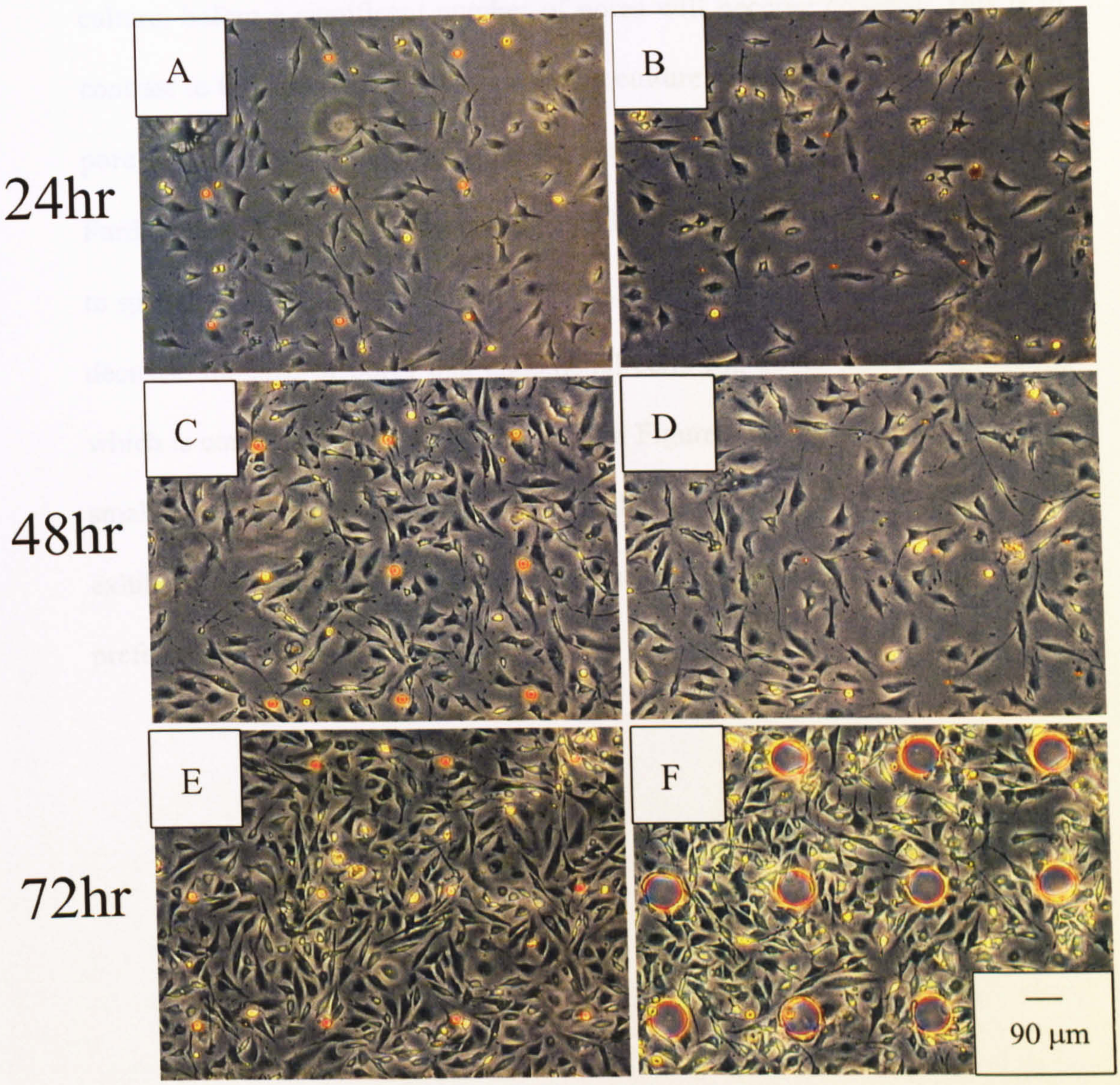

Figure 4.17 Selection of phase contrast microscopy images showing endothelial cells and 3T3 fibroblasts in co-culture between day 1 and 3.

Whilst the larger pores were not covered by the endothelial cells in either single or co-culture, the endothelial cells will cover pores in the 50 to 5μm range. However, they appear to require a critical cell density within the co-culture, before a significant number of pores will become covered. This is in contrast to the endothelial cells in a single culture, where the probability that a pore was covered was increasing monotonously with total pore coverage. Furthermore, Figure 4.16 shows that endothelial cells in co-culture are not able to spread as effectively as endothelial cells in single culture. This will therefore decrease the size of pores that endothelial cells can cover through spreading, which is confirmed in the data presented in Figure 4.9. However, despite their smaller sizes, endothelial cells in co-culture, as illustrated in Figure 4.17 exhibited behaviour similar to the single culture of endothelial cells, showing a preferential attachment to pores.

4.4 Conclusion

The colonisation of biodegradable polymer scaffolds with cell populations has become established as the foundation for the engineering of a number of tissues, including cartilage, liver and bone. The formation of tissues *in vivo* necessitates the vascularization of such scaffolds if blood vessels are to reach the tissue. The infiltration of fibrous vascularized tissue results however in decreased porosity within the scaffold. Predicting the interactions between these cells and pores is important if scaffold characteristics are to be optimised.

This study of cells over defined pore features has determined that cell behaviour is interlinked by three factors:

1. Cell type
2. Pore size
3. Cell density

It has also been shown that the cells respond to the pores as topographical discontinuities. The difference in behaviour of the two cell types is related to the cytoskeletal structure and actin monomer content. Fibroblast cells displayed greater mobility and a co-operative pattern of cell spreading in which pores with diameters greater than the cell dimensions were bridged by groups of cells using their neighbours as supports. In co-culture, this behaviour was inhibited to some extent by the endothelial cells by preventing fibroblast-to-fibroblast interactions.

Endothelial cells were unable to use neighbours as support structures and failed to bridge pores greater than the cell diameter in either single or co-culture. The endothelial cells appeared to attach preferentially to pores treating them as topographical discontinuities. Movement by these cells was then limited to around the pore feature. Furthermore, the large spread of endothelial cells is inhibited by fibroblasts in co-culture.

In both cell types, cell density and pore size affected percentage pore coverage significantly. These results confirm that within a tissue engineering scaffold cells displaying fibroblast behaviour will tend to block pores even where the pore diameter is greater then the cell diameter, but that this behaviour can be modulated by the addition of non-fibroblastic cell types.

These results show that the ability to control pore size is essential in controlling cell behaviour. This, therefore, provides the impetus for the manufacture of an injectable scaffold with highly porous morphology.

CHAPTER 5

PHYSICO-CHEMICAL CHARACTERISATION OF AN *IN SITU* SELF-ASSEMBLING POROUS SCAFFOLD FOR TISSUE ENGINEERING.

5.1 Introduction.

A major goal of tissue engineering as described in Chapter 1, is the concept of growing cells within three-dimensional support scaffolds (Hutmacher 2000). Scaffold materials must satisfy a number of requirements. The solid phase must be biocompatible and promote cell adhesion and growth. Over time, as the cells produce their own ECM, the scaffold should degrade. Processing techniques must be able to produce irregular shapes to match those of the tissue to be replaced. High porosity is needed for cell seeding, ingrowth and successful vascularization of the scaffold. The material must also have sufficient mechanical strength for handling and *in vivo* loading.

In broad terms, scaffolds are either a pre-formed water-insoluble matrix, with large interconnected pores, within which cells are seeded or a hydrogel that solidifies around the cell population (Burg *et al.* 2000; Kuo and Ma 2001). The

matrix scaffold is formed before cells are seeded and then it is either placed in a bioreactor for *in vitro* tissue formation or implanted into a patient for augmented *in vivo* tissue regeneration. Whilst, the three-dimensional cell culture environment within these porous scaffolds is favourable to tissue regeneration, the need to pre-form the scaffold before seeding and implantation is problematic. Cell seeding methods are inefficient due to poor transport of the cells through the matrix and cell damage. In terms of implantation, the scaffold must be shaped to fill a cavity within the body, requiring knowledge of the cavity dimensions and limiting the shape of cavity that can be filled. In addition, an invasive operation is required to deliver the large biomaterial.

In contrast, a number of hydrogel materials have been designed that can be delivered directly into the body through a syringe. The gel forms within the body following a trigger signal. These include thermosensitive, biodegradable hydrogels consisting of blocks of poly (ethylene oxide) and poly (lactic acid) that display an upper critical solution temperature, forming liquids that are injectable at temperatures around 45°C and gels at body temperature (Jeong *et al.* 1997). Other systems include the use of acrylated PEG as a non-toxic crosslinking reagent to produce polymer networks with acrylated polylactic acid and acrylated copolymers based on lactic acid, which can be polymerised *in situ* (Han and Hubbell 1997) (Elisseeff *et al.* 1997). Water-insoluble interpolymeric complexes (IPC) containing poly (methacrylic acid) (PMA) 15 kDa and polyethylene glycol (PEG), 20 kDa, in an organic solvent system that undergoes a sol-gel phase transformation when injected into a pH 7.4 buffer and the release of calcium from lipids to cross link alginates also demonstrate the wide variety of *in situ* transformations that are possible (Joshi *et al.* 1999)

(Westhaus and Messersmith 2001). A comprehensive review of *in situ* transforming biomaterials can be found in Chapter 1

Such systems have the advantage that they can fill cavities of any shape without prior knowledge of the cavity dimensions. However, such hydrogels lack large interconnected porous networks, and hence the barrier of diffusion to signalling and nutrient molecules limits tissue formation. The lack of a porous structure also significantly reduces the scaffold's ability for vascularization. In addition, the mechanism of gelation may damage cells, hence prohibiting co-administration of cells.

The aim of this work was to combine the advantages of injectable scaffolds with the necessary porosity of traditional water-insoluble scaffolds. Such a scaffold would require a trigger to transform once *in situ*, must be biodegradable and cell interactive. In Chapters 5 and 6, the development of a new porous scaffold is described that can be delivered by syringe into a tissue or cavity as a polymer and/or cell slurry. Immediately following delivery, the slurry would potentially self-assemble into a porous scaffold with cells distributed throughout. Self-assembly involves the cross-linking of polymer particles by the avidin-biotin mediated interaction. The self-assembly process could occur under physiological conditions and does not require cell harmful trigger signals such as UV irradiation. This is achieved by forming the polymer component of the scaffold, with microparticles manufactured from the biodegradable PLA-PEG-biotin synthesized in Chapter 3. The use of PLA-PEG microparticles in drug delivery and tissue engineering is established and thus common methods could be employed to signal to the cells within the scaffold

through growth factor delivery or integrin-mediated adhesion (Cannizzaro *et al.* 1998; Babensee *et al.* 2000).

The potential for avidin to act as a crosslinking agent in aggregation has been previously described for a number of biotinylated moieties. For an example, in a study based on the aggregation kinetics in affinity purification of biotinylated liposomes, Lynch *et al* showed that the aggregation kinetics were primarily determined by the biotin density on the liposome surface, the stochiometric ratio of avidin molecules to liposomes and the liposome concentration (Lynch *et al.* 1996; Lynch *et al.* 1996). Although liposomes as drug delivery and tissue engineering devices suffer from inherent problems such as low encapsulation efficiencies, rapid leakage of water-soluble drugs in the presence of blood components and poor storage stability (Soppimath *et al.* 2001), the parameters for aggregation used in their studies are likely to be significant for the aggregation of PLA-PEG-biotin microparticles. Further studies on the organization of inorganic nanoparticles using biotin-streptavidin connectors for the manufacture of ferritin-based arrays have been carried out by Li *et al.* It was found that there was a critical ratio of avidin to biotinylated ferritin molecules for supramolecular structures to be formed. Above and below these critical amounts of avidin, the turbidity decreased: thus indicating that the aggregate size was smaller (Li *et al.* 1999). Finally Chiruvolu *et al* showed higher order self-assembly of vesicles could be achieved by utilizing the biotin-avidin interaction in a two stage self-assembly process. In the primary self-assembly process, lipid molecules self-assembled into spherical vesicles as a result of non-specific intermolecular forces. These spherical vesicles then self-

assembled into the higher order structures using the biotin-streptavidin mediated interaction (Chiruvolu *et al.* 1994)

In Chapter 5, the manufacture of the microparticles that form the foundation of the self-assembling scaffolds is described. Evidence that these particles will undergo the binding process is assessed by SPR. The aggregation process is then probed and optimized using a variety of quantitative and qualitative techniques and finally the viscoelastic properties of the scaffold are evaluated. For the tailoring of mechanical properties, a gel-forming component, biotin-PEG-biotin is introduced and its impact on the scaffold assessed.

5.2 Methods and materials

5.2.1 Preparation of PLA-PEG-biotin

PLA-PEG-biotin was synthesised as described in Chapter 3.

5.2.2 Preparation of Biotin-PEG-Biotin

α-ω-bis(amine) PEG (1g) was dissolved into acetonitrile (2ml), methylene chloride (1ml), Et_3N (80μl) and NHS-Biotin (0.50g). The reactants were stirred overnight under argon and then worked-up by diethyl ether (40ml) to precipitate the polymer. The isolated material was then dissolved in hot isopropanol (70°C) to give an opaque-cloudy solution. On cooling, the product was filtered and lyophilised.

5.2.3 Preparation of nano/microparticles

500mg of PLA-PEG-biotin was dissolved in 20ml of dichloromethane (DCM) to produce a 25mg/ml solution. PVA (250000 Mw) [88% hydrolysed] was dissolved into ELGA water (0.25g into 250 ml) to make a 0.1% w/v solution. The PLA-PEG-biotin solution was then added to a homogenised PVA solution using a 5ml Gilson pipette. The mixture was homogenised for a further 10 minutes at 1500 rpm and then left stirring overnight for DCM to evaporate and microparticles to form. Nanoparticles were prepared as above with a 9% PVA solution and homogenisation at 5000 rpm and a 5mg/ml solution of PLA-PEG-

biotin. Further nano/microparticles were manufactured using 0.1, 1 and 9% PVA at stirring rates of 1500, 3500 and 5000 rpm.

5.2.4 Preparation of scaffold composites

Avidin saturated microparticles were prepared by placing PLA-PEG-biotin particles in an excess of avidin, centrifuging and washing. The excess amount of avidin was determined on the basis of aggregation studies. This quantity increased with decreasing size of particles. A typical batch was prepared by introducing 10 mg microparticles into a stirring 10 ml aqueous solution of 20 mg avidin.

Biotin-PEG-biotin was introduced to scaffolds by dissolving the biotin-PEG-biotin in water and introducing this solution to the avidin bound microparticles. Where percentage proportions of the scaffold are quoted, these are weight-by-weight proportions e.g. a 10 mg (30% biotin-PEG-biotin/50% avidin saturated microparticle) scaffold will be made up of 3mgs biotin-PEG-biotin dissolved in 2 mg water which has then been introduced to 6 mgs avidin saturated microparticles. For the purposes of measuring the effects of avidin on aggregation and rheometry of microparticles where the quantities of material tested varied, the ratio of the microparticles to the avidin on a weight by weight basis are quoted. In the aggregation studies, the avidin activity was not assayed and this data must therefore be considered qualitative. However, data on the molar binding affinity of the biotin in PLA-PEG-biotin can be found in chapter 3. Avidin has an activity of 10-15 units per mg, where 1 unit will bind 1 μg of d-biotin

5.2.5 Surface plasmon resonance (SPR)

The SPR equipment (Ortho Clinical Diagnostics, Chalfont, St-Giles, UK) employs a Kretschmann configuration with a monochromatic laser source of 780nm wavelength and silver coated glass slides biotinylated by incubating in a 0.1 mg/ml solution of N-([6-biotinamido-]hexyl-)3'-[2'pyridylthio] propionamide in TFE. PLA-PEG-Biotin nanoparticles (250nm) were saturated in excess avidin and washed using centrifugation. The avidin-saturated nanoparticles (1.5×10^{-7} M), were then prepared in 10 mM sodium phosphate buffer (pH 7.4). For the purposes of a stable baseline reading, a sodium phosphate buffer wash (10mM, pH 7.4) was first passed over the biotin-HPDP functionalised surface for 100 s. Avidin functionalised surfaces were then obtained by flowing avidin solution (1.5×10^{-7} M) over the biotinylated slides. To remove any excess avidin, sodium phosphate buffer (10mM, pH 7.4) was then washed over the surface. Then biotin-PEG(3350)-biotin (1×10^{-6} M) was flowed across the sample surface, followed by a buffer wash. Avidin-saturated nanoparticles (1.5×10^{-7} M) were then flowed over the surface followed by a buffer wash. As a control experiment, unsaturated PLA-PEG-Biotin nanoparticles (1.5×10^{-7} M, 250nm), were injected in place of the avidin-saturated nanoparticles following the avidin and biotin-PEG-biotin injections. A further control involved injecting avidin alone over the experimental time period. The flow rate was 0.24 mL/min with results taken from at least 8 repeats. The change in the SPR angle was monitored over time, in units of millidegrees angles (mDA) where 1 mDA = 0.001°.

5.2.6 Microscopy

Phase contrast images were taken on an optical microscope (Leica DMIRB) attached to a Leica Q500 IW using a colour video camera (JVC TK-C1380). This was equipped with a fluorescence filter to enable fluorescein imaging.

5.2.7 Transmission Electron Microscopy

Visual evaluation of the nanoparticles before and after the addition of avidin was performed using transmission electron microscopy (TEM). 20 µl of sample (5 µg/ml) in PBS were placed onto copper grids for 5 minutes. Excess liquid was blotted with filter paper, and the process was repeated. Following air-drying, grids were then negatively stained by floating on a drop of phosphotungstic acid solution (3% w/v) (adjusted to pH 4.74 with KOH) for 20 minutes, after which they were washed once in 50% ethanol and then twice in distilled water, prior to being air-dried again. Grids were analysed on Jeol Jem 1010 TEM (Jeol (UK) Ltd, Welwyn Garden City, UK), operating at a voltage of 80 kV.

5.2.8 Cryo Scanning Electron Microscopy (Cryo-SEM)

CryoSEM was chosen over traditional SEM so that aggregated microparticles detected were as a result of the receptor-mediated binding interaction and not dehydration. Samples were prepared by mixing samples of microparticles with the optimum amounts of avidin for aggregation in distilled water. These samples were then placed onto the sample holder coated in colloidal graphite

and rapidly frozen in liquid nitrogen (-210°C), etched under vacuum (-80°) and gold-coated. Images were obtained at 25 KeV on a Philips 505 scanning electron microscope equipped with a Hexland CT1000 cryostation, maintaining the specimen at –180°C throughout.

5.2.9 Nanoparticle Size analysis:

Nanoparticle size was determined using photon correlation spectroscopy (PCS) (Malvern S4700 PCS system, Malvern Instruments Ltd, Malvern, UK). The analysis was performed at a scattering angle of 90°C and at a temperature of 25°C using 1 ml samples diluted with filtered water (0.2 μm filter, Minisart®, Germany). For each sample, the mean diameter ± standard deviations of six determinations were calculated applying multimodal analysis. Values shown are the mean diameter for two replicate samples. The final concentrations of nanoparticles were prepared by suspending 50 μg of the nanoparticles in 1, 2 and 10ml of water. Varying avidin quantities were then introduced to stirring or agitated suspensions of the nanoparticles. Random 100 μl samples were then taken and diluted to 1 ml with filtered water.

5.2.10 Spectrophotometer sedimentation studies

10 mg samples of PLA-PEG-biotin microparticles (≈10 micron) were prepared in 1 ml aliquots of water with varying concentrations of avidin (0 to 10 mg). Kinetic studies over a period of 60 minutes were carried out using the 1ml samples on the Beckman DU640 spectrophotometer with an analytical

wavelength of 700 nm at 37°C with a read average time of 5 seconds. Gradients were calculated using linear lines of best fit.

5.2.11 Particle size measurement

The evolution of size of the aggregates was monitored using a particle size analyser (Coulter LS230). The instrument applies the principle of forward light scattering by particles to measure the particle size distributions. The size distributions were estimated by fitting the intensity of the scattered light (λ = 750 nm) as a function of the scattering angle (θ = 0.017-34°C). They were then compared by the instrument to the scattering patterns of spherical particles of the same size calculated by the Mie model of light scattering by particles. Significant differences from this model occur, only if particles are very non-spherical. The critical concentration of samples required for each measurement varied and therefore the ratio of avidin to microparticles within each sample is quoted on a weight-by-weight basis.

5.2.12 Oscillatory shear measurements

Oscillatory shear measurements was performed using a controlled stress rheometer (CS10, Bohlin) fitted with a cone and plate (4° geometry) and used a frequency range of 0.1 –5 rad/s at 37°C. The linear viscosity region (where stress is proportional to strain) was determined by stress sweep measurements in order to carry out measurements at stresses that did not damage the scaffold structure. Tan δ = G''/G' where G' and G'' are the storage and loss modulus and δ is the loss angle. A gel structure normally results in G' being greater than G'' whilst a non-gel structure will result in G''>G'. Measurements dependent on shear rate were made over the 0.1 - 100 s^{-1} region.

5.3 Results and discussion

The novel scaffold described in this chapter possesses the advantages of both porous matrices and *in situ* forming gels, generating porous scaffolds that self-assemble at the site of injection. Figure 5.1 is a schematic representation of the process of scaffold self-assembly. We start with particles of poly (lactic acid)-poly (ethylene glycol)-biotin (PLA-PEG-biotin) (Cannizzaro *et al.* 1998) that are formed using a single emulsion method. The particles are then crosslinked together by co-injection with the cross-linking protein avidin, to form an interconnected macroporous structure.

In the development of the scaffold, the first step was to manufacture the nano and microparticles from PLA-PEG-biotin, which was synthesized and characterised in Chapter 3. The use of microparticles has been described in many tissue-engineering applications. Examples include microparticles that have been used for a variety of tissue regenerative purposes from tissue bulking in urinary incontinence, regeneration of dermis-like tissues through the release of basic fibroblast growth factor to delivering nerve growth factor to enhance axonal regeneration following injury to the central nervous system (CNS)(Cao and Shoichet 1999; Kawai *et al.* 2000). The potential of combining the avidin-biotin system with nanoparticle technology has also been recently demonstrated in carrier systems with biotinylated drug derivatives for antisense therapy for HIV infections (Coester *et al.* 2000).

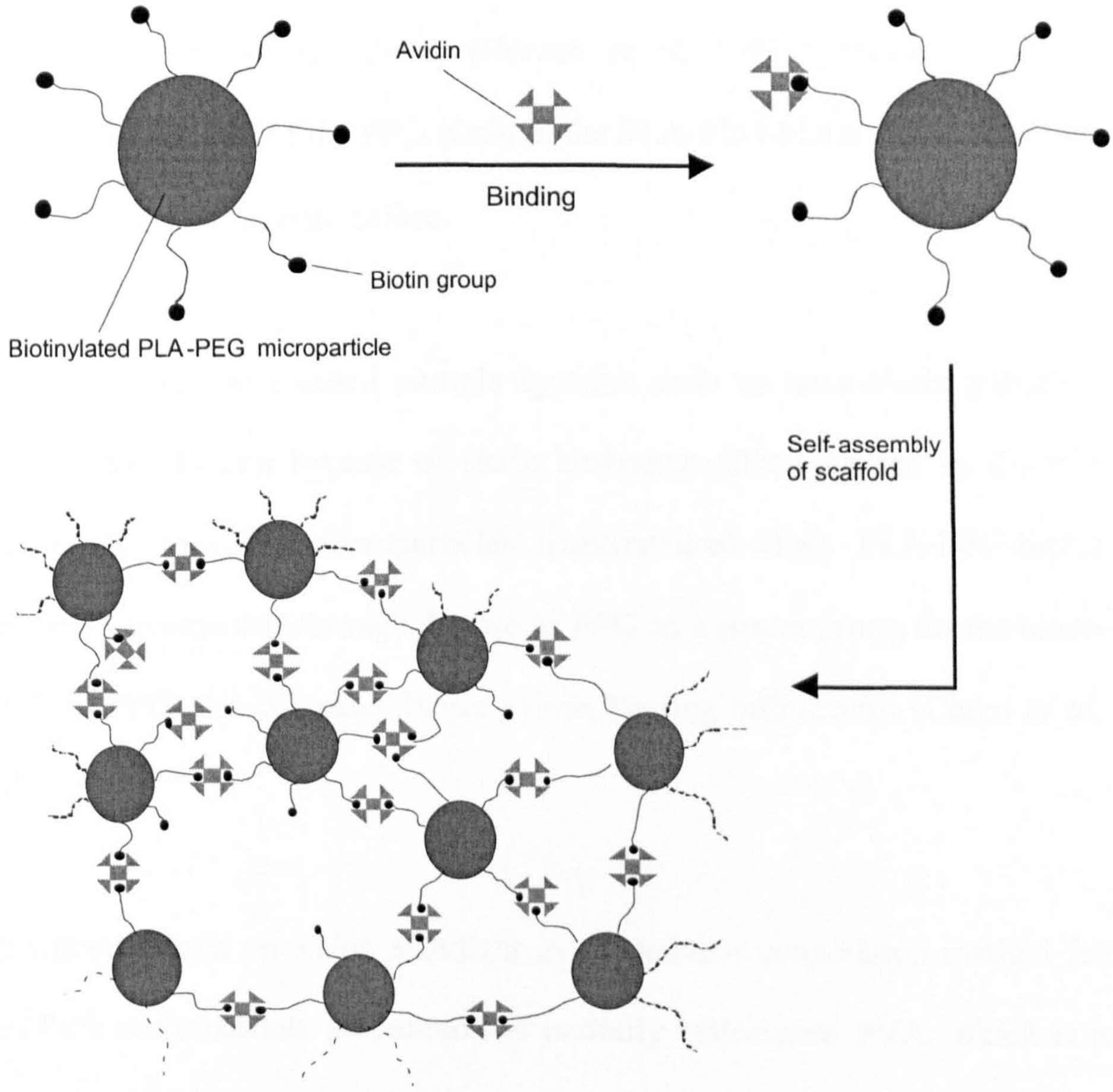

Figure 5.1 Schematic of the process of scaffold self- assembly.

5.3.1 Manufacturing of microparticles

As described in Chapter 1, PLA-PEG copolymers display hydrophobic-hydrophilic type characteristics that result in a PEG enriched surface when manufactured into microparticles (Hrkach *et al.* 1997). Because biotin is tethered onto the end of the PEG chain in the PLA-PEG-biotin copolymer, this also results in a biotin rich surface.

Whilst previous biotinylated particle systems such as latex-biotin particles, were not able to link because of steric hindrance effects caused by the two approaching particles; microparticles manufactured from PLA-PEG-biotin polymer overcome this through the use of PEG as a spacer group for the biotin unit. The PEG also increases biotin-avidin binding efficiencies (Chern *et al.* 1996).

A commonly used emulsion stabilizer in the solvent evaporation method for PLA-PEG microparticle preparation is partially hydrolyzed PVA, which is a copolymer of poly (vinyl acetate) and poly (vinyl alcohol). The choice of an 88% hydrolysed PVA was made because a study by Murakami *et al* found this to be the optimum degree of hydrolyzation of PVA for the manufacture of nano/microparticles (Murakami *et al.* 1997).

The binding of PVA to the microparticles may be through the interpenetration of PVA and PLA-PEG molecules. The irreversible binding of PVA on the microparticle surface is likely to happen when the organic solvent is removed from the interface in which interpenetration of PVA and PLA-PEG molecules

occur. The impact of a mixed PVA interfacial zone with the PEG enriched surface will be in the masking of biotin binding sites at the PEG end groups. However, previous work by SPR has shown that significant avidin immobilisation still occurs after PVA adsorption with masking up to only 30%, suggesting that there are sufficient biotin binding sites retained on the surface of the microparticle (Black *et al.* 1999).

The ability to control particle size is demonstrated in Table 5.1, where particle size is governed by the stirring rate, with the minimum sizes of the microparticles determined by the PVA concentrations of the continuous phase. This is important not only in dictating the porosity of our scaffolds through the interstitial spaces generated through aggregation of the microparticles, but also because it has been found that there is a linear relationship between the degradation rate and particle size, with larger particles degrading faster. In smaller particles, degradation products formed within the particle can diffuse easily to the surface, while in larger particles degradation products have a longer path to the surface of the particle during which autocatalytic degradation of the remaining polymer can occur (Dunne *et al.* 2000).

It is also possible to control the porosity of the individual microparticles to have a secondary form of control over the scaffold's overall porous structure. This is advantageous because particles with varying porosities can alter release rates of growth factors or allow cell infiltration. This could be achieved by using higher temperatures during the manufacture, which results in rapid solvent evaporation.

PVA conc. (%, w/w)	Stirring rate (rev./min)	Average Size (micron)	Polydispersity
0.1	1500	9.9	0.29
	3500	5.2	0.31
	5000	2.1	0.33
1	1500	3.2	0.26
	3500	1.9	0.35
	5000	1.7	0.39
9	1500	1.4	0.34
	3500	0.6	0.39
	5000	0.25	0.55

Table 5.1 Parameters controlling microparticles size.

This causes local explosion inside the droplets and leads to the formation of porous structures throughout the microspheres (Jain 2000; Yang *et al.* 2000). This is illustrated in Figure 5.2 by a batch of PLA-PEG-biotin microparticles that were manufactured at the higher temperature of 37°C.

In the case of tissues where increased load bearing was necessary, an additional gel-forming component biotin-PEG-biotin could be added to a mixture of avidin-saturated particles to enhance the mechanical properties of the scaffold. The self-assembly was achieved in these examples by the biotin-avidin mediated interaction between the biotin unit attached to the PEG and the avidin on the surface of the nanoparticles. The next stage was to therefore assess the binding processes involved in the scaffold formation.

5.3.2 Surface Plasmon Resonance (SPR) binding studies

The mechanisms of self-assembly were explored by SPR analysis. The specific receptor-mediated nature of the crosslinking is demonstrated in the SPR data in Figure 5.3. The silver coated SPR slides were modified with a biotin-presenting monolayer by exposure to N-([6-biotinamido-]hexyl-)3'-[2'pyridylthio]propionamide. Successive layers of avidin, biotin-PEG-biotin, avidin and PLA-PEG-biotin nanoparticles were then built upon this surface. The addition of each layer, via specific avidin-biotin interactions, was detected by an increase in the SPR angle.

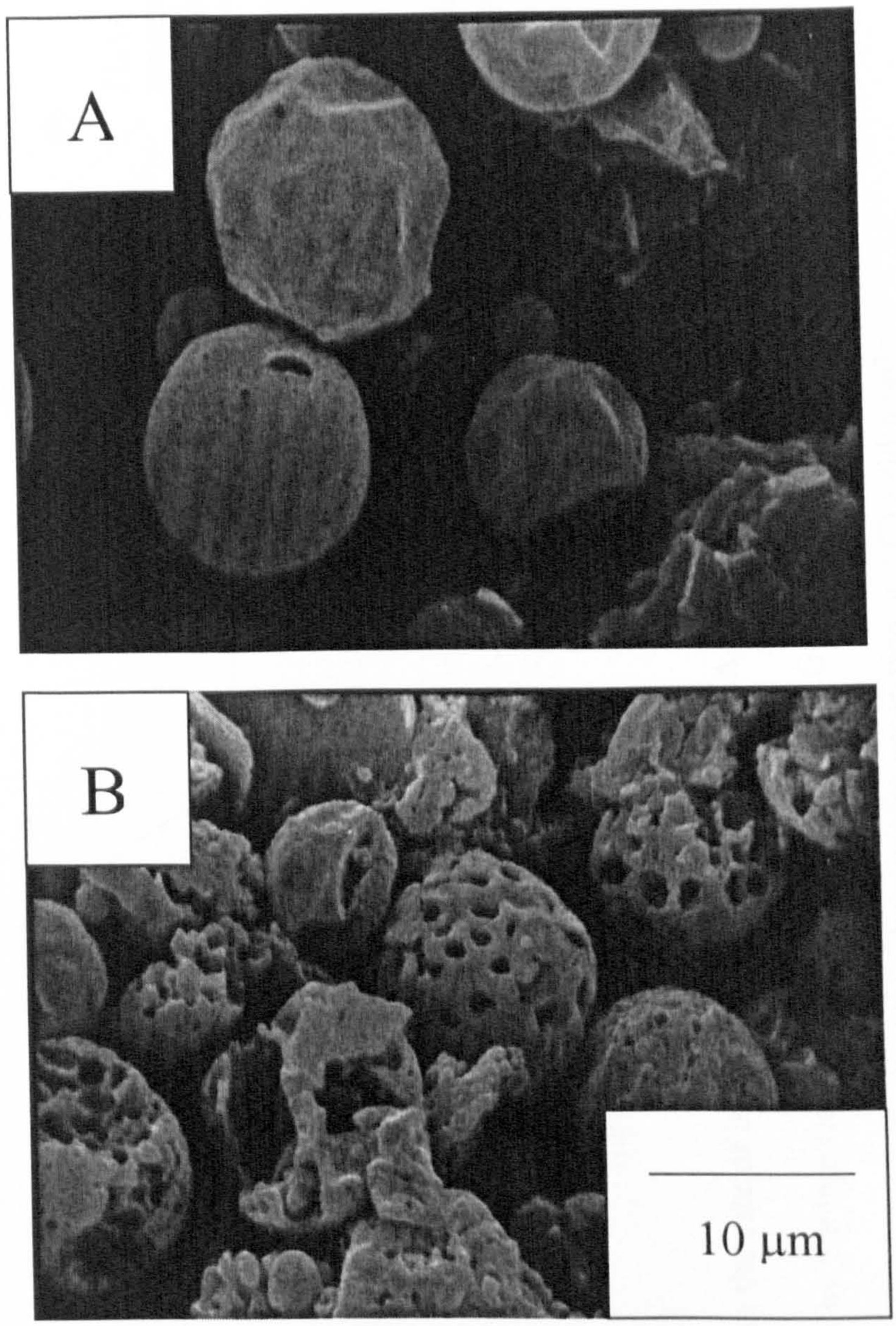

Figure 5.2 SEM image of microparticles manufactured at A) 24°C and B) 37°C showing that the increased temperature for solvent evaporation results in highly porous microparticles.

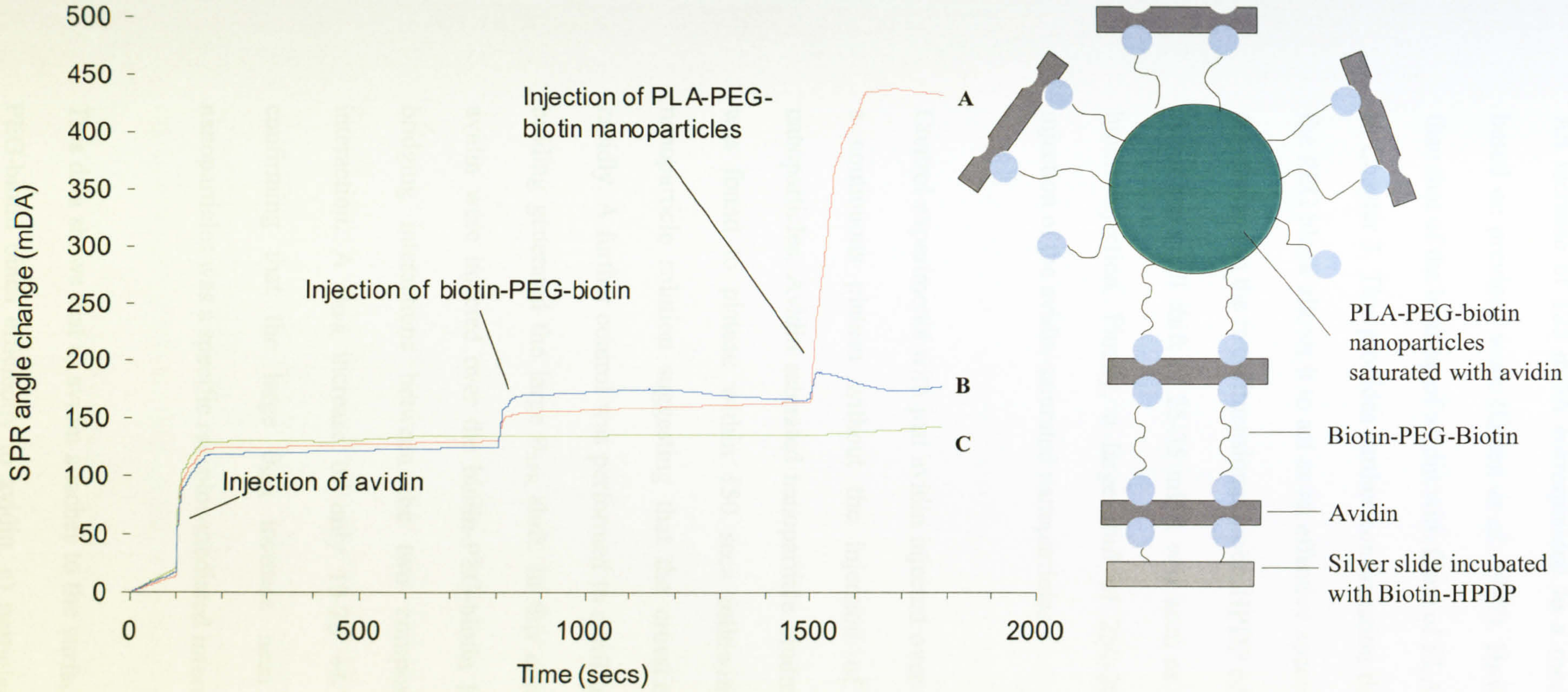

Figure 5.3 SPR experiment to determine the rate of binding of avidin saturated PLA-PEG-biotin nanoparticles with biotin-PEG-biotin. Spectra for the **A)** injection of avidin, followed by the injection and binding of a biotin-PEG-biotin layer and finally binding of nanoparticles saturated with avidin. Controls included **B)** the injection of nanoparticles without avidin saturation and **C)** avidin only.

An increase of 125 mDA corresponded to a monolayer of protein coverage based on previous work (Green *et al.* 1997). However, the shift was smaller than that of the binding of avidin with films of PLA-PEG-biotin (181.58 mDA) in Chapter 3. This provides further confirmation that the hydrophilic nature of the PEG block allows it to act as an effective spacer molecule for the biotin, in comparison to the two-dimensional biotin-HPDP adsorbed onto the silver slide. A further small shift of 25-35 mDA was seen as a result of the biotin-PEG-biotin injection. Finally, a large shift of 250-260 mDA was detected on injection of the avidin-saturated nanoparticles.

Control experiments with just avidin injected over the biotin surface produced a continuous plateau without the injection of biotin-PEG-biotin or the nanoparticles. Avidin saturated nanoparticle binding to the biotin-PEG-biotin was found to plateau within 150 secs following the introduction of the nanoparticle solution suggesting that the crosslinking process could occur rapidly. A further control was performed to confirm that specific avidin-biotin binding generated the large θ_{SPR} shift. In this control, nanoparticles without avidin were injected over the biotin-PEG-biotin layer hence preventing any bridging interactions between the two components through the avidin interaction. A θ_{SPR} increase of only 10-20 +/- 2/3 mDA was recorded confirming that the large θ_{SPR} increase seen for the avidin-saturated nanoparticles was a specific receptor-mediated interaction.

This data shows that a) avidin attaches to the surface of the particles b) biotin-PEG-biotin binds efficiently to avidin, c) particles coated in avidin bind to biotin-PEG-biotin and d) the biotin-avidin mediated interaction is a specific

instantaneous binding process. Having shown that each component of the scaffold had maintained their binding properties after manufacture, it was then necessary to optimise the aggregation process.

5.3.3 Aggregation studies on nanoparticles

The initial plan for scaffold formation was to be dependent on the linking of particles through the avidin-biotin mediated interaction. Aggregation studies were carried out to determine optimum particle:avidin ratios. The ability to control the porosity in the self-assembling scaffolds is achieved through control of particle size, which then determines the size of the interstitial spaces generated when the particles aggregate together. Thus to prove that porosity could be controllable within the scaffold, it was necessary to show that aggregation could be achieved with both nanoparticles and microparticles.

Starting with nanoparticles, particle size analysis was conducted using photon correlation spectroscopy (PCS) and transmission electron microscopy (TEM). Figure 5.4 shows the aggregation data of 50 μg samples of 250 nm PLA-PEG-biotin particles. Up to 0.1mg of avidin had negligible effects on the aggregation of the nanoparticles. It is possible that small aggregates may have formed but were not sufficiently present to be selected during random sampling of the suspension. Increasing up to 0.4 mg of avidin showed a consistent increase in the size of aggregates reaching optimum aggregation levels at 0.35 mg. Beyond this quantity of avidin, a decrease in aggregate size was detected.

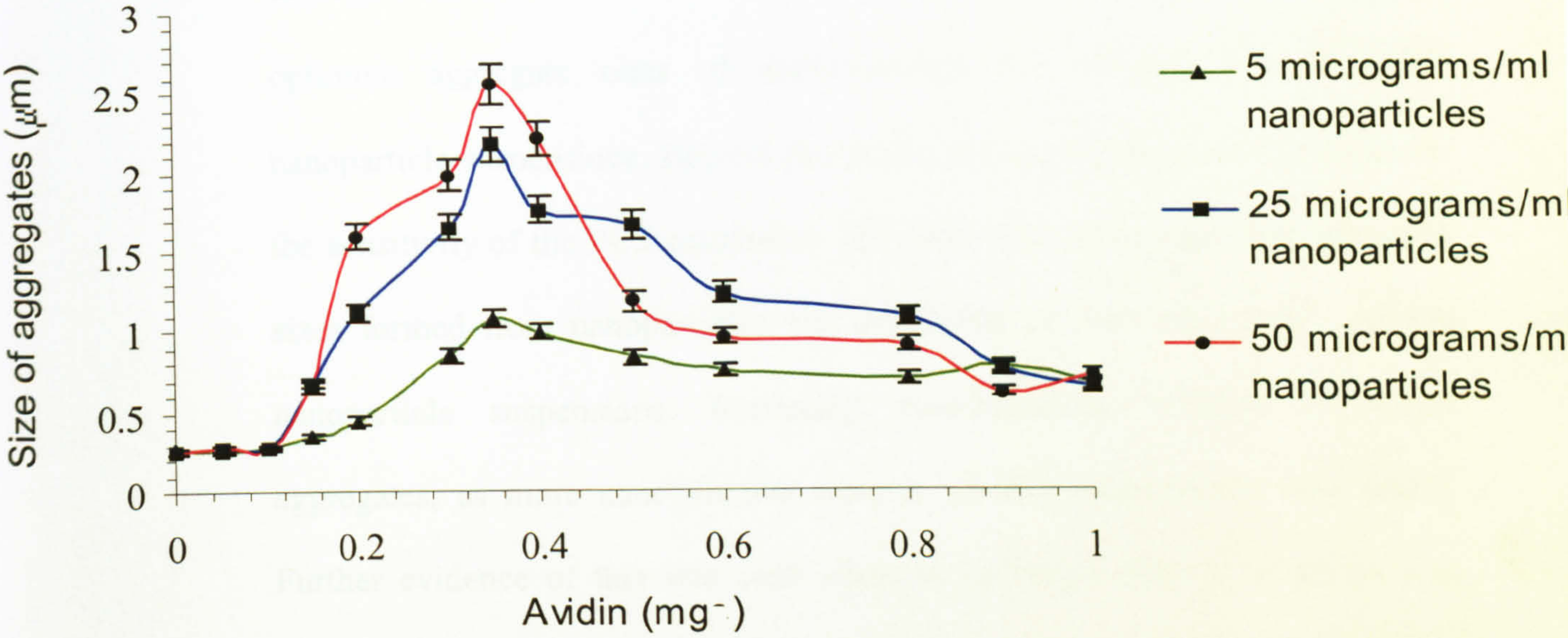

Figure 5.4. Photon correlation spectroscopy (PCS) data on the aggregation of different dilutions of PLA-PEG-biotin nanoparticles with the addition of avidin to determine nanoparticle concentration and avidin to nanoparticle ratio effects on aggregation.

Increasing avidin further resulted in further falls in the overall aggregate size until a plateau was observed after 0.9mg of avidin.

Assessment was then made on the influence of the concentration of the suspensions of nanoparticles. The optimum aggregate size increased as the concentration of the nanoparticle suspension increased. At 5 μg/ml, optimum aggregate sizes around the 1-micron size were observed. This increased to optimum aggregate sizes of approximately 2.5 microns for 50 μg/ml nanoparticle suspensions. Beyond this point, the aggregates were too large for the sensitivity of the PCS equipment. However it could be seen that aggregate sizes formed from nanoparticles was dependent on the concentration of the nanoparticle suspensions. Increasing concentrations resulted in larger aggregates, as more nanoparticles were in contact when avidin was added. Further evidence of this was seen when an optimum amount of avidin was added to a concentrated suspension of nanoparticles and assessed by TEM. Figure 5.5 shows the nanoparticles before and after addition of avidin clearly illustrating the aggregating effect of the avidin-biotin binding process. Having shown that it was possible to optimise nanoparticle aggregation, it was necessary to show that aggregation of microparticles could also be optimised.

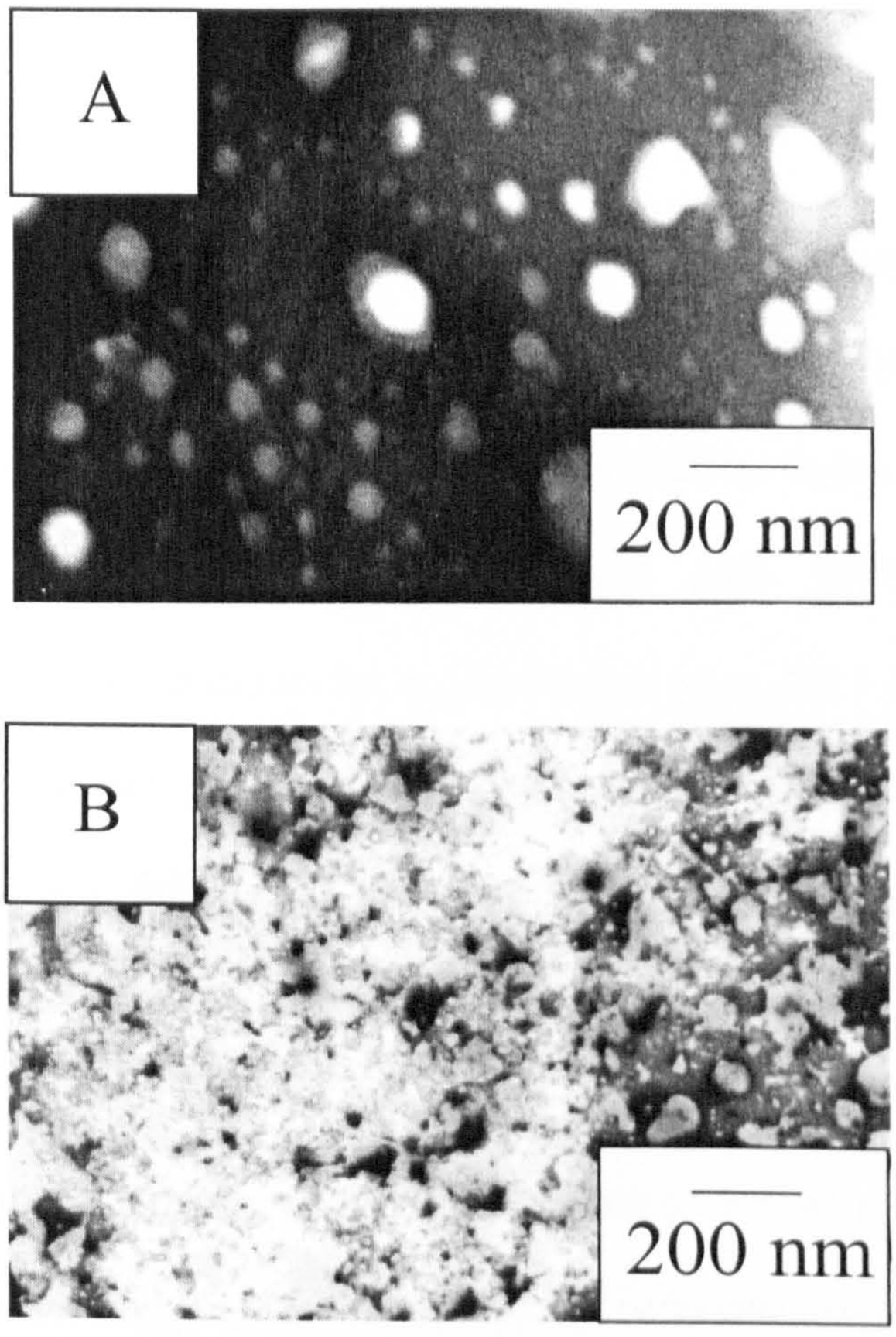

Figure 5.5 TEM images of A) PLA-PEG-biotin nanoparticles without avidin and B) after addition of avidin.

5.3.4 Aggregation studies on microparticles

An initial assessment on whether PLA-PEG-biotin microparticles would crosslink together upon addition of avidin was made by mixing 10-micron particles with rhodamine-conjugated avidin (Av-Rh) (Figure 5.6). Microscopy images of large aggregates up to 1 mm in size were observed.

Because the microparticles were above the sensitivity range of the PCS equipment, aggregation studies were carried out using two alternative methods; sedimentation and particle size analysis (Coulter LS230). These complimentary techniques were chosen because individually each method has some drawbacks. Particle size analysis by sedimentation provides a simple effective non-destructive method of measuring aggregate sizes, where the apparent volume fraction is a function of the light obscured in the sample, but the method lacks the accuracy of the particle size analyser (Coulter LS230). The size distribution measured by the particle size analyser is an equivalent volume based size distribution for particles, as calculated by the Mie theory from the scattering patterns of aggregates. However, the software assumes all particles are spherical, but when particles aggregate together, many different shapes can be formed. These do not necessarily correspond to the shape of the primary particles. Measurements also take place under agitated stirring conditions. Clearly, restructuring of this nature could have a substantial effect on the size of aggregates, as the undisturbed aggregate with more tenuous structure occupies a larger space than that of the restructured aggregate.

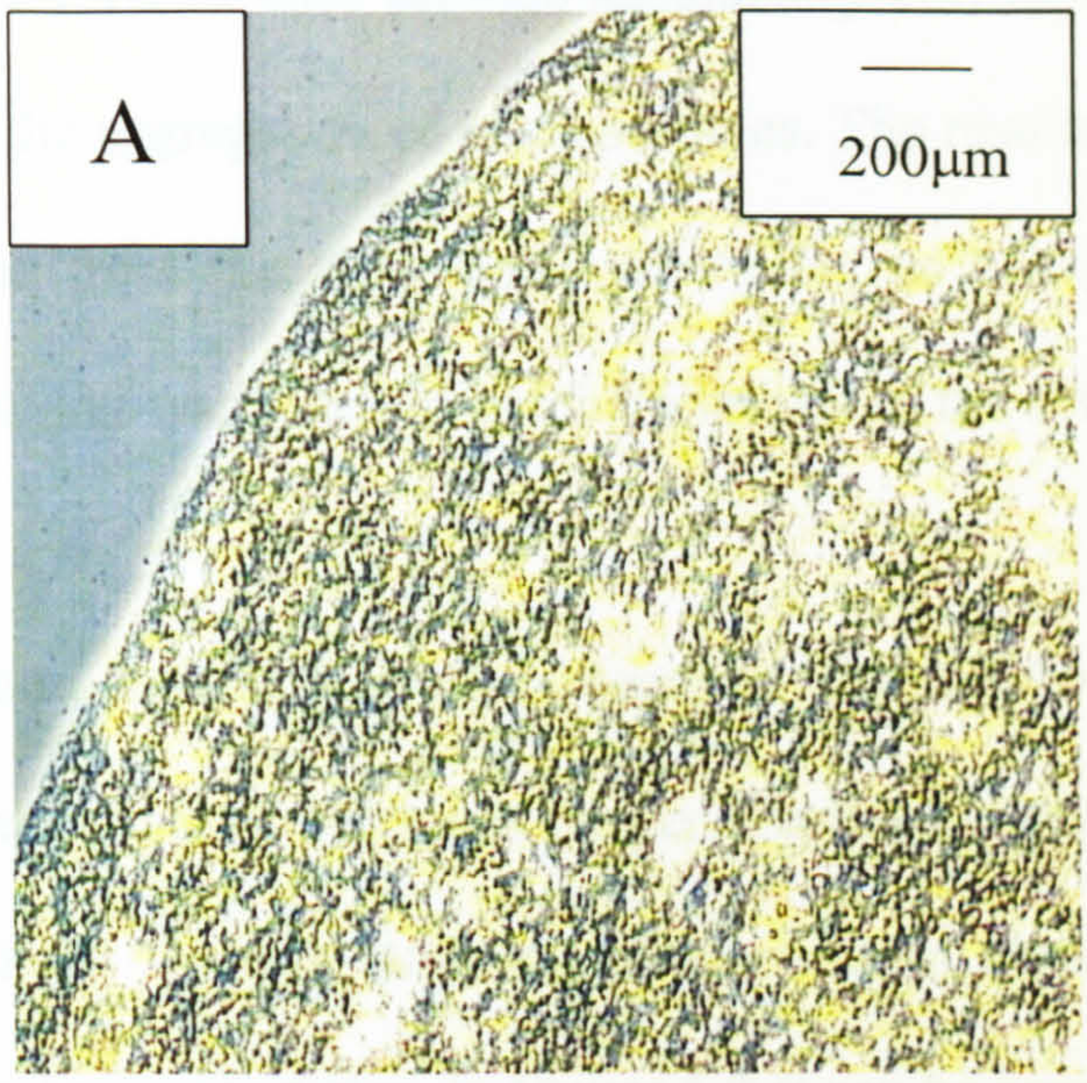

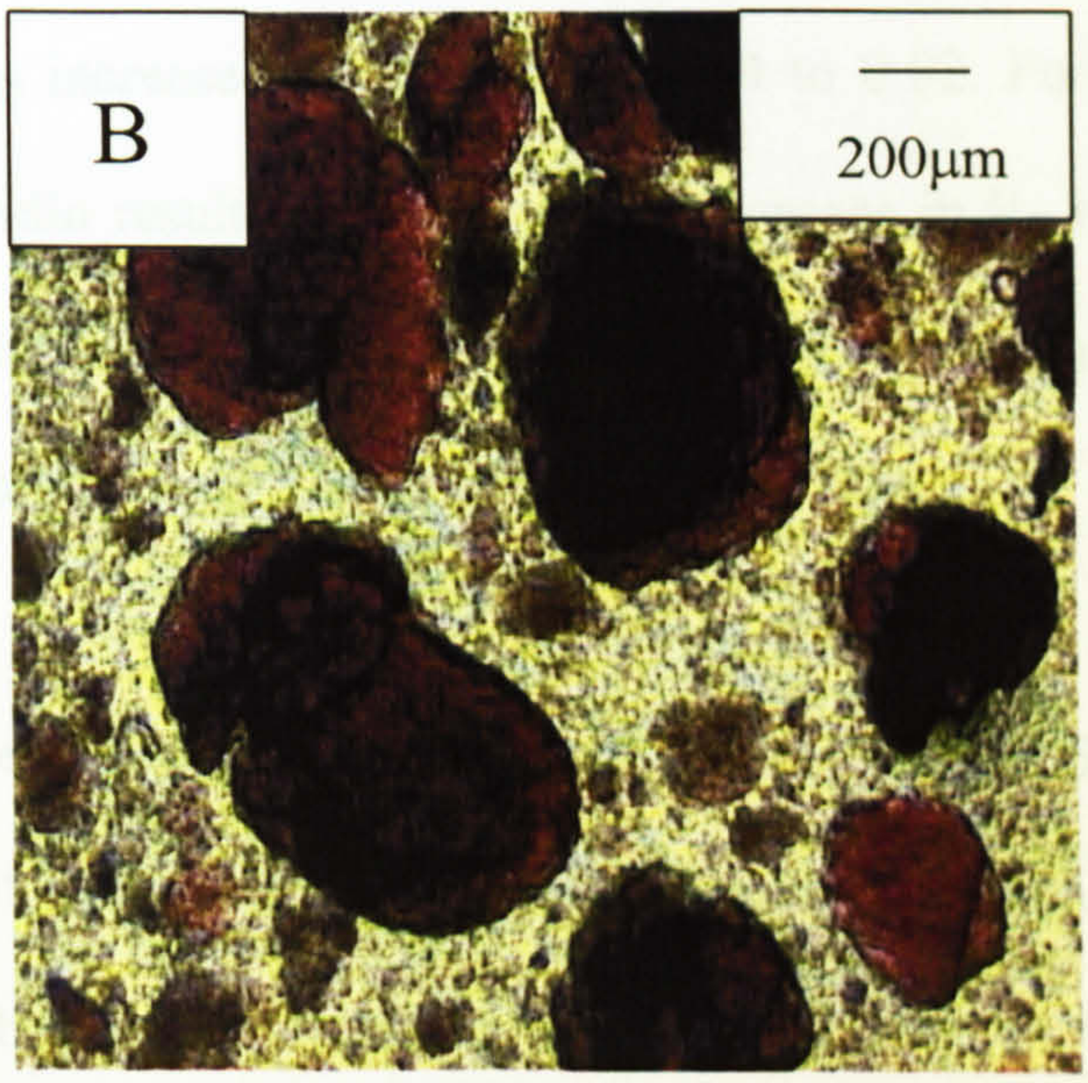

Figure 5.6 Microscopy images of PLA-PEG-biotin microparticles **A)** showing small unaggregated microparticles before addition of rhodamine conjugated avidin and **B)** after addition of the fluorescently labelled crosslinking agent showing large aggregates.

However, a comparison of the particle size analysis by sedimentation with that by the Coulter LS 230 does provide satisfactory correlation on the effects of the avidin on the aggregation of microparticles. The results presented have also been produced from the same batch of avidin, as a key difficulty in these aggregation studies was batch-to-batch variations in the activity of the avidin.

In sedimentation studies, the rate of decrease (R_D) in absorbance increased as the size of the aggregates increased (larger aggregates settle out faster allowing more light to get through quicker). Sedimentation studies were carried out using 10 mg/ml microparticles. In Figure 5.7 it can be seen that up to 0.1 mg of avidin, the R_D increased sharply from 0.004 to 0.02. Further increases in the amount of avidin resulted in more gentle increase in R_D reaching an optimum 0.0285 at 2mg avidin. Further amounts of avidin then resulted in the R_D decreasing again, falling to 0.01 for 10mg of avidin.

Similarly, the Coulter LS230 data shown in Figure 5.8 showed a single distribution of 10-micron particles without avidin. Upon addition of avidin, the distribution became multimodal showing increasing aggregate sizes with increasing amounts of avidin up to 2mg. Saturation of the microparticles with avidin also resulted in a multimodal distribution but with aggregate sizes significantly smaller indicating that an excess of avidin prevents optimal aggregation from occurring.

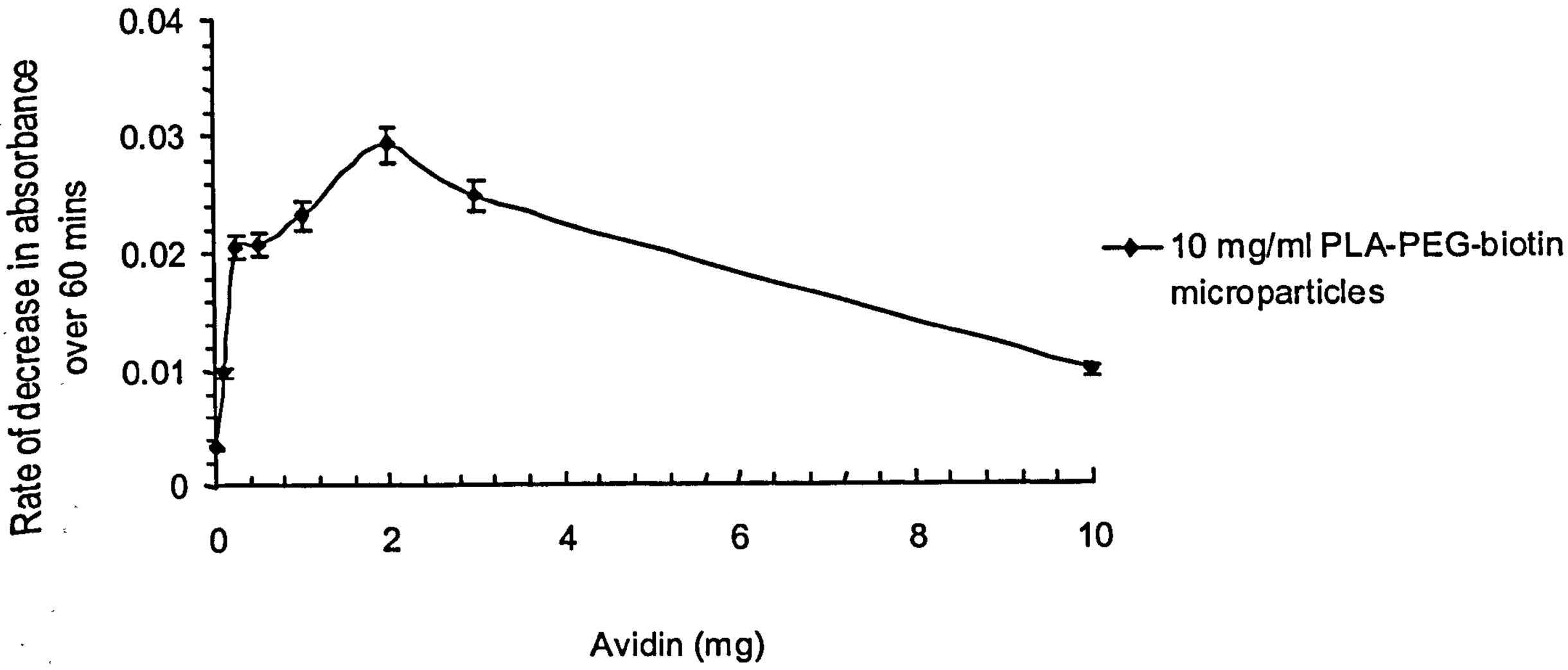

Figure 5.7 Aggregation studies using sedimentation to show rate of decrease in absorbance for 10 mg/ml PLA-PEG-biotin particles (≈10 μm) with varying concentrations of avidin

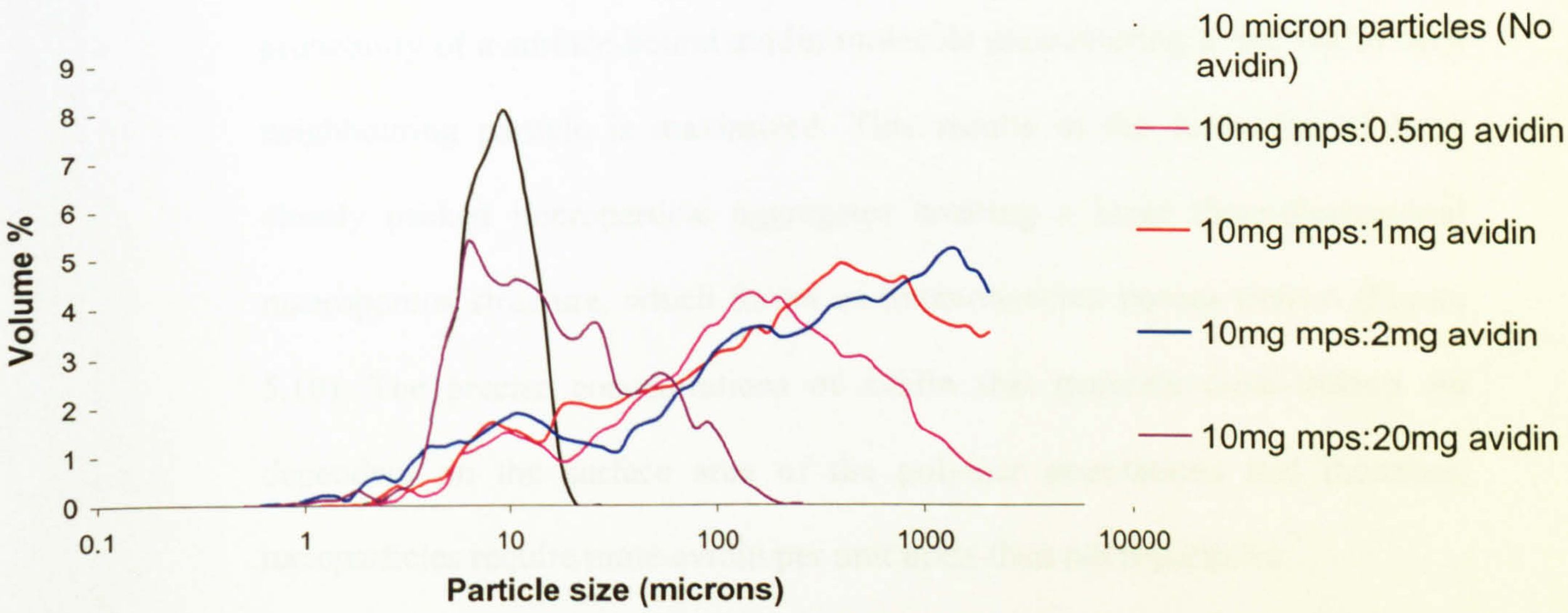

Figure 5.8 Aggregate distributions determined by Coulter LS230 studies on PLA-PEG-biotin particles (≈10 μm) with varying concentrations of avidin.

This data reveals a consistent relationship between particle surface area, avidin concentration, and aggregation. At low avidin concentrations there are insufficient bridging points due to the scarcity of the protein. At high avidin, concentrations there are insufficient free biotin molecules on the surfaces of the particles to achieve cross-linking. This is illustrated in Figure 5.9 by CryoSEM images of PLA-PEG-biotin microparticles placed in an excess of avidin, resulting in limited aggregation. At intermediate avidin concentrations, the probability of a surface-bound avidin molecule encountering a free biotin on a neighbouring particle is maximized. This results in the formation of large closely packed microparticle aggregates creating a large three-dimensional macroporous structure, which forms an interconnected porous system (Figure 5.10). The precise concentrations of avidin that generate cross-linking are dependent on the surface area of the polymer populations and therefore, nanoparticles require more avidin per unit mass than microparticles.

5.3.5 Rheological determination of mechanical properties

Scaffolds for tissue regeneration purposes require defined mechanical properties. A proposed advantage of the scaffold presented is the ability to tailor the viscoelastic properties of the scaffold to that of the area in which tissue regeneration is required.

Rheological measurements on microparticle aggregates whilst demonstrating the crosslinking properties of avidin highlighted the lack of mechanical strength of these scaffolds. This was a problem both in terms of rheological characterisation through seepage of the composites and reaching targeted

mechanical requirements of traditional scaffolds described in Chapter 1. In order to strengthen the scaffold, biotin-PEG-biotin was introduced. The binding affinity of biotin-PEG-biotin was first probed in SPR analysis but the complexities of introducing avidin to a biotin-PEG-biotin solution meant that avidin could not be used as the crosslinking agent. The most obvious hurdle was that avidin was binding to the biotin-PEG-biotin and therefore not crosslinking the microparticles. This was overcome by preparing the microparticles with avidin first as described previously. Solutions of biotin-PEG-biotin were then introduced to the avidin-bound microparticles as the crosslinking agent. Biotin-PEG-biotin was first used at a constant proportion to investigate the impact of the percentage of microparticles by weight in these scaffold composites and the impact of the ratio of microparticles to avidin.

Figure 5.11 show that the addition of avidin results in a transition in the mechanical properties of the scaffold. The avidin appears to impact on the scaffold in two ways.

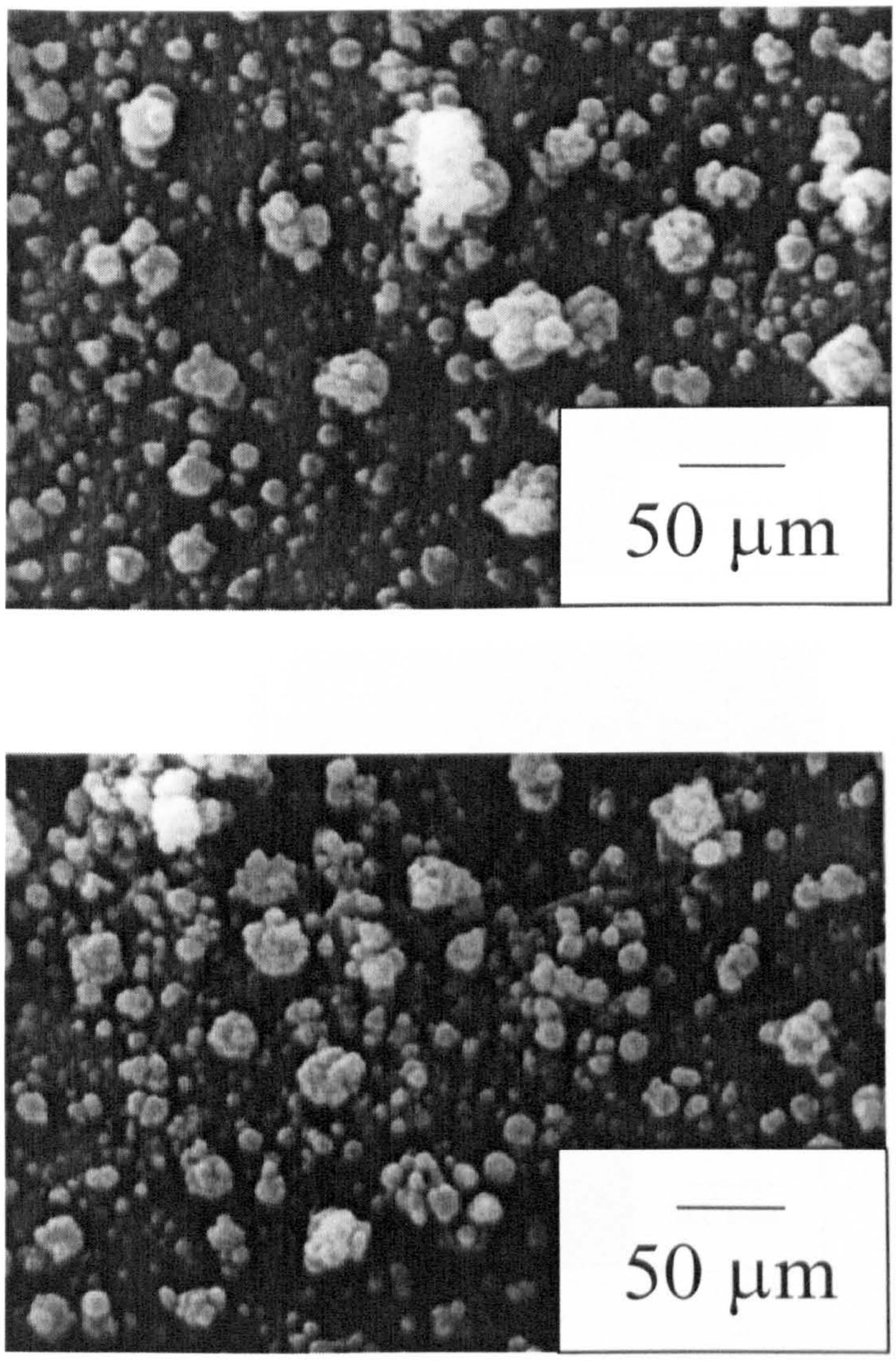

Figure 5.9 CryoSEM images of 10-micron PLA-PEG-biotin microparticles saturated in avidin showing limited aggregation.

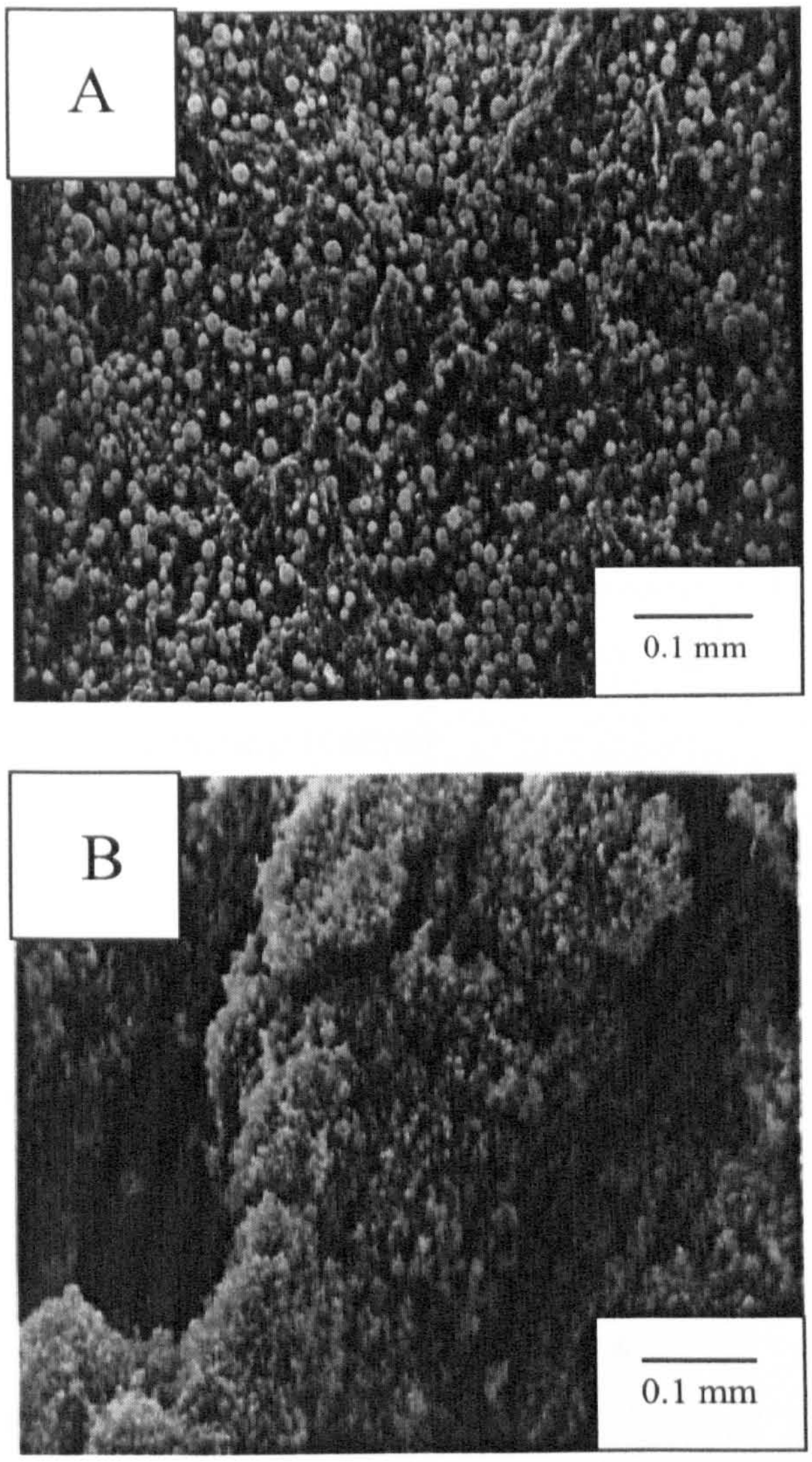

Figure 5.10 CryoSEM images of **A)** 10 micron PLA-PEG-biotin microparticles without avidin and **B)** after addition of avidin showing the interconnected macroporous structure of the large aggregates formed.

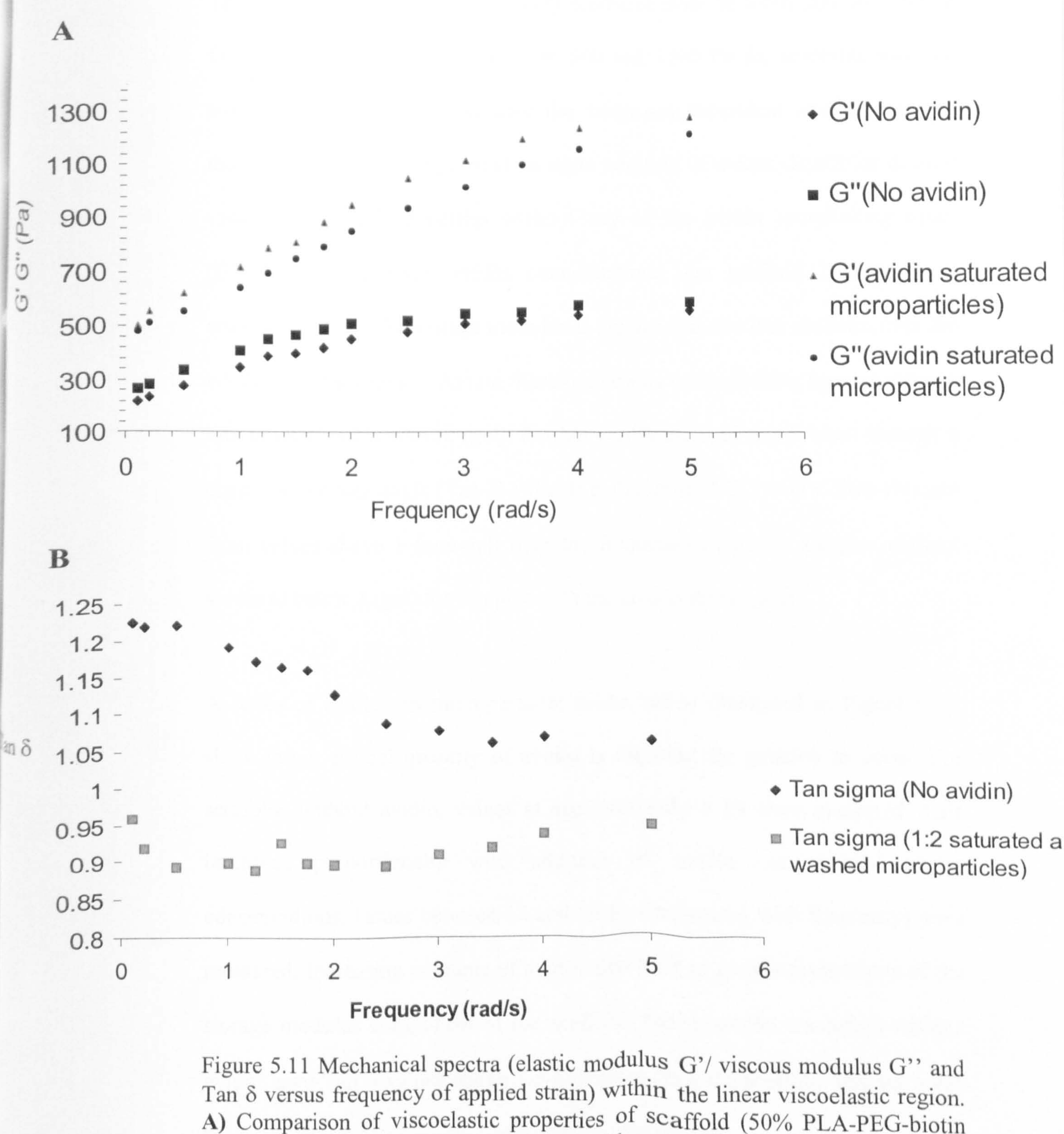

Figure 5.11 Mechanical spectra (elastic modulus G'/ viscous modulus G'' and Tan δ versus frequency of applied strain) within the linear viscoelastic region. **A)** Comparison of viscoelastic properties of scaffold (50% PLA-PEG-biotin microparticles/25%PEG-biotin) at 37°C with and without avidin treatment and **B)** plot of Tan δ over a 0.1 -5 Hz frequency range with 50% PLA-PEG-biotin microparticles/25% Biotin-PEG-Biotin without avidin and with saturated and washed microparticles with avidin. The 1:2 ratio denotes saturation of microparticles with twice the amount of avidin on a weight-by-weight basis prior to washing and centrifugation.

The first is that the overall viscosity increases from between 200 and 500 Pa for avidin free scaffolds to between 500 and 1200 Pa for scaffolds with the crosslinking protein. Furthermore the frequency dependent studies illustrate that the scaffolds undergo gelation upon addition of avidin. Scaffolds display viscoelastic liquid properties without any of the avidin crosslinking agent (G''>G'). At optimum avidin concentrations, the scaffold behaves as a viscoelastic solid: the storage modulus is greater than the loss modulus over the whole frequency range. Avidin therefore acts as a crosslinking agent creating a multidimensional network (gel). Further clarification of this is seen through a change in the loss angle (Tan δ) value (i.e. the ratio of G'' to G'). This changes from values above 1 (non-gel) over the frequency range for samples without avidin to below 1 (gel) for samples with the crosslinking agent.

A series of studies on microparticle: avidin ratios illustrated in Figure 5.12, show that a critical quantity of avidin is required for gelation to occur. For scaffolds without avidin, values at approximately 4 Pa were measured. This increased proportionally with addition of avidin. At optimal avidin concentrations, values between 12 and 19 Pa (increasing with frequency) were measured. Increasing amounts of avidin also lead to greater proportions of the storage modulus component of the scaffold. For example, a scaffold without avidin gave Tan δ values above 1.5 indicating that the scaffold was not a gel. Low microparticle to avidin ratios (20:1), whilst lowering the Tan δ value to between 1.1 and 1.2, were not sufficient to form the gel structure.

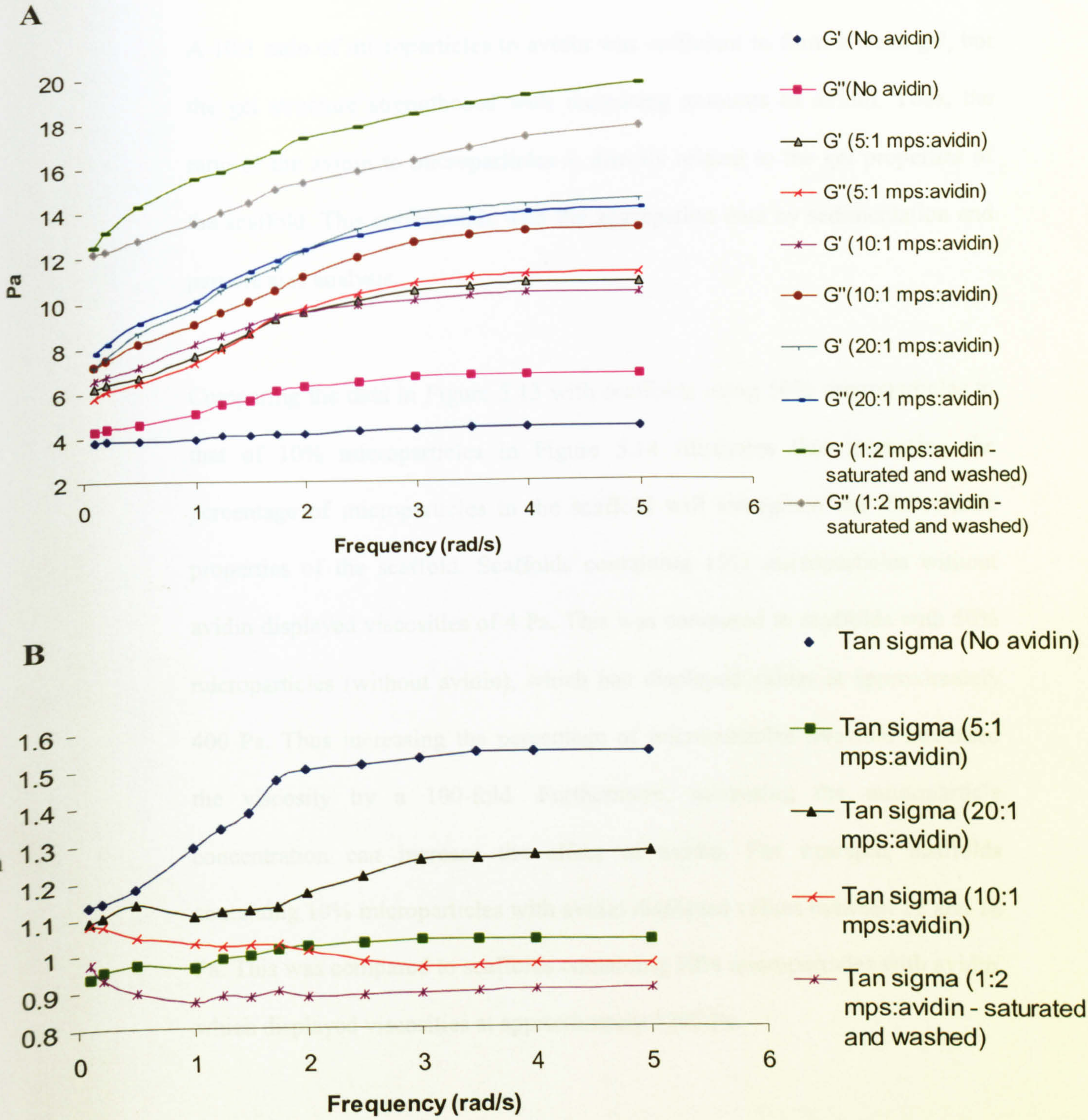

Figure 5.12 Mechanical spectra (elastic modulus G'/ viscous modulus G'' and Tan δ versus frequency of applied strain) within the linear viscoelastic region. **A)** Plot of G' and G" values over a 0.1 - 5Hz frequency range with varying PLA-PEG-biotin microparticles to avidin compositions (10% microparticles in 25% Biotin-PEG-biotin) and **B)** plot of Tan δ over a 0.1- 5Hz frequency range with varying PLA-PEG-biotin microparticle to avidin compositions (10% microparticles in 25% Biotin-PEG-biotin)

A 10:1 ratio of microparticles to avidin was sufficient to form a weak gel, but the gel structure strengthened with increasing amounts of avidin. Thus, the ratio of the avidin to microparticles is directly related to the gel properties of the scaffold. This corresponds with the aggregation data by sedimentation and particle size analysis.

Comparing the data in Figure 5.13 with scaffolds using 50% microparticles to that of 10% microparticles in Figure 5.14 illustrates that increasing the percentage of microparticles in the scaffold will strengthen the viscoelastic properties of the scaffold. Scaffolds containing 10% microparticles without avidin displayed viscosities of 4 Pa. This was compared to scaffolds with 50% microparticles (without avidin), which had displayed values at approximately 400 Pa. Thus increasing the percentage of microparticles five-fold increased the viscosity by a 100-fold. Furthermore, increasing the microparticle concentration can increase the effect of avidin. For example, scaffolds containing 10% microparticles with avidin displayed values between 12 and 18 Pa. This was compared to scaffolds containing 50% microparticles with avidin, which displayed viscosities at approximately 1200 Pa.

5.3.5.1. The impact of biotin-PEG-biotin on the mechanical properties

Shear rate dependent studies have also highlighted the influence of the proportion of biotin-PEG-biotin on the viscoelastic properties of the scaffold. A comparison of microparticles before and after the addition of avidin was performed over a 0.01 to 100 s^{-1} range (Figure 5.13). The mechanical spectra show that avidin increases the overall viscosity of the samples, providing further evidence of the crosslinking process.

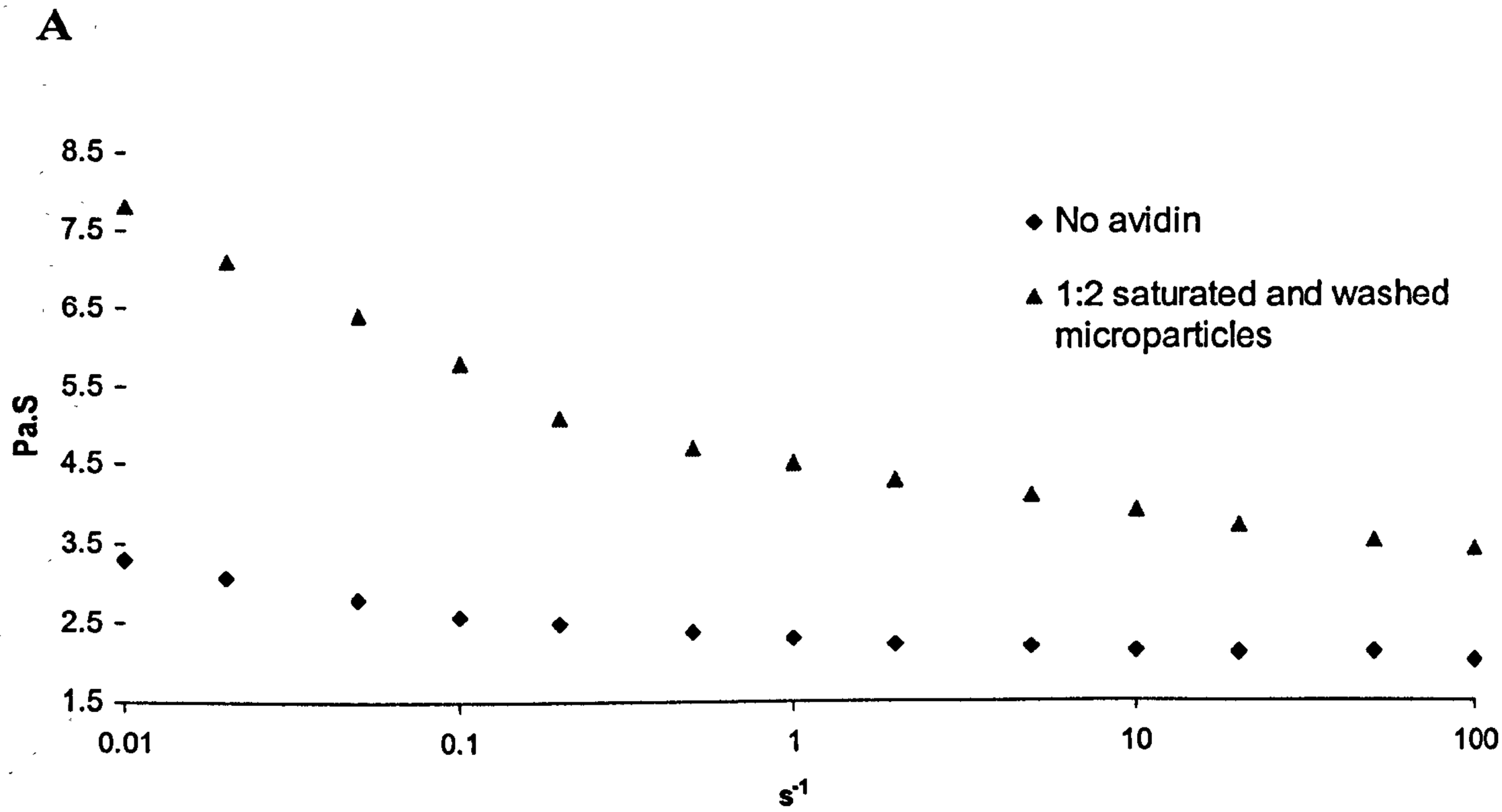

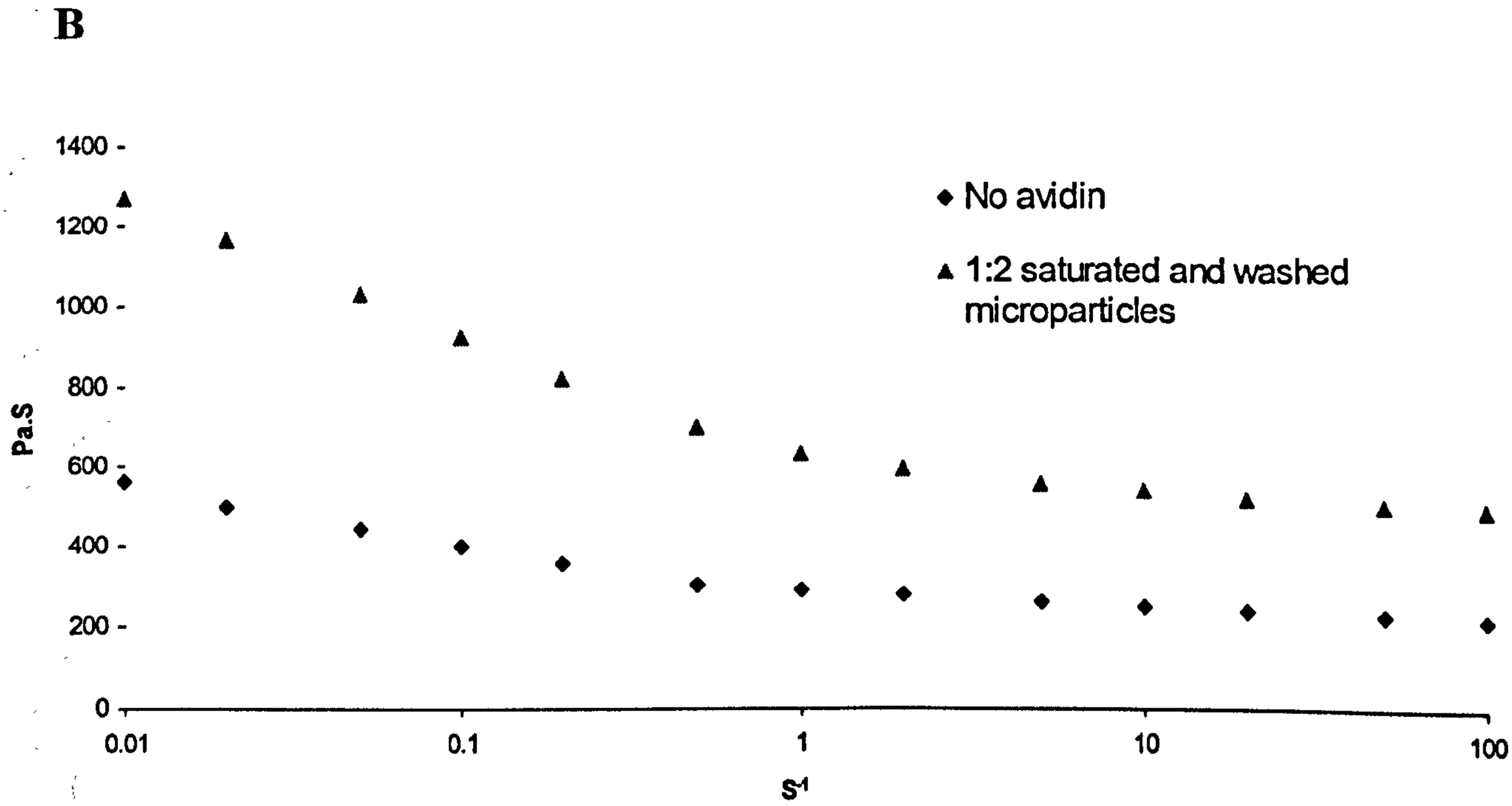

Figure 5.13 Shear rate dependent studies over a 0.1 - 100 s^{-1} range comparing scaffolds before and after crosslinking with avidin using **A)** 50% microparticles and **B)** 50% microparticles/ 25% biotin-PEG-biotin. The 1:2 ratio denotes saturation of microparticles with twice the amount of avidin on a weight-by-weight basis prior to washing and centrifugation.

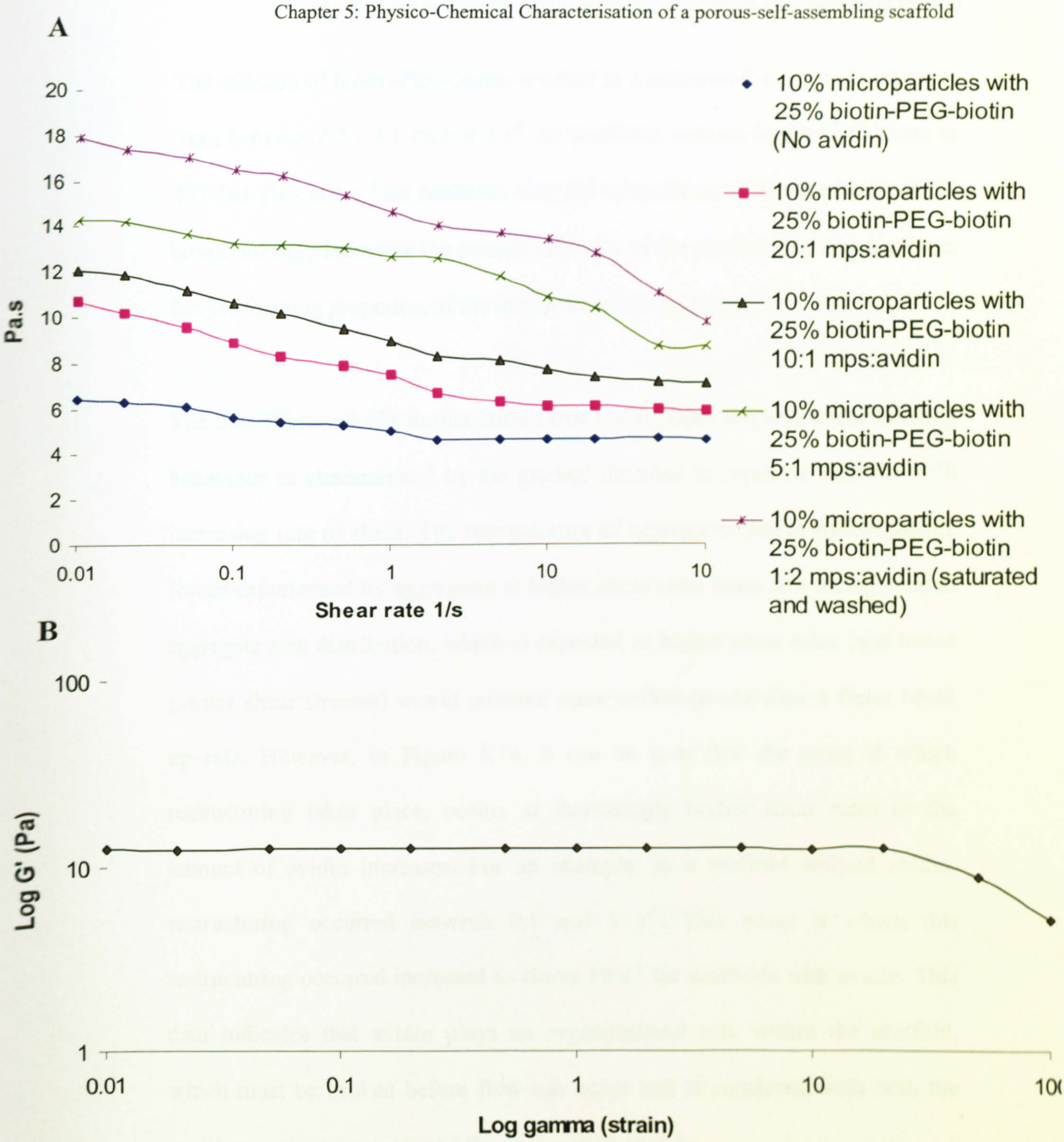

Figure 5.14 Shear rate dependent studies over a 0.1 - 100 s^{-1} range **A)** Plot of 10% microparticles (10 μm)/25% biotin-PEG-biotin with varying ratios of avidin and **B)** an amplitude sweep for 10% avidin saturated microparticles to determine linear viscoelastic region.

The addition of biotin-PEG-biotin resulted in a substantial increase in viscosity from between 2.2 - 4.1 Pa.s at 5 s^{-1} for scaffolds without biotin-PEG-biotin to 267-561 Pa.s at 5 s^{-1} for scaffolds with the bifunctional PEG. The biotin-PEG-biotin not only increases the overall viscosity of the scaffold but also increases the gel-forming properties of the avidin crosslinking agent.

The data (Figure 5.13) further shows that the scaffold displays shear thinning behaviour as characterised by the gradual increase in apparent viscosity with increasing rate of shear. The restructuring of aggregates due to hydrodynamic forces experienced by aggregates at higher shear rates leads to a steady state in aggregate size distribution, which is expected as higher shear rates (and hence greater shear stresses) would promote more collisions and thus a faster break up rate. However, in Figure 5.14, it can be seen that the point at which restructuring takes place, occurs at increasingly higher shear rates as the amount of avidin increases. For an example, in a scaffold without avidin, restructuring occurred between 0.1 and 1 s^{-1}. This point at which this restructuring occurred increased to above 10 s^{-1} for scaffolds with avidin. This data indicates that avidin plays an organisational role within the scaffold, which must be broken before flow can occur and is consistent with both the oscillatory measurements and the aggregation studies.

Thus rheological data has shown that controlling the concentrations of the various components within the scaffold can alter mechanical viscoelastic properties. For an example, increasing the proportions of microparticles, avidin or biotin-PEG-biotin can increase the overall viscosity of the scaffold and thus its load-bearing properties.

5.4 Conclusion

A fundamental physico-chemical study on the potential for a porous *in situ* solidifying scaffold has been presented. The main component, biodegradable PLA-PEG microparticles are sterically stabilised in a physiological liquid prior to scaffold formation. These microparticles have been demonstrated by SPR to have sufficient biotin units on the surface to undergo binding with avidin rapidly and specifically.

At precise concentrations of avidin, a cross-linking of the microparticles occurs and a scaffold forms. Above and below these concentrations, optimal aggregation is prevented through insufficient binding sites or saturation of the binding sites.

Tailoring the individual components of the scaffold may be used to optimise the mechanical properties. Where increased load bearing properties are necessary, bi-functional PEG can be added to increase the gel-forming component in the scaffold.

The procedure has also been demonstrated with nanoparticles (≈250 nm diameter) and microparticles (≈10 μm diameter) of PLA-PEG-biotin to illustrate the possibility of controllable properties such as porosity and degradation rates through variation in particle size.

Having shown that PLA-PEG-biotin microparticles will self-assemble to form scaffolds with gel-like structural properties, the next stage was to identify potential applications for the scaffold. In Chapter 6, the use of the self-assembling process in cell delivery and in forming defined three-dimensional scaffolds is investigated.

CHAPTER 6

THREE-DIMENSIONAL POROUS POLYMER AND CELL COMPOSITES THAT SELF ASSEMBLE *IN SITU*

6.1 Introduction.

Injectable gels have found many applications as cell delivery devices in tissue engineering. For example, Cao *et al.* have demonstrated the use of PEO/PPO/PEO copolymers mixed with isolated chondrocytes, to initiate formation of a layer of cartilage on host bone. The painted chondrocytes-polymer solution formed a semi-solid sticky gel within minutes. This newly formed cartilage then infiltrated the underlying osseus substrate to form a bone-cartilage interface. Such cell/polymer suspensions have been used for the formation of cartilage on the dorsum of mice using injectable systems (Vacanti *et al.* 1991; Cao *et al.* 1997; Temenoff and Mikos 2000). The delivery of chondrocytes within injectable gels has also been described for a number of other materials. These include alginate and PEO gels that have been used to produce injectable three-dimensional templates for cartilage formation,

although alginates are immunogenic and have poor resorbability and PEO based gels are not biodegradable (Atala *et al.* 1993).

These hydrogels however do not have large interconnected porous networks and, hence, the barrier of diffusion to signaling and nutrient molecules limits tissue formation. In addition, the mechanism of gelation as described in Chapter 5 may damage cells.

Furthermore the formation of defined three-dimensional scaffolds has to date been restricted to materials that are not capable of undergoing injection. Such scaffolds are generally processed using toxic solvents and require pre-fabrication prior to cell transplantation. This results in inefficient cell seeding, as isolated cells need to be transported throughout the scaffold.

In Chapter 5, a novel self-assembling scaffold was described that combined the benefits of water-insoluble porous scaffolds and injectable gels. The mechanism of self-assembly was based on the avidin-biotin mediated interaction. Having shown that the microparticles would self-assemble upon addition of a critical quantity of avidin, the next stage was to assess potential applications. The gel-like properties of the scaffold (G''<G') induced by the addition of avidin indicate that complex three-dimensional shapes could be formed. Furthermore, the receptor-ligand mediated method of self-assembly suggests that cells could be entrapped within the scaffold without harmful trigger signals such as UV exposure or temperature changes.

6.2 Methods and Materials

6.2.1 Formation of three-dimensional scaffolds

A poly(dimethyl siloxane) (PDMS) mould was formed by curing its prepolymer (Sylgard 184, Dow Corning) on a defined square based pyramidal shape. The PDMS mould was peeled off and washed with ethanol, hexane and de-ionized water. A scaffold (30% biotin-PEG-biotin, 60% avidin saturated PLA-PEG-biotin microparticles) was then injected into the mould. Following crosslinking of the two components of the scaffold, the mould was cut away to reveal the scaffold in the pyramidal shape of the mould into which it was injected. A further scaffold was manufactured (30% biotin-PEG-biotin, 60% PLA-PEG-biotin microparticles) without any avidin. Further PDMS moulds were made using a cube and round tablet like shape. Scaffolds in the shapes of these moulds were then also prepared with and without avidin. These were then assessed by SEM.

6.2.2 Cell culture experiments

3T3 fibroblasts (ATCC) and bovine aortic endothelial cells (ECACC) were cultured in DMEM supplemented with 10% foetal calf serum, 2 mM L-glutamine, 100 U/ml penicillin, 100 μg/ml streptomycin and 0.25 μg/ml amphotericin B. Cell cultures were incubated at 37°C in a 5% CO_2 enriched atmosphere. Approximately 1 x 10^6 of the 3T3 fibroblasts were placed into a mixture of 50% PLA-PEG-biotin microparticles and an optimum amount of

avidin (2mgs) was added to this to aggregate the microparticles and entrap the cells. This same procedure was then completed using 1 x 10^6 bovine aortic endothelial cells (BAECs). Scaffolds were then prepared for SEM by fixing the cells on the scaffold using 1ml of a 3% glutaraldehyde in 0.1 M phosphate buffer (pH 7.2) and leaving at 4°C overnight. The scaffolds were then washed 3 times in phosphate buffer for 15 minutes at a time. The fixative was poured off and then 1ml of 1% OsO_4 solution was added to fix the cells and provide a conductive coating of osmium. This improved the final image quality by reducing charging under the electron beam and enhancing the secondary electron emission. The scaffolds were washed 3 times in distilled water and dehydrated through a series of ethanol concentrations. Samples were then gold-coated and examined as described previously.

Human Osteoblast Sarcoma (HOS) cells were cultured in Dulbecco's modified Eagle's Medium (DMEM) supplemented with 10% foetal calf serum (FCS), 2 mM L-glutamine, 100 U/ml penicillin, 100 μg/ml streptomycin and 0.25 μg/ml amphotericin B (antibiotic/antimycotic), 1 x NEAA and 75 mg ascorbic acid. Cell cultures were incubated at 37°C in a 5% CO_2 enriched atmosphere. Every 2-3 days the cells were passaged, using 0.25% trypsin/ 1mM EDTA in PBS, and reseeded. Cells were incubated with Cell Tracker™ green CMFDA (5-chloromethylfluorescein diacetate) fluorescent stain (Molecular Probes), by reconstituting the material in 11 μl DMSO and adding this solution to the media of a confluent monolayer of cells for 45 min. The medium was then replaced and the cells incubated for a further hour. Following trypsinization and resuspension, the cells were centrifuged and resuspended in DMEM.

Approximately 1 x 10^6 cells were placed into a mixture of 50% avidin saturated PLA-PEG-biotin microparticles and 25% biotin-PEG-biotin was added to this to aggregate the microparticles and entrap the cells. Scaffolds were examined using a confocal microscope.

6.2.3 Injected scaffold stability studies

Agarose gels were prepared at 0.5, 1 and 2% concentrations. Initial studies using PLA-PEG microparticles indicated that diffusion of microparticles was best achieved using 0.5% Agarose gels. Scaffolds using 25% biotin-PEG-biotin, 50% avidin saturated PLA-PEG-biotin microparticles and 1 x 10^6 HOS cells were injected (2 ml) into the agarose gels. As a control, 25% biotin-PEG-biotin and 50% PLA-PEG-biotin microparticles (without avidin) and 1 x 10^6 HOS cells were injected (2 ml) into the agarose gels. A further control was to inject (2 ml) a scaffold using 25% Biotin-PEG-biotin, 50% avidin saturated PLA-PEG-biotin microparticles with no cells.

6.2.4 The Alamar blue assay for cell viability

An Alamar blue 10% working solution was prepared by mixing 1ml of an Alamar blue stock solution (Serotec) with 9 ml of Hanks Balanced Salts Solution (HBSS) without Phenol Red (Sigma) and sterilised using a 0.2 μm filter. The Alamar blue assay was carried out using 1 x 10^6 HOS cells entrapped within scaffolds prepared as described previously. Blanks using tissue culture plastic, cell free scaffolds and cells alone were carried out as comparisons. 100 μl samples were taken from each sample and placed into a

96 well plate, which was gently shaken for 5 minutes. Measurements were made using a plate reader (Ex 530 nm/Emm 590 nm) with a sensitivity setting at 50.

6.2.5 *In vivo* studies of polymer and cell composites.

In vivo studies on the self-assembling scaffold were carried out in conjunction with Dr Richard Orrefo of the University of Southampton.

Defined defects within chicken bones were filled *in situ* with self-assembled scaffolds containing 1 * 10^6 osteoprogenitor cells obtained from a young human. These were then placed onto the chorioallantoic membranes of chick embryos (CAMs). The CAMs were incubated for a period of up to 7 days before sample preparation. A total of 21 CAMs were included in the *in vivo* studies. This comprised of 4 controls without cells and 4 samples with additional BMP2 growth factor. The remaining CAMs were then included in the studies for repeatability controls.

6.3 Results and Discussion

Having established that PLA-PEG-biotin microparticles would self-assemble together upon addition of optimum quantities of avidin, the potential for this system as an injectable cell delivery device for tissue engineering was assessed. This could be achieved as illustrated schematically in Figure 6.1, by taking a mixture of microparticles and crosslinking with avidin as described in Chapter 5, but this time adding cells to the microparticle suspension thereby entrapping the cells within the aggregating particles. The interconnected porous structure as characterised in Chapter 5 would then allow the cells to spread and infiltrate the rest of the scaffold.

6.3.1 Formation of three-dimensional scaffolds

Mechanical testing of scaffolds in Chapter 5 had indicated that the microparticle aggregates had gel-like properties. Thus, such a system had potential for the formation of complex three-dimensional shapes using mould casting. Initially cell free scaffolds were formed. Such scaffolds could be used to fill a cavity within a patient and then promote infiltration of cells from neighbouring sites via scaffold-loaded signals. Figure 6.2 demonstrates the manufacturing process for the scaffold. In this process, avidin saturated PLA-PEG-biotin microparticles (60%) are co-injected with biotin-PEG-biotin (30%) into a PDMS cast of a defined pyramidal shape. Following crosslinking, the PDMS mould was cut away to reveal a porous scaffold that conformed to the pyramidal shape of the mould into which it was injected.

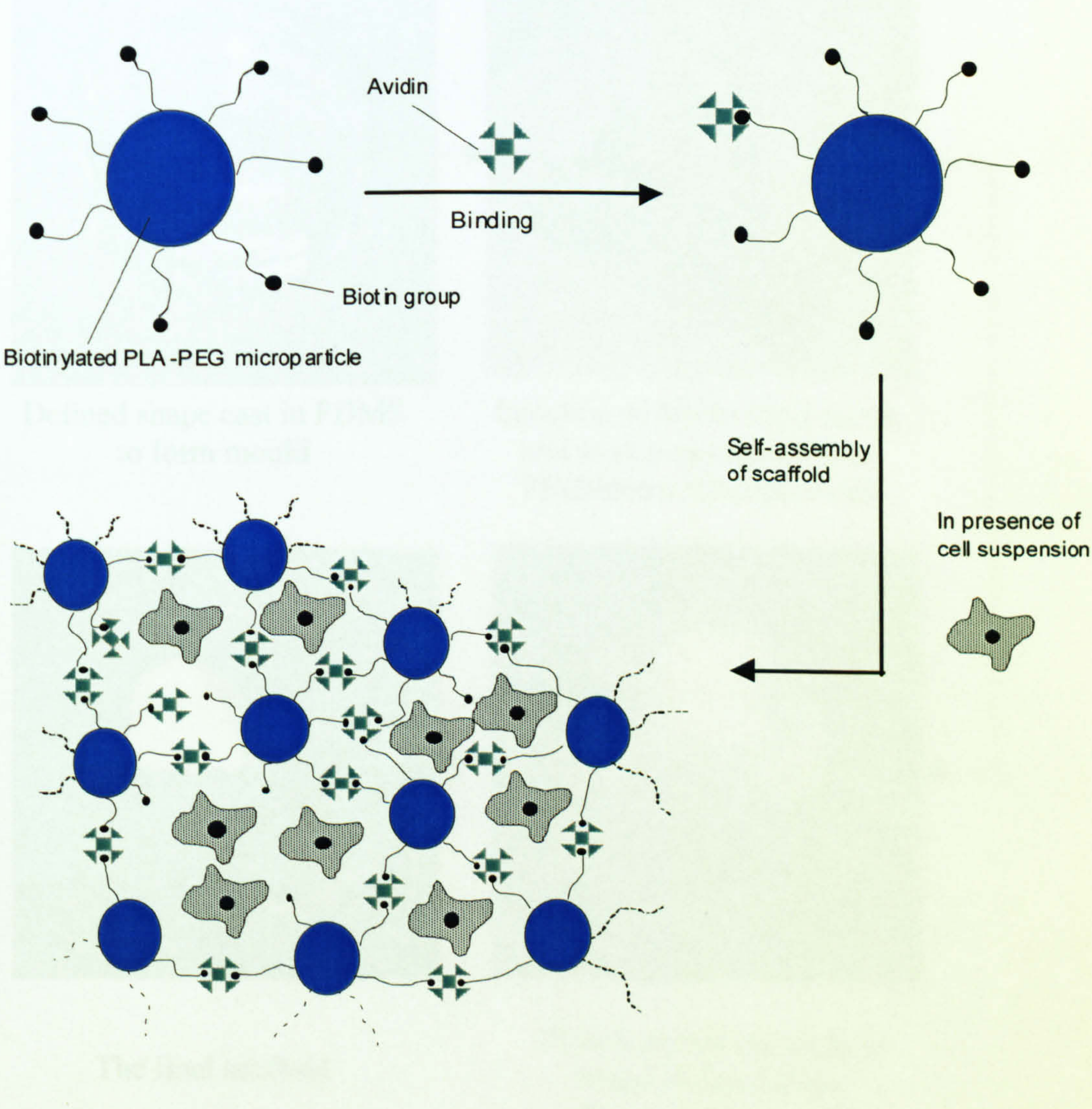

Figure 6.1 Schematic of the process of the self- assembly of porous polymer and cell composites.

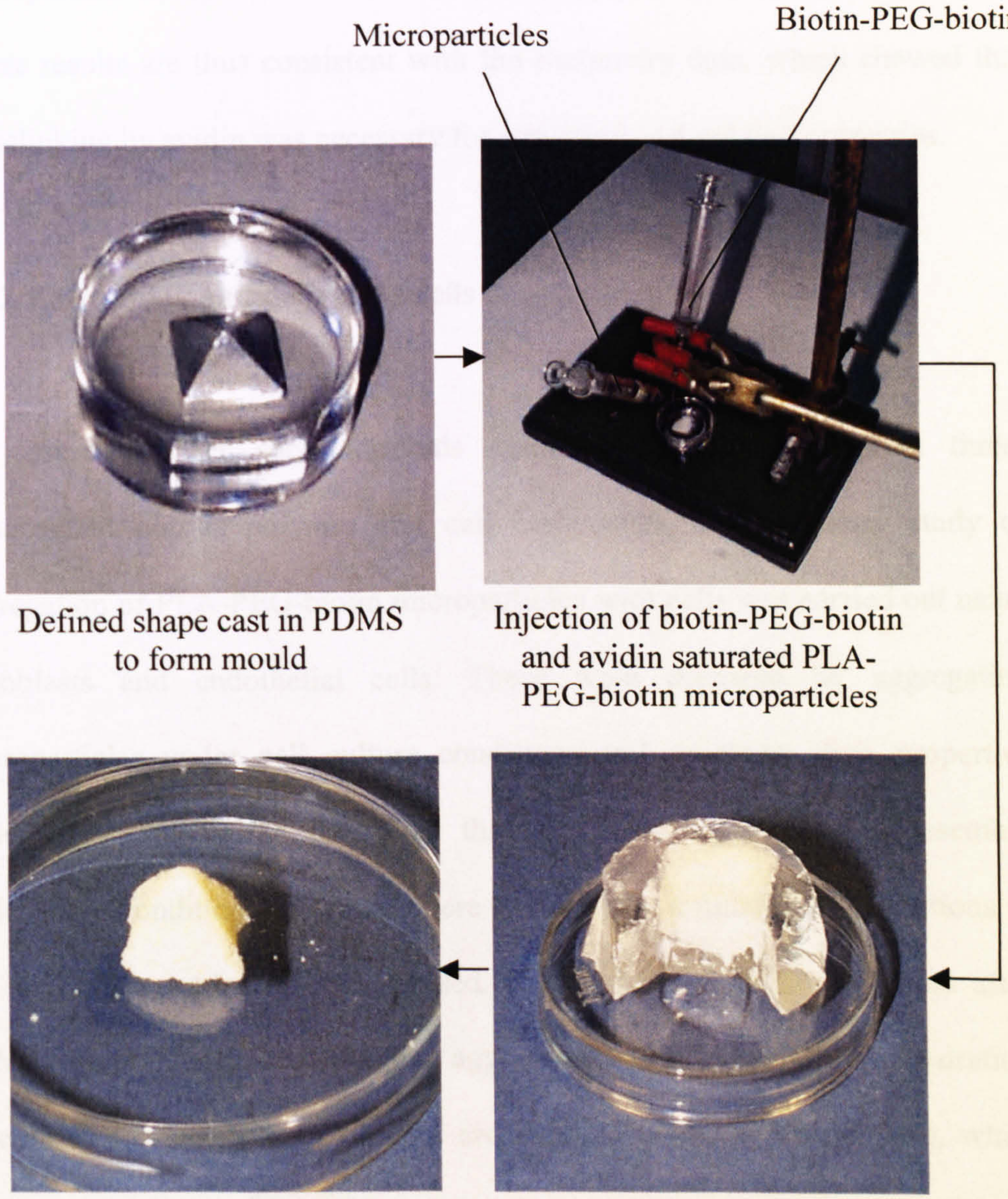

Figure 6.2 Defined three-dimensional pyramid scaffold fabricated with avidin saturated microparticles and biotin-PEG-biotin in PDMS mould

The SEM images in Figure 6.3 demonstrate the versatile range of shapes that this system can produce. In the absence of the cross-linker, avidin, the microparticle slurry fails to maintain the shape on removal from the mould. These results are thus consistent with the rheometry data, which showed that crosslinking by avidin was necessary for structural and gel like properties.

6.3.2 Entrapping and delivering cells

To assess whether such scaffolds could self-assemble to form three-dimensional porous polymer and cell composites, a preliminary study of aggregation of PLA-PEG-biotin microparticles with cells was carried out using fibroblasts and endothelial cells. These were prepared by aggregating microparticles under cell culture conditions and assessing their properties under SEM. Figure 6.4 illustrated that microparticles would self-assemble under these conditions; however, there were clearly a number of limitations in the study that needed to be addressed. Firstly, it was difficult to assess after SEM sample processing, whether aggregation was because of dehydration (necessary for cell fixation) or the crosslinking process. Furthermore, while SEM images appear three-dimensional, they preclude quantification of bulk interior structure. Whilst fibroblasts with good morphology could be seen with microparticles on the fringe of the scaffold aggregates (Figure 6.4), it was difficult to assess the entrapped cells within the scaffold.

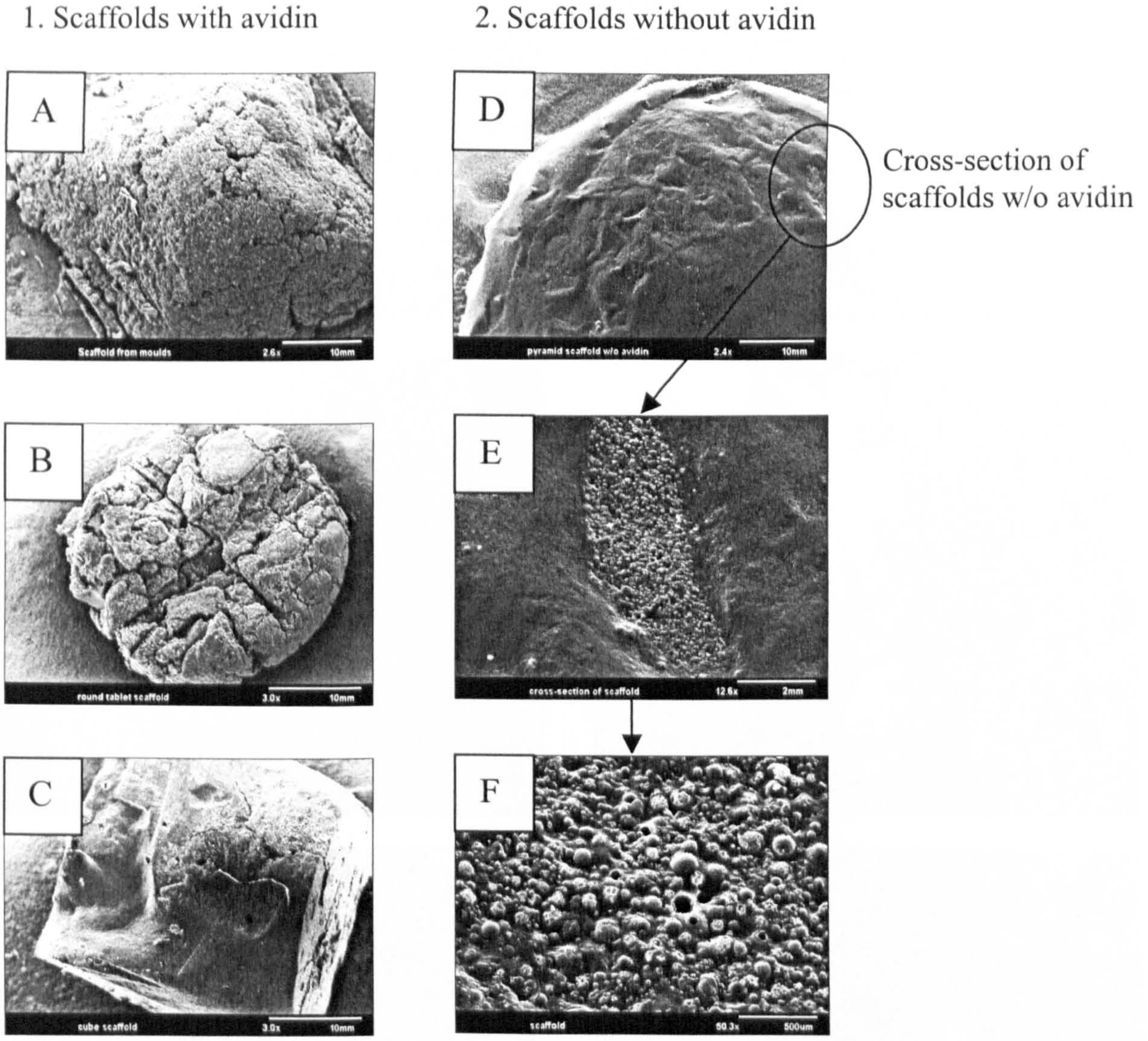

Figure 6.3 The formation of three dimensional structures using PDMS moulds:

A) Square based pyramid, B) Round Tablet, C) Cube, D) Square based pyramid scaffold formed without avidin showing scaffold's failure to maintain shape and E/F) Close-up of a cross-section of the scaffold without avidin.

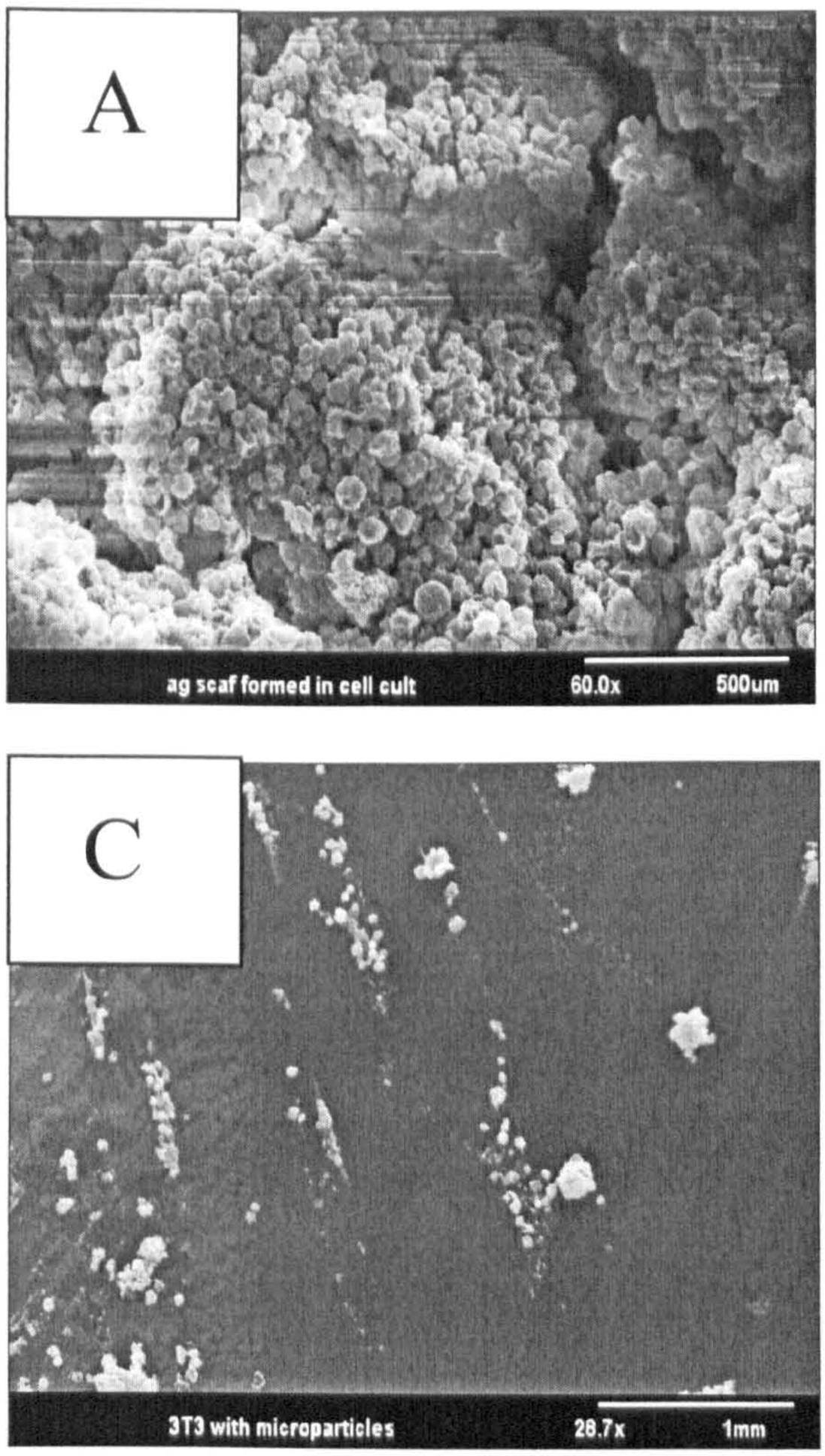

Figure 6.4 Preliminary study of aggregation of microparticles under cell culture condition (DMEM with FCS, ABAM, L-glutamine, 37°C, 3T3 fibroblasts or BAECs). SEM samples fixed with glutaraldehyde, coated with OsO4 and dehydrated and then gold coated. **A/B)** Microparticles aggregating under cell culture conditions. **C/D)** 3T3 Fibroblasts associating with microparticles on the fringe of scaffold aggregates **E/F)** BAECS on an aggregated microparticle scaffold

Finally, in assessing potential applications for the scaffold, it was determined that the repair of damaged bone type tissues such as that found in the spinal column would be an ideal candidate for delivering cells such as osteoblasts within the injectable scaffold, given the delicate nature of surgical procedures around this region. For this reason, a pyramidal shaped scaffold with $1x10^6$ human osteoblast sarcoma (HOS) cells entrapped within the structure was formed.

Confocal microscopy has been demonstrated to be a powerful tool in the analysis of three-dimensional porous scaffolds (Tjia and Moghe 1998) and was thus used to produce optically sectioned serial 2-D images of human osteoblasts entrapped within our self-assembled scaffold. The confocal fluorescence images in Figure 6.5 display the distribution of cell populations through sections of the scaffold with the cells identified by a fluorescent marker (green/excitation 488nm) and the PLA-PEG-biotin microparticles identified by the reflected light signal (red/RT 30/70). Confocal images were taken throughout the scaffold and displayed single cells and small clusters of cells distributed evenly.

6.3.3 Scaffold formation in simulated tissues

To demonstrate that the cross-linking process for the formation of a 3D scaffold within a simulated tissue was feasible; 0.5% agarose gels were prepared and microparticles, biotin-PEG-biotin and cells were injected without avidin, through a syringe needle.

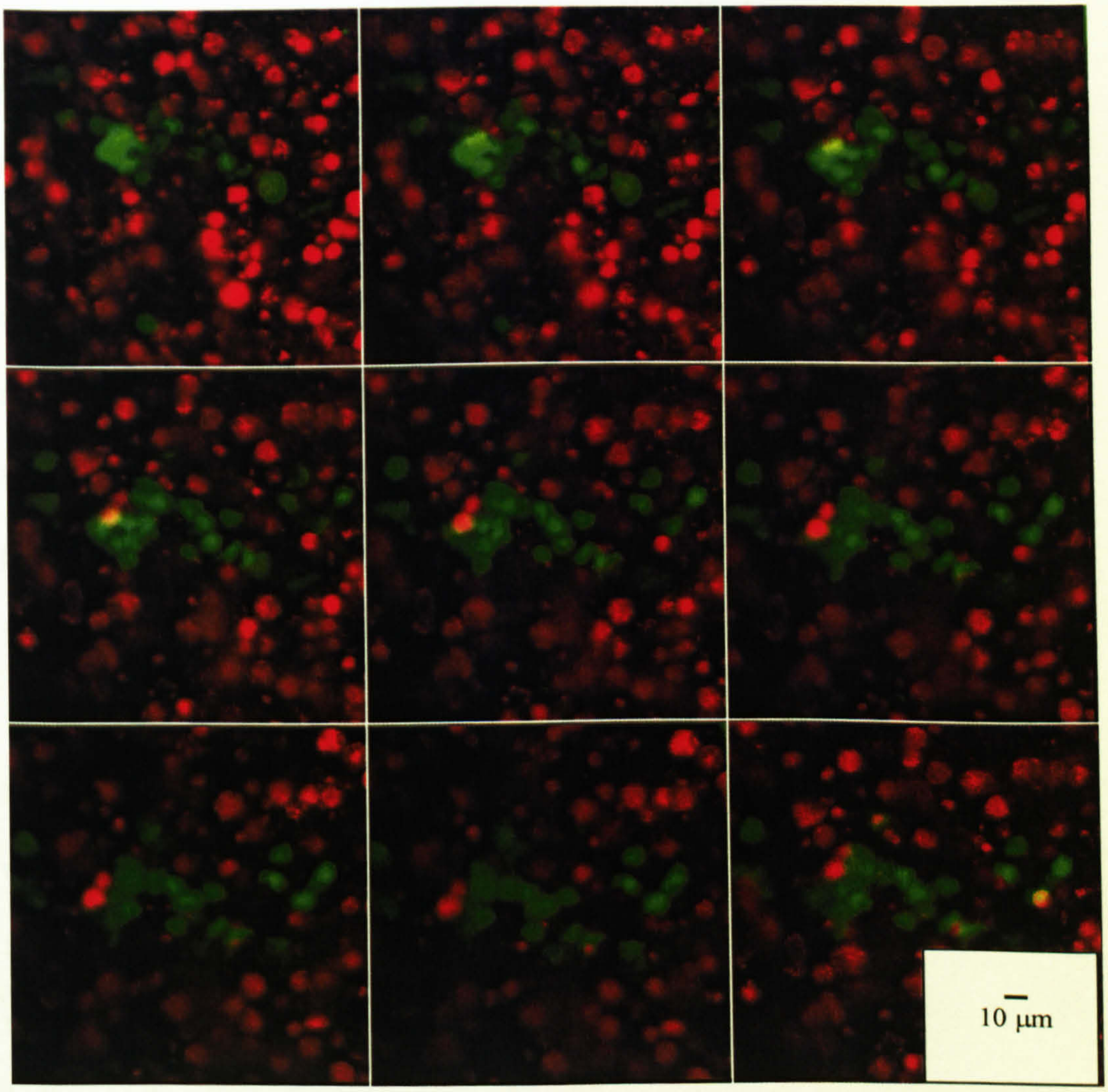

Figure 6.5 Series of Confocal microscopy images of cross-sections of scaffold (red reflectance) displaying entrapped osteoblasts (green, CellTracker™).

The microparticles were able to diffuse through the agarose and, hence, did not form a scaffold (Figure 6.6). Higher concentrations of agarose at 1% and 2% were not suitable because microparticles without avidin did not diffuse through

The experiment was then repeated but this time avidin was co-injected with the saturated microparticles. Agarose images in Figure 6.6 display the ability of the injected scaffold containing the avidin crosslinking agent with entrapped cells to maintain shape in comparison to injected scaffolds without avidin. The scaffold structure shown in Figure 6.6 instantly formed as a result of the self-assembly process converting the colloidal injection into a solid mass. Such a procedure could be used to inject cells into soft tissue sites forming scaffolds within a restricted region.

Scaffolds formed in the simulated tissues were then tested for cell viability using the Alamar blue test. The Alamar blue assay incorporates a fluorometric/colourimetric growth indicator based on the detection of metabolic activity. The system incorporates an oxidation-reduction (RE DOX) indicator that both fluoresces and changes colour in response to a chemical reduction of growth medium resulting from cell metabolism. As cells grow in culture, innate metabolic activity results in a chemical reduction of the immediate surrounding environment. Continued viability maintains a reduced environment while inhibition of viability maintains an oxidized environment. Reduction related to metabolism causes the REDOX indicator to change from oxidised (non-fluorescent, blue) to a reduced form (fluorescent, red).

The microparticles were able to diffuse through the agarose and, hence, did not form a scaffold (Figure 6.6). Higher concentrations of agarose at 1% and 2% were not suitable because microparticles without avidin did not diffuse through

The experiment was then repeated but this time avidin was co-injected with the saturated microparticles. Agarose images in Figure 6.6 display the ability of the injected scaffold containing the avidin crosslinking agent with entrapped cells to maintain shape in comparison to injected scaffolds without avidin. The scaffold structure shown in Figure 6.6 instantly formed as a result of the self-assembly process converting the colloidal injection into a solid mass. Such a procedure could be used to inject cells into soft tissue sites forming scaffolds within a restricted region.

Scaffolds formed in the simulated tissues were then tested for cell viability using the Alamar blue test. The Alamar blue assay incorporates a fluorometric/colourimetric growth indicator based on the detection of metabolic activity. The system incorporates an oxidation-reduction (RE DOX) indicator that both fluoresces and changes colour in response to a chemical reduction of growth medium resulting from cell metabolism. As cells grow in culture, innate metabolic activity results in a chemical reduction of the immediate surrounding environment. Continued viability maintains a reduced environment while inhibition of viability maintains an oxidized environment. Reduction related to metabolism causes the REDOX indicator to change from oxidised (non-fluorescent, blue) to a reduced form (fluorescent, red).

Figure 6.6 **A)** Scaffolds using 25% biotin-PEG-biotin, 50% avidin saturated PLA-PEG-biotin microparticles and 1 x 10^6 human osteoblast sarcoma (HOS) cells injected (2ml) into 0.5% agarose gels. **B)** As a control, 25% biotin-PEG-biotin, 50% PLA-PEG-biotin microparticles (without avidin) and 1 x 10^6 HOS cells were injected (2ml) into 0.5% agarose gels and failed to hold a scaffold shape.

Cells entrapped within the scaffold, demonstrated viability, with an initial fluorescence of 1854 at 30 minutes, increasing to 4563 at the 4-hour time point (Figure 6.7). It is worth noting that the period of time over which this assay was performed was not enough to elucidate growth statistics. The lack of a suitable standard also means that no conclusions other than viability of the cells can be drawn from this data. Furthermore, the scaffolds tested were in their untreated form and with the use of targeted cell adhesive biotinylated peptides and/or appropriate growth factors, cell spreading and viability could be increased (Cannizzaro *et al.* 1998).

6.3.5 *In vivo* performance of scaffold/cell composites

Having shown that cells remained viable within the scaffold, the next stage was to assess the scaffold's performance *in vivo.* Osteoprogenitor cells obtained from a young human were used to produce polymer and cell composites within bone defects. These were then tested on the chorioallantoic membranes of chick embryos over a period of up to 7 days. Whilst this model lacks a full immunogenic system, initial results as illustrated in Figure 6.8 indicate that bone defects filled with scaffold-cell composites will become vascularized and this therefore holds great potential for further development.

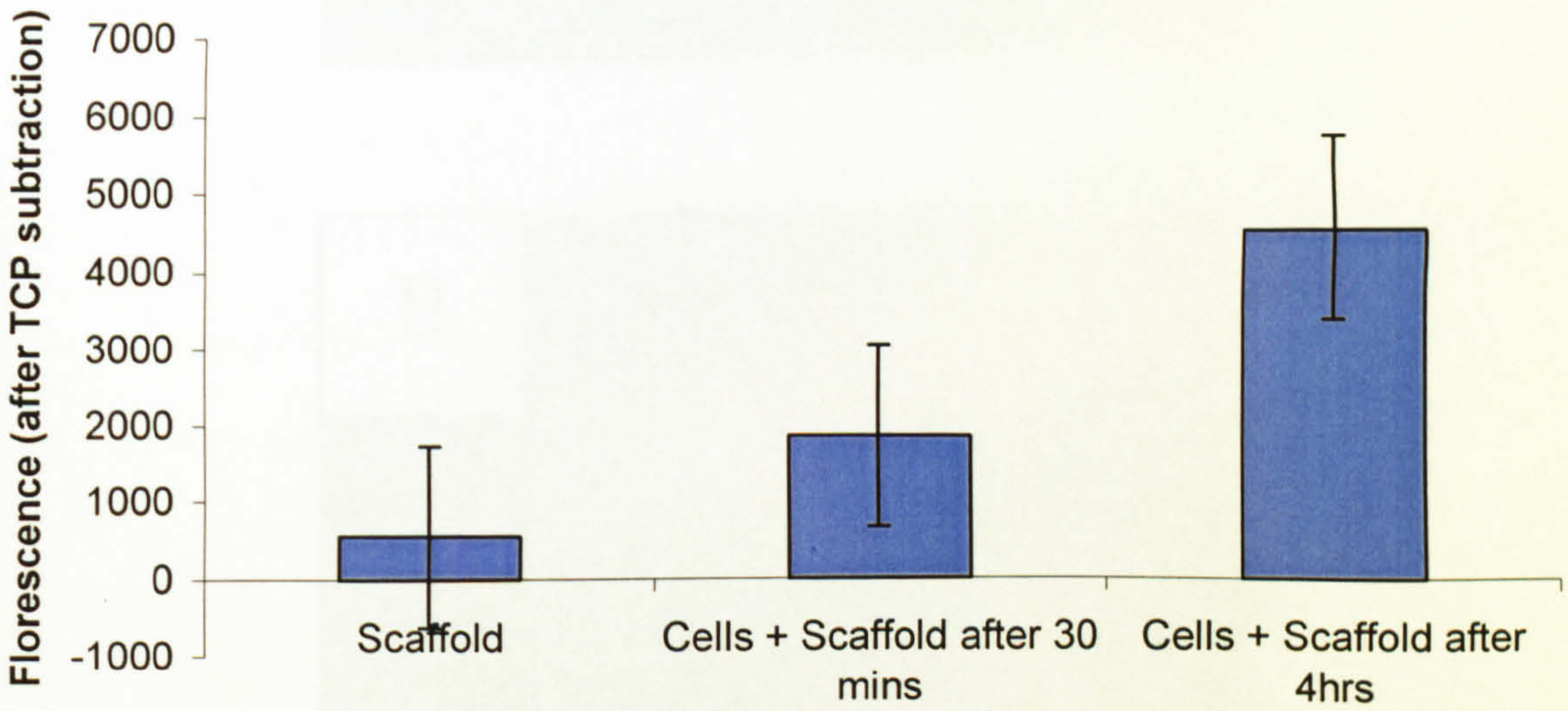

Figure 6.7 Alamar Blue assay results on entrapped HOS cells ($1x10^6$) after injection and crosslinking in scaffold.

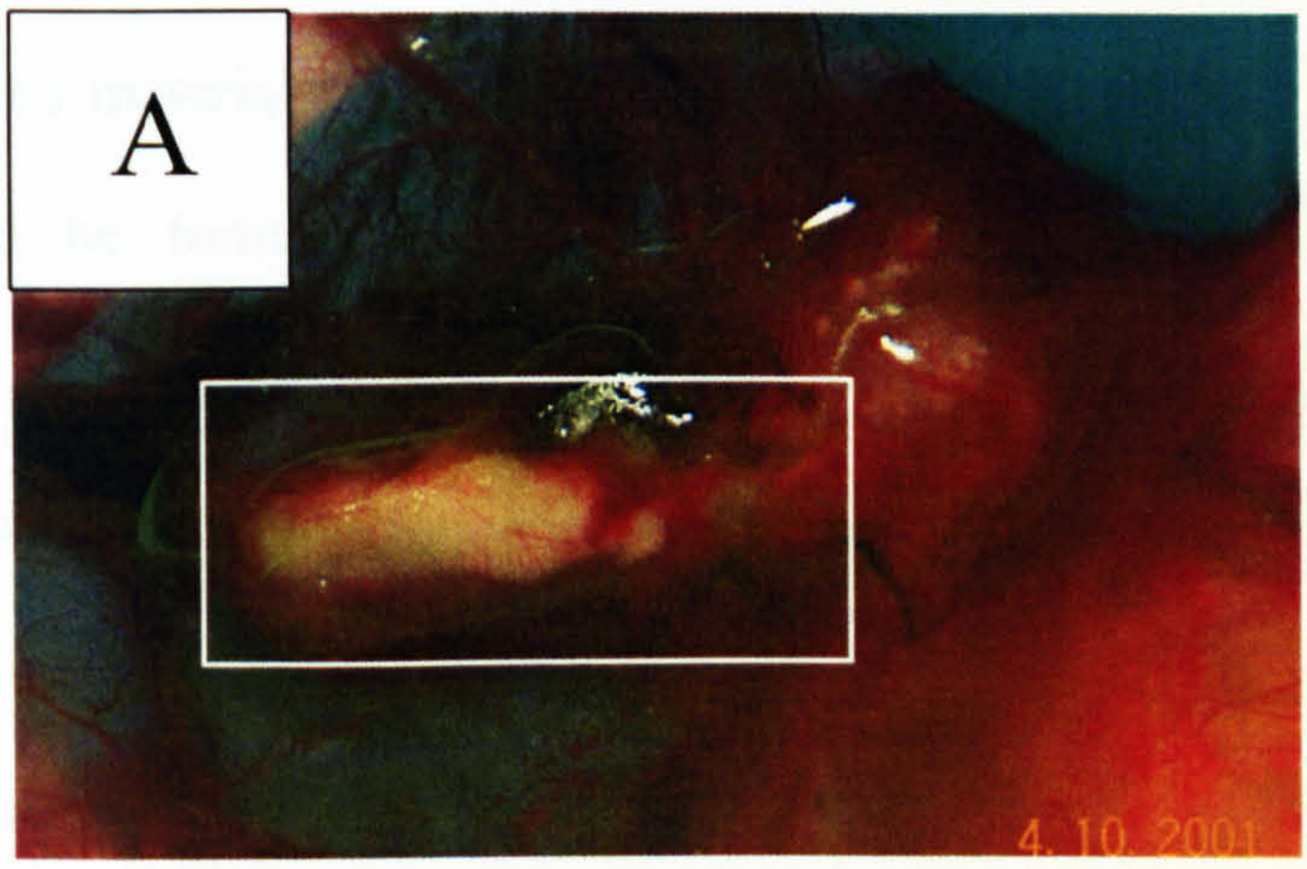

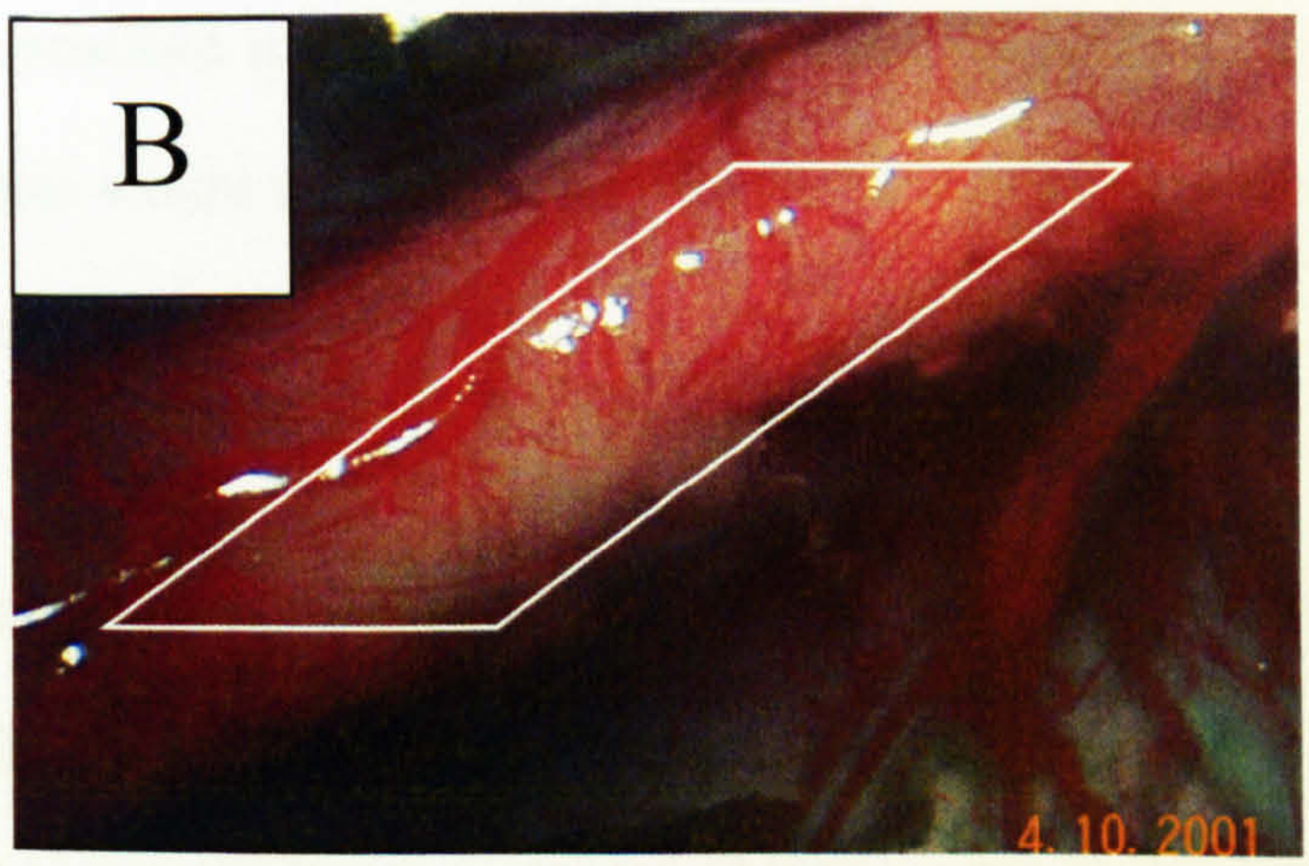

Figure 6.8 *In vivo* images showing vascularization of bone defects filled with self-assembling osteoprogenitor/scaffold composites. A) Top view of bone and B) bottom view of bone on the membrane of the chick embryo. (White boxes indicate section of bone filled with self-assembling scaffold)

(Courtesy of R.Oreffo, University of Southampton)

6.4 Conclusion

The novel molecular-interaction mechanism of self-assembly of these scaffolds differentiates this material from other injectable systems. Cell and polymer composites can be formed *in situ*, using an injectable system, without transformation via cell harmful trigger signals. Furthermore, scaffolds are formed with interconnected porous structures allowing cell infiltration.

Using PDMS moulds, defined three-dimensional scaffolds were produced. These failed to maintain their shape without the addition of avidin. Similarly injection of the scaffold in simulated tissues using weak agarose gels showed that microparticles would diffuse without avidin but maintained shape with the crosslinking agent.

In vitro studies have demonstrated that cells entrapped within the self-assembled scaffolds are well distributed and remain viable. *In vivo* studies using chick embryos were than carried out with osteoprogenitor cells entrapped within self-assembled scaffolds. These polymer and cell composites were shown to be capable of undergoing vascularization and promoting tissue ingrowth.

Whilst avidin has generated immune responses *in vivo*; concerns over the long term *in vivo* potential of the self-assembling scaffold due to the antigenicity of the avidin molecule are countered by the use of PEG, which reduces immune responses to avidin significantly (Marshall and Pedley 1996).

This self-assembling material thus has a wide variety of applications from the formation of preformed defined three-dimensional scaffolds without the use of toxic solvents to the injectable delivery of viable cells within a porous matrix.

CHAPTER 7

CONCLUSIONS

An aim in tissue engineering is to achieve natural regeneration of tissues and organs by utilising the natural healing process. Often it is necessary to use a scaffold to support tissue growth. This can be with or without cell transplantation within the scaffold. Scaffolds without cells could promote cell ingrowth and vascularization using controlled release of growth factors in a process known as tissue induction.

The use of scaffolds with cells is necessary because isolated cells injected into the body at random cannot form new tissue on their own. Within scaffolds however, the cells can begin to secrete their own extracellular matrix, the polymer scaffold degrades and is eventually eliminated from the body, resulting in completely natural tissue replacement.

Scaffolds must satisfy a number of requirements for use in cell transplantation. They must have cell-interactive surface properties, porosity, biodegradability

and suitable mechanical properties. The scaffold should also be ideally capable of controlled release.

To date, research has been focussed on two areas of scaffolds for tissue regeneration. These have been water-insoluble porous scaffolds or injectable gels. Water-insoluble scaffolds have traditionally been based on synthetic biodegradable biomaterials that are established as surgical materials. In contrast, research on injectable gels has been directed towards natural materials. These natural materials can suffer from a variety of problems relating to immunogenicity and lack of mechanical strength. A number of synthetic injectable materials have also been developed. However, these synthetic materials generally require cell harmful trigger signals for the transformation to gel, such as UV exposure, pH changes or sudden temperature changes. The most significant difficulty with injectable materials, however, lies in the lack of porosity within these gels limiting tissue formation and vascularization to the barrier of diffusion of signalling and nutrient molecules.

Traditional water-insoluble scaffolds have been designed to be porous, biodegradable, cell interactive and with tailored mechanical strength. However, these materials require invasive surgical procedures and prior knowledge of the shape of the defect/cavity. Furthermore, cell seeding can suffer from poor transport of the cell through the scaffold.

The purpose of the work presented in this thesis was to combine the benefits of traditional scaffolds with those of the injectable materials. In Chapter 3, the

synthesis of a novel biomaterial with self-assembling properties that can integrate biological activity into its surface chemistries is described. PLA-PEG-biotin combines the benefits of PLA-PEG based copolymer systems with the advantages of the universal avidin-biotin linkage system. Using ^{1}H-NMR spectroscopic, DSC, GPC, SPR analysis and fluorescent spectroscopy studies, the synthesis of PLA-PEG-biotin was shown to maintain the integrity of the functionalised end-group without affecting the bulk properties. The synthesis thus provides us with a material that can form the foundation of our proposed self-assembling porous scaffold.

As described, the potential for controllable porosity by our proposed self-assembling scaffold is a considerable advantage over other injectable *in situ* transforming biomaterials. Therefore before manufacturing the scaffold, a comprehensive study of two model cell types involved in vascularization processes was carried in out Chapter 4, over a series of defined pore features.

This study of cells over defined pore features determined that cell behaviour is interlinked by three factors: 1) cell type, 2) cell density and 3) pore size. These observations were important because the proposed scaffold would be able to control pore size and its self-assembling process could control distribution of cells throughout the scaffold. Therefore the next stage was to manufacture and conduct a systematic physico-chemical study on the potential of the self-assembling porous scaffold.

In Chapter 5, using a single emulsion method, microparticles were manufactured with the PLA-PEG-biotin synthesised in Chapter 3. SPR analysis demonstrated that the microparticles would bind with avidin. Aggregation studies revealed that by using precise concentrations of avidin, a cross-linking of the microparticles occurs and a scaffold forms. Above and below these concentrations, optimal aggregation is prevented through insufficient binding sites or saturation of the binding sites. Tailoring the individual components of the scaffold was shown to control the mechanical properties. Where increased load bearing properties were necessary, bi-functional PEG could be added to increase the gel-forming component in the scaffold. To demonstrate the possibility of controllable properties such as porosity, the scaffold formation was carried out using both nano and microparticles.

Next, potential applications of this self-assembling scaffold were assessed. In Chapter 6, the use of the self-assembling process in cell delivery and in forming defined three-dimensional scaffolds was investigated. Using simulated environments, the scaffold was able to form defined three-dimensional shapes within defined cavities or soft-tissues. Polymer and cell composites were formed using human osteoblast sarcoma cells. The Alamar blue assay confirmed these cells remained viable once seeded within the scaffold. *In vivo* studies were then carried out with chick embryos using human osteoprogenitor cells entrapped within the self-assembling scaffolds. These studies showed that such polymer and cell composites were capable of tissue ingrowth and would therefore readily undergo vascularization.

The novel scaffold presented in this thesis combines the benefits of both traditional water-insoluble scaffolds and injectable biomaterials. The novel self-assembling process produces a scaffold that can form *in situ* using a binding mechanism that does not interfere with cells. Thus the scaffold is capable of highly efficient well-distributed cell seeding. The interconnected porous structure of the scaffold once formed allows cell infiltration and thus vascularization. The basic component of the scaffold is a biodegradable microparticle that can be formed from any of the poly (α-hydroxyacids) or indeed other polymers. Hence, conventional controlled release technologies and surface engineering can be combined with the self-assembly to form biomimetic scaffolds that stimulate integrin-mediated cell adhesion and then release growth factors. The ability of the scaffold to form a versatile range of shapes *in situ* with porous morphology and favourable rheological properties thus has potential for a variety of tissue engineering and drug delivery applications.

7.1 Further work.

The numerous advantages presented by the scaffold include the use of controlled release of growth factors from the microparticles and surface engineering of the scaffolds through cell adhesive peptides. Therefore future work may include studies that combine these modifications with the scaffold.

The potential for the scaffold to self-assemble *in vivo* is in part dependent on the delivery vehicle. Therefore the development of a syringe system that can

deliver both the crosslinking factor and the cells and/or microparticles is a further area of investigation.

Finally, the potential for microparticles to aggregate is not restricted to the avidin-biotin interaction. Therefore, given the possible immunogenic responses to the avidin within the scaffold, it is a desirable strategy to search for alternative crosslinking processes. For example, microparticles manufactured from a positively charged polymer could potentially aggregate upon addition of negatively charged ions.

REFERENCES

Agrawal, C. M. (1998). Reconstructing the human body using biomaterials. *Journal of the Minerals, Metals and Materials Society* **50**(1): 31-35.

Atala, A., L. G. Cima, *et al.* (1993). Injectable Alginate Seeded With Chondrocytes As a Potential Treatment For Vesicoureteral Reflux. *Journal of Urology* **150**(2): 745-747.

Atala, A. and L. M. Nyberg (2000). Tissue engineering. *World Journal of Urology* **18**(1): 1-1.

Athanasiou, K. A., J. P. Schmitz, *et al.* (1998). The effects of porosity on *in vitro* degradation of polylactic acid polyglycolic acid implants used in repair of articular cartilage. *Tissue Engineering* **4**(1): 53-63.

Babensee, J. E., J. M. Anderson, *et al.* (1998). Host response to tissue engineered devices. *Advanced Drug Delivery Reviews* **33**(1-2): 111-139.

Babensee, J. E., L. V. McIntire, *et al.* (2000). Growth factor delivery for tissue engineering. *Pharmaceutical Research* **17**(5): 497-504.

Baldwin, S. P. and W. M. Saltzman (1996). Polymers for tissue engineering. *Trends in Polymer Science* **4**(6): 177-182.

Barrera, D. A., E. Zylstra, *et al.* (1993). Synthesis and RGD peptide modification of a new biodegradable copolymer: Poly(lactic acid-co-lysine). *Journal of the American Chemical Society* **115**: 11010-11011.

Bates, H. A. and S. B. Rosenblum (1985). 300 Mhz H-1-Nmr Spectra and Conformations of Biotin and Related Hexahydrothienoimidazolone Derivatives. *Tetrahedron* **41**(12): 2331-2336.

Bellamkonda, R. and P. Aebischer (1994). Review: Tissue engineering in the nervous system. *Biotechnology and Bioengineering* **43**: 543-554.

Black, F. E., M. Hartshorne, *et al.* (1999). Surface Engineering and Surface Analysis of a Biodegradable Polymer with Biotinylated End Groups. *Langmuir* **15**(9): 3157-3161.

Bonassar, L. J. and C. A. Vacanti (1998). Tissue engineering: The first decade and beyond. *Journal of Cellular Biochemistry*(S30-31): 297.

Brauker, J. H., V. E. Carrbrendel, *et al.* (1995). Neovascularization of Synthetic Membranes Directed By Membrane Microarchitecture. *Journal of Biomedical Materials Research* **29**(12): 1517-1524.

Brunette, D. M. (1986). Fibroblasts On Micromachined Substrata Orient Hierarchically to Grooves of Different Dimensions. *Experimental Cell Research* **164**(1): 11-26.

Brunette, D. M. (1986). Spreading and Orientation of Epithelial-Cells On Grooved Substrata. *Experimental Cell Research* **167**(1): 203-217.

Burg, K. J. L., W. D. Holder, *et al.* (2000). Comparative study of seeding methods for three-dimensional polymeric scaffolds. *Journal of Biomedical Materials Research* **51**(4): 642-649.

Burkoth, A. K. and K. S. Anseth (2000). A review of photocrosslinked polyanhydrides: in situ forming degradable networks. *Biomaterials* **21**(23): 2395-2404.

Campbell, C. E. and A. F. Von Recum (1989). Microtopography and soft tissue response. *Journal of Investigative Surgery* **2**: 51-74.

Cannizzaro, S. M., R. F. Padera, *et al.* (1998). A novel biotinylated degradable polymer for cell-interactive applications. *Biotechnology and Bioengineering* **58**(5, June 5th): 529-535.

Cao, X. D. and M. S. Shoichet (1999). Delivering neuroactive molecules from biodegradable microspheres for application in central nervous system disorders. *Biomaterials* **20**(4): 329-339.

Cao, Y. L., J. P. Vacanti, *et al.* (1997). Transplantation of chondrocytes utilizing a polymer-cell construct to produce tissue-engineered cartilage in the shape of a human ear. *Plastic and Reconstructive Surgery* **100**(2): 297-302.

Cavallaro, J. F. and P. D. Kemp (1994). Collagen fabrics as biomaterials. *Biotechnology and Bioengineering* **43**: 781-791.

Chen, X., S. P. McCarthy, *et al.* (1997). Synthesis and characterization of (L)-lactide-ethylene oxide multiblock copolymers. *Macromolecules* **30**: 4295-4301.

Chenite, A., C. Chaput, *et al.* (2000). Novel injectable neutral solutions of chitosan form biodegradable gels in situ. *Biomaterials* **21**(21): 2155-2161.

Chern, C. S., C. K. Lee, *et al.* (1996). Biotin-modified submicron latex particles for affinity precipitation of avidin. *Colloids and Surfaces B-Biointerfaces* **7**(1-2): 55-64.

Chiruvolu, S., S. Walker, *et al.* (1994). Higher-Order Self-Assembly of Vesicles By Site-Specific Binding. *Science* **264**(5166): 1753-1756.

Christenson, L. (1999). Tissue engineering update - Broadening the scope of applications. *Genetic Engineering News* **19**(8): 7-+.

Christenson, L., A. G. Mikos, *et al.* (1997). Biomaterials for tissue engineering: Summary. *Tissue Engineering* **3**(1): 71-76.

Chuang, W. Y., T. H. Young, *et al.* (1999). Properties of the poly(vinyl alcohol)/chitosan blend and its effect on the culture of fibroblast in vitro. *Biomaterials* **20**(16): 1479-1487.

Cima, L. G., D. E. Ingber, *et al.* (1991). Hepatocyte culture on biodegradable polymeric substrates. *Biotechnology and Bioengineering* **38**: 145-158.

Cima, L. G., J. P. Vacanti, *et al.* (1991). Tissue engineering by cell transplantation using degradable polymer substrates. *Journal of Biomechanical Engineering* **113**(May): 143-149.

Clark, P. (1994). Cell behaviour on micropatterned surfaces. *Biosensors & Bioelectronics* **9**: 657-661.

Clark, P., P. Connolly, *et al.* (1987). Topographical Control of Cell Behavior .1. Simple Step Cues. *Development* **99**(3): 439-448.

Clark, P., P. Connolly, *et al.* (1990). Topographical Control of Cell Behavior .2. Multiple Grooved Substrata. *Development* **108**(4): 635-644.

Clark, P., P. Connolly, *et al.* (1991). Cell Guidance By Ultrafine Topography In vitro. *Journal of Cell Science* **99**: 73-77.

Clowes, A. W., T. R. Kirkman, *et al.* (1986). Mechanisms of Arterial Graft Healing - Rapid Transmural Capillary Ingrowth Provides a Source of Intimal Endothelium and Smooth-Muscle in Porous Ptfe Prostheses. *American Journal of Pathology* **123**(2): 220-230.

Clowes, A. W., R. K. Zacharias, *et al.* (1987). Early Endothelial Coverage of Synthetic Arterial Grafts - Porosity Revisited. *American Journal of Surgery* **153**(5): 501-504.

Coester, C., J. Kreuter, *et al.* (2000). Preparation of avidin-labelled gelatin nanoparticles as carriers for biotinylated peptide nucleic acid (PNA). *International Journal of Pharmaceutics* **196**(2): 147-149.

Cook, A. D., J. S. Hrkach, *et al.* (1997). Characterization and development of RGD-peptide-modified poly(lactic acid-co-lysine) as an interactive, resorbable biomaterial. *Journal of Biomedical Materials Research* **35**: 513-523.

Cook, J. R., B. E. Crute, *et al.* (1989). Microporosity of the Substratum Regulates Differentiation of Mdck Cells-Invitro. *In Vitro Cellular & Developmental Biology* **25**(10): 914-922.

Cosnier, S. and A. Lepellec (1999). Poly(pyrrole-biotin): a new polymer for biomolecule grafting on electrode surfaces. *Electrochimica Acta* **44**(11): 1833-1836.

Curtis, A. and C. Wilkinson (1997). Topographical control of cells. *Biomaterials* **18**(24): 1573-1583.

Curtis, A. and C. Wilkinson (2001). Nantotechniques and approaches in biotechnology. *Trends in Biotechnology* **19**(3): 97-101.

Curtis, A. S. G. (1994). Nanofabrication and its applications in medicine and biology. *Engineering and Physical Processes* **Chapter 3**: 41-55.

Curtis, A. S. G. and P. Clark (1990). The Effects of Topographic and Mechanical-Properties of Materials On Cell Behavior. *Critical Reviews in Biocompatibility* **5**(4): 343-362.

Davis, M. and J. P. Vacanti (1996). Toward development of an implantable tissue engineered liver. *Biomaterials* **17**: 365-372.

Deible, C. R., P. Petrosko, *et al.* (1998). Molecular barriers to biomaterial thrombosis by modification of surface proteins with polyethylene glycol. *Biomaterials* **19**(20): 1885-1893.

Den Dunnen, W. F. A., B. Van Der Lei, *et al.* (1993). Long-term evaluation of nerve regeneration in a biodegradable nerve guide. *Microsurgery* **14**: 508-515.

Denbraber, E. T., J. E. Deruijter, *et al.* (1995). Effect of Parallel Surface Microgrooves and Surface-Energy On Cell-Growth. *Journal of Biomedical Materials Research* **29**(4): 511-518.

Deng, X. M., C. D. Xiong, *et al.* (1990). Synthesis and Characterization of Block Copolymers From D,L-Lactide and Poly(Ethylene Glycol) With Stannous Chloride. *Journal of Polymer Science Part C-Polymer Letters* **28**(13): 411-416.

Diamandis, J. P. and T. K. Christopoulos (1991). The biotin-(strept)avidin system: Principles and applications in biotechnology. *Clinical Chemistry* **37**: 625-636.

Ding, Z. L., C. J. Long, *et al.* (1999). Temperature control of biotin binding and release with a streptavidin-poly(N-isopropylacrylamide) site-specific conjugate. *Bioconjugate Chemistry* **10**(3): 395-400.

Drumheller, P. D. and J. A. Hubbell (1995). Surface immobilization of adhesion ligands for investigation of cell-substrate interactions. *Tissue engineering*: 1583-1581.

Drumheller.P, H. C., Hubbell.J (1998). Bioactive Peptides and Surface Design. Frontiers in Tissue Engineering. C. W. P. Jr, Pargamon: 273-310.

Eaglstein, W. H. and V. Falanga (1998). Tissue engineering for skin: An update. *Journal of the American Academy of Dermatology* **39**(6): 1007-1010.

Edelman, E. R. (1999). Vascular tissue engineering - Designer arteries. *Circulation Research* **85**(12): 1115-1117.

Eisenbarth, E., J. Meyle, *et al.* (1996). Influence of the surface structure of titanium materials on the adhesion of fibroblasts. *Biomaterials* **17**(14): 1399-1403.

Elisseeff, J., K. Anseth, *et al.* (1997). Synthesis and characterization of photo-gross-linked polymers based on poly(L-lactic acid-co-L-aspartic acid). *Macromolecules* **30**(7): 2182-2184.

Evans, G. R. D., K. Brandt, *et al.* (1999). In vivo evaluation of poly(L-lactic acid) porous conduits for peripheral nerve regeneration. *Biomaterials* **20**(12): 1109-1115.

Fausto, N., A. D. Lairdo, *et al.* (1995). Role of growth factors and cytokines in hepatic regeneration. *The FASEB Journal* **9**: 1527-1536.

Fewster, S. D., R. R. H. Coombs, *et al.* (1994). Precise Ultrafine Surface Texturing of Implant Materials to Improve Cellular Adhesion and Biocompatibility. *Nanobiology* **3**(3-4): 201-210.

Flemming, R. G., C. J. Murphy, *et al.* (1999). Effects of synthetic micro- and nano-structured surfaces on cell behavior. *Biomaterials* **20**(6): 573-588.

Freed, L. E., G. Vunjak-Novakovic, *et al.* (1994). Biodegradable polymer scaffolds for tissue engineering. *Biotechnology* **12**(July): 689-693.

Fujisato, T., T. Sajiki, *et al.* (1996). Effect of basic fibroblast growth factor on cartilage regeneration in chondrocyte-seeded collagen sponge scaffold. *Biomaterials* **17**(2): 155-162.

Ganachaud, F., A. Theretz, *et al.* (1995). Synthesis and Characterization of Bioreactive-End-Group- Containing Azoinitiators and Their Use For Preparing End- Functionalized Polyvinylpyrrolidone. *Journal of Applied Polymer Science* **58**(10): 1811-1824.

González, M., L. A. Bagatolli, *et al.* (1997). Interactions of biotin with streptavidin. *The Journal of Biological Chemistry* **272**: 11288-11294.

Gopferich, A. (1996). Mechanisms of polymer degradation and erosion. *Biomaterials* **17**(2): 103-114.

Green, N. M. (1965). A spectrophotometric assay for avidin and biotin based on binding of dyes by avidin. *Biochem. J.* **94**: 23c-24c.

Green, R. J., J. Davies, *et al.* (1997). Surface plasmon resonance for real time analysis of protein adsorption to polymer surfaces. *Biomaterials* **18**: 405-13.

Green, R. J., M. C. Davies, *et al.* (1999). Competitive protein adsorption as observed by surface plasmon resonance. *Biomaterials* **20**(4): 385-391.

Han, D. K. and J. A. Hubbell (1996). Lactide-based poly(ethylene glycol) polymer networks for scaffolds in tissue engineering. *Macromolecules* **29**(15): 5233-5235.

Han, D. K. and J. A. Hubbell (1997). Synthesis of polymer network scaffolds from L-lactide and poly(ethylene glycol) and their interactions with cells. *Macromolecules* **30**: 6077-6083.

He, S. L., M. J. Yaszemski, *et al.* (2000). Injectable biodegradable polymer composites based on poly(propylene fumarate) crosslinked with poly(ethylene glycol)-dimethacrylate. *Biomaterials* **21**(23): 2389-2394.

Healy, K. E., C. H. Thomas, *et al.* (1996). Kinetics of bone cell organization and mineralization on materials with patterned surface chemistry. *Biomaterials* **17**(2): 195-208.

Heller, J. (1994). Use of poly(ortho esters) and polyanhydrides in the development of peptide and protein delivery systems. *ACS Symposium Series* **567**: 292-305.

Hench, L. L. (1998). Biomaterials: a forecast for the future. *Biomaterials* **19**(16): 1419-1423.

Hollinger, J. O. and K. Leong (1996). Poly(alpha-hydroxy acids): Carriers for bone morphogenetic proteins. *Biomaterials* **17**(2): 187-194.

Holmberg, K., F. Tiberg, *et al.* (1997). Grafting with hydrophilic polymer chains to prepare protein-resistant surfaces. *Colloids and Surfaces a-Physicochemical and Engineering Aspects* **123**: 297-306.

Holy, C. E., S. M. Dang, *et al.* (1999). In vitro degradation of a novel poly(lactide-co-glycolide) 75/25 foam. *Biomaterials* **20**(13): 1177-1185.

Howdle, S. M., M. S. Watson, *et al.* (2001). Supercritical fluid mixing: preparation of thermally sensitive polymer composites containing bioactive materials. *Chemical Communications*(01): 109-110.

Hrkach, J. S., J. Ou, *et al.* (1995). Synthesis of Poly(L-Lactic Acid-Co-L-Lysine) Graft-Copolymers. *Macromolecules* **28**(13): 4736-4739.

Hrkach, J. S., M. T. Peracchia, *et al.* (1997). Nanotechnology for biomaterials engineering: Structural characterization of amphiphilic polymeric nanoparticles by H-1 NMR spectroscopy. *Biomaterials* **18**(1): 27-30.

Hubbell, J. A. (1996). Hydrogel systems for barriers and local drug delivery in the control of wound healing. *Journal of Controlled Release* **39**(2-3): 305-313.

Hubbell, J. A. (1996). In situ material transformations in tissue engineering. *Mrs Bulletin* **21**(11): 33-35.

Hubbell, J. A. (1998). Synthetic biodegradable polymers for tissue engineering and drug delivery. *Current Opinion in Solid State & Materials Science* **3**(3): 246-251.

Hutmacher, D. W. (2000). Scaffolds in tissue engineering bone and cartilage. *Biomaterials* **21**(24): 2529-2543.

Ishaug-Riley, S. L., G. M. Crane-Kruger, *et al.* (1998). Three-dimensional culture of rat calvarial osteoblasts in porous biodegradable polymers. *Biomaterials* **19**(15): 1405-1412.

Ito, Y. (1998). Tissue engineering by immobilized growth factors. *Materials Science & Engineering C-Biomimetic Materials Sensors and Systems* **6**(4): 267-274.

Jain, R. A. (2000). The manufacturing techniques of various drug loaded biodegradable poly(lactide-co-glycolide) (PLGA) devices. *Biomaterials* **21**(23): 2475-2490.

Jeong, B., Y. H. Bae, *et al.* (1997). Biodegradable block copolymers as injectable drug-delivery systems. *Nature* **388**(6645): 860-862.

Joshi, R., D. H. Robinson, *et al.* (1999). In vitro properties of an in situ forming gel for the parenteral delivery of macromolecular drugs. *Pharmaceutical Development and Technology* 4(4): 515-522.

Kaasgaard, T., O. G. Mouritsen, *et al.* (2001). Screening effect of PEG on avidin binding to liposome surface receptors. *International Journal of Pharmaceutics* **214**(1-2): 63-65.

Kaiser, K., M. Marek, *et al.* (1997). Basic studies on heterobifunctional biotin-PEG conjugates with a 3- (4-pyridyldithio)propionyl marker on the second terminus. *Bioconjugate Chemistry* 8(4): 545-551.

Kalb, B. and A. J. Pennings (1980). General crystallization behaviour of poly(l-lactic acid). *Polymer* **21**(June): 607-612.

Kaufmann, P. M., S. Heimrath, *et al.* (1997). Highly porous polymer matrices as a three-dimensional culture system for hepatocytes. *Cell Transplantation* 6(No. 5): 463-468.

Kawai, K., S. Suzuki, *et al.* (2000). Accelerated tissue regeneration through incorporation of basic fibroblast growth factor-impregnated gelatin microspheres into artificial dermis. *Biomaterials* **21**(5): 489-499.

Kim, B. S. and D. J. Mooney (1998). Development of biocompatible synthetic extracellular matrices for tissue engineering. *Trends in Biotechnology* **16**(5): 224-230.

Kohn, J. (1996). Tissue engineering: An overview. *Mrs Bulletin* **21**(11): 18-19.

Kricheldorf, H. R. and C. Boettcher (1993). Polylactones .27. Anionic-Polymerization of L-Lactide - Variation of Endgroups and Synthesis of Block-Copolymers With Poly(Ethylene Oxide). *Makromolekulare Chemie-Macromolecular Symposia* **73**: 47-64.

Kricheldorf, H. R., J. M. Jonte, *et al.* (1985). Polylactones .3. Copolymerization of Glycolide With L,L-Lactide and Other Lactones. *Makromolekulare Chemie-Macromolecular Chemistry and Physics*(S12): 25-38.

Kricheldorf, H. R. and I. Kreiser (1987). Polylactones .11. Cationic Copolymerization of Glycolide With L,L- Dilactide. *Makromolekulare Chemie-Macromolecular Chemistry and Physics* **188**(8): 1861-1873.

Kricheldorf, H. R. and I. KreiserSaunders (1996). Polylactides - Synthesis, characterization and medical application. *Macromolecular Symposia* **103**: 85-102.

Kricheldorf, H. R., I. Kreisersaunders, *et al.* (1995). Polylactones .31. Sn(Ii)Octoate-Initiated Polymerization of L-Lactide - a Mechanistic Study. *Polymer* **36**(6): 1253-1259.

Kricheldorf, H. R. and J. Meierhaack (1993). Polylactones .22. Aba Triblock Copolymers of L-Lactide and Poly(Ethylene Glycol). *Makromolekulare Chemie-Macromolecular Chemistry and Physics* **194**(2): 715-725.

Kue, R., A. Sohrabi, *et al.* (1999). Enhanced proliferation and osteocalcin production by human osteoblast-like MG63 cells on silicon nitride ceramic discs. *Biomaterials* **20**(13): 1195-1201.

Kuo, C. K. and P. X. Ma (2001). Ionically crosslinked alginate hydrogels as scaffolds for tissue engineering: Part 1. Structure, gelation rate and mechanical properties. *Biomaterials* **22**(6): 511-521.

Labrador, R. O., M. Buti, *et al.* (1998). Influence of collagen and laminin gels concentration on nerve regeneration after resection and tube repair. *Experimental Neurology* **149**(1): 243-252.

Lackey, C. A., N. Murthy, *et al.* (1999). Hemolytic activity of pH-responsive polymer-streptavidin bioconjugates. *Bioconjugate Chemistry* **10**(3): 401-405.

Langer, R. and J. P. Vacanti (1993). Tissue Engineering. *Science* **260**(5110): 920-926.

Lawes, R. (1994). Microstructures and microengineering. *Engineering and Physical Processes* **Chapter 4**: 57-73.

Lawes, R. A. (1996). Fabrication technology for microengineering. *Sensor Review* **16**(2): 16-22.

Leary, J. J., D. J. Brigati, *et al.* (1983). Rapid and Sensitive Colorimetric Method For Visualizing Biotin- Labeled Dna Probes Hybridized to Dna or Rna Immobilized On Nitrocellulose - Bio-Blots. *Proceedings of the National Academy of Sciences of the United States of America-Biological Sciences* **80**(13): 4045-4049.

LeBaron, R. G. and K. A. Athanasiou (2000). Ex vivo synthesis of articular cartilage. *Biomaterials* **21**(24): 2575-2587.

Lee, K. Y. and D. J. Mooney (2001). Hydrogels for tissue engineering. *Chemical Reviews* **101**(7): 1869-1879.

Lee, K. Y., M. C. Peters, *et al.* (2000). Controlled growth factor release from synthetic extracellular matrices. *Nature* **408**(6815): 998-1000.

Li, M., H. Schnablegger, *et al.* (1999). Coupled synthesis and self-assembly of nanoparticles to give structures with controlled organization. *Nature* **402**(6760): 393-395.

Li, R. H., M. White, *et al.* (1998). Poly(vinyl alcohol) synthetic polymer foams as scaffolds for cell encapsulation. *Journal of Biomaterials Science-Polymer Edition* **9**(3): 239-258.

Li, S. M. and S. McCarthy (1999). Further investigations on the hydrolytic degradation of poly(DL- lactide). *Biomaterials* **20**(1): 35-44.

Li, S. M., I. Rashkov, *et al.* (1996). Synthesis, characterization, and hydrolytic degradation of PLA/PEO/PLA triblock copolymers with long poly(L-lactic acid) blocks. *Macromolecules* **29**(1): 57-62.

Li, Y. X. and T. Kissel (1993). Synthesis and Properties of Biodegradable Aba Triblock Copolymers Consisting of Poly(L-Lactic Acid) or Poly(L-Lactic-Co-Glycolic Acid) a-Blocks Attached to Central Poly(Oxyethylene) B-Blocks. *Journal of Controlled Release* **27**(3): 247-257.

Lindqvist, Y. and G. Schneider (1996). Protein-biotin interactions. *Current Opinion in Structural Biology* **6**: 798-803.

Lu, L., S. J. Peter, *et al.* (2000). In vitro and in vivo degradation of porous poly(DL-lactic-co- glycolic acid) foams. *Biomaterials* **21**(18): 1837-1845.

Lu, L. C. and A. G. Mikos (1996). The importance of new processing techniques in tissue engineering. *Mrs Bulletin* **21**(11): 28-32.

Lu, L. C., S. J. Peter, *et al.* (2000). In vitro degradation of porous poly(L-lactic acid) foams. *Biomaterials* **21**(15): 1595-1605.

Lunt, J. (1998). Large-scale production, properties and commercial applications of polylactic acid polymers. *Polymer Degradation and Stability* **59**(1-3 SISI): 145-152.

Lynch, N. J., P. K. Kilpatrick, *et al.* (1996). Aggregation of ligand-modified liposomes by specific interactions with proteins. 1: Biotinylated liposomes and avidin. *Biotechnology and Bioengineering* **50**: 169-183.

Lynch, N. J., P. K. Kilpatrick, *et al.* (1996). Aggregation of ligand-modified liposomes by specific interactions with proteins. 2: Biotinylated liposomes and antibiotin antibody. *Biotechnology and Bioengineering* **50**(2): 151-168.

Mahal, L. K., K. J. Yarema, *et al.* (1997). Engineering Chemical Reactivity on Cell Surfaces Through Oligosaccharide Biosynthesis. *Science* **276**: 1125-1128.

Marler, J. J., J. Upton, *et al.* (1998). Transplantation of cells in matrices for tissue regeneration. *Advanced Drug Delivery Reviews* **33**(1-2): 165-182.

Marshall, D. and R. B. Pedley (1996). Polyethylene glycol modification of a galactosylated streptavidin clearing agent: effects on immunogenicity and clearance of a biotinylated anti-tumour antibody. *British Journal of Cancer* **73**: 565-572.

Massia, S. P. and J. A. Hubbell (1990). Covalent surface immobilization of Arg-Gly-Asp and Tyr-Ile-Gly-Ser-Arg-containing peptides to obtain well-defined cell-adhesive substrates. *Analytical Biochemistry* **187**: 292-301.

Massia, S. P. and J. A. Hubbell (1991). An RGD spacing of 440nm is sufficient for integrin $\alpha_v\beta_3$–mediated spreading and 140nm for focal contact and stress fiber formation. *The Journal of Cell Biology* **114**(5): 1089-1100.

Matsusue, Y., T. Yamamuro, *et al.* (1992). Invitro and Invivo Studies on Bioabsorbable Ultrahigh-Strength Poly(L-Lactide) Rods. *Journal of Biomedical Materials Research* **26**(12): 1553-1567.

Menger, M. D., P. Walter, *et al.* (1990). Quantitative-Analysis of Neovascularization of Different Ptfe- Implants. *European Journal of Cardio-Thoracic Surgery* **4**(4): 191-196.

Meyle, J., K. Gultig, *et al.* (1994). Contact Guidance of Fibroblasts On Biomaterial Surfaces. *Journal of Materials Science-Materials in Medicine* **5**(6-7): 463-466.

Mi, Y. L. and S. X. Zheng (1998). A new study of glass transition of polymers by high pressure DSC. *Polymer* **39**(16): 3709-3712.

Mikos, A. G., G. Sarakinos, *et al.* (1993). Prevascularization of Porous Biodegradable Polymers. *Biotechnology and Bioengineering* **42**(6): 716-723.

Moghe, P. V. (1996). Soft-tissue analogue design and tissue engineering of liver. *Mrs Bulletin* **21**(11): 52-54.

Mooney, D. J., D. F. Baldwin, *et al.* (1996). Novel approach to fabricate porous sponges of poly(D,L-lactic- co-glycolic acid) without the use of organic solvents. *Biomaterials* **17**(14): 1417-1422.

Mooney, D. J., C. Breuer, *et al.* (1995). Fabricating tubular devices from polymers of lactic and glycolic acid for tissue engineering. *Tissue Engineering* **1**(2): 107-118.

Mooney, D. J., P. M. Kaufmann, *et al.* (1996). Localised Delivery of Epidermal Growth Factor Improves the Survival of Transplanted Hepatocytes. *Biotechnology and Bioengineering* **50**: 422-429.

Mooney, D. J., K. Sano, *et al.* (1997). Long-term engraftment of hepatocytes transplanted on biodegradable polymer sponges. *Journal of Biomedical Materials Research* **37**(3): 413-420.

Mooney, D. T., C. L. Mazzoni, *et al.* (1996). Stabilized polyglycolic acid fibre based tubes for tissue engineering. *Biomaterials* **17**(2): 115-124.

Murakami, H., Y. Kawashima, *et al.* (1997). Influence of the degrees of hydrolyzation and polymerization of poly(vinylalcohol) on the preparation and properties of poly(DL-lactide-co-glycolide) nanoparticle. *International Journal of Pharmaceutics* **149**(1): 43-49.

Niklason, L. and R. S. Langer (1997). Advances in Tisssue Engineering of Blood Vessels and Other Tissues. *Transplant Immunology* **5**: 303-306.

Otsuka, H., Y. Nagasaki, *et al.* (1998). Reactive PEG-polylactide block copolymer for tissue engineering. *Abstracts of Papers of the American Chemical Society* **216**: 249-POLY.

Pachence, J. M. (1996). Collagen-based devices for soft tissue repair. *Journal of Biomedical Materials Research* **33**(1): 35-40.

Padera, R. F. and C. K. Colton (1996). Time course of membrane microarchitecture-driven neovascularization. *Biomaterials* **17**(3): 277-284.

Park, Y. J., Y. M. Lee, *et al.* (2000). Platelet derived growth factor releasing chitosan sponge for periodontal bone regeneration. *Biomaterials* **21**(2): 153-159.

Patel, N., R. Padera, *et al.* (1998). Spatially controlled cell engineering on biodegradable polymer surfaces. *Faseb Journal* **12**(14): 1447-1454.

Penco, M., S. Marcioni, *et al.* (1996). Degradation behaviour of block copolymers containing poly(lactic- glycolic acid) and poly(ethylene glycol) segments. *Biomaterials* **17**(16): 1583-1590.

Penco, M., E. Ranucci, *et al.* (1998). A new chain extension reaction on poly(lactic-glycolic acid) (PLGA) thermal oligomers leading to high molecular weight PLGA-based polymeric products. *Polymer International* **46**(3): 203-216.

Peng, T. and Y. L. Cheng (2001). PNIPAAm and PMAA co-grafted porous PE membranes: Living radical co-grafting mechanism and multi-stimuli responsive permeability. *Polymer* **42**(5): 2091-2100.

Peppas, N. A. and R. Langer (1994). New challenges in biomaterials. *Science* **263**(25 March): 1715-1720.

Peter, S. J., M. J. Miller, *et al.* (1998). Polymer concepts in tissue engineering. *Journal of Biomedical Materials Research* **43**(4): 422-427.

Peter, S. J., J. A. Nolley, *et al.* (1997). In vitro degradation of a poly(propylene fumarate)/beta- tricalcium phosphate composite orthopaedic scaffold. *Tissue Engineering* **3**(2): 207-215.

Quirk, R. A., M. C. Davies, *et al.* (2000). Surface engineering of poly(lactic acid) by entrapment of modifying species. *Macromolecules* **33**(2): 258-260.

Rashkov, I., N. Manolova, *et al.* (1996). Synthesis, characterization, and hydrolytic degradation of PLA/PEO/PLA triblock copolymers with short poly(L-lactic acid) chains. *Macromolecules* **29**(1): 50-56.

Ratner, B. D., D. G. Castner, *et al.* (1990). Biomolecules and Surfaces. *Journal of Vacuum Science & Technology a-Vacuum Surfaces and Films* **8**(3 Pt2): 2306-2317.

Ronneberger, B., T. Kissel, *et al.* (1997). Biocompatibility of ABA triblock copolymer microparticles consisting of poly(L-lactic-co-glycolic-acid) A-blocks attached to central poly(oxyethylene) B-blocks in rats after intramuscular injection. *European Journal of Pharmaceutics and Biopharmaceutics* **43**(1): 19-28.

RothenWeinhold, A., K. Besseghir, *et al.* (1997). Analysis of the influence of polymer characteristics and core loading on the in vivo release of a somatostatin analogue. *European Journal of Pharmaceutical Sciences* **5**(6): 303-313.

Ruoslahti, E. (1997). Cell biology - Stretching is good for a cell. *Science* **276**(5317): 1345-1346.

Ruoslahti, E. and B. Obrink (1996). Common principles in cell adhesion. *Experimental Cell Research* **227**(1): 1-11.

Salzmann, D. L., L. B. Kleinert, *et al.* (1997). The effects of porosity on endothelialization of ePTFE implanted in subcutaneous and adipose tissue. *Journal of Biomedical Materials Research* **34**(4): 463-476.

Schacht, E., J. Vandorpe, *et al.* (1996). Biomedical applications of degradable polyphosphazenes. *Biotechnology and Bioengineering*: 102-108.

Selomulya, C., R. Amal, *et al.* (2001). Evidence of shear rate dependence on restructuring and breakup of latex aggregates. *Journal of Colloid and Interface Science* **236**(1): 67-77.

Sharkawy, A. A., B. Klitzman, *et al.* (1997). Engineering the tissue which encapsulates subcutaneous implants .1. Diffusion properties. *Journal of Biomedical Materials Research* **37**(3): 401-412.

Sharkawy, A. A., B. Klitzman, *et al.* (1998). Engineering the tissue which encapsulates subcutaneous implants. II. Plasma-tissue exchange properties. *Journal of Biomedical Materials Research* **40**(4): 586-597.

Sharkawy, A. A., B. Klitzman, *et al.* (1998). Engineering the tissue which encapsulates subcutaneous implants. III. Effective tissue response times. *Journal of Biomedical Materials Research* **40**(4): 598-605.

Shastri, V. P., I. Martin, *et al.* (2000). Macroporous polymer foams by hydrocarbon templating. *Proceedings of the National Academy of Sciences of the United States of America* **97**(5): 1970-1975.

Sheridan, M. H., L. D. Shea, *et al.* (2000). Bioadsorbable polymer scaffolds for tissue engineering capable of sustained growth factor delivery. *Journal of Controlled Release* **64**(1-3): 91-102.

Singhvi, R., A. Kumar, *et al.* (1994). Engineering Cell-Shape and Function. *Science* **264**(5159): 696-698.

Singhvi, R., G. Stephanopoulos, *et al.* (1994). Effects of Substratum Morphology On Cell Physiology - Review. *Biotechnology and Bioengineering* **43**(8): 764-771.

Smith, M. S. and J. D. Browne (1998). The effect of endothelial cell growth factor on peripheral nerve regeneration. *Otolaryngology-Head and Neck Surgery* **118**(2): 178-182.

Sondell, M., G. Lundborg, *et al.* (1999). Vascular endothelial growth factor has neurotrophic activity and stimulates axonal outgrowth, enhancing cell survival and Schwann cell proliferation in the peripheral nervous system. *Journal of Neuroscience* **19**(14): 5731-5740.

Soppimath, K. S., T. M. Aminabhavi, *et al.* (2001). Biodegradable polymeric nanoparticles as drug delivery devices. *Journal of Controlled Release* **70**(1-2): 1-20.

Stayton, P. S., T. Shimoboji, *et al.* (1995). Control of protein-ligand recognition using stimuli-responsive polymer. *Nature* **378**: 472-474.

Steendam, R., M. J. van Steenbergen, *et al.* (2001). Effect of molecular weight and glass transition on relaxation and release behaviour of poly(DL-lactic acid) tablets. *Journal of Controlled Release* **70**(1-2): 71-82.

Stock, U. A. and J. P. Vacanti (2001). Tissue engineering: Current state and prospects. *Annual Review of Medicine* **52**: 443-451.

Temenoff, J. S. and A. G. Mikos (2000). Review: tissue engineering for regeneration of articular cartilage. *Biomaterials* **21**(5): 431-440.

Thomson, R. C., M. C. Wake, *et al.* (1995). Biodegradable Polymer Scaffolds to regenerate Organs. *Advances in Polymer Science* **122**: 245-274.

Thomson, R. C., M. J. Yaszemski, *et al.* (1995). Fabrication of Biodegradable Polymer Scaffolds to Engineer Trabecular Bone. *Journal of Biomaterials Science-Polymer Edition* **7**(1): 23-38.

Tjia, J. S. and P. V. Moghe (1998). Analysis of 3-D microstructure of porous poly(lactide-glycolide) matrices using confocal microscopy. *Journal of Biomedical Materials Research* **43**(3): 291-299.

Tonan, K., K. Adachi, *et al.* (1998). NMR study of selective H-D exchange of amide protons of D-biotin with deuterium oxide in dimethyl sulfoxide. *Spectrochimica Acta Part a-Molecular and Biomolecular Spectroscopy* **54**(7): 989-997.

Tracy, M. A., K. L. Ward, *et al.* (1999). Factors affecting the degradation rate of poly(lactide-co- glycolide) microspheres in vivo and in vitro. *Biomaterials* **20**(11): 1057-1062.

Tziampazis, E., J. Kohn, *et al.* (2000). PEG-variant biomaterials as selectively adhesive protein templates: model surfaces for controlled cell adhesion and migration. *Biomaterials* **21**(5): 511-520.

Uhrich, K. E., S. M. Cannizzaro, *et al.* (1999). Polymeric systems for controlled drug release. *Chemical Reviews* **99**(11): 3181-3198.

Ural, E., K. Kesenci, *et al.* (2000). Poly(D,L-cactide/epsilon-caprolactone)/hydroxyapatite composites. *Biomaterials* **21**(21): 2147-2154.

Vacanti, C. A., R. Langer, *et al.* (1991). Synthetic-Polymers Seeded With Chondrocytes Provide a Template For New Cartilage Formation. *Plastic and Reconstructive Surgery* **88**(5): 753-759.

Vacanti, C. A. and J. P. Vacanti (2000). The science of tissue engineering. *Orthopedic Clinics of North America* **31**(3): 351-+.

Vacanti, C. A., J. P. Vacanti, *et al.* (1994). Tissue Engineering Using Synthetic Biodegradable Polymers. Polymers of Biological and Biomedical Significance. **540:** 16-34.

Vacanti, J. P. (2001). Looking back and looking ahead. *Tissue Engineering* 7(2): 107-109.

Vacanti, J. P. and R. Langer (1999). Tissue engineering: the design and fabrication of living replacement devices for surgical reconstruction and transplantation. *Lancet* **354**: SI32-SI34.

Veronese, F. M. (2001). Peptide and protein PEGylation: a review of problems and solutions. *Biomaterials* **22**(5): 405-417.

Vonrecum, A. F. and T. G. Vankooten (1995). The Influence of Micro-Topography On Cellular-Response and the Implications For Silicone Implants. *Journal of Biomaterials Science-Polymer Edition* **7**(2): 181-198.

Wake, M. C., C. W. Patrick, *et al.* (1994). Pore Morphology Effects on the Fibrovacular Tissue Growth in Porous Polymer Substrates. *Cell Transplatation* **3**(4): 339-343.

Westhaus, E. and P. B. Messersmith (2001). Triggered release of calcium from lipid vesicles: a bioinspired strategy for rapid gelation of polysaccharide and protein hydrogels. *Biomaterials* **22**(5): 453-462.

Whang, K., D. C. Tsai, *et al.* (1998). Ectopic bone formation via rhBMP-2 delivery from porous bioabsorbable polymer scaffolds. *Journal of Biomedical Materials Research* **42**(4): 491-499.

Williams, S. K., S. S. Berman, *et al.* (1997). Differential healing and neovascularization of ePTFE implants in subcutaneous versus adipose tissue. *Journal of Biomedical Materials Research* **35**(4): 473-481.

Winn, S. R., H. Uludag, *et al.* (1999). Carrier systems for bone morphogenetic proteins. *Clinical Orthopaedics and Related Research*(367): S95-S106.

Wintermantel, E., J. Mayer, *et al.* (1996). Tissue engineering scaffolds using superstructures. *Biomaterials* **17**(2): 83-91.

Wojciakstothard, B., A. S. G. Curtis, *et al.* (1995). Role of the Cytoskeleton in the Reaction of Fibroblasts to Multiple Grooved Substrata. *Cell Motility and the Cytoskeleton* **31**(2): 147-158.

Yang, Y. Y., H. H. Chia, *et al.* (2000). Effect of preparation temperature on the characteristics and release profiles of PLGA microspheres containing protein fabricated by double-emulsion solvent extraction/evaporation method. *Journal of Controlled Release* **69**(1): 81-96.

Yin, M. and G. L. Baker (1999). Preparation and characterization of substituted polylactides. *Macromolecules* **32**(23): 7711-7718.

Zhang, P. and J. S. Moore (2000). Synthesis and characterization of PEE-PEO diblock copolymers with complementary end-groups for hydrogen-bond heteroassociation. *Journal of Polymer Science Part a-Polymer Chemistry* **38**(1): 207-219.

Zhu, K. J., X. Z. Lin, *et al.* (1990). Preparation, Characterization, and Properties of Polylactide (Pla) Poly(Ethylene Glycol) (Peg) Copolymers - a Potential-Drug Carrier. *Journal of Applied Polymer Science* **39**(1): 1-9.